Improving 3D Matrices for Tissue Engineering Using Advanced Drug Delivery Techniques

Yiwei Wang

Report submitted in partial fulfilment of the requirements for the admission to the Doctor of Philosophy (Pharmacy)

Faculty of Science

Kingston University, London

October 2007

Acknowledgements

This project would not have been possible if not for my outstanding and experienced director of studies, Professor Allan Coombes, who provided invaluable professional guidance throughout the course of my PhD studies. I have learned a great deal from his supervision and knowledge. I am greatly indebted to him for his continuous encouragement and helpful advice. Sincerely and heartily, I would like to thank him with great gratitude and appreciation.

I would like to give Dr David Wertheim very special thanks for his tireless efforts to provide an enriching experience in Micro-CT image analysis. I am also grateful to Dr Allan Jones of the University of Sydney for his valuable time and instruction in Micro-CT and sample analysis.

I would like to thank Dr Hsin-I Chang and Associate Professor Chris Jackson of the University of Sydney for their insightful comments, advice and instruction during the first year of my PhD study.

I greatly appreciate the advice and technical assistance with biodynamic testing given by Dr Paul Tomlins, Dr Jenny Lam and Dr Bufa Zhang of the National Physical Laboratory.

I extend my special appreciation to Professor Oyar Alpar and Dr Xiongwei Li of the School of Pharmacy, University of London for their intellectual support and advice on cell culture.

My life at Sydney University and Kingston University, London was enriched by many people around me. I am indebted to many people in the Faculty of Pharmacy, University of Sydney and the Materials Group, School of Pharmacy and Chemistry, Kingston University, for their support. Thanks especially to my colleagues, Kevin Cheung-Yuan Lai, Baljit Ghatora, Seema Pillia Jing Xu, Philip Kwon, Rina Khatwa, Antonella Ciocce, Zaid Abbas, Moayad Almasri, Hugh O'Malley, Sarah Banfield.

Most importantly, I wish to express my deepest gratitude to my parents. Their support and selfless affection made my studies possible. If it were not for them, this would not have happened.

Abstract

Micro/macroporous matrices comprising a continuous phase of poly(ε-caprolactone) (PCL) and a dispersed phase of water soluble particles (lactose and gelatin) with defined size range (45-90, 90-125 and 125-250μm) were produced by rapid cooling solutions of PCL in acetone followed by solvent extraction from the hardened material. This novel approach enables high loading (29-44% w/w) of particles (lactose and gelatin) to be achieved in PCL matrices by suspension of particulates in the PCL solution prior to casting. Highly efficient protein release (90%) was obtained over time periods of 3 days to 3 weeks by variation of particle loading and particle size range. The good particle distribution throughout the matrix and efficient extraction of the water-soluble phase allows formation of a macroporous structure with defined pore architecture by incorporation of particles of a specific shape and size range. SEM analysis revealed the porous surface morphology. Micro computed tomography (micro-CT) and image analysis enabled visualization of the internal 3-D pore structure, quantification of the frequency distribution of equivalent pore diameter and porosity (%) in PCL matrices. Micro/macroporous PCL tubes exhibited a burst strength of 125 to 145MPa under hydrostatic loading at 37°C and good recovery of tube diameter following short-duration flow rates of 1000 ml/min under continuous increasing and pulsatile conditions. Sustained release of incorporated enzymes (lysozyme, collagenase and catalase) occurred over 11 days from the PCL matrices, with retained activity dependent on the particular enzyme used (collagenase 100% at 11 days, lysozyme 75-80% at 11 days, catalase 10-20 % at 5 days). Swiss3T3 fibroblasts exhibited strong attachment and successful colonization of the surface of PCL matrices over 8 to 15 days in cell culture. These findings demonstrate the potential of micro/macroporous PCL matrices for scaffold production in tissue engineering and for controlling drug delivery.

List of Tables

Table 1.1 Optimal pore size for cell infiltration and host tissue ingrowth

Table 1.2 Methods of scaffold/matrix manufacture

Table 1.3 Growth factors used in tissue engineering applications (adapted from Whittaker, M.J. et al)

Table 1.4 Polymers used for production of reservoir systems

Table 1.5 Properties of synthetic polymers

Table 1.6 Biomedical application of PCL and its blends

Table 3.1 Influence of cooling time in dry ice on shrinkage of unloaded-PCL

Table 3.2 Weight distribution of gelatin particles (125-250μm) in PCL matrices produced using 12.5%, 15% and 20% w/v PCL solution

Table 3.3 Thermal properties and porosity of PCL matrices and lactose-loaded PCL matrices

Table 3.4 Thermal properties and porosity of PCL tubular castings

Table 4.1 Typical information generated on the pore structure within a sample
Table 4.2 Theoretical porosity of PCL matrices

Table 4.3 Macroporosity of PCL matrices determined by analysis of micro-CT images using low threshold (150)

Table 4.4 Macroporosity of PCL matrices determined by analysis of micro-CT images

Table 5.1 The effect of conditions of pulsatile flow on the deformation of microporous PCL tubes

Table 5.2 Burst strength of microporous PCL tubes, gelatin-loaded PCL tubes and macroporous PCL tubes formed by gelatin extraction

Table 6.1 Thermal properties of PCL and lysozyme-loaded PCL matrices

Table 6.2 Activity of lysozyme solution following powder exposure to organic

solvents

Table 6.3 Thermal properties of PCL and collagenase-loaded PCL matrices

Table 6.4 Activity of collagenase following exposure of powder in organic solvent

Table 6.5 Thermal properties of catalase-loaded PCL matrices produced using methanol or ethanol as a non-solvent

Table 6.6 Activity of catalase following exposure of the powder to organic solvents

Table 6.7 Thermal properties of drug free-PCL matrices and dexamethasone-loaded PCL matrices produced by precipitation casting using 12.5% w/v PCL solutions

List of Figures

Figure 1.1 Biodegradable 3D scaffold used to promote cell attachment, proliferation and differentiation. The scaffold with or without cells and/or biological signaling molecules (e.g. growth factor, cytokines, chemokines and genes) is applied to a defect to induce in vivo regeneration of tissue and organs

Figure 1.2 The steady-state concentration profile of a drug in a reservoir-type polymeric system. Cr = concentration of drug in the reservoir, Ci = concentration of drug at the site of implantation

Figure 1.3 Scheme of drug delivery from porous matrices

Figure 1.4 Drug release by diffusion through a non-degradable polymeric matrix

Figure 1.5 Chemical structures of natural polymers

Figure 1.6 Chemical structure of soluble synthetic polymers

Figure 1.7 Chemical structure of synthetic hydrogels

Figure 1.8 Chemical structure of non-biodegradable synthetic polymers

Figure 1.9 Chemical structure of biodegradable synthetic polymers

Figure 1.10 Mechanisms of polymerization of poly (ε-caprolactone)

Figure 2.1 Formulation of microporous PCL matrices

Figure 2.2 The liquid displacement method for porosity measurement

Figure 2.3 The principle of computed micro-tomography (Micro-CT)

Figure 2.4 Schematic representation of diameter measurement using a laser micrometer

Figure 2.5 The Bose-Enduratec biodynamic chamber

Figure 2.6 Schematic representation of a biodynamic chamber

Figure 2.7 Schematic representation of the test facility used for burst testing PCL tubes

Figure 3.1 Microporous PCL matrices in the form of cylinders, tubes, and ring-shaped insert

Figure 3.2 Temperature profile of PCL solution in acetone on immersing in dry ice

Figure 3.3 Surface morphology of PCL matrices formed using (A) methanol (B) ethanol (C) water as a non-solvent

Figure 3.4 The weight distribution of lactose in microporous PCL matrices produced using various particle size ranges (starting suspension loading 29% w/w)

Figure 3.5 Cumulative lactose release from microporous PCL matrices (29% w/w particle loading) containing discrete particle size ranges

Figure 3.6 Scanning electron micrographs of (A) unloaded PCL matrix (B) Lactose (90-125μm): PCL matrix before release (C,D) Lactose (90-125μm): PCL matrix after release

Figure 3.7 Scanning electron micrographs of lactose particles (A) before PCL matrix production (B, C) recovered from PCL matrix

Figure 3.8 The weight distribution of gelatin particles in microporous PCL matrices produced using various particle size ranges (A) matrices prepared from 29% w/w particle suspensions (B) matrices prepared from 38% w/w particle suspensions (C) matrices prepared from 44% w/w particle suspensions

Figure 3.9 Cumulative gelatin release (%) from microporous PCL matrices containing particles of discrete size ranges. Matrices produced from (A) 29% w/w (B) 38% w/w (C) 44% w/w particle suspensions

Figure 3.10 Scanning electron micrographs.(A) 29% w/w gelatin (125-250μm): PCL matrix before release (B, C) 29% w/w gelatin (125-250μm): PCL matrix after release (D) cross section of 44% w/w gelatin (90-125μm)-loaded PCL matrix after release (E) cross section of 44% w/w gelatin (125-250μm)-loaded PCL matrix after release

Figure 3.11 Scanning electron micrographs of 125-250μm gelatin particles (A) before PCL matrix formulation (B) following extraction from PCL matrices

Figure 3.12 Light micrograph of 3T3 fibroblasts cultured on TCP at day 5

Figure 3.13 Proliferation rates of 3T3 mouse fibroblasts on TCP and porous PCL matrices produced by extraction of lactose particles (* $P<0.05$)

Figure 3.14 Proliferation rates of 3T3 fibroblasts on TCP and porous PCL matrices produced by extraction of gelatin particles (* $P<0.01$)

Figure 3.15 Scanning electron micrographs of 3T3 fibroblasts cultured for 1 day on a

PCL matrix formed by extraction of lactose particles

Figure 4.1 2D shadow images of (A) PCL matrix (B) 29% w/w gelatin (90-125μm): PCL matrix (polymer phase) after release (C) 29% w/w gelatin (125-250μm): PCL matrix (polymer phase) after release

Figure 4.2 Internal microtomographs of (A) Polymeric phase of PCL matrix (B) Polymeric phase of 29% w/w gelatin (90-125 μm): PCL matrix before release
(C) Polymeric phase of 29% w/w gelatin (45-90 μm): PCL matrix after release
(D) Polymeric phase of 23% w/w gelatin (125-250 μm): PCL matrix after release
(E) Pore phase of 29% w/w gelatin (45-90μm): PCL matrix after particle release
(F) Pore phase of 23% w/w gelatin (125-250μm): PCL matrix after particle release

Figure 4.3 2D shadow images of (A) 38% w/w gelatin (90-125μm): PCL matrix (polymer phase) after release (B) 38% w/w gelatin (90-125μm): PCL matrix (polymer phase) after release (C) 44% w/w gelatin (45-90μm): PCL matrix (polymer phase) after release (D) 44% w/w gelatin (90-125,125-250μm): PCL matrix (polymer phase) before/after release

Figure 4.4 Internal microtomographs of (A) Polymeric phase of 44% w/w gelatin (90-125 μm): PCL matrix before release (B) Polymeric phase of 80% w/w gelatin (45-90 μm): PCL matrix after release (C) Polymeric phase of 38 % w/w gelatin

(90-125 μm): PCL matrix after release (D) Polymeric phase of 38% w/w gelatin (125-250 μm): PCL matrix after release (E) pore structure of 38% w/w gelatin (45-90 μm): PCL matrix after release (F) pore structure of 38% w/w gelatin (90-125 μm): PCL matrix after release

Figure 4.5 Internal microtomographs (A) pore structure of 44% w/w gelatin (45-90 μm): PCL matrix after release (complete section) (B) pore structure of 44% w/w gelatin (125-250 μm):PCL matrix after release (complete section) (C) pore structure of 44% w/w gelatin (45-90 μm): PCL matrix after release (half section) (D) pore structure of 44 % w/w gelatin (45-90 μm): PCL matrix after release (quarter section)

Figure 4.6 Step-by-step process of image processing of 2D shadow images from Micro-CT data of PCL matrices (A) 2D image showing the difference after filtering (B) 2D image showing the difference after contrast adjustment (C) 2D image showing the image after threshold adjustment (D) Modified 2D image and a defined square area of interest (E) Final image used for quantitative analysis

Figure 4.7 Image processing of MicroCT data. Original shadow image (A), and grey-scale image analysis using a threshold of 150 (B) and 230 (C)

Figure 4.8 Illustration of the variation of pore shape in a 2-D image sample

Figure 4.9 (A) Grey scale micro-CT image of a PCL matrix following extraction of

38 % w/w gelatin particles (90-125μm). (A) original defined area of interest (B) Image analysed after exclusion of pores on edge of area of interest

Figure 4.10 Analysis of macroporosity using micro-CT images of PCL matrices following extraction of 29% w/w lactose particles (A) Variation in equivalent pore diameter (90-125μm lactose-loaded PCL) (B) Frequency distribution of equivalent pore diameter (90-125μm lactose-loaded PCL) (C) Variation in equivalent pore diameter (125-250μm lactose-loaded PCL) (D) Frequency distribution of equivalent pore diameter (125-250μm lactose-loaded PCL)

Figure 4.11 Analysis of macroporosity using micro-CT images of PCL matrices following extraction of 29 %w/w gelatin particles (A) Variation in equivalent pore diameter (90-125μm gelatin-loaded PCL) (B) Frequency distribution of equivalent pore diameter (90-125μm gelatin-loaded PCL) (C) Variation in equivalent pore diameter (125-250μm gelatin-loaded PCL) (D) Frequency distribution of equivalent pore diameter (125-250μm gelatin-loaded PCL)

Figure 4.12 Schematic illustrating the difference between pore size measurement using Micro-CT and sieving

Figure 4.13 Analysis of macroporosity using micro-CT images of PCL matrices following extraction of 38% w/w gelatin particles (A) Variation in equivalent pore

diameter (45-90μm gelatin-loaded PCL) (B) Frequency distribution of equivalent pore diameter 4(5-90μm gelatin-loaded PCL)(C) Variation in equivalent pore diameter (90-125μm gelatin-loaded PCL (D) Frequency distribution of equivalent pore diameter (90-125μm gelatin-loaded PCL) (E) Variation in equivalent pore diameter (125-250μm gelatin-loaded PCL)(F) Frequency distribution of equivalent pore diameter (125-250μm gelatin-loaded PCL)

Figure 4.14 Analysis of macroporosity using micro-CT images of PCL matrices following extraction of 44% w/w gelatin particles (A) Variation in equivalent pore diameter (45-90μm gelatin-loaded PCL) (B) Frequency distribution of equivalent pore diameter (45-90μm gelatin-loaded PCL) (C) Variation in equivalent pore diameter (90-125μm gelatin-loaded PCL) (D) Frequency distribution of equivalent pore diameter (90-125μm gelatin-loaded PCL) (E) Variation in equivalent pore diameter (125-250μm gelatin-loaded PCL(F) Frequency distribution of equivalent pore diameter (125-250μm gelatin-loaded PCL)

Figure 4.15 (A) Variation in equivalent pore diameter (125-250μm) (B) frequency distribution of equivalent pore diameter following gelatin particle (125-250μm) extraction from 44% w/w loaded PCL matrices. Sequential images starting from No.36

Figure 4.16 Step-by-step process of porosity analysis using micro-CT images

(A) 3D view of pore structure (B) 3D view of sample with 2D view in x-y, x-z and y-z

direction (C) Pores were rendered in red before analysis (D) All rendered pores were selected for analysis (E) Presentation of results

Figure 4.17 Internal macropores in PCL matrices detected using (A) low threshold (150) (B)high threshold (230) processing of micro-CT images. Matrices produced by extraction of 44% w/w gelatin particles (125 -250 μm) using high threshold (230)

Figure 5.1 The changes in outer diameter of a microporous PCL tube over 1 hr at 37°C under a constant flow rate of 300ml/min

Figure 5.2 The changes in outer diameter of microporous PCL tubes containing (A) 29%, (B) 38% and (C) 44% w/w gelatin particles over 1 hour under a constant flow rate of 300ml/min at 37 °C

Figure 5.3 The changes in outer diameter of microporous PCL tubes after (A) 29%, (B) 38% and (C) 44% w/w gelatin extraction. Tubes tested for 1 hour under a constant flow rate of 300 ml/min at 37 °C

Figure 5.4 The amount of gelatin released from microporous PCL tubes in distilled water at 37°C

Figure 5.5 Scanning electron micrographs of 44% w/w gelatin-loaded PCL tube before gelatin release (A, B) after gelatin release (C, D)

Figure 5.6 Explanation of the reduction in outer diameter determination of gelatin-loaded PCL tubes under flow conditions

Figure 5.7 The changes in outer diameter of a microporous PCL tube under increasing continuous flow rates at 37°C

Figure 5.8 The changes in outer diameter of (A) 29% (B) 38% and (C) 44%

gelatin-loaded PCL tubes under continuous increasing flow conditions at 37°C

Figure 5.9 The changes in outer diameter of macroporous PCL tubes produced by gelatin extraction under continuous increasing flow conditions at 37°C. (A) 13% macroporosity (B) 19% macroporosity(C) 23% macroporosity

Figure 5.10 The changes in outer diameter of microporous PCL tube under pulsatile flow conditions at 37 °C

Figure 5.11 The changes of outer tube diameter and internal pressure during burst testing of PCL tubes

Figure 5.12 Scanning electron micrographs of fracture surface of PCL tubes following burst testing (A, B) microporous PCL (C) 13% macroporous PCL (D) 19% macroporous PCL (E) 23% macroporous PCL

Figure 6.1 Native structure of chicken egg white lysozyme

Figure 6.2 The weight distribution of lysozyme in microporous PCL matrices

Figure 6.3 Cumulative lysozyme release from microporous PCL matrices in PBS at 37°C

Figure 6.4 Activity of lysozyme solution in PBS following storage at - 20°C

Figure 6.5 Activity of lysozyme solution in PBS following storage at 37°C

Figure 6.6 Activity of lysozyme released from PCL matrices into PBS at 37°C (A) during 8 hours (B) during 11 days

Figure 6.7 Scanning electron micrographs (A) 20% w/w lysozyme: PCL matrix before release (B) lysozyme: PCL matrix after release (C) lysozyme particles

Figure 6.8 The weight distribution of collagenase in microporous PCL matrices

Figure 6.9 Cumulative collagenase release from miroporous PCL matrices.

Figure 6.10 Activity of collagenase solution in PBS stored at -20°C

Figure 6.11 Activity of collagenase solution in PBS stored at 37°C

Figure 6.12 Activity of collagenase released from PCL matrices in PBS at 37°C (A) during 8 hours (B) during 11days

Figure 6.13 Scanning electron micrographs of (A) external surface of 20% w/w collagenase-loaded PCL matrices (B) cross section of 20% w/w collagenase-loaded PCL matrices (C) collagenase particles

Figure 6.14 Native structure of catalase

Figure 6.15 The weight distribution of catalase in microporous PCL matrices produced using methanol as a non-solvent and 10, 20% and 50% w/w particle suspensions.

Figure 6.16 The weight distribution of catalase in microporous PCL matrices produced using ethanol as a non-solvent and 10, 20% and 40% w/w particle suspensions

Figure 6.17 Activity of catalase solution in PBS following storage at 37 °C (A) during 8 hours (B) during 7 days

Figure 6.18 Cumulative catalase release from microporous PCL matrices produced using methanol as a non-solvent

Figure 6.19 Cumulative catalase release from microporous PCL matrices produced using ethanol as the non-solvent (PBS 37°C)

Figure 6.20 Activity of catalase released from PCL matrices (A) during 8 hours (B)

during 10 days in PBS at 37°C

Figure 6.21 Scanning electron micrographs of 20% w/w catalase-loaded: PCL matrix produced using methanol as the non-solvent (A) surface region (B) section through matrix and using ethanol as the non-solvent (C) surface region (D) section through matrix (E) catalase powder

Figure 6.22 The weight distribution of dexamethasone in PCL matrices produced using 5% and 10%w/w concentration drug solution

Figure 6.23 Release of dexamethasone (μg) from microporous PCL matrices containing 3.9% and 7.9% w/w initial drug loading

Figure 6.24 Cumulative release of dexamethasone (%) from PCL matrices containing 3.9% and 7.9% w/w initial drug loading

Figure 6.25 Scanning electron micrographs of 7.9% w/w dexamethasone-loaded PCL matrix produced using the co-solution technique (A) Surface region (B) section through matrix

List of Abbreviations

BCA: Bicinchoninic acid

CAD: Computer-aided design

DCM: Dichloromethane

DDS: Drug delivery system

DMEM: Dulbecco's modified eagle's medium

DSC: Differential scanning calorimetry

ECM: Extracellular matrix

FGF: Fibroblast growth factor

FN: Fibronectin

GDT: Gray-weighted distance transform

hPTH: Human parathyroid hormone

ICM: inflection count metric

KGF: Keratinocyte growth factor

LN: Laminin

MicroCT: Micro-computed tomography

MPC: Methacryloyloxyethyl phosphorylcholine

NGF: Epidermal growth factor

NMR: Nuclear magnetic resonance

PBS: Phosphate buffered saline

PCL: Polycaprolactone

PDGF: Platelet-derived growth factor

PEG: Polyethylene glycol

PEO: Polyethylene oxide

PET: Polyethylene terephthalate

PEU: Polyurethane

PGA: Polyglcolic acid

PHEMA: Polyhyroxyethyl methacrylate

pHEMA: Poly(2-hydroxyethyl methacrylate)

PHPMA: Polyhydroxypropyl methacrylamide

PLA: Polylactic acid

PLGA: Polylactic-glycolic acid copolymer

PLLA: Poly-L-Lactic acid

PMMA: Poly(methyl methacrylate)

PP: Polypropylene

PTFE: Poly(tetrafluorethylene)

PU: Ployurethanes

PVA: Poly(vinyl alcohol)

PVP: Polyvinylpyrrolidone

RGD: Arg-Gly-Asp

SEM: Scanning electron microscopy

SLS: Selective laser sintering

TCP: Tissue culture plastic

TCPS: Tissue culture polystyrene

TIPS: Thermal induced phase separation

VEGF: vascular endothelial growth factor

VN: Vitronectin

Table of Content

ACKNOWLEDGEMENTS ..... **I**

ABSTRACT ..... **III**

LIST OF TABLES ..... **IV**

LIST OF FIGURES ..... **VI**

LIST OF ABBREVIATIONS ..... **XVII**

TABLE OF CONTENT ..... **XX**

CHAPTER 1 ..... **1**

INTRODUCTION **1**

1.1 EXTRACELLULAR MATRIX AND THE DESIGN OF ARTIFICIAL SCAFFOLDS 3

1.2 THE IMPORTANCE OF SCAFFOLD POROSITY AND ITS CHARACTERISATION 5

1.3 SCAFFOLD PRODUCTION 10

1.4 GROWTH FACTORS, ENZYMES AND CONTROLLED DRUG DELIVERY 12

1.4.1 Controlled drug delivery *15*

1.5 CONTROLLED DRUG DELIVERY IN TISSUE ENGINEERING 20

1.6 CELL INTERACTION WITH POLYMERIC SCAFFOLDS 21

1.7 APPLICATION OF POLYMERS IN SCAFFOLD MANUFACTURE 25

1.7.1 Natural polymers *25*

1.7.2 Synthetic polymers *27*

1.7.3 Polycaprolactone *34*

1.8 PROJECT AIMS AND OUTLINE 40

CHAPTER 2 ..... **42**

MATERIALS AND METHODS **42**

2.1 MATERIALS 42

2.2 PREPARATION OF MICROPOROUS PCL MATRICES 42

2.3 INVESTIGATION OF PCL MATRIX SHRINKAGE DURING PREPARATION MATRIX DENSITY 43

2.4 THE EFFECT OF COOLING TIME ON PCL MATRIX FORMULATION AND CHARACTERISTICS 44

2.5 THE EFFECT OF PCL SOLUTION CONCENTRATION ON PCL MATRIX FORMULATION AND PARTICLE LOADING 44

2.6 PREPARATION OF LACTOSE-LOADED PCL MATRICES BY RAPID COOLING IN DRY ICE 45

2.6.1 Determination of the lactose content of PCL matrices *45*

2.6.2 In vitro release of lactose from microporous PCL matrices *46*

2.7 PREPARATION OF GELATIN-LOADED PCL MATRICES 46

2.7.1 Determination of the gelatin content of PCL matrices *47*

2.7.2 In vitro release of gelatin from microporous PCL matrices *47*

2.8 DENSITY MEASUREMENT OF PCL MATRICES 48

2.9 MEASUREMENT OF THE POROSITY OF PCL TUBULAR MATRICES 48

2.10 THERMAL ANALYSIS OF MICROPOROUS PCL MATRICES, LACTOSE-LOADED AND GELATIN-LOADED MATRICES 49
2.11 CHARACTERIZATION OF THE MORPHOLOGY OF PCL MATRICES USING SCANNING ELECTRON MICROSCOPY (SEM) 50
2.12 INVESTIGATION OF THE MORPHOLOGY OF LACTOSE AND GELATIN PARTICLES BEFORE AND AFTER MATRIX PRODUCTION 50
2.13 FIBROBLAST INTERACTION WITH PCL MATRICES IN CELL CULTURE 50
2.13.1 Preparation of Swiss 3T3 fibroblast cell culture 50
2.13.2 Growth of 3T3 fibroblasts on PCL matrices having various pore size ranges produced by lactose or gelatin extraction 51
2.13.3 SEM analysis of fibroblast attachment on microporous PCL matrices 52
2.14 QUALITATIVE AND QUANTITATIVE ASSESSMENT OF THE INTERNAL PORE STRUCTURE OF PCL MATRICES USING COMPUTED MICRO-TOMOGRAPHY (MICRO-CT) 53
2.14.1 Image processing 55
2.15 THE DEFORMATION BEHAVIOUR OF MICROPOROUS PCL TUBES UNDER HYDROSTATIC AND HYDRODYNAMIC LOADING CONDITIONS 56
2.15.1 Measurement of the changes in diameter of PCL tubes under a constant fluid flow rate of 300ml/min at 37°C 58
2.15.2 Measurement of the changes in outer diameter of PCL tubes under continuous and pulsatile flow conditions at 37°C 60
2.15.3 Investigation of the burst strength of PCL tubes at room temperature and 37°C 61
2.15.4 SEM examination of the fracture surface of PCL tubes 62
2.16 PREPARATION AND CHARACTERISATION OF ENZYME-LOADED AND DEXAMETHASONE-LOADED PCL MATRICES 63
2.16.1 Materials 63
2.16.2 Preparation of lysozyme-loaded PCL matrices 63
2.16.3 Measurement of the lysozyme content of PCL matrices 64
2.16.4 In vitro release of lysozyme from PCL matrices 64
2.16.5 Analysis of lysozyme activity 65
2.16.6 Investigation of lysozyme activity in control solutions and in the solvents used for PCL matrix formulation 66
2.16.7 Investigation of lysozyme activity following release from PCL matrices 66
2.17 PREPARATION OF COLLAGENASE-LOADED PCL MATRICES 66
2.17.1 Measurement of collagenase content in PCL matrices 67
2.17.2 In vitro release of collagenase from PCL matrices 67
2.17.3 Determination of collagenase activity in PBS 68
2.17.4 Investigation of collagenase activity in control solutions and in the solvents used for PCL matrix formulation 69
2.17.5 Investigation of collagenase activity following release from PCL matrices 70
2.18 PREPARATION OF CATALASE-LOADED PCL MATRICES 70
2.18.1 Measurement of catalase content in PCL matrices 70
2.18.2 In vitro release of catalase from PCL matrices 71
2.18.3 Analysis of catalase activity in PBS (control solution) 71
2.18.4 Investigation of catalase activity under matrix formulation conditions and following

release from PCL matrices ... 72
2.19 PREPARATION OF DEXAMETHASONE-LOADED PCL MATRICES ... 73
2.19.1 Determination of dexamethasone content in PCL matrices ... 74
2.19.2 In vitro release of dexamethasone from PCL matrices ... 74
2.19.3 Thermal analysis of enzyme-loaded and dexamethasone-loaded PCL matrices ... 75
2.19.4 SEM investigation of surface morphology of enzyme-loaded and dexamethasone-loaded PCL matrices ... 75

CHAPTER 3 ... 76

FORMULATION AND CHARACTERISATION OF POLYCAPROLACTONE-BASED MATRICES FOR PROTEIN DELIVERY AND SOFT TISSUE ENGINEERING ... 76

3.1FORMULATION OF PCL MATRICES BY LOW TEMPERATURE CASTING ... 76
3.2 EFFECT OF PCL SOLUTION CONCENTRATION ON PARTICLE LOADING ... 79
3.3 MORPHOLOGY OF UNLOADED PCL MATRICES ... 80
3.4 PREPARATION AND CHARACTERIZATION OF LACTOSE-LOADED PCL MATRICES ... 82
3.4.1 Lactose release from PCL matrices having various particle size ranges ... 83
3.4.2 Morphology of lactose-loaded PCL matrices ... 85
3.4.3 Morphology of lactose particles before and after matrix formulation ... 86
3.4.4 Thermal properties and porosity analysis of PCL and lactose-loaded PCL matrices ... 88
3.5 PREPARATION AND CHARACTERISATION OF GELATIN-LOADED PCL MATRICES ... 89
3.5.1 Gelatin release from PCL matrices having various particle size ranges and loading percentages ... 91
3.5.2 Morphology of gelatin-loaded PCL matrices ... 94
3.5.3 Morphology of gelatin particles before and after matrix formulation ... 97
3.5.4 Thermal properties and porosity analysis of PCL matricesand gelatin-loaded PCL matrices ... 98
3.6 GROWTH OF 3T3 FIBROBLASTS ON PCL MATRICES ... 98
3.6.1 SEM analysis of 3T3 fibroblasts on PCL matrices ... 102
3.10 DISCUSSION AND CONCLUSIONS ... 103

CHAPTER 4 ... 109

QUANTIFICATION OF THE INTERNAL PORE STRUCTURE OF PCL MATRICES USING MICRO-CT ... 109

4.1 QUALITATIVE ASSESSMENT OF THE INTERNAL PORE STRUCTURE OF PCL MATRICES ... 110
4.2 QUANTITATIVE ASSESSMENT OF THE INTERNAL PORE STRUCTURE OF PCL MATRICES ... 116
4.2.1 Image processing ... 116
4.2.2 Determination of pore size and frequency distribution of equivalent pore diameter ... 122
4.2.3 Matrix homogeneity and reproducibility of image analysis ... 130
4.3 MICRO-CT EVALUATION OF MACROPOROSITY OF PCL MATRICES PRODUCED BY GELATIN PARTICLE EXTRACTION ... 131
4.4 DISCUSSION AND CONCLUSIONS ... 137

CHAPTER 5 ... 141

CHARACTERISATION OF MICROPOROUS PCL TUBES FOR VASCULAR TISSUE

ENGINEERING UNDER FLUID FLOW CONDITIONS **141**

5.1 MEASUREMENT OF THE CHANGES IN DIAMETER OF PCL TUBES UNDER A CONSTANT FLOW RATE OF 300 ML/MIN AT 37°C 143

5.1.1 Gelatin release from microporous PCL tubes in distilled water at 37°C *148*

5.1.2 Morphology of the external surface of microporous PCL tubes before and after gelatin release *149*

5.2 MEASUREMENT OF THE CHANGES IN OUTER DIAMETER OF MICROPOROUS PCL TUBES UNDER CONTINUOUS FLOW CONDITIONS AT 37°C 151

5.2.1 Measurement of the changes in diameter of gelatin-loaded PCL tubes under continuous flow conditions at 37 °C *153*

5.2.2 Measurement of the changes in outer diameter of macroporous PCL tubes (formed by gelatin extraction) under continuous flow conditions at 37°C *155*

5.3 MEASUREMENT OF THE CHANGES IN DIAMETER OF MICROPOROUS PCL TUBES UNDER PULSATILE FLOW CONDITIONS AT 37°C 157

5.4 BURST TESTING OF MICROPOROUS, GELATIN-LOADED AND MACROPOROUS PCL TUBES 160

5.4.1 Morphology of fracture surface of PCL tubes following burst testing *162*

5.5 DISCUSSION AND CONCLUSIONS 164

CHAPTER 6 ..... **168**

CONTROLLED DELIVERY OF ENZYMES AND A STEROID, DEXAMETHASONE, FROM MICROPOROUS PCL MATRICES **168**

6.1 PREPARATION AND ANALYSIS OF LYSOZYME-LOADED PCL MATRICES 169

6.1.1 Lysozyme as a model protein in tissue engineering *169*

6.1.2 Formulation of lysozyme-loaded PCL matrices *170*

6.1.3 Thermal properties of lysozyme-loaded PCL matrices *171*

6.1.4 Lysozyme release from microporous PCL matrices *172*

6.1.5 Biological activity of lysozyme *173*

6.1.6 Investigation of lysozyme activity following release from PCL matrices *176*

6.1.7 Morphology of lysozyme-loaded PCL matrices *179*

6.2 PREPARATION AND ANALYSIS OF COLLAGENASE-LOADED PCL MATRICES 180

6.2.1 Formulation of collagenase-loaded PCL matrices *180*

6.2.2 Thermal properties of collagenase-loaded PCL matrices *181*

6.2.3 Collagenase release from microprous PCL matrices in vitro *182*

6.2.4 Investigation of collagenase activity in solution and after exposure to the solvents used for matrix formulation. *184*

6.2.5 Bioactivity of collagenase released from PCL matrices *187*

6.2.6 Surface morphology of collagenase-loaded PCL matrices *189*

6.3 FORMULATION AND ANALYSIS OF CATALASE-LOADED PCL MATRICES 190

6.3.1 Formulation of catalase-loaded PCL matrices *191*

6.3.2 Thermal properties of catalase-loaded PCL matrices produced using methanol or ethanol as the non-solvent *194*

6.3.3 Bioactivity of catalase *194*

6.3.4 Catalase release from microporous PCL matrices produced using methanol or ethanol as a non-solvent *198*

6.3.6 Biological activity of catalase released from microporous PCL matrices *200*
6.3.7 Morphology of catalase-loaded PCL matrices *202*
6.4. FORMULATION AND CHARACTERIZATION OF DEXAMETHASONE-LOADED PCL MATRICES 204
6.4.1 Thermal properties of dexamethasone-loaded PCL matrices *205*
6.4.2 Dexamethasone release from microporous PCL matrices in vitro *206*
6.4.3 Morphology of dexamethasone-loaded PCL matrices *208*
6.5 DISCUSSION AND CONCLUSIONS 209

CHAPTER 7 ..... **213**

OVERALL CONCLUSIONS AND FUTURE WORK **213**

REFERENCES **218**

CURRICULUM VITAE **237**

Chapter 1

Introduction

Although tissue transplantation has been performed since ancient times, tissue engineering as a new concept has existed only for the last twenty to thirty years. There is no precise definition of tissue engineering, but it involves several elements including the introduction of biological entities in vivo (e.g. cells, growth factors) that facilitate tissue regeneration and the use of synthetic components (implants) to replace or repair damaged tissue [1]. Tissue engineering spans two research fields: regenerative medicine and organ substitution and continues to be a focus for worldwide research because of the shortage of donor tissue or organs. Tissue transplantation is one of the few effective options available for patients with certain chronic conditions. In the past century, many of the obstacles in the way of successful organ transplantation have been cleared through use of immunosuppressive drugs and advanced surgical techniques. However, prolonged drug use often causes side-effects such as the high possibility of infection, carcinogenesis and viral infection [1]. Reconstructive surgery provides an alternative to organ transplants but biomedical devices such as joint prostheses cannot provide a complete substitute for biological function and cannot prevent progressive deterioration of the injured tissue or organ. In addition, surgical reconstruction can cause long-term problems, such as the development of colon cancer after incontinence treatment due to urine entry [2]. Tissue engineering is expected to overcome the limitations referred to above by

developing new approaches for encouraging tissue growth and repair. One approach attempts to form new tissue by seeding cells on a mimic or artificial extracellular matrix (scaffold) ex-vivo. The cell-scaffold construct is implanted in the body where tissue development continues. In a second approach, cell-free scaffolds are implanted and serve as a substrate for growth of host cells. Several tissue engineering designs including skin substitutes and chondrocyte implantation for repair of articular cartilage defects are being tested in patients [3]. These studies have revealed that novel tissue replacement strategies can work in certain cases, but success does not come easily and hybrid approaches involving cultured cells, support scaffolds or matrices and advanced materials are required.

Three key components govern the formation of new tissue: (i) cells (ii) the extracellular matrix (ECM) which is required for cell attachment, proliferation and differentiation (iii) growth factors for promoting tissue regeneration. Detailed studies have shown that stem cells play a key role in tissue regeneration [4]. However, stem cells are not extensively used in tissue regeneration at present because they are not clearly identified and cell culture of the large cell population required for tissue manufacture has proved problematical.

1.1 Extracellular matrix and the design of artificial scaffolds

The natural extracellular matrix (ECM) is a complex, cross-linked network of proteins and glycosaminoglycans which is not only a physical support for cell attachment and growth but also provides a three-dimensional environment to organize cells in space. In addition the ECM provides cells with environmental signals to direct site-specific cellular regulation, which contribute to tissue regeneration and organogenesis [5]. In tissue engineering, it is difficult to repair a large tissue defect by only supplying cells to the defect-site because the natural ECM is absent. Therefore, a scaffold or artificial ECM is necessary, at least initially, to assist cell attachment and subsequent proliferation and differentiation.

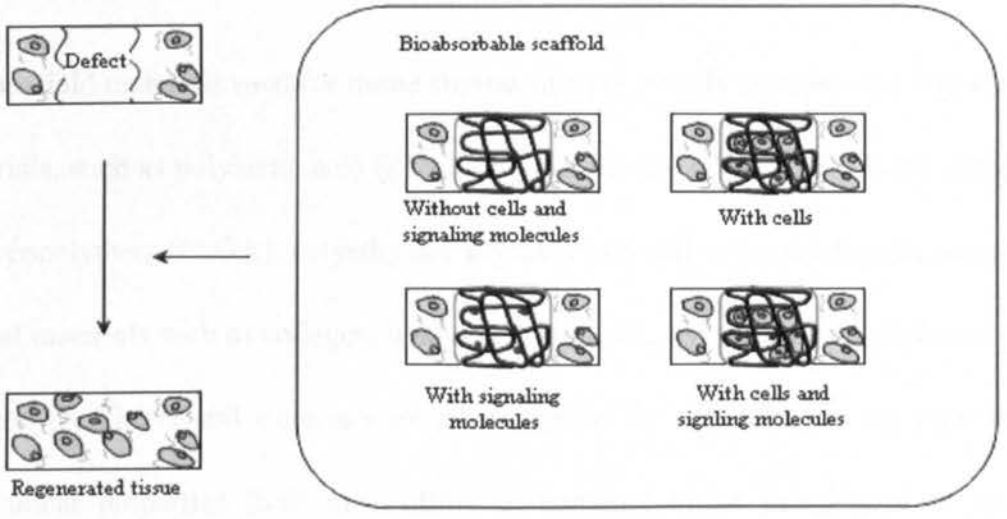

Figure 1.1 Biodegradable 3D scaffold used to promote cell attachment, proliferation and differentiation. The scaffold with or without cells and/or biological signaling molecules (e.g. growth factor, cytokines, chemokines and genes) is applied to a defect to induce in vivo regeneration of tissue and organs

A key technology in tissue engineering, therefore, is the preparation of an artificial scaffold for cell attachment, proliferation and differentiation (Figure 1.1). A wide range of biomaterials have been used to provide 3-D scaffolds or carriers for cell seeding and for encapsulating cells to protect them against immuno-rejection. Ideally, the material will degrade in vivo to be replaced by natural ECM molecules [6, 7]. Thus, the degradation rate of the scaffold represents an additional and important parameter in determining the properties of the scaffold and can be tuned (in theory) to the needs of specific cells and tissue development. For example, fibroblasts that proliferate rapidly may require scaffolds with high degradation rates, whereas tissue structures such as bone that require longer periods of stability for strength development may benefit from longer-lasting support scaffolds.

The scaffold materials used for tissue engineering are usually synthetic biodegradable materials, such as polylactic acid (PLA), polyglcolic acid (PGA), poly(lactic-glycolic acid) copolymers (PLGA), polyethylene glycol (PEG) and polypropylene fumarate or natural materials such as collagen, hyaluronic acid, silk, hydroxyapatite, chitosan, and alginate [6, 7]. Natural materials are advantageous for cell adhesion but their poor mechanical properties limit their utility in complex organ substitution or tissue regeneration. The properties of synthetic materials [8] such as mechanical properties, degradation rate, morphology and porosity are more easily controlled. Composites of natural and synthetic materials have also been used extensively in tissue engineering to combine the advantages of both types of material. [9].

1.2 The importance of scaffold porosity and its characterisation

On a macroscopic level, the overall shape of the scaffold provides boundaries for tissue regrowth. On a microscope level, the material provides a framework for local cell growth and tissue organization, permitting cell attachment, distribution and proliferation within a controllable microenvironment [10]. Scaffold porosity in particular controls the key processes of nutrient supply to cells, metabolite dispersal, local pH stability and cell signaling. The pore size can affect the proximity of cells during seeding and the amount of space the cells have for 3-D organization in the later stages of tissue growth. To date cell seeding on 2-D scaffold surfaces has been shown to be easy to perform but the preparation of 3-D cell-scaffold constructs for regeneration of organs is far more complex. For example, pores of adequate size allow cells to migrate or adhere to the surface of a material, but interconnecting pores are necessary to permit cell growth into the scaffold interior.

Specific cells require different pore sizes for optimal attachment and growth (Table 1.1) [11]. As a result, much research in tissue engineering is aimed at obtaining polymeric and bioceramic scaffolds with a very high porosity and simultaneous good control over pore size and morphology [12]. The presence of pores smaller than 160μm in PLA and PLGA scaffolds, produced by salt leaching, has been reported to be optimal for attachment of human skin fibroblasts [13]. Bony ingrowth was found to predominate in porous PMMA implanted in bone when the pore size was around

450μm [14]. Connective tissue formed when the pore size was below 100μm and extensive vascular infiltration was only observed with pores around 10000μm. In the case of polyurethane meniscal implants, structures comprising macropores (150-300 μm), highly interconnected by micropores (<50 μm) have been found to be conducive to ingrowth of fibrocartilaginous tissue [15]. The cell infiltration depth (120μm in 28 days) found in elastin scaffolds, for example, probably results from the material's high porosity and inter-connectivity [16]. It has been shown in previous studies that cell-scaffold binding can block pores of inadequate size and geometry [17, 18]. High inter-connectivity of pores is also essential to supply nutrients and allows oxygen exchange in the inner regions of a scaffold to maintain cell viability, especially for complex tissue engineering of organs.

Table 1.1 Optimal pore size for cell infiltration and host tissue ingrowth

Cell/tissue type	Optimal pore size (μm)	Scaffold material	Reference
Human skin fibroblasts	<160μm	PLA/PLG	[13]
Bone	450μm	PMMA	[14]
Bone	>100-150μm	Bioceramic	[19]
Fibrocartilaginous tissue	150-300μm	Polyurethane	[15]
Adult mammalian skin cells	20-125μm	Collagen-glycocaminoglycan (CG)	[20]
Osteogenic cells	100-150μm	Collagen-GAG	[21]
Smooth muscle cells	60-150μm	PLA	[22]
Endothelial cells	<80μm	Silicon nitride	[23]

A variety of techniques have been used to evaluate scaffold porosity including theoretical assessment, scanning electron microscopy (SEM), mercury porosimetry, gas pycnometry and adsorption. Theoretical methods based on two main approaches (cube analysis and mass technique) have been applied to characterize the porosity of regular honeycombed scaffolds, fabricated via rapid prototyping [24, 25]. Other theoretical calculations such as Archimedes method have been used in analysis of micro-tubular polymer scaffolds [26] and liquid displacement techniques have been developed to measure the porosity of hydroxyapaptite implants and scaffolds [27-29]. SEM analysis complements the theoretical calculations of porosity [24, 30, 31] and allows direct measurements of pore size and wall thickness. However, SEM cannot examine the scaffold interior without sample sectioning which introduces uncertainty due to unwanted material compression and edge effects. Mercury porosimetry is a well known and established method, but it neither measures small mesopores (2-50nm pores) due to lack of mercury penetration nor measures very large pores as the mercury penetrates the structure before measurements can be made. Furthermore, mercury porosimetry does not account for closed pores as mercury does not intrude into them and it only measures the distribution of constrictions in a pore network. The gas adsorption method is relevant to the study of porosity in nano-featured and nano-modified scaffolds [32], and is based on the electrical forces of attraction that bind atoms in solids. To counter the net inward attractive forces, surface atoms bind surrounding gas molecules via Van der Waals and electrical forces. Researchers have used gas adsorption to assess scaffolds with pore sizes ranging from 0.35-400 nm or

3.5 to 2000μm but the analysis does not evaluate closed pore content and it is time-consuming. Flow porosimetry is a non-destructive approach that has been used to measure the pore sizes of materials such as filtration media and paper products, but no publications in the biomaterials and tissue engineering fields have been reported.

Feldkamp et al [33] pioneered micro-computed tomographic (micro-CT) imaging technology to analyze trabecular bone samples at a spatial resolution of 50μm. Since then, micro-CT has been used extensively in the study of bone architecture and other tissue types. Micro-CT images the specimen through exposure to small quantities of ionizing radiation and corresponding measurements of absorption. The resulting grey-scale images form a series of 2-D sequential slices which build up into a density map of the sample. With relevant computerized reconstruction, micro-CT provides precise quantitative and qualitative information on the 3D morphology of specimens [34-38] and the interior can be studied in great detail without resorting to physical sectioning or the use of toxic chemicals. Williams et al [34] recently used Micro-CT to visualize PCL scaffolds produced by selective laser sintering (SLS) and to assess the porosity and subsequent bone formation following cell seeding and implantation in mice. Micro-CT has also been used to quantify scaffold micro-architectural parameters related to compressive mechanical properties [39]. Thurner et al [37] explored X-ray Micro-CT for morphological characterisation of cell cultures on filamentous 3-D scaffolds and Synchrotron Micro-CT has highlighted the subtlety of cell-scaffold interactions - fibroblasts tend to span between multi-filament yarns

whereas osteoblast-like cells are confined to the filament surface [38]. Ongoing development of micro-CT techniques is improving qualitative and quantitative analysis of tissue engineering scaffolds. Jones et al [19] applied three algorithms to identify pores, interconnects and pore size distribution in bioceramic scaffolds to predict the permeability of the pore network and thus optimize bioreactor conditions for cell seeding.

Beyond the fundamental requirements of adequate pore size and inter-connectivity, pore tortuosity also plays a key role in matrix and scaffold function. Tortuosity is defined as the ratio of the actual path length through connected pores to the Euclidean distance (shortest linear distance). Tortuosity is a key factor in tissue scaffold performance but rarely quoted in the literature. A common method to calculate tortuosity is via the results from dissolution measurements. In this method, the tortuosity is calculated from several parameters related to the dissolution of a drug from a matrix [40, 41]. However this approach can result in unrealistic values of more than one thousand [42] or below one [40]. Tortuosity can also be measured from the porosity and diffusion coefficients obtained from spin echo NMR measurements [43]. Mercury intrusion porosimetry has also been suggested for determining tortuosity. Another example of tortuosity calculating is to use the inflection count metric (ICM). This approach adds the number inflections of a 3-D frame representation of a pore connecting two points and multiplies this number by the path length [44]. Wu et al [43] recently described a method to find the shortest route through the pores in images of

compacts using an algorithm called 'grey-weighted distance transform (GDT)' which provide precise measurements of tortuosity.

1.3 Scaffold production

Numerous techniques have been employed to prepare polymer matrices with controlled pore size, shape and connectivity to optimize cell-scaffold interaction, including solvent-casting/particle leaching [13] gel casting [45] solid free form fabrication such as selective laser sintering (SLS) [34] and super critical fluid processing [46] (Table 1.2 adapted from Whitaker, M.J. et al [47]). Thermally induced phase separation (TIPS) including liquid-liquid phase separation [48] and solid-liquid-phase separation [26] have been extensively investigated. In these methods, solvent removal by extraction or sublimation has frequently been used to prepare polymeric structures with controlled porosity [8]. The morphologies and properties of the resultant scaffolds largely depend on the phase separation mechanism [49]. Liquid-liquid phase separation involves cooling a polymer solution to produce a polymer-rich phase and a polymer-lean phase, followed by solvent removal. This approach gives rise to isotropic pores of 1-30 μm in diameter, depending on the process parameters and the thermodynamics of the polymer/solvent system. Solid-liquid phase separation of polymer solutions involves solvent solidification (e.g. dioxane) at low temperatures in the region of -18°C followed by freeze drying to remove the solvent. This leads to ladder or sheet-like anisotropic morphologies, which strongly depend on the quenching rate [49]. In general, solvent freezing at a relatively

high temperature induces a low nucleation rate and a low crystal growth rate, which leads to a small number of large size solvent crystals. As a result, the average pore size obtained in the final scaffold increases with increasing freezing temperature [29]. Other techniques investigated for producing porous scaffolds include particulate leaching in combination with gas foaming [50], precipitation casting [51] and compression moulding [52].

Table 1.2 Methods of scaffold/matrix manufacture

Material	Scaffold fabrication method	Reference
Poly(α-hydroxy acid)	Fibre mesh	[53-56]
(e.g. PLA, PGA, PLGA,	Particulate leaching	[46, 57-59]
PLA-ε-caprolacotone)	Extrusion and particulate leaching	[60]
	Microsphere leaching	[52]
	Emulsion freeze-drying	[31]
	Particulate leaching and gas foaming	[46, 61, 62]
	Supercritical carbon dioxide	[63, 64]
	3D printing	[65, 66]
PEG hydrogels	Photopolymerization	[67-70]
Lactic acid-PEG hydrogels	Photopolymerization	[71, 72]
Poly-L-lactic acid-co-L-aspartic acid hydrogels	Photopolymerization	[73]
Fibrin	Enzymatic polymerization	[74]
Polyproplylene fumarate	Photopolymerization	[75, 76]
PVA	Sponges	[77-79]
Polyethylene terepthalate	Fiber mesh	[80, 81]
Natural substances (e.g. collagen, gelatin)	Sponges, gels	[82, 83]

More recently, rapid prototyping techniques involving polymer melts and powders, such as precise extrusion [84] three-dimensional printing techniques [85, 86] and fused deposition modeling [87] have received considerable interest. Selective laser sintering (SLS) has been used to fabricate PCL scaffolds with porosity ranging from 37-55%, compressive modulo ranging from 52 to 68MPa, and strength ranging from 2.0 to 3.2 MPa [39]. Complex structures can be readily produced from computer-aided design (CAD) models. However, these techniques are time consuming and require sophisticated equipment [12].

The material type, pore size and structure and degradation characteristics determine the scaffold mechanical properties [88]. Providing adequate mechanical support is a critical scaffold requirement for attached cells since it influences cell growth, differentiation, and organization during tissue formation [89]. It is considered that if the scaffold is unable to provide a stiffness (Young modulus) in the range of (10-1,500MPa) [90] for hard tissue or (0.4-350MPa) for soft tissues then any nascent tissue formation will probably fail due to excessive structural deformation [88].

1.4 Growth factors, enzymes and controlled drug delivery

After seeding on a porous scaffold, cells often form multilayers on the scaffold surface due to insufficient cell penetration into the interior. Moreover, it has been observed that few cells are retained within highly porous structures with large open pores [34]. Therefore, the scaffold alone may not induce uniform 3-D cell distribution

and tissue regeneration. As a result, biomimetic peptides, growth factors, cytokines, chemokines, genes and/or surface adhesion factors have been incorporated within scaffolds to promote or prevent cell differentiation, motility and adhesion [91]. Examples of growth factors previously applied in tissue engineering systems are listed in Table 1.3. Growth factors may be secreted by several different cells and the same growth factor can also affect more than one cell type. Taking skin regeneration as an example, growth factors and cytokines, such as fibroblast growth factor (FGF), keratinocyte growth factor (KGF, interleukin-1α and vascular endothelial growth factor (VEGF) are released within the wound bed to trigger cell proliferation, macrophage activation and angiogenesis [47]. Thus, growth factor delivery needs to be precisely controlled in either space or time. Platelet-derived growth factor (PDGF), FGF, nerve growth factor, epidermal growth factor, VEGF have all been incorporated in a variety of scaffolds in attempts to enhance the performance of tissue engineering constructs [55, 92-94]. However, in general, growth factors and other biological signaling molecules are unstable in vivo, making it necessary to administer them by drug delivery systems (DDS) to improve stability, control release, prolong half-life and achieve cell targeting.

Table 1.3 Growth factors used in tissue engineering applications (adapted from Whittaker, M.J. et al [47])

Growth factor	Action	Use	Delivery method	Ref.
Platelet-derived growth factor (PDGF)	Endothelial cell proliferation	Angiogenesis Wound healing	Implanted EVA rods Alginate hydrogels PLLA, PLGA, PLA microspheres	[55, 94-96]
Fibroblasts growth factor (FGF)	Cell proliferation	Bone and cartilage regeneration Nerve growth Endothelial cell proliferation Angiogenesis	Hydrogels PLGA Cross-linked fibrin and collagen Heparinized fibrin	[93, 97-99]
Nerve growth factor (NGF)	Axonal growth and cholinergic cell survival	Neurite extension in central and peripheral nervous systems	PLGA/poly(caprolactone) encapsulation	[74, 92, 100-102]
Epidermal growth factor (EGF)	Cell proliferation	Migration and differentiation of neural stem cells	Surface immobilization on polymers PLGA microshperes Photoimmobilazation	[103, 104]
Vascular endothelial growth factor (VEGF)	Endothelial cell proliferation	Angiogenesis	Alginate hydrogels PLGA-PEG microspheres Heprinized fibrin	[105-108]
Bone morphogenetic ptrotein-2 (BMP-2)	Cell proliferation	Bone regeneration	Hydrogels PLGA	[109]
Transforming growth factor-β (TGF-β)	Extracellular matrix (ECM) production	Bone and cartilage regeneration Stimulates ECM synthesis	Surface immobilization EVA rods PLA Chitosan	[55, 82, 110, 111]

1.4.1 Controlled drug delivery

Controlled drug delivery applications include both sustained delivery of bioactives in body tissue or blood over days/weeks/months/years and targeted delivery to specific sites such as tumours or tissues such as diseased blood vessels and bone, on a one-time or sustained basis. Drug release from a delivery system can be zero-order, variable or bioresponsive and the release rate can generally be controlled by five mechanisms: 1.Diffusion 2.Dissolution 3.Osmosis 4.Mechanical-control 5.Bio-responsive control

Diffusion controlled drug delivery systems can be divided into reservoir systems and matrix systems. In a reservoir device (e.g. films, capsules, particles, fibers) drugs are surrounded by a rate-controlling polymer membrane which can be non-porous, or micro-porous Table 1.4. For drugs in solution, the reservoir is bound by a polymeric membrane which has a compact, non-porous structure. In a matrix device, the drug is distributed throughout a continuous phase composed of either biodegradable or non-biodegradable synthetic polymers, formed as tablets, films, beads, cylinders or fibers. In both cases, drug release is governed by diffusion of the drug through the polymer membrane or the polymeric matrix and is controlled by the physicochemical characteristics of the drug, polymer chemical structure and morphology.

In reservoir systems, penetration of fluid into the polymeric membrane is followed by drug dissolution (if the drug is in solid form) and drug diffusion. Diffusion through

non-porous polymer membranes depends on the size of the drug molecules and the space available between the polymeric chains. For transport though non-porous membranes, there are three barriers to be circumvented (Figure1.2). The drug molecules in the reservoir compartment initially partition into the membrane then diffuse through it. Finally drug partition occurs into the implantation site or release medium.

Table 1.4 Polymers used for production of reservoir systems

Polymers providing solution-diffusion mechanism	**Polymers providing pore-diffusion mechanism**
Silicone rubber, Silastic	Cellulose esters, Cellulose triacetate
Poly(ethylene-vinyl acetate),	Modified insoluble collagen
Polyethylene, Polyurethane	Polycarbonates, Polyamides,
Polyisopropene, Polyamide,	Polyethylene oxide, Polyvinyl alcohol,
Polyethylene oxide, Polyvinyl alcohol,	Polyvinyl pyrrolidone
Polyvinyl pyrrolidone	

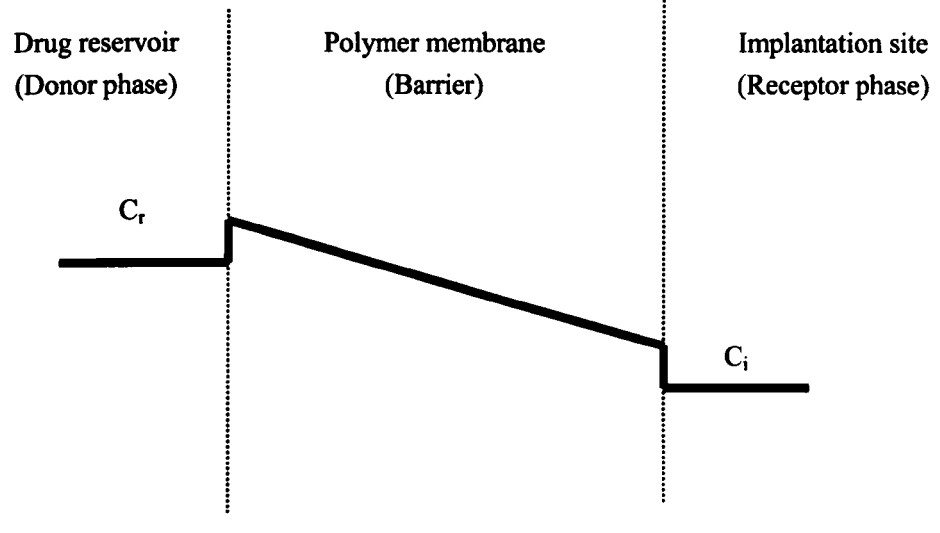

Figure 1.2 The steady-state concentration profile of a drug in a reservoir-type polymeric system. Cr = concentration of drug in the reservoir, Ci = concentration of drug at the site of implantation

The rate of drug diffusion through non-porous membranes follows Fick's law (Equation 1.1) and is thus dependent on the partition and diffusion coefficient of the drug in the membrane, the available surface area of the membrane, the membrane thickness and the drug concentration gradient.

$$dm/dt = (DK/h) \,.\, A.\, \Delta C \qquad \text{(Equation 1.1)}$$

dm/dt = the rate of drug diffusion

D = drug diffusion coefficient in the membrane

K = the partition coefficient of the drug in the membrane

h = membrane thickness

A = available surface area of the membrane

ΔC= concentration change ($C_r - C_i$)

In cases where drug molecules are released through a porous polymer membrane (or matrix) diffusion through micropores has also to be considered. The micropores may be filled with a fluid such as water, oil (e.g. silicone, castor and olive oil), body fluid or release medium. The transport of drug through pores is termed pore-diffusion and the pathway of drug transport is no longer straight, but tortuous Figure 1.3. Thus the porosity of the membrane (ε) and the tortuosity of the pathway (τ) must be considered and equation 1.1 is modified for a porous polymeric membrane as follows:

$$dm / dt = Ds \,.\, A \,.\, Cs \,.\, \varepsilon / \tau h \qquad \text{(Equation 1.2)}$$

where Cs, the drug solubility in a solvent and Ds is the drug diffusion coefficient in the solvent.

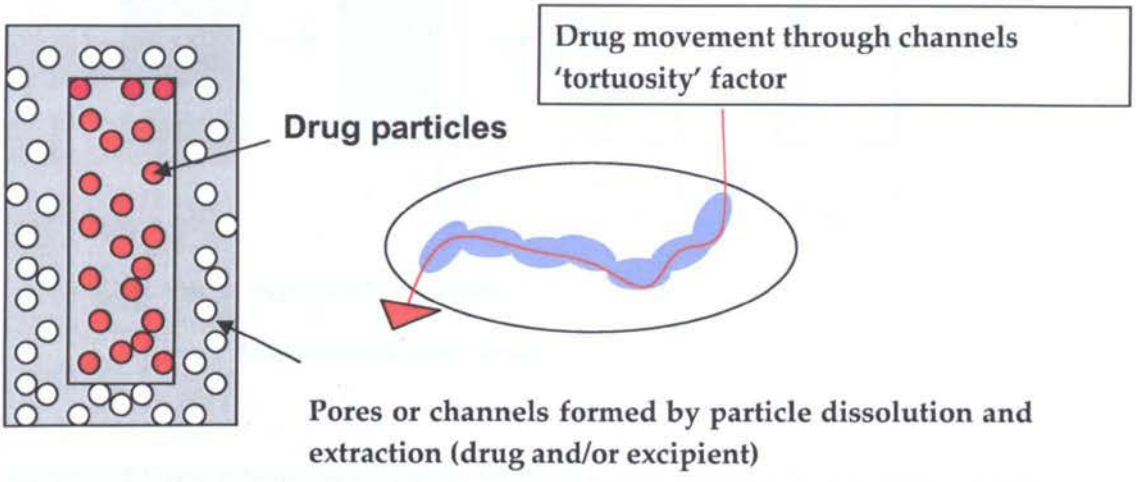

Figure 1.3 Scheme of drug delivery from porous matrices

In matrix-type systems, the drug is distributed throughout a polymeric phase by mixing the drug with polymer powder or solution and shaping the mixture into various geometries by solvent casting, compression/injection moulding, super critical point molding or screw extrusion [13, 46, 52]. Regardless of a drug's physical state in the polymeric matrix, the release rate decreases over time, thus zero-order drug release is not usually obtained. Drug molecules closest to the surface are released initially. As release continues, molecules must travel a longer distance to reach the exterior of the device and thus the time required for release is increased (Figure1.4). The increased diffusion path length results in a decrease in the release rate of drug molecules with time.

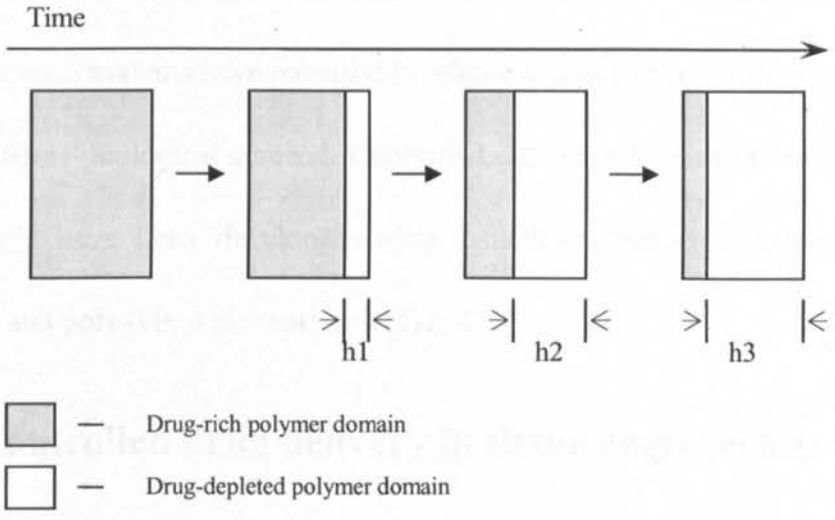

Figure 1.4 Drug release by diffusion through a non-degradable polymeric matrix

In **dissolution-controlled systems**, drug release is controlled by the dissolution rate of the polymer membrane surrounding the drug core (reservoir devices) or the polymer matrix. Dissolution-controlled reservoir devices are often used for oral drug delivery (eg. Spansule, Sequel and SODAS capsules).

Osmosis-controlled drug delivery systems are designed to deliver drugs at a constant rate due to the increased osmotic pressure caused by fluid movement through a semi-permeable membrane. ALZET® and DUROS® implants are examples of osmosis-controlled devices for peptide and protein delivery. **Mechanically-controlled delivery systems** are commonly used for intravenous administration of drugs in the hospital setting. Precise infusion rates enable zero-order controlled drug release to be easily achieved. **Bio-responsive controlled systems** modulate drug release in response to changes in the external environment. Ionic strength and pH changes for

example, are used to affect the swellability of a polymeric device and hence drug release. Such systems have potential to release a drug in a pulsatile manner, according to a patients' biological demand. Controlled delivery of insulin from glucose-sensing hydrogels have been developed using 2-methacryloyloxyethyl phosphorylcholine (MPC) and poly (vinyl alcohol) gels [112, 113].

1.5 Controlled drug delivery in tissue engineering

Controlled drug delivery systems (DDS) have been studied for many decades and used to influence a diverse range of medical conditions from pregnancy prevention (Norplant®) [114] to eradication of brain tumours (Gliadel®) [115]. DDS technology using biodegradable materials has been applied to deliver a wide range of biopharmaceuticals including growth factors [116, 117], hormones [118], antibodies [119], antigens [120-122] and DNA [123, 124]. Biodegradable materials also offer significant advantages in tissue engineering [10] since new tissue could be formed as cells infiltrate the scaffold from the surrounding healthy tissue and the scaffold resorbs. However, presentation of bioactive molecules is generally required in association with the scaffold due to the low concentration of cells and/or host growth factors responsible for new tissue generation. Delivery of genes encoding growth factors has been investigated as an alternative to proteinaceous growth factors in tissue engineering [125]. If a growth factor encoding a gene is transfected into cells existing at the site of regeneration, it is possible that these cells will secrete the potential growth factor needed to promote tissue regeneration. Gene therapy based on

production of angiogenic growth factors, VEGF and basic fibroblast growth factor (bFGF) has been reported for treatment of ischemic disease [126]. However the vectors used for gene transfer do not display adequate biosafety or efficacy to date and progress in this area has been disappointing so far. In an alternative approach, sustained release of plasmid DNA from a collagen sponge has been investigated for bone tissue regeneration [127]. The plasmid encoded a secreted peptide fragment of human parathyroid hormone (hPTH). Pictogram quantities of hPTH were produced for six weeks in animal studies and bone regeneration was achieved at the defect site. Although DDS technology has been shown to enhance the efficiency of growth factors in vivo in certain cases, a major problem of loss of bioactivity can occur during scaffold formulation due to protein denaturation and deactivation on contact with the polymer matrix for example [128]. Exposure to harsh environmental conditions during formulation, such as heating, sonication and organic liquids can also result in a loss of biological activity [129].

1.6 Cell interaction with polymeric scaffolds

In order to produce an optimized scaffold or matrix, it is necessary to understand the influence of the scaffold structure on cell viability, growth and function. Cellular response to a material surface is governed by a number of factors which include surface chemistry, tomography, surface charge, structural heterogeneity, cell culture conditions, mechanical properties of the scaffold and the physiological environment. Since the growth and function of many tissue-derived cells require attachment and

spreading on a solid surface, the events surrounding cell adhesion are fundamentally important. For example, the strength of cell adhesion is an important determinant of the rate of cell spreading, cell migration and differentiated cell function. A number of studies have shown that cell adhesion appears to be maximized on surfaces with intermediate wettability [130, 131]. For most surfaces, adhesion requires the presence of serum [132] and adhesion is enhanced on positively charged surfaces [131]. The surface morphology of an implanted material is known to have a significant effect on cell behavior. Cultured cells react differently to rough or smooth surfaces. In many cases, cells orient and migrate along fibers or ridges in the surface, a phenomenon called contact guidance from early studies on neuronal cell cultures [133]. Fibroblasts have also been observed to orient on grooved surfaces, particularly when the texture dimensions are 1-8μm [134].

Polymeric scaffolds may not interact with cells in a desired manner since their surface chemistry may not promote adequate cell adhesion [135] and may induce toxic and inflammatory reactions [136]. Biomaterials can frequently be made more suitable for cell attachment and growth by surface modification. Early work used long chains of ECM proteins such as fibronectin (FN), vitronectin (VN) and laminin (LN) for surface modification to utilize their inherent cell-binding properties. In addition, the use of short peptide fragments corresponding to cell biding domains, such as RGD (Arg-Gly-Asp) has in certain cases proved to be advantageous over the use of the long chain of native ECM proteins [137, 138]. Synthetic RGD-containing peptides have

been immobilized to poly(tetrafluorethylene) (PTFE), PET, polyacrylamide, polyurethane (PU), PED, poly(vinyl alcohol) (PVA) and PLA to bind receptors on cell surfaces and mediate cell adhesion [139]. On the other hand, some reports have identified specific chemical groups at the polymer surface-such as hydroxyl (-OH) [140, 141] C-O [142] which enhance cell attachment, growth and functionality and are therefore as important factors in modulating the behavior of surface-attached cells.

The migration of cells within a tissue is a critical element in the formation of the complex architecture of organs. Thus, cell migration is also likely to be an important factor in tissue engineering, either on or through the scaffold or assemblies of other cells to form new tissue. Surface modification of biomedical devices with cell binding peptides may not provide effective in vivo. Bulk modification of biomaterials by cell-signaling peptides is necessary if the complex structure of host tissue at defect sites is to be reproduced. Several cell binding peptides, containing RGD sequences have been introduced into three dimensional networks by physical, chemical photochemical and ionic cross-linking [143-145] and peptide-modified hydrogels have promoted soft tissue augmentation in vivo [146].

For a tissue engineered substitute to have a wide impact on patient treatment, it will need to be available 'off-the-shelf'. Autologous cells are generally used in early clinical trails to bypass immunogenicity issues [147]. However, commercial products would need to recruit autologous cells directly from the host or use allogeneic cells.

Cell differences are not only associated with species variation, but also with location in the body [148] and age of donor [149, 150]. In addition, certain cells such as vascular endothelial cells provide complex multi-functional roles such as antigen presentation and blood vessel lining. Thus adult stem cells, such as the bone marrow-derived stem/progenitor cells, or human embryonic stem cells are being investigated extensively in regenerative medicine to provide a source of correctly differentiated and functioning cells [151].

If allogeneic cells are used to achieve 'off-the-shelf' availability, then a strategy is required for overcoming immune rejection. One possibility is lifelong use of immunosuppressive drugs such as cyclosporin used in organ transplantation although there is a drawback associated with serious side effects (e.g. renal dysfunction, hypertension). Other approaches include costimulatory blockade [152] or the use of multi-potent or pluri-potent stem cells [153]. The ability to manipulate the immune system will have important implications in regenerative medicine to address the major issue of immunogenicity of both the scaffold and cell component of tissue engineering constructs.

The mechanical properties of the scaffold are also important for promoting cell growth and tissue development. In the case of vascular tissue engineering, the regenerated blood vessel should mimic the native blood vessel in both architecture and function. Adequate haemodynamic burst resistance, visco-elstic properties and

fatigue life corresponding to the native blood vessels are desirable to ensure long term patency [154]. There are several different approaches being pursued in vascular tissue engineering to achieve the above properties including the use of intact elastin scaffolds obtained from digested animal arteries; scaffolds woven from elastin mimetic fibers and the use of cells genetically engineered to exhibit elevated elastin production and assembly.

1.7 Application of polymers in scaffold manufacture

1.7.1 Natural polymers

In the last few decades, natural polymers and synthetic polymers have been widely used as biomaterials in controlled drug delivery and tissue engineering. Natural polymers (albumin, chitosan, chitin and fibrin) (Fig.1.5) are isolated from a variety of sources, animal (collagen, gelatin), seaweed (agarose, alginate) or bacteria. They are soluble in aqueous or buffer solutions and are biodegradable in vivo. Collagen and gelatin, which are protein-based polymers, have been fabricated as sponges, films, matrices, gels and microspheres for pharmaceutical and medical applications due to their biodegradability and biocompatibility [155, 156]. Collagen sponge scaffolds demonstrate strong attachment and proliferation of endothelial cells, epithelial cells and bone marrow cells [157]. In addition, collagen sponges incorporating growth factors (VEGF and b-FGF) have been used to stimulate angiogenesis and accelerate cartilage regeneration [158]. Biobrane™, Transcyte®, Apligraf® and Integra® (commercial collagen sponges with or without neonatal fibroblasts) have been applied

clinically for wound healing and as tissue-engineered skin. Gelatin is derived from collagen and is extensively used for pharmaceutical and medical purposes. The biosafety of gelatin has been proved through long clinical usage as a plasma expander, as an excipient in drug formulation, and as a sealant for vascular prostheses [159]. Gelatin microspheres, foams, films, biocomposites and hydrogels have been produced for sustained delivery of growth factors and low molecular weight drugs [160, 161]. The material has also been used for production of cell-support structures due to its inherent cell adhesion properties, good biocompatibility and low antigenicity [162, 163]. However, in common with natural polymers, gelatin suffers from batch to batch variation during processing and purification and loses mechanical integrity due to rapid biodegradation.

Alginate, chitosan and chitin have been used in various forms for drug delivery and tissue engineering, such as wound healing, bone scaffolds and nerve regeneration [158, 164, 165]. Chitosan fibers have been utilized as sutures and wound dressings and micro/nano particles have been formulated to deliver anti-cancer drugs such as doxorubicin and 5-flurouracil [166]. Commercial alginate biomedical products which include Algisite®, algonsteril® and kaltogel® are used for wound healing and alginate scaffolds have been used for delivery of VEGF to stimulate angiogenesis [164, 167].

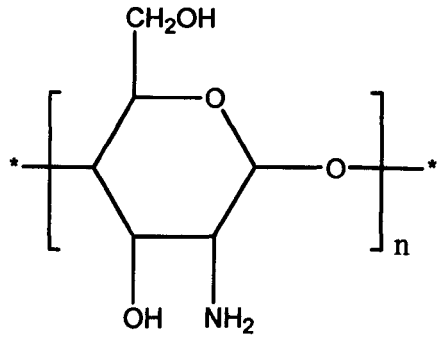

Chitosan

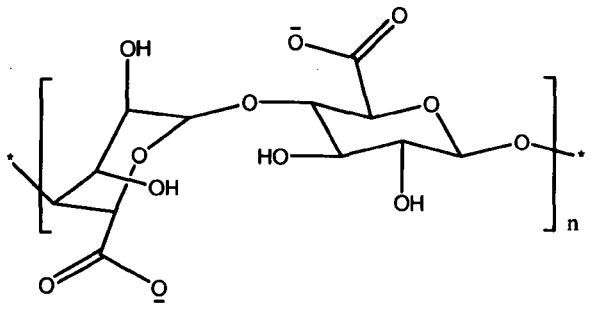

Alginate

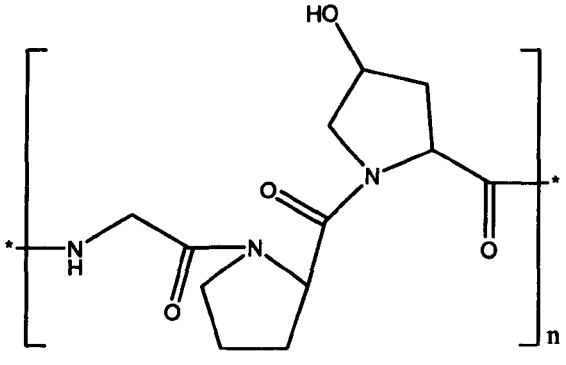

Collagen

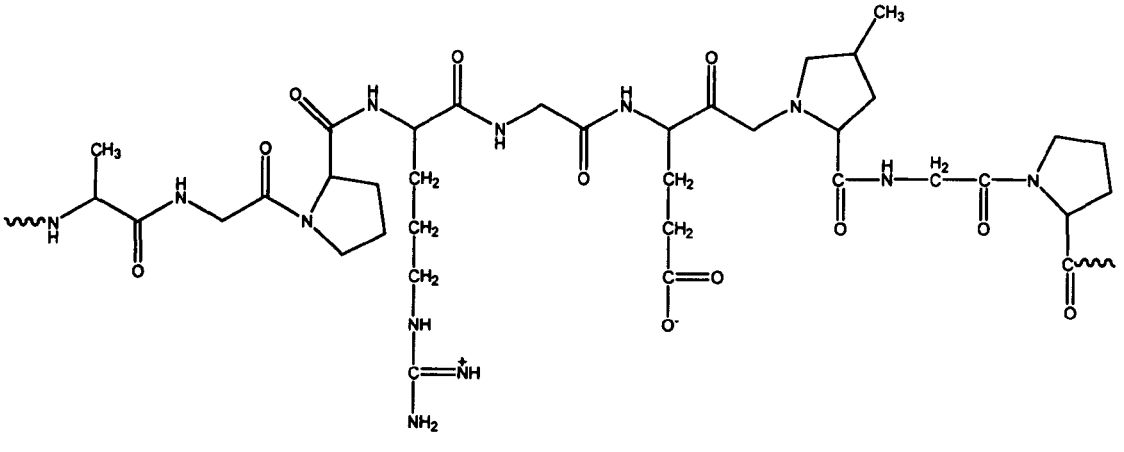

Gelatin

Figure 1.5 Chemical structures of natural polymers

1.7.2 Synthetic polymers

Synthetic polymers have been used in controlled drug delivery and tissue engineering

for several decades. They can be classified into five groups: 1) soluble 2) insoluble 3) hydrogels 4) non-biodegradable and 5) biodegradable. With ongoing developments in pharmaceutical science, more than 20 polymers have been fabricated as films, micro/nano-particles, fibres, inserts and matrices for application in controlled drug delivery or regenerative medicine. The properties of several of these polymers are summarized in Table1.5.

Table 1.5 Properties of synthetic polymers

Material	Tg (℃)	Tm (℃)	Density (g/cm^3)	Strength (MPa)	Semicrystallinity (SC) Amorphous (A)	Applications
PVA		180-190				
PVC	75-105				A	Surgical packaging, IV sets
PMMA	105		1.15-1.19	65 (tensile)	A	Blood pump, Implantable ocular lens
PET		265			SC	Implantable suture, mesh, artificial vascular grafts and heart valve
PTFE			2.15-2.2		SC	Catheter and artificial vascular grafts
PGA	35-40	225-230		890 (compressive)	SC	Suture, prosthetics and controlled drug delivery
PLA	60-65	173-178		--	A	Suture and prosthetics
PCL	-62	57		--	SC	Drug delivery and soft tissue engineering

☐ ~ Non-biodegradable
☐ ~ Biodegradable

Soluble synthetic polymers such as polyethylene glycol (PEG), polyvinyl alcohol (PVA), polyvinyl pyrrolidone (PVP), hydroxypropyl methyl cellulose and polyhydroxypropyl methacrylamide (PHPMA) are soluble in aqueous media because of their constituent hydrophilic polymer chains (Figure 1.6). These polymers may be used in solution to modify other materials or as solid, dissolvable matrices. They are advantageous for transport of drugs via body fluids to target sites and for temporary organ substitution. The anti-cancer drug, Doxorubicin has been linked to PHPMA for use in chemotherapy [168] and pilocarpine-loaded PVA films have been applied as ocular inserts to provide gradual dissolution and drug release in tear film [169].

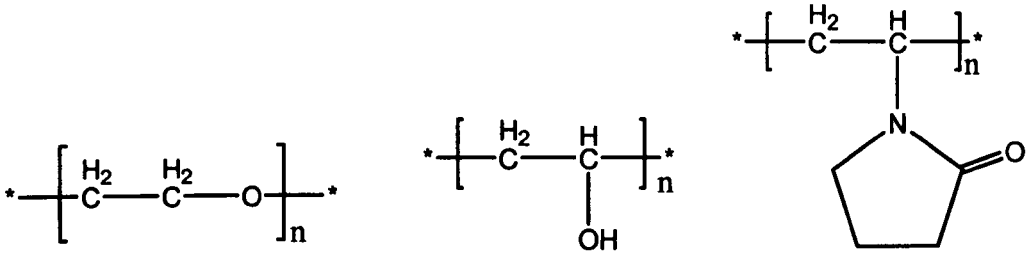

polyethylene glycol **polyvinyl alcohol** **polyvinyl pyrrolidone**

Figure 1.6 Chemical structure of soluble synthetic polymers

Synthetic hydrogels are water-swollen polymers with water content ranging from 30-90% depending on the polymer properties. The most commonly used hydrogels in the biomedical field are polyhydroxyethyl methacrylate (PHEMA), cross-linked PEG, PVA, PVP and polyacrylamide [170] (Figure 1.7). Hydrogels are produced by crosslinking soluble polymers via chemical bonding or physical interaction of

polymer chains. Such interactions can be achieved by exposure to UV light or pH variation[164]. Synthetic polymer hydrogels have been used extensively in soft tissue implants due to their high water content and compliance. PVA has been used as an adhesion shield in tendon regeneration [164] while PLA-PEG and PHEMA hydrogels have been investigated for growth factor delivery in tissue engineering. Bone morphogenic proteins released from PLA-PEG hydrogels, for example, has been shown to regenerate dentin and b-FGF released from PHEMA enhances proliferation of endothelial cells [171].

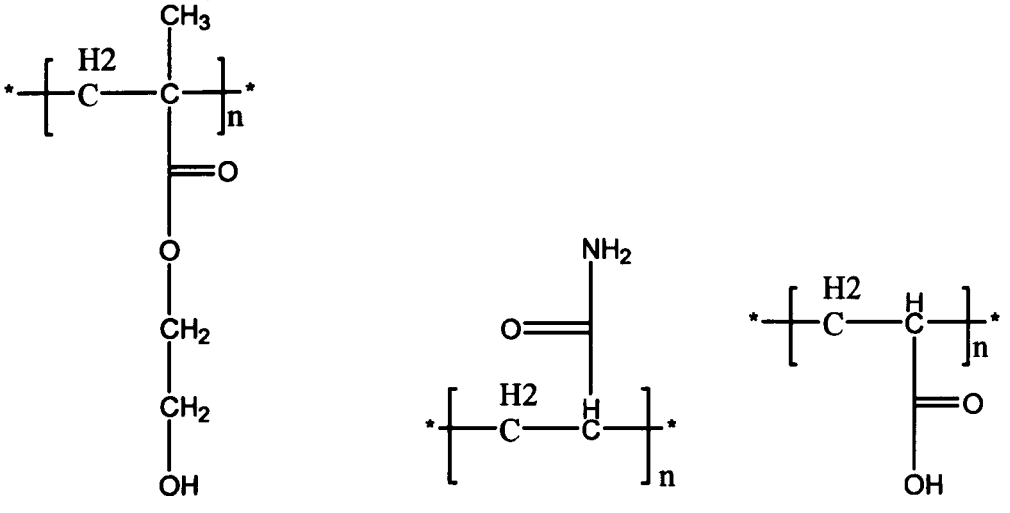

polyhydroxyethylmethacrylate **polyacrylamide** **polyacrylic acid**

Figure 1.7 Chemical structure of synthetic hydrogels

Non-biodegradable, water insoluble, synthetic polymers are composed of hydrophobic chains. Silicone elastomer, polyethylene (PE), polyethylene terephthalate (PET), polyurethanes (PU) and polytetrafluoroethylene (PTFE) (Figure 1. 8) are the most widely used in clinical applications, due to their properties of mechanical strength, stiffness retention over time, favorable biocompatibility and long-term

stability. PE and PMMA are widely used in tissue engineering for orthopaedic, joint replacement and vascular prosthesis [172, 173]. PTFE, more commonly known as Teflon® (DuPont™), expanded PTFE (Goretex®), and PET fibres (Dacron™) are still the only biomaterials used for large diameter vascular graft production. Silicone elastomers have been widely used in vascular and dental applications [166, 172] and in controlled drug delivery systems [174, 175]. Silicone elastomer devices have been used to deliver steroids for long-term contraception and anti-viral drugs due to the polymer's biocompatibility, ease of fabrication and high permeability to low molecular weight drugs [176]. Two commercial contraception products (Norplant® and Jadelle®) provide long term sustained release of levonorgestrel over 5 years after subdermal implantation in patients. Silicone elastomer intra-vaginal ring inserts have also been investigated for controlled release of anti-HIV drugs (eg. Nonoxynol 9) [177].

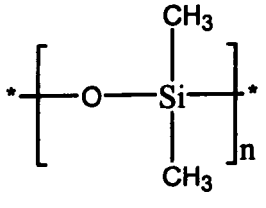

Silicone

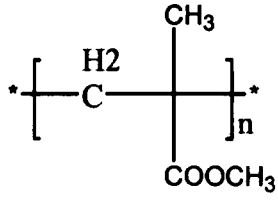

polymethyl methacylate

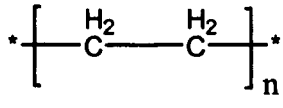

polyethylene

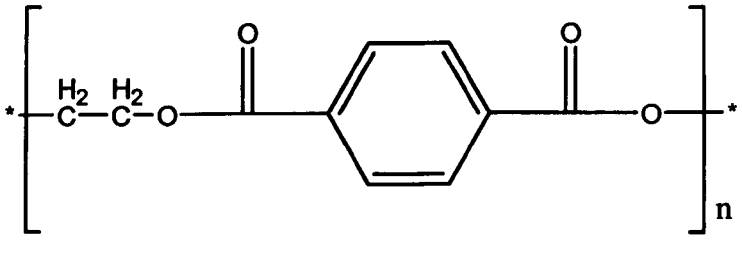

Polyethyleneterephthalate

Figure 1.8 Chemical structure of non-biodegradable synthetic polymers

Biodegradable synthetic polymers such as polyglycolic acid and polylactic acid are water-insoluble but slowly resorb in vivo via chemical hydrolysis or enzymatic cleavage (Figure 1.9). Five principal families of biodegradable polymers have been synthesized and characterized for clinical applications, polyester, polyanhydrides, polyamides, polyortheoesters and phosphorous-based polymers. Polyglycolic acid (PGA), polylactic acid (PLA), polycaprolactone (PCL) and copolymers of lactide/glycolide are among the most commonly used resorbable polyesters for drug delivery and tissue engineering [20]. They display good biocompatibility, low antigenicity and controlled degradation rate. The early development of successful suture materials based on polyesters (PCL, PLA, PGA (Dexon®), polydioxanone (PDS®) and polyglactin) have led to several decades experience with these materials in humans, so that their safety is now well documented [172, 178]. The first reported biomedical applications of poly (lactic acid) polymers involved their use as sutures and bone substitutes [179]. In the early 1970s controlled delivery of narcotic antagonists from poly(lactic acid) films was investigated [180] and microspheres of poly(d,l-lactic acid) were used to delivery contraceptive steroids [181, 182].

Poly(sebacic acid), poly(adipic acid) and poly(terephthalic acid) are polyanhydrides of the linkages that commonly occur in polymers, the anhydride linkage is one of the least stable in the presence of water which makes them unsuitable for many applications. However, the potential for rapid hydrolysis of the polymer backbone makes anhydride-based polymers attractive candidate biodegradable materials. A

common materials design approach for medical applications is to produce polymers which degrade into non-toxic components. For this reason, polyamino acids are advantageous for production of new polymeric biomaterials. Polyorthosesters are synthesized by addition of polyols to diketene acetals and the mechanical properties can be varied by selecting appropriate diols or mixture of diols. Delivery of 5-flurouracil for chemotherapy and tetracycline for treatment of periodontal disease has been successfully achieved using polyorthoesters [183].

Biodegradable polymers, particularly the polyesters, have been manufactured in various forms (e.g. films, matrices, macro particles, nanoparticles and fibers) for application in tissue engineering and controlled drug delivery. Copolymers of DL-lactic acid and glycolic acid have been converted into rods (Zoladex®) and microspheres (Lupron Depot) for the treatment of prostate cancer or endometriosis [184, 185].

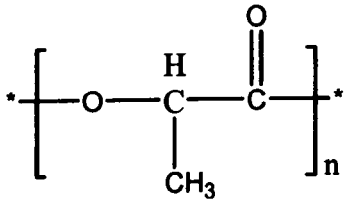

polylactic acid

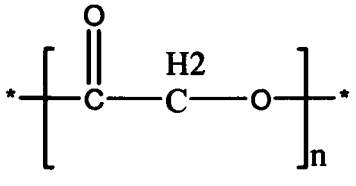

polyglycolic acid

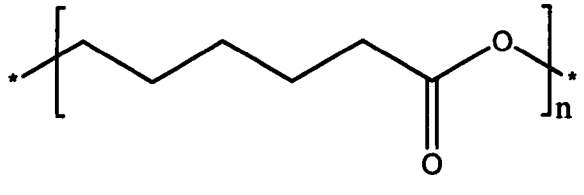

polycaprolactone

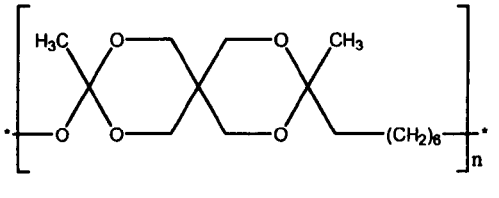

polyorthoester

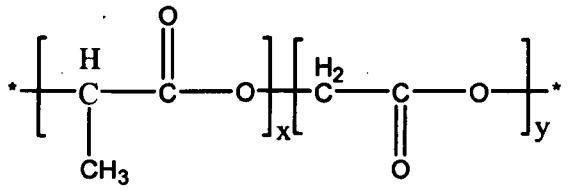

PLGA: copolymers of DL-lactic acid and glycolic acid

Figure 1.9 Chemical structure of biodegradable synthetic polymers

1.7.3 Polycaprolactone

Polycaprolactone (PCL) is semi-crystalline, slowly-resorbing, aliphatic polyester which is biocompatible with soft and hard tissue and has been widely investigated as the scaffold component of tissue engineering constructs for hard and soft tissue repair [9, 34, 36]. PCL may be synthesized by the ring opening polymerization of ε-caprolactone via four different mechanisms (Figure 1.10): anionic, cationic, coordination and radical polymerization. Each method has unique attributes, providing different degrees of control over molecular weight and molecular weight distribution, end-group composition, and the chemical structure and sequence (block versus random) distribution of copolymers.

Anionic polymerisation

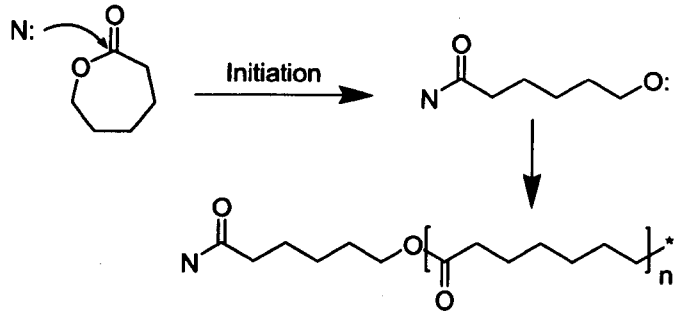

Cationic polymerization

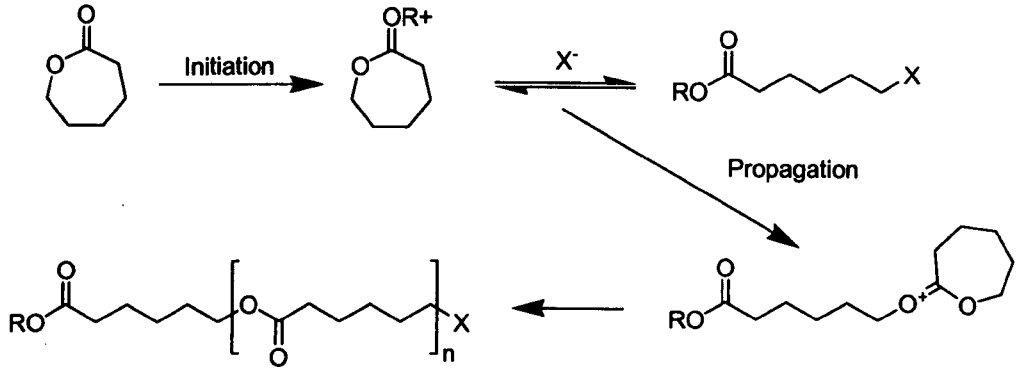

Coordination polymerization

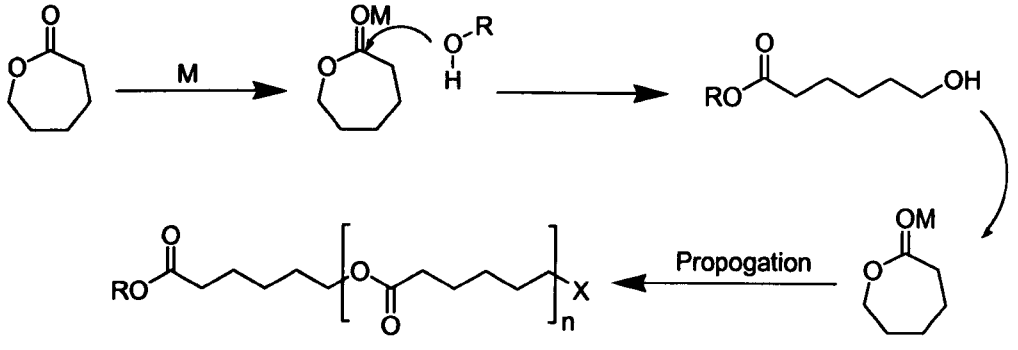

Radical polymerization

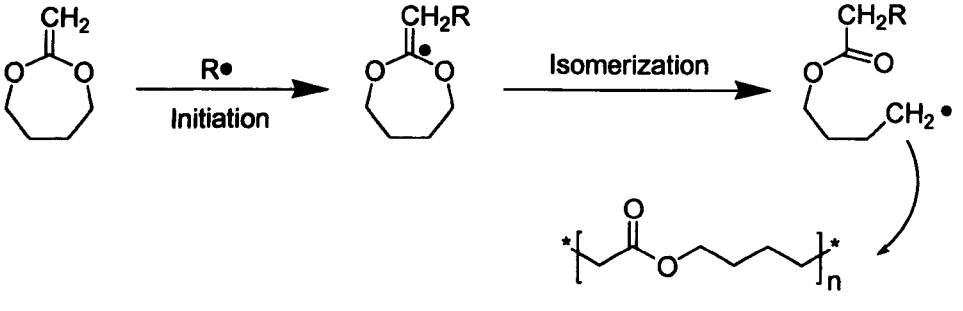

Figure 1.10 Mechanisms of polymerization of poly (ε-caprolactone)

PCL exhibits a melting point (Tm) in the range of 59-64°C and a glass transition temperature (Tg) at -60°C. Because of its low Tg, the melt cannot be quenched to a glass. Polymers with a Tg > 37°C are in the glassy state at body temperature while those having a Tg < 37°C are in the rubbery state. Polymers in the glassy state tend to be brittle and inflexible with low permeability to drugs and therefore have limited application as tissue engineering scaffolds. In contrast, polymers in the rubbery state exhibit high permeability to drugs due to the increase in free volume, but their lower mechanical strength needs to be considered when developing tissue engineering scaffolds. The heat of fusion (ΔH_f) of 100% crystalline PCL is reported to be 139.5 J/g [186], and this value has been used to estimate the crystallinity of PCL and its copolymers using differential scanning calorimetry (DSC). Polymer crystallinity is important in determining physical properties such as degradation time, permeability, density and melting point. For example an increase in crystallinity increases the amount of regular packing of constituent chair molecules and reduces the permeability to body fluids. The biodegradation rate is simultaneously reduced by the decrease in accessible ester bonds. Semi-crystalline polymers are characterized by a degree of crystallinity above 50% whereas amorphous polymers are non-crystalline. The crystallinity of PCL is affected by molecular weight, for example, such that a crystallinity decrease from 80-40% results on increasing the molecular weight from 5000-100,000 [187].

The degradation behavior of PCL (films and rods) has been investigated following

subdermal implantation in animals. Degradation of PCL begins by random hydrolytic chain scission of the ester linkages, manifested by a reduction in the viscosity and molecular weight of the polymer [186, 188]. This process is not considered to involve enzymatic attack because the same degradation rate is indicated in vivo and in vitro in water at 40°C. A second phase of PCL degradation usually commences when the molecular weight decreases to approximately 5000 and the rate of chain scission falls, but weight loss stars. Weight loss can be attributed to the increased probability that chain scission of a low molecular weight polymer will produce a fragment small enough to diffuse out of the polymer bulk. Physical break down of the polymer mass finally occurs to produce smaller particles with an increased probability of phagocytosis [187, 189]. Previous *in vivo* studies have shown that the molecular weight of PCL decreased from 50,000 to 5000 over 100 weeks and required three years for total removal from the body [190]. Such long-term degradation characteristics suggest application of PCL in bone, cartilage and vascular regeneration. Although PCL applied as a 1 year contraceptive delivery system did not show any significant side effects, the long term toxicity of PCL in vivo still needs to be considered for clinical use.

The toxicology of PCL has been studied in conjunction with evaluations of Capronor® which is an implantable 1-year contraceptive delivery system composed of levonorgestrel in a PCL capsule. An early initial 90-day trial of Capronor in 1984 in female rats and guinea pigs revealed no toxic effects [191]. Clinical observations,

physical examinations, qualitative food consumption, urinalysis, and ophthalmoscopic analysis showed no significant differences between the test and control group during a two year period [192]. PCL implants have also been assessed for toxicity based on cell ultrastructure in organ cultures, cell surface characteristics and cell population doubling times [193]. Only a minimal tissue reaction, which could not be scored, was stated in the above test. A clinical trail of Capronor involving 48 women found that the PCL implant was well tolerated by subjects with no adverse systemic side effects during the 40 weeks study [194].

Due to its good biocompatibility, PCL has been fabricated using numerous techniques into various forms such as films, membranes, fibers, micro/nano particles, capsules and reservoir devices for tissue engineering and/or drug delivery (Table.1.6). Blending of polymers to achieve a balance in material properties has been applied extensively in biomedical materials and drug delivery research. Microporous, bone graft substitutes have been produced by blending fast resorbing PLG and slow resorbing PLA to adjust the resorption rate and dimensional stability of implants. PCL is much more permeable than PLG for delivery of certain drugs but degrades very slowly. Blending of PCL with PLG has been shown to result in retention of permeability and shape stability while increasing the overall degradation rate of the material compared with PLG. In addition, biocomposites of natural and synthetic polymers offset the disadvantages of natural materials and exploit the wide range of physico-chemical properties and processability of synthetic polymers. For example,

the poor cell adhesion properties normally associated with poly(2 hydroxyethylmethacrylate) [poly(HEMA)] have been mitigated by blending with gelatin [162]. PCL-collagen films, prepared by impregnating lyophilized collagen mats with PCL solutions, have been investigated as scaffolds for human osteoblasts and skin substitutes [9, 195]. This approach avoided the need for crosslinking of the collagen phase to improve stability and retained the good cell adhesion properties of the protein.

Table 1.6 Biomedical application of PCL and its blends

Polymer	Forms	Fabrication method	Application	Ref.
PCL	films	Melt-processing	Progesterone and levonorgestrel delivery	[196]
	disks	Solvent casting		[197]
	membranes	Solvent casting		[198]
	tubes	Melt extrusion at 160°C		
	capsules			
	rod		Tobramycin sulphate antibiotic delivery	[199, 200]
	matrices	Solvent-casting/ particulate-leaching	Support osteoblast growth for bone tissue engineering	[201]
	scaffolds			
PCL/hydronyapatite	scaffolds		Support rabbit bone marrow stromal cells	[202]
PCL/collagen	films	Impregnation of freeze-dried collagen with PCL solution	Support human osteoblasts and mouse fibroblast growth	[9, 195, 203]
PCL	micro/ nano particles	Solvent evaporation/ extraction	Lipophilc drugs, hydrophilic drugs and protein delivery	[204-207]
	Hollow fibres	Melt spinning Dry and wet spinning Electrospinning	Delivery of tetracycline antibiotic	
PLA-PCL	hollow fibres	Dry and wet spinning	Drug-loaded nanoparticles	[208]
PCL	fibres	Gravity spinning	Support growth of fibroblasts and myoblasts. Delivery of protein, progesterone and gentamicin sulfate	[209-211]

1.8 Project aims and outline

This thesis focuses on the formulation and characterisation of polycaprolactone-based matrices with the aim of improving scaffold performance in tissue engineering and the function of drug delivery devices. PCL micro/macroporous matrices containing high protein loading (29-44% w/w) were produced by rapid cooling of a PCL solution in dry ice followed by solvent extraction from the hardened material using methanol.

Chapter 1 presents an introduction to the field of tissue engineering and controlled drug delivery.

Chapter 2 describes the formulation of PCL matrices incorporating protein, enzymes and a steroid (dexamethasone) respectively. The methods used for characterising the release behaviour, internal pore structure of PCL matrices (micro-CT), thermal behaviour, mechanical testing under fluid flow conditions, cell culture and enzyme bioactivity assay are also included in the chapter.

Chapter 3 details the formulation, release behaviour, morphology, thermal properties and biocompatibility (using cultures of 3T3 fibroblasts) of PCL matrices incorporating lactose and gelatin particles. These investigations revealed the potential of the matrices for controlling growth factor delivery in tissue engineering.

Chapter 4 describes a quantitative and qualitative analysis of the internal pore structure of PCL matrices using micro-CT. Detailed information regarding pore structure, the range of equivalent pore diameter, frequency distribution of equivalent pore diameter and macroporosity is presented. The results are useful for understanding the kinetics of drug delivery from matrix-type devices and predicting cell ingrowth behaviour in tissue engineering scaffolds.

Chapter 5 is concerned with the mechanical characterisation (dimensional changes, burst strength) of PCL tubes for vascular tissue engineering under fluid flow conditions (constant, continuous increasing and pulsatile conditions).

Chapter 6 describes the formulation, morphology, thermal properties and release behaviour of PCL matrices incorporating lysozyme, collagenase and catalase. The activity of released enzyme is reported. Dexamethasone release behaviour from PCL matrices is also described in this chapter.

Chapter 7 presents an overall summary and conclusions of the study with suggestions for future work.

Chapter 2

Materials and Methods

2.1 Materials

PCL (*M*w 115,000 Da, Capa 650) was obtained from Solvay Interox, Warrington, UK. Lactose powder (β-lactose, L3750) and gelatin powder (bloom 125), phosphate buffered saline (PBS) and bicinchoninic acid (BCA) reagents were purchased from Sigma-Aldrich Chemicals. Acetone, dichloromethane (DCM) and methanol were obtained from Fisher Scientific.

2.2 Preparation of microporous PCL matrices

PCL (1.7 g) was dissolved in 10 ml acetone by gentle heating at approximately 50°C to produce a 17% w/v solution. This PCL solution was transferred into a mould comprising a 3 ml polypropylene (PP) syringe body with a centrally located 1 ml PP syringe body. The tubular casting obtained (6.5 mm internal diameter, 7.5 mm external diameter, 55 mm long) was of interest for fabrication of substitute blood vessels. After rapid cooling in dry ice (-78°C) for 2-5 minutes to induce rapid crystallization and hardening of the polymer, the matrices were carefully removed from the mould and it was immersed in methanol (50 ml) for 24 h to extract the acetone. Finally, the tubular castings were removed from the methanol bath and the acetone/methanol remaining in the matrices was allowed to evaporate in air under

ambient conditions. Two further processing techniques were investigated 1) the hardened matrices were allowed to dry in the mould without methanol addition until the diameter was constant 2) methanol was introduced on top of the matrices in the mould and left for 24h to extract acetone, followed by matrix drying in the mould.

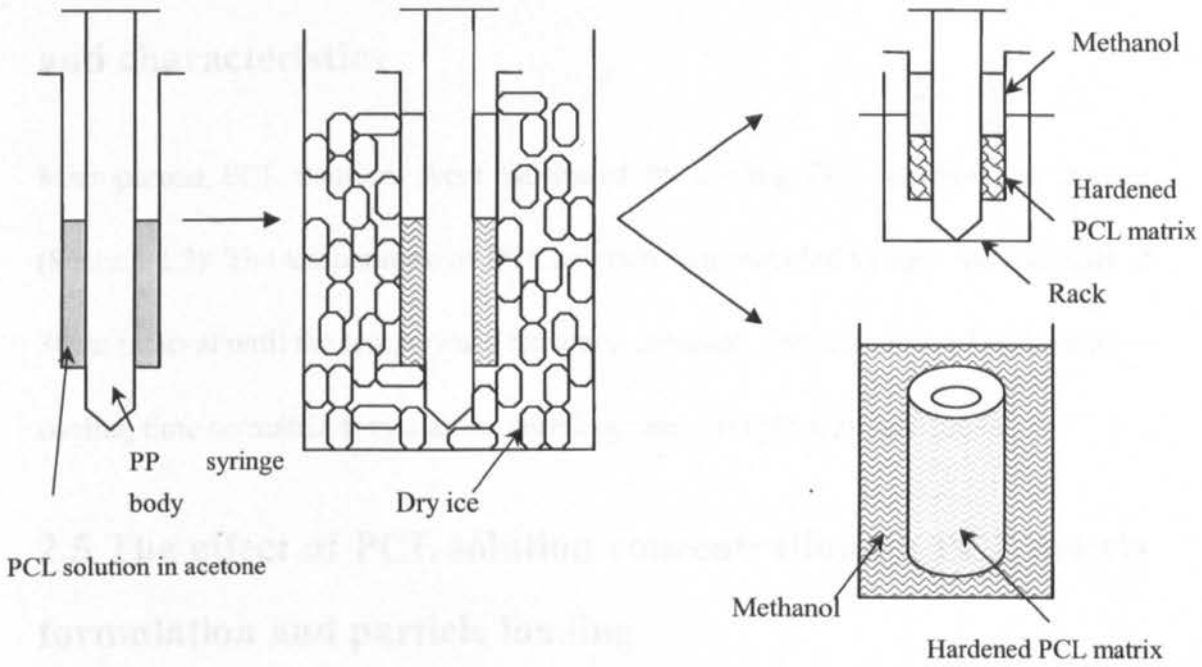

Figure 2.1 Formulation of microporous PCL matrices

2.3 Investigation of PCL matrix shrinkage during preparation matrix density

The diameters of PCL tubes were measured at key points in the manufacturing process namely 1) after casting in dry ice 2) following solvent extraction in methanol and 3) after sample drying. The diameter of the casting was also measured following the two different drying approaches maintained above namely 1) drying in the mould without methanol addition and 2) addition of methanol on top of the hardened matrix

in the mould, followed by drying in the mould. The diameters were record using a micrometer until they remained constant. The weight, length and internal/external diameter of samples of PCL matrices were measured to calculate the density as gm/cm^3.

2.4 The effect of cooling time on PCL matrix formulation and characteristics

Microporous PCL matrices were fabricated by cooling PCL solutions in dry ice (Section 2.2). The temperature of PCL solution was recorded using a thermometer at 30sec interval until the temperature remained constant. The influence of PCL solution cooling time on matrix formulation, shrinkage and strength was determined.

2.5 The effect of PCL solution concentration on PCL matrix formulation and particle loading

This study was performed to determine the optimal PCL solution concentration and particle loading for production of high protein loading PCL matrices. Gelatin loaded PCL matrices in tubular form were produced as described above in Section 2.2. Gelatin particles in the size range of 45-90 and 90-125 μm respectively were added to a 17% w/v PCL solution to give a protein concentration of 29%, w/w. Gelatin powder (insoluble in acetone) was sieved to obtain a particle size range of 125-250 μm and suspended in 5, 12.5 and 20% w/v) PCL solutions to give a final loading of 29, 38 and 44% w/w The suspensions were used to formulate particle-loaded PCL matrices

by rapid cooling in dry ice (Section 2.2).

2.6 Preparation of lactose-loaded PCL matrices by rapid cooling in dry ice

Lactose particles in three size ranges (45-90, 90-125, 125-250 μm) were obtained by sieving the as-received powder. Lactose particles (insoluble in acetone) of each defined size range were dispersed in 17% w/v PCL solution using a glass rod to give a final loading of 29% w/w. The lactose suspension was transferred into a mould comprising a 3 ml polypropylene (PP) syringe body with a centrally located 1 ml PP syringe body. Following crystallization and hardening of the PCL phase in dry ice for 3min, the lactose-loaded matrices were removed from the mould and immersed in methanol (50 ml) for 24 h to extract acetone. Acetone/methanol remaining in the matrices was allowed to evaporate in air under ambient conditions.

2.6.1 Determination of the lactose content of PCL matrices

The distribution of lactose in the matrices was measured to assess the influence of the casting method on loading uniformity and lactose release rate. Three individual samples from the top 5mm, mid-region, and base of lactose-loaded PCL tubes were each dissolved in 2ml DCM. The polymer was precipitated by addition of distilled water (8 ml) and the sample tubes were shaken overnight on a Vibrax VXR system to evaporate the DCM. The lactose concentration in distilled water was determined by HPLC (Waters, Milford, MA, USA) with refractive Index detection and compared

with a calibration curve constructed using a series dilution of lactose in distilled water (20-1000 μg/ml). The lactose loading of the PCL matrices was subsequently calculated as % w/w.

2.6.2 In vitro release of lactose from microporous PCL matrices

Samples of lactose-loaded PCL matrices (approximately 100mg) taken from tubular castings were accurately weighed and immersed in 10 ml distilled water at 37°C for 15 days. The release medium was replaced completely by fresh distilled water at 1 day intervals and the concentration of lactose in the samples was determined by HPLC (Waters). The amount of lactose release was calculated using a calibration curve as described above (Section 2.6) and expressed as cumulative release (%) versus time.

2.7 Preparation of gelatin-loaded PCL matrices

Gelatin powder (insoluble in acetone) was sieved to obtain particle size ranges of 45-90, 90-125 and 125-250 μm and dispersed, respectively, in 17% w/v PCL solution to produce three protein concentrations of 29 38 and 44% w/w respectively. The suspensions were transferred into a PP mould to produce PCL tubular matrices as described in Section 2.2. Following crystallization and hardening of the PCL phase in dry ice for 3min, the gelatin-loaded matrices were removed from the mould and immersed in methanol (50 ml) for 24 h to extract the acetone. Acetone/methanol

remaining in the matrices was allowed to evaporate in air under ambient conditions.

2.7.1 Determination of the gelatin content of PCL matrices

The distribution of gelatin in the PCL matrices was measured to assess the influence of the casting method on loading uniformity and gelatin release rate. Three individual samples from the top (5mm), middle and base of gelatin-loaded PCL matrices were each dissolved in 2 ml DCM. PBS (8ml) was added to precipitate the PCL and the sample tubes were shaken overnight using a Vibrax VXR shaker to evaporate the solvent. Samples of gelatin in PBS solution were analysed in triplicate to determine the protein content using the BCA assay. Aliquots (10 μl) were transferred to a glass tube and 2 ml BCA working reagent were added. A series dilution of gelatin in PBS was used to produce calibration samples (0-800 μg/ml). All test and calibration samples were incubated at 37°C for 30 min before measuring the absorbance using a Hitachi U2000 spectrophotometer at a wavelength of 562 nm. The protein content in PBS was subsequently compared with the calibration curve to calculate the gelatin loading of PCL matrices as % w/w.

2.7.2 In vitro release of gelatin from microporous PCL matrices

Accurately weighed samples of PCL matrices (100mg) containing gelatin powder of various particle size ranges and loading were immersed in 10 ml PBS (pH 7.4). The sample tubes were retained at 37°C for 21 days and the release medium was replaced

completely by fresh PBS at 1 day intervals. The amount of gelatin in the release medium was analysed using the BCA total protein assay after 24 h and then every 2 days up to 21 days by comparison with a calculation curve produced using a series dilution of gelatin in PBS. Gelatin release from the matrices was expressed as cumulative release (%) versus time.

2.8 Density measurement of PCL matrices

The weight, length, external and internal diameter of lactose or gelatin-loaded PCL matrices in tubular form was measured to calculate the sample density.

2.9 Measurement of the porosity of PCL tubular matrices

The porosity of PCL matrices in tubular form after release of lactose and gelatin respectively was measured by Archimedes' principle [212, 213]. Briefly, ethanol was used as the displacement liquid, since it easily penetrates the pores of the matrices without causing sample shrinkage or swelling. A 5ml glass measuring cylinder was filled with ethanol (density ρ_e) and weighed (W_1). A PCL matrix sample of weight (W_s) was transferred to the cylinder and sonicated in a water bath (Unisonics, Sydney Australia) for 30 min to displace air bubbles and allow ethanol to fill the pores. Ethanol above the mark of 5ml was removed and the cylinder containing ethanol and the PCL sample was weighed (W_2). The PCL sample saturated with ethanol was removed from the cylinder and the cylinder was weighed (W_3). The sample porosity (ε) was calculated using the following equations.

Vp (matrix pore volume) = $(W_2 - W_3 - W_s) / \rho_e$

Vs (matrix solid volume) = $(W_1 - W_2 + W_s) / \rho_e$

ρ_s (matrix density) = $W_s/Vs = W_s \rho_e / (W_1 - W_2 + W_s)$

$\varepsilon = Vp / (Vp+Vs) = (W_2 - W_3 - W_s)/ (W_1 - W_3)$

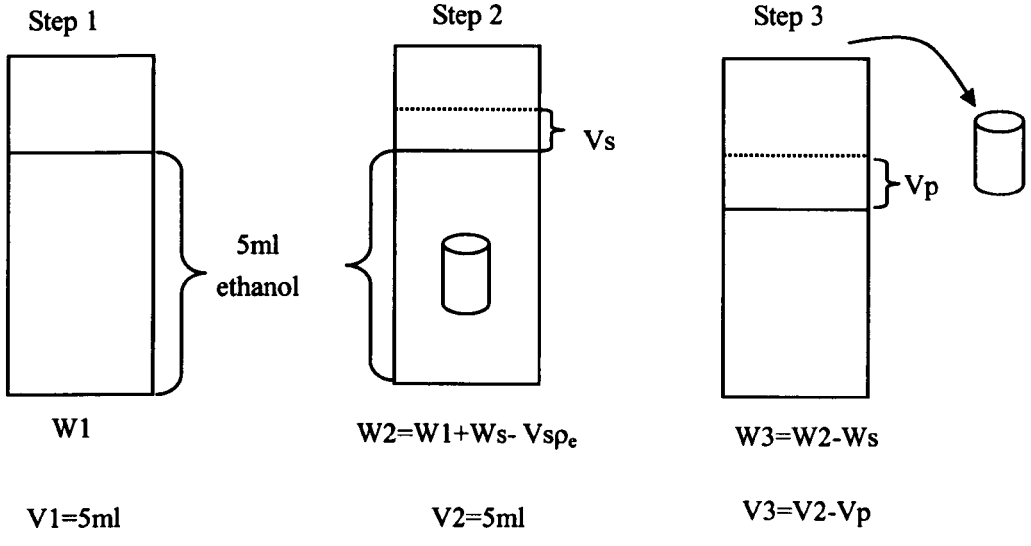

Figure 2.2 The liquid displacement method for porosity measurement

2.10 Thermal analysis of microporous PCL matrices, lactose-loaded and gelatin-loaded matrices

The thermal characteristics (peak melting point (T_m) and percentage crystallinity) of PCL matrices, lactose-loaded and gelatin-loaded matrices were determined using a TA Instruments DSC 2920. Specimens were accurately weighed (minimum 5 mg), sealed in aluminum pans and programme-heated from 0°C to 90°C at a rate of 10°C/min. Sample percentage crystallinity was estimated from the reported heat of fusion of 139.5 J/g for fully crystalline PCL [186].

2.11 Characterization of the morphology of PCL matrices using scanning electron microscopy (SEM)

The morphology of PCL, lactose-loaded and gelatin-loaded PCL matrices before and after release was examined using a Philips XL30 scanning electron microscope (SEM). Specimens were mounted on aluminum sample stubs and sputter-coated with platinum using an Edward E30GA automatic mounting press prior to examination in the SEM at a voltage of 15 kV. Sections through PCL, lactose-loaded and gelatin-loaded PCL tubes were also examined.

2.12 Investigation of the morphology of lactose and gelatin particles before and after matrix production

As received lactose or gelatin particles were examined using a Philips X30 SEM as described above (Section 2.11). Lactose and gelatin particles (insoluble in DCM) were recovered from PCL matrices by dissolving the PCL in DCM, followed by washing the sedimented powder 3 times with fresh DCM to remove residual PCL. The extracted lactose and gelatin particles were dried under ambient conditions before sputter coating with platinum and examination using SEM respectively.

2.13 Fibroblast interaction with PCL matrices in cell culture

2.13.1 Preparation of Swiss 3T3 fibroblast cell culture

Swiss 3T3 mouse fibroblasts were obtained from the European Collection of Cell Culture (ECACC). Dulbecco's modified eagle's medium (DMEM), L-glutamine and

fetal bovine serum were purchased from Sigma Aldrich. Cell culture plates (48 wells) were obtained from Fisher Scientific.

Swiss 3T3 fibroblast cells (European Collection of Cell Culture) were transferred into a 75cm^2 tissue culture flask (TCF) containing culture medium after thawing in a water bath at 37 °C. The fibroblast culture medium was prepared using standard DMEM containing 10% v/v fetal bovine serum (FBS), 1% v/v L-glutamine (2mM/L final conc.) and 1% v/v antibiotics solution (100 IU/ml penicillin and 100 μg/ml gentamicin) and was pre-warmed at 37 °C in a water bath. Once fibroblast colonisation of around 80-90% was achieved in TCF, the cell culture medium was removed and 3ml of 0.25% trypsin-EDTA solution was added for 5min to detach the cells followed by addition of 5 ml DMEM-L-glutamine culture medium to protect the cells. The fibroblast suspension in DMEM-L-glutamine was centrifuged at 1000 rpm/min (about 200×g) for 10mins to separate dead cells. The cells remaining in the base of the centrifuge tube were resuspended in DMEM for storage or for use in the following experiments.

2.13.2 Growth of 3T3 fibroblasts on PCL matrices having various pore size ranges produced by lactose or gelatin extraction

Swiss 3T3 fibroblasts (10×10^3 cells/cm^2) were seeded in 48-well tissue culture plastic plates (TCP) containing PCL matrices with various pore size ranges (45-90, 90-125,

125-250μm). Cells were also seeded on TCP as a control. The microporous matrices were produced by solubilisation and extraction of 85-99% of the lactose or gelatin particles incorporated in 29% w/w loaded matrices (Samples were immersed in distilled water or PBS at 37 °C for over 2 weeks to remove the soluble phase). Samples of microporous matrices in the form of disks (1cm in diameter) were cut from tubular castings using a razor. All PCL matrices and TCP were sterilized under UV light in a cell culture hood overnight (12h). Samples in three specific pore size ranges were seeded in triplicate to gain measurements of cell numbers on each type of matrix at each time point. Plates were incubated at 37 °C and 5% CO_2 and the culture medium was replaced with fresh DMEM every two days. Growth of cells was allowed for 8 days and cell numbers were counted at day 1, 5, and 8. Each matrix with attached fibroblasts in the 48-well TCP plate was washed using sterile PBS to remove residual culture medium. For cell detachment, 0.25% trypsin solution in EDTA (0.3ml) was added to each sample well followed by incubating at 37 °C for 5min. Trypsin was inactivated by adding 0.5ml culture medium to each well and the number of cells detached from the porous matrices was counted using a Weber's haemocytometer.

2.13.3 SEM analysis of fibroblast attachment on microporous PCL matrices

The morphology of Swiss 3T3 fibroblasts attached at 1, 3 and 5 days on PCL matrices having various pore size ranges produced via gelatin extraction was examined using a Philips XL30 scanning electron microscope. PCL matrices with attached fibroblasts

were removed from the 48-well TCP plates, transferred to 10ml centrifuge tubes and residual culture medium was replaced by sterile PBS (pH 7.4). After rinsing three times with PBS, fibroblasts on the surface of the PCL matrices were fixed by addition of 2.5% glutaraldehyde in 0.1M sodium cacodylate buffer for 30min (1^{st} fixation). Samples were rinsed with PBS (3×5min) before the 2^{nd} fixation using 2% Osmium tetroxide in 0.2M sodium cacodylate buffer for 1 hour. The fixed cells attached to matrices were washed with sodium cacodylate buffer and dehydrated in a series of ethanol dilutions (50-100%) for 5min, twice per dilution. The specimens with attached cells were dried in a Critical Point dryer, mounted on aluminum sample stubs and sputter-coated with platinum prior to examination in the SEM at a voltage of 15 kV.

2.14 Qualitative and quantitative assessment of the internal pore structure of PCL matrices using computed micro-tomography (Micro-CT)

The internal 3D pore structure of PCL matrices was analysed by computed micro-tomography (Micro-CT). Micro-CT combines X-ray transmission techniques with computed tomographical reconstruction to enable collection of detailed 3-D information about the internal microstructure of a material (Figure 2.3). In micro-CT, a scanning X-ray beam transmits through the specimen to form a set of flat, 2-D shadow images (absorption images) due to density differences in internal areas of the specimen that affects the intensity of transmitted X-rays. Internal areas can be

reconstructed using a set of flat cross-sections and further analysed to provide two and three-dimensional morphological parameters such as pore shape, connectivity and pore distribution.

Longitudinal samples (approximately 2×2×10 mm in length) were cut from microporous PCL tubes and analysed using a Skyscan1072 (Skyscan, Aartselaar, Belgium) desktop X-ray CT scanner at 15 μm voxel resolution (50× magnification), X-ray tube current of 173 μA and voltage of 30 kV. Specimens were mounted vertically on a plastic support and rotated through 360 degrees around the long axis (z-axis) of the sample. The absorption image was recorded every 0.225° of rotation. These projection radiographs were then used in standard cone-beam reconstruction software to generate a series of 1024 8bit axial slices, each of 1024x1024 pixels, that had Z-dimensional spacing equal to the within slice pixel spacing. The resulting 3D data sets were hence isotropic with voxel spacing of 15 μm over the entire 1024^3 spatial range. Three-dimensional reconstruction of the internal pore morphology was carried out using these axial bitmap images and analysed by VG Studio Max 1.2 software (Volume Graphics GmbH, Heidelberg, Germany).

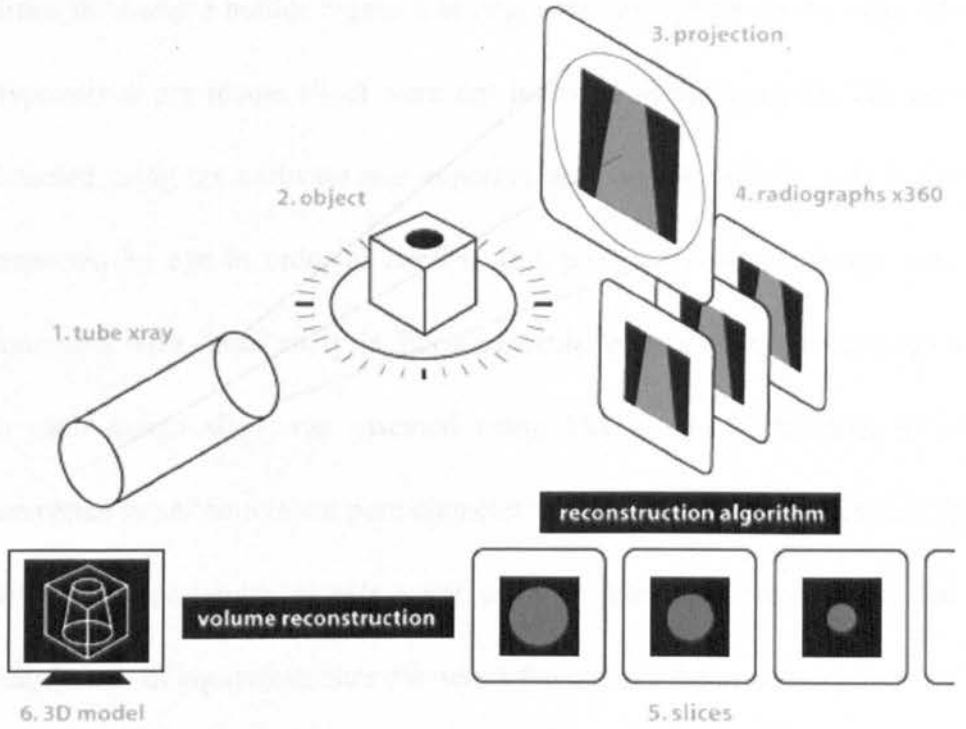

Figure 2.3 The principle of computed micro-tomography (Micro-CT)

2.14.1 Image processing

Analysis of transverse Micro-CT images obtained at 1000μm intervals along the sample long-axis was performed to provide quantitative estimates of pore size distribution in the matrices. After conversion to grey scale using Paint Shop Pro (Jasc Software Inc., USA) images were processed to detect pores by in-house developed software using MATLAB (The MathWorks Inc, USA). The grey-scale images were filtered, the contrast adjusted and a threshold applied to detect the dark regions of the pores. The same threshold was used for all images in a particular data set, although different thresholds were applied for each sample (eg 90-125 and 125-250μm gelatin-loaded PCL). Higher level processing involved removing small objects, filtering and removing the sample border region prior to calculation of pore areas.

Since the sample border region was neglected, any pores on the edge of the sample (typically 6 per image slice) were not included in the analysis. The pore boundary detected using the software was superimposed on the original grey-scale image and inspected by eye in order to confirm that pore detection by image processing was consistent with visual analysis. For a particular matrix type, the variation of pore area in each image slice was assessed using MATLAB (MathWorks Inc, USA) and converted to an 'equivalent pore diameter'. In addition the pore area data for all image slices of a particular sample were used to provide a measure of the frequency distribution of equivalent pore diameters throughout the matrix.

The porosity (%) of PCL matrices after gelatin extraction was assessed using Amira 4.0 (Mercury Computer System Inc, USA) which provides a 3-D data set by reconstruction of the sequential grey-scale images modified by Paint Shop Pro as described above. The porosity was calculated by comparing the total pore volume with the total volume of a sample cube (pore phase plus polymeric phase). Each sample of PCL matrix analysed provided 1000 sequential grey- scale images. Blocks of 300 images from top to base through the sample were reconstructed as 3D images to assess the uniformity of porosity and to characterise the internal pore structure.

2.15 The deformation behaviour of microporous PCL tubes under hydrostatic and hydrodynamic loading conditions

The mechanical behaviour (burst strength, diameter increase (dilation)) of

microporous PCL tubes with/without gelatin loading was investigated using the Bose-Enduratec biodynamic system under hydrostatic and hydrodynamic conditions. PCL tubes with internal diameter of 6.5 mm, external diameter of 7.5 mm and length 50 mm were produced by rapid cooling in dry ice as described in Section 2.2. Microporous PCL tubes with gelatin loading of 29, 38 and 44% w/w respectively were produced using gelatin particles with a size range of 90-125μm. The changes in the diameter of the PCL tubes during the study were measured using a laser scanning micrometer (Mitutoyo LSM 301) configured as a simple shadowgraph detector (Figure 2.4). The PCL tube, when placed perpendicular to a parallel beam of light produces a shadow on the detector that can be captured and analysed for changes in tube diameter. Data were captured at a rate of 1-10 measurements per second at 16 bit resolution and all data were logged using a Labview 8.0 based programme (National Instruments, US). The laser micrometer has a resolution of ± 0.1μm.

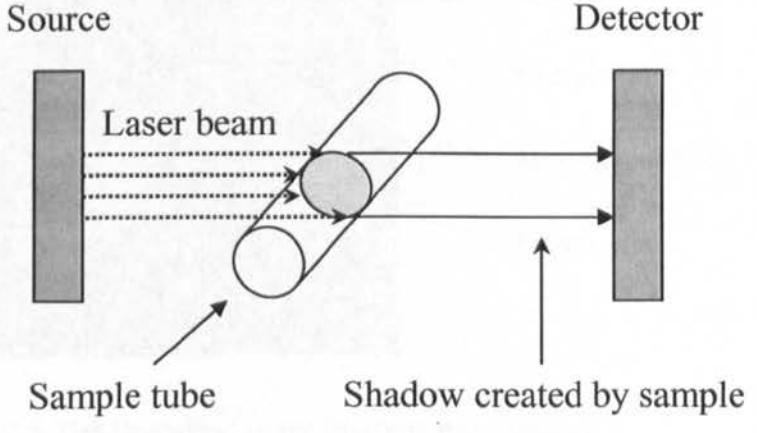

Figure 2.4 Schematic representation of diameter measurement using a laser micrometer.

2.15.1 Measurement of the changes in diameter of PCL tubes under a constant fluid flow rate of 300ml/min at 37 °C

A Bose-Enduratec BioDynamic chamber for modeling cardiovascular flow conditions (BOSE, Minnesota, USA) (Figure 2.4) was used to mimic human blood flow rate and pulsatile flow conditions at 37 °C. The principle of operation is shown schematically in Figure 2.5. Basically, fluid is pumped from a reservoir to a mixing chamber before passing through the sample tube and the volume of fluid is controlled by a piston stroke. A sensor sited in the mixing chamber records changes in fluid pressure. Flow rates from 0-1500ml/min can be applied.

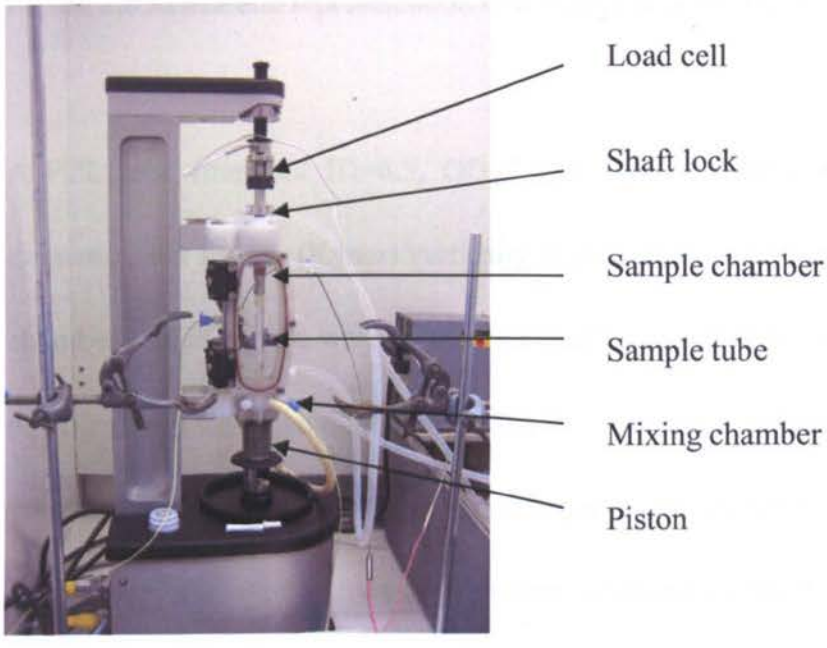

Figure 2.5 The Bose-Enduratec biodynamic chamber

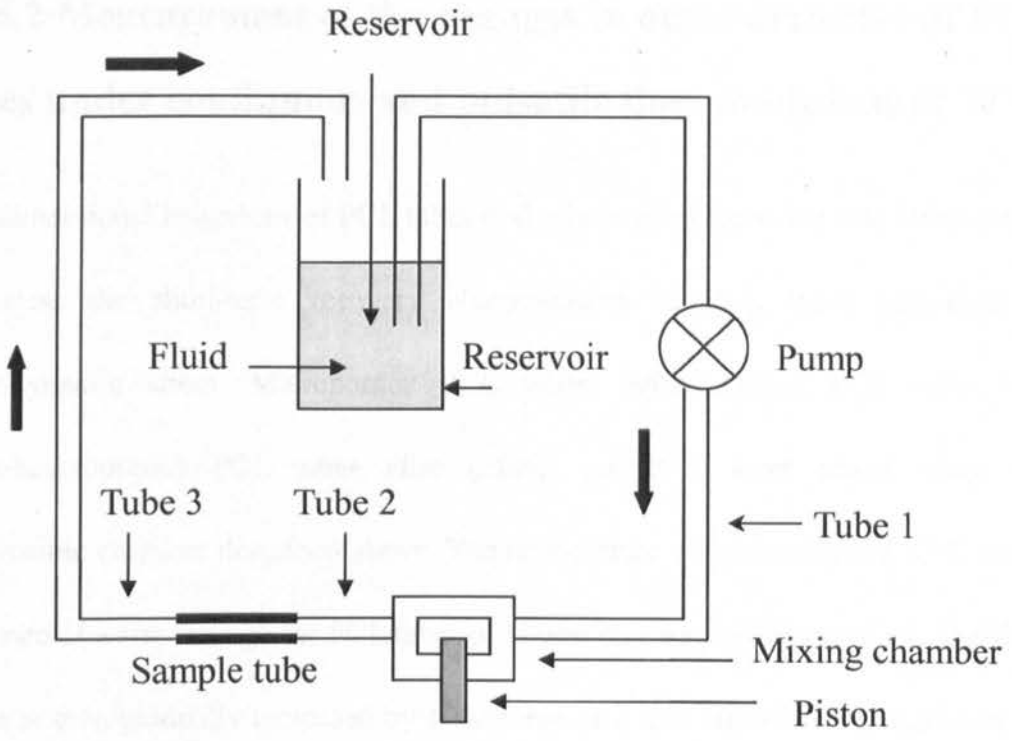

Figure 2.6 Schematic representation of a biodynamic chamber

A PCL tube (nominal ID=6.5, OD=7.5, length= 60 mm) was mounted on 6mm diameter Luer fittings (Kynar) vertically in the center of the biodynamic chamber. The chamber and PCL tube were filled with distilled water at 37 °C. A constant flow rate of 300ml/min was maintained inside the PCL tube to simulate flow conditions in the vasculature using a computer controlled pump. At the same time, a laser scanning micrometer was used to measure the outer diameter of the PCL tubes at 1 scan per second intervals over 1 hour. Data were recorded and analysed using Labview 8.0 (National Instruments, US). Samples of microporous PCL tubes, gelatin-loaded PCL tubes and micro/macroporous PCL tubes following gelatin extraction were tested in triplicate.

2.15.2 Measurement of the changes in outer diameter of PCL tubes under continuous and pulsatile flow conditions at 37°C

The dimensional behaviour of PCL tubes under increasing flow rate was investigated to assess the short-term recovery characteristics of PCL tubes subjected to hydrodynamic stress. Microporous PCL tubes, gelatin-loaded PCL tubes and micro/macroporous PCL tubes after gelatin extraction were tested using the biodynamic chamber described above. The temperature was controlled at 37°C and a flow rate of water through the PCL tubes of 100ml/min was initially applied. The flow rate was then gradually increased by 100ml/min at 2 min intervals to a maximum of 1000ml/min. After 2 minute at 1000ml/min, the flow rate was reduced to the initial flow rate of 100ml/min and the test was repeated two more times. The changes in outer diameter of the tubes (dilation) under increasing flow rate were recorded using a Mitutoyo LSM 301 laser scanning micrometer at 10 scans/sec and analysed by computer program.

Steady state flow of a fluid through a straight tube can be described by Poiseuille's law

$$\Delta p = \frac{8\eta L}{\pi a^4} Q$$

This states that there will be pressure drop, ΔP along the length of the tube, L. which is directly proportional to the flow rate Q (ml/s) and the viscosity of the fluid, η (Pa.s) and inversely proportional to the fourth power of the tube radius. Due to the pressure

drop along the tube, laser scanning micrometer was positioned to measure the outer diameter at the mid section of the PCL tube.

A wall shear stress, σ_w is generated in the tube under fluid flow conditions defined according to:

$$\sigma_w = \frac{4Q\eta}{\pi a^3}$$

σ_w is inversely proportional to the cube of the tube radius.

2.15.3 Investigation of the burst strength of PCL tubes at room temperature and 37°C

The burst strength of microporous PCL tubes was investigated under hydrostatic conditions using the test set-up shown in Figure 2.7. PCL tubes (55mm long, outer diameter 7.5mm, internal diameter 6.5mm) filled with distilled water were immersed horizontally in a water bath retained at 25°C or 37°C. Silicone elastomer tubing was used to connect one end of the PCL sample tube to the pressure system via a clamp. Another length of silicone tube was used to seal the other end of the PCL tube. A pressure of 102,400Pa was applied initially to the sample tube following temperature equilibration and increased at a rate of 50-100Pa/sec until the burst point of the PCL tube. Samples of microporous PCL tubes, gelatin-loaded and micro/macroporous PCL tubes produced by gelatin extraction were tested in triplicate to determine the mean burst strength. The change in tube diameter with increasing pressure was measured using a Mitutoyo LSM 301 laser scanning micrometer at a scan speed of 10 scans/sec.

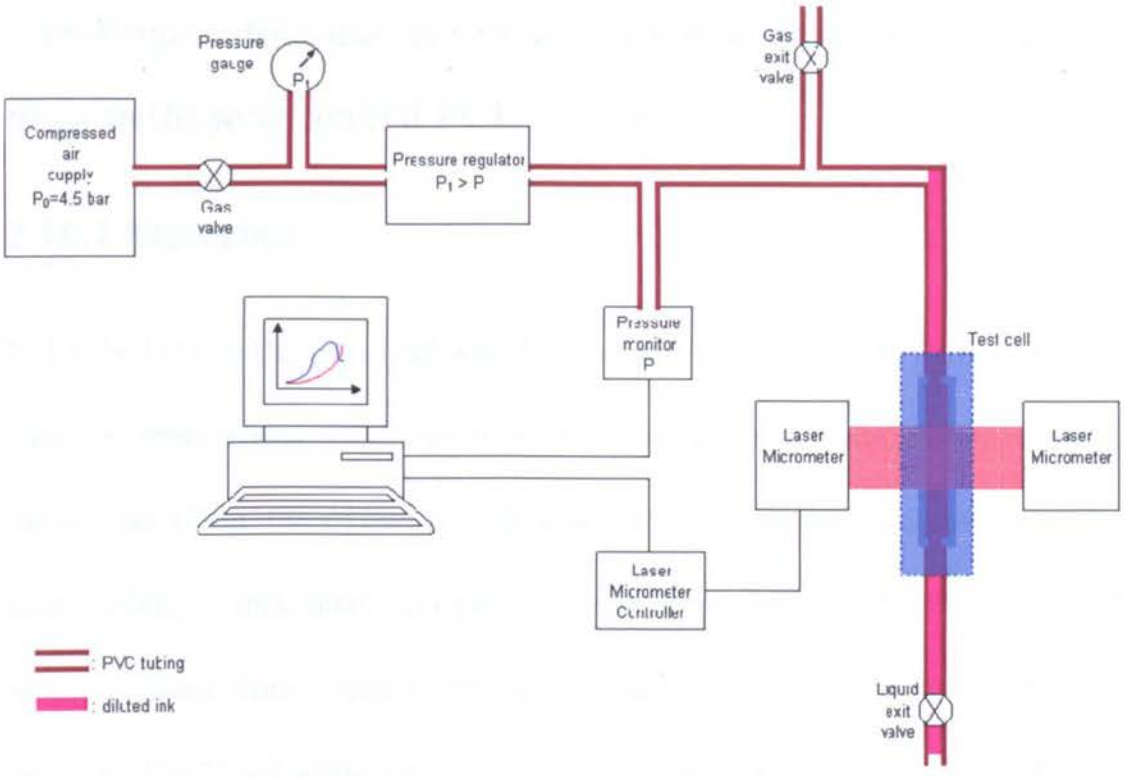

Figure 2.7 Schematic representation of the test facility used for burst testing PCL tubes.

2.15.4 SEM examination of the fracture surface of PCL tubes

The fracture surface after burst testing of microporous PCL tubes, gelatin-loaded tubes and micro/macroporous PCL tubes (formed by particle extraction was examined using a ZEISS EVD 50 (Germany) scanning electron microscope. Samples were attached to aluminum SEM stubs using carbon tabs and sputter coated with platinum using an Edward E30GA automatic mounting press prior to examination in the SEM at a voltage of 10 kV.

2.16 Preparation and characterisation of enzyme-loaded and dexamethasone-loaded PCL matrices

2.16.1 Materials

PCL (*M*w 115,000 Da, Capa 650) was obtained from Solvay Interox, Warrington, UK. Catalase (from bovine liver), lysozyme (from chicken egg white, 50400 unit/mg), collagnease (from *Clostridium histolyticum*), Dexamethasone, phosphate buffered saline (PBS), bicinchoninic acid (BCA) reagents and QuantiPro™ BCA assay kit were purchased from Sigma Chemicals Company, UK. Collagenase substrate kit (code no. 27670), anhydrous citric acid, calcium acetate, nihydrin, 2-methoxyethanol, tin (II) chloride dehydrate, acetic acid and 1-propanol were purchased from Fluka, UK. Lysozyme assay kit (VXE22013), acetone, dichloromethane (DCM), ethanol and methanol were obtained from Fisher Scientific, UK.

2.16.2 Preparation of lysozyme-loaded PCL matrices

Lysozyme-loaded microporous PCL matrices were prepared by rapid cooling in dry ice as described in Section 2.2. Lysozyme crystal particles (insoluble in acetone) were ground to small particulates and dispersed in a 17% w/v PCL solution to produce a 10, 20 or 40% w/w enzyme-loaded PCL suspension, respectively. The lysozyme suspension was then poured into a PP mould designed to produce a tubular casting (OD= 7.5 mm, ID= 6.5mm length= 55mm) and cooled in dry ice for 2-3 min to allow crystallization and hardening of the PCL phase.

2.16.3 Measurement of the lysozyme content of PCL matrices

Samples approximately 100mg were cut from tubes of lysozyme-loaded PCL matrices and accurately weighed. Samples were dissolved in 1ml dichloromethane (DCM) and 9ml PBS was added to precipitate the PCL polymer. The sample was sonicated for 30min to assist extraction of lysozyme into the PBS phase before shaking overnight on a Vibrax VXR system to evaporate DCM. The lysozyme concentration in PBS was determined by BCA total protein assay and compared with a calibration curve constructed using a series dilution of lysozyme in PBS (200-1000μg/ml). The enzyme loading of the matrix was subsequently calculated as % w/w and used to assess the influence of loading uniformity of the matrix and the influence of lysozyme content of the matrix on enzyme release rate.

2.16.4 In vitro release of lysozyme from PCL matrices

Accurately weighed samples of PCL matrices loaded with lysozyme powder in various loading percentages were retained in 10ml PBS at 37 °C in a water bath. At 1 day intervals, the release medium was removed completely and replaced by fresh PBS. The amount of lysozyme in the release medium was analysed after 24h and then every 2 days up to 12 days using the BCA assay and expressed as cumulative release (%) versus time.

2.16.5 Analysis of lysozyme activity

Lysozyme activity was evaluated using the EnzChek® Lysozyme Assay kit. This fluorescence-based assay is based on a modified *Micrococcus lysodeikticus* assay. Lysozyme activity reduces the quenching, yielding a dramatic increase in the fluorescence caused by labeled *Micrococcus lysodeikticus* cells, the increase is proportional to lysozyme activity.

Lysozyme stock solution (1000U/ml) was prepared by dissolving 1000U lysozyme from chicken egg white in 1ml of deionized water. DQ™ lysozyme substrate stock was prepared by suspending 1mg fluorescent labeled *Micrococcus lysodeikticus* in 1ml of deionized water (dH_2O). A lysozyme standard curve was prepared by adding 50μl of 0.1M sodium phosphate buffer (pH 7.4) to each of 8 wells of a 96-well microplate followed by addition of 50μl of (1000U/ml) stock of lysozyme solution to the first well. After mixing by pipetting, 50μl of the mixed solution was transferred to the second well. This process was repeated from one well to the next, except that 50μl from the mixture in the seventh well was discarded and no reagents were added to the eighth well. Thus, the lysozyme concentration ranges from 500U/ml to 0U/ml in the final 100 μl volumes. The DQ lysozyme substrate working suspension was prepared by diluting the 1mg/ml stock 20-fold in 0.1M sodium phosphate buffer. For the activity assay, 50 μl of the 50 μg/ml DQ lysozyme substrate working preparation was added to each microplate well which contained the standard samples or experimental (test) samples respectively. After incubating the mixtures at 37 °C for 30 minutes, the

fluorescence absorption was measured at 494nm and fluorescence emission was measured at 518nm.

2.16.6 Investigation of lysozyme activity in control solutions and in the solvents used for PCL matrix formulation

Lysozyme powder was dissolved in PBS (pH 7.4) to produce a 1000U/ml solution as described above (Section 2.16.5) and stored at 20° C or 37° C for 8 hours or 1 week. Lysozyme powder (100mg) was also suspended in 10ml methanol or acetone for 24 hours to simulate exposure to the solvents used in the matrix formulation process. Following methanol or acetone evaporation, lysozyme was redissolved in PBS to produce a 1000U/ml solution. The biological activity of the above solutions was evaluated as described in Section 2.16.5.

2.16.7 Investigation of lysozyme activity following release from PCL matrices

The lysozyme release medium was collected every two days and stored at -20° C prior to activity testing using the fluorescent- *Micrococcus lysodeikticus* assay (Section 2.16.5). Fresh lysozyme solution and lysozyme solution stored at -20° C and 37° C were used as controls.

2.17 Preparation of collagenase-loaded PCL matrices

Collagenase-loaded PCL microporous matrices were prepared by rapid cooling of suspension in dry ice as describe in Section 2.2. Collagenase powder from

Clostridium histolyticum (insoluble in acetone) was dispersed in 17% w/v PCL solution to produce a 10, 20 or 40% w/w enzyme-loaded PCL suspension, respectively. The suspension was then poured into a PP mould and cooled in dry ice for 2-3 min to allow crystallization and hardening of the PCL phase.

2.17.1 Measurement of collagenase content in PCL matrices

Three samples from the top, mid-region and base of collagenase-loaded PCL tubes were each dissolved in 1ml dichloromethane (DCM) and 9ml PBS were added to precipitate the PCL polymer. The sample tube was shaken for 30 minutes (IKA Vibrax, VXR) to obtain thorough mixing of DCM and PBS and left overnight to evaporate DCM. The concentration of collagenase in PBS was determined using the BCA total protein assay by comparison with a calibration curve constructed using a series dilution of collagenase in PBS (200-1000 μg/ml). The collagenase loading of the PCL matrices was subsequently calculated as % w/w.

2.17.2 In vitro release of collagenase from PCL matrices

Samples of collagenase-loaded PCL matrices (approximately 100mg) were accurately weighed and immersed in 5 ml PBS at 37°C for 20 days. The release medium was replaced completely by fresh PBS at 1 day intervals and the concentration of collagenase in the samples was determined using a QuantiPro™ BCA assay kit. The amount of collagenase release was calculated using a calibration curve as described above Section 2.17.1 and expressed as cumulative release (%) versus time.

2.17.3 Determination of collagenase activity in PBS

Collagenase activity was evaluated using an assay kit based on the collagenase-substrate (carbobenzoxy-Gly-Pro-Gly-Gly-Pro-Ala-OH). The substrate can be hydrolysed in a quantitative manner by collagenase to carbobenzoxy-Gly-Pro-Gly and Gly-Pro-Ala which react with ninhydrin to allow spectroscopic determination.

A stock solution of collagenase (1000μg/ml) was prepared by dissolving 50mg collagenase powder from *Clostridium histolyticum* in 50ml of PBS solution. Citrate buffer A (0.1M pH 6.3) was prepared by dissolving 0.96g citric acid and 79.1mg calcium acetate hydrate in 40ml distilled water and the pH was adjusted with 1N NaOH to 6.3 before dilution to 50ml in total with distilled water. Citrate buffer B (0.2M pH 5.0) was prepared by dissolving 1.92g citric acid in 40ml distilled water and the pH was adjusted to 5.0 with NaOH. Ninhydrin reagent solution was prepared by dissolving 0.2g ninhydrin in 5ml 2-methoxyethanol with 5ml citrate buffer B. Propanol (25ml) was diluted to a final volume of 50ml with distilled water and tin (II) chloride (32mg) dissolved in 2ml 0.1N HCL. Collagenase substrate solution (Component A) was prepared by dissolving 2.4mg carbobenzoxy-Gly-Pro-Gly-Gly-Pro-Ala-OH in 10ml citrate buffer A. Collagenase substrate standard (Component B) was prepared by dissolving 2mg Gly-Pro-Ala in 10 ml citrate buffer A.

Collagenase substrate (carbobenzoxy-Gly-Pro-Gly-Gly-Pro-Ala-OH) solution (0.5ml) and 0.1ml citrate buffer A was added into test tubes, while Gly-Pro-Ala solution in citrate buffer A (0.6ml) was used as a standard. Aliquots (0.1ml) of a series concentration of collagenase solution (100μg-1000μg/ml) in PBS were added to the tubes containing collagenase substrate solution in citrate buffer A. After 5 minutes incubation at 37°C, 0.15ml of the collagenase substrate/collagenase solution mixture was collected and added to a separate tube containing 0.6ml ninhydrin reagent solution and 0.03ml tin (II) chloride solution. The contents were mixed by swirling and heated at 100°C for 15 minutes before cooling to room temperature in a water bath. Finally, the UV/Vis absorption of the mixture (0.2ml) with added 50% propanol solution (1ml) was measured at 565nm using spectrophotometer (Hitachi U2000).

2.17.4 Investigation of collagenase activity in control solutions and in the solvents used for PCL matrix formulation

Collagenase powder was dissolved in PBS (0.1mM pH 7.4) to give a concentration of 1mg/ml and stored at 37°C or -20°C respectively for 8 hours or 2 weeks. The biological activity of collagenase in PBS was examined every two days to provide a control for comparison of the activity of collagenase released from PCL matrices.

In addition, collagenase powder (1mg) was exposed to 5ml acetone and 5ml methanol respectively for 24 hours, followed by drying under vacuum for 24-48 hours. The dry

powder was redissolved in PBS to produce a 1mg/ml solution and the bioactivity of collagenase was subsequently measured to investigate the effect of powder exposure to the solvents used in matrix fabrication.

2.17.5 Investigation of collagenase activity following release from PCL matrices

The PBS medium containing collagenase released from microporous PCL matrices was collected every day and stored immediately at -20°C prior to testing. Enzyme activity was measured as described in Section 2.17.3. Measurements were performed in triplicate for each sample of release medium and the mean was calculated.

2.18 Preparation of catalase-loaded PCL matrices

Catalase powder was ground to fine particles using a glass pestle and mortar and catalase-loaded PCL matrices in tubular form were produced as described above for lysozyme-loaded matrices (Section 2.16.2).

2.18.1 Measurement of catalase content in PCL matrices

Samples approximately 100mg were cut from tubes of catalase-loaded PCL matrices and accurately weighed. Samples were dissolved in 1ml dichloromethane (DCM) and 9ml methanol was added to precipitate PCL. The sample tube was sonicated for 30min to assist extraction of catalase into methanol before shaking overnight on a Vibrax VXR system to evaporate DCM. The resulting catalase solution in methanol was added to PBS solution in the ratio 10% v/v. The catalase concentration in

PBS/10% methanol was determined by BCA total protein assay and compared with a calibration curve constructed using a serious dilution of catalase in PBS/methanol (200-1000μg/ml). The enzyme loading of the matrix was subsequently calculated as % w/w and used to assess the influence of loading uniformity of the matrix and the influence of catalase content of the matrix on enzyme release rate.

2.18.2 In vitro release of catalase from PCL matrices

Three samples of catalase-loaded PCL matrices (approximately 100mg) were cut from tubular mouldings having a specific enzyme loading and accurately weighed. Each sample was placed in 10ml PBS solution at 37° C in a water bath for 12 days. The complete release medium was collected and replaced with fresh PBS at 1 day intervals. The BCA total protein assay was used to determine the concentration of catalase in the release medium. The catalase release amount was calculated by comparison with a calibration curve constructed using a series dilution of catalase in PBS (200-1000μg/ml) and expressed as cumulative release (%) versus time.

2.18.3 Analysis of catalase activity in PBS (control solution)

A series concentration of catalase in PBS (20-50μg /ml) was prepared by dissolving 10-25mg of catalase in 50ml of pH 7.4 PBS followed by 10 times dilution. The effect of enzyme concentration on catalase activity was subsequently determined over 8 hours and 12 days storage. The catalase solution was filtered using a PVDF syringe filter (0.2μm, Whatman, UK) to produce a sterilized catalase stock. The UV

absorbance at 405nm of fresh catalase solution was determined using a spectrophotometer before storage at -20 °C or 37 °C. The biological activity of catalase in PBS was measured every 1 hour or 2 days to provide a control for comparison of catalase activity on release from microporous PCL matrices.

The substrate for assay of catalase biological activity was prepared by diluting 140μl of 30% H_2O_2 into 100ml of 0.05M phosphate buffer solution. The absorbance of the substrate at 240nm was between 0.52 and 0.55. For the catalase activity assay, the spectrophotometer was pre-warmed at 25°C for 30min and the wavelength was set at 240nm. Substrate (2.9ml H_2O_2 in PBS) was placed in a UV cuvette and incubated in the spectrophotometer at 25°C for 3-4min to reach temperature equilibration. An aliquot (100μl) of the diluted enzyme solution was added to the UV cuvette containing the substrate and allowed to mix immediately. The initial absorbance at 240nm (A_{240}) was found to exceed 0.45. The required function time (Δt) was recorded when A_{240} decreased from 0.450 to 0.400. A standard curve was constructed by plotting the reciprocal of Δt (min^{-1}) versus enzyme concentration for standard solutions (20-50 μg/ml).

2.18.4 Investigation of catalase activity under matrix formulation conditions and following release from PCL matrices

The PBS medium containing catalase released from PCL matrices was collected every

1 hour or at 1 day intervals and the enzyme activity was analysed using the H_2O_2 method as described above (Section 2.18.3). Measurements were performed in triplicate for each sample of release medium and the mean was calculated.

Catalase powder (1mg) was suspended in 5 ml acetone, 5 ml ethanol or 5 ml methanol for 24h, followed by drying under ambient conditions for 24h. The powder was redissolved in PBS to produce a 50μg/ml solution and activity of catalase was subsequently measured to investigate the influence of powder exposure to the solvents used in matrix production.

2.19 Preparation of dexamethasone-loaded PCL matrices

PCL (1.25g) was dissolved in 10ml acetone with gentle heating to produce a 12.5% w/v solution. Dexamethasone (62.5 or 125mg) was dissolved in 10ml of a 12.5% PCL solution to give a concentration of 5% and 10% (w/w) respectively. Aliquots (3 ml) were poured into a 5ml polypropylene syringe body and allowed to stand at room temperature for 30 minutes. Methanol (3 ml) was added slowly into the syringe to form a layer on top of the PCL/dexamethasone solution. The samples were retained at room temperature for 24-48 hours to produce initial hardening of the PCL matrices by polymer precipitation and the dexamethasone-containing microporous PCL matrices were allowed to dry in the mould by solvent evaporation under ambient conditions.

2.19.1 Determination of dexamethasone content in PCL matrices

Disks of dexamethasone-loaded PCL matrices (9mm diameter, approximately 2mm thick) with a theoretical 5 or 10% w/w drug loading were cut from various locations along the length of the moulding and accurately weighed. Each disk was initially dissolved in 0.5 ml DCM. Methanol (9.5ml) was added to precipitate the PCL and to act as a receiver phase for the steroid. Sample tubes were shaken for 30 minutes (IKA Vibrax, VXR) to obtain thorough mixing of DCM and methanol and left overnight to evaporate DCM. The concentration of dexamethasone in the methanol phase was determined by measuring the UV absorbance at 236 nm (Unicam Helios Beta scanning UV-Vis spectrometer) and comparing this with a calibration curve constructed using a series dilution of the steroid in methanol (10-30 μg/ml). The steroid loading of the PCL matrix was subsequently calculated as % w/w.

2.19.2 In vitro release of dexamethasone from PCL matrices

Three disks of dexamethasone-loaded PCL matrices (30mg) were each placed in closed polypropylene tubes containing 10 ml of PBS (pH 7.4). Samples were retained at 37 ^{o}C in a water bath. At 4 hour time intervals over 8 days, the release medium was removed completely and replaced with fresh medium. The steroid concentration in the release medium was obtained by measuring the UV absorbance at a wavelength of 236nm and comparing this with a calibration curve constructed using a series dilution of dexamethasone in PBS (10-30μg/ml).

2.19.3 Thermal analysis of enzyme-loaded and dexamethasone-loaded PCL matrices

The thermal behavior of enzyme-loaded PCL matrices prepared by the rapid cooling method or dexamethasone-loaded PCL matrices produced by precipitation casting was investigated using a TA instrument DSC2920. Samples (minimum 5mg) were sealed in aluminum pans and programme-heated from 0°C to 90°C at a rate of 10°C/min. The percentage crystallinity was estimated using a value of 139.5 J/g for fully crystalline PCL [186].

2.19.4 SEM investigation of surface morphology of enzyme-loaded and dexamethasone-loaded PCL matrices

The morphology of catalase, lysozyme, collagenase or dexamethasone-loaded PCL matrices before and after release was examined using a ZEISS EVD 50 (Germany) scanning electron microscope (SEM). Specimens were mounted on aluminum sample stubs and sputter-coated with platinum using an Edward E30GA automatic mounting press prior to examination in the SEM at a voltage of 15 kV.

Chapter 3

Formulation and characterisation of polycaprolactone-based matrices for protein delivery and soft tissue engineering

3.1Formulation of PCL matrices by low temperature casting

Microporous PCL matrices in the form of thick-section cylinders, tubes and ring-shaped inserts (Figure 3.1) were produced by rapid cooling in dry ice, solutions of polycaprolactone (PCL) in acetone, followed by solvent extraction from the hardened material using methanol. The process stages involve: 1) addition of PCL solution in acetone to a PP mould 2) The mould is placed in dry ice for 2-5 min. 3) Removed of the hardened matrix from the mould 4) Immersion of the hardened matrix in methanol or ethanol (non-solvent) normally for 24 hours 5) Air drying of the matrix until the diameter and weight are constant. The PCL matrix may also be retained in or outside the mould to allow solvent evaporation in air, but this approach results in distortion of the material.

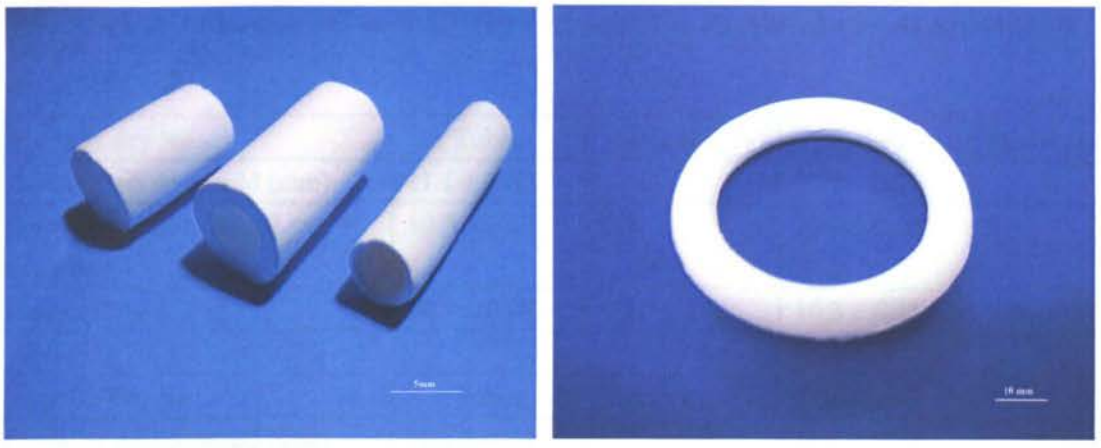

Figure 3.2 Microporous PCL matrices in the form of cylinders, tubes, and ring-shaped insert

The dried castings present a soft textured, porous and highly flexible character, free of large scale cracks and voids in the surface and interior. Cylindrical matrices prepared from 17% w/v PCL solutions were characterized by diameters of 8.5-10mm depending on the mould size and a density of 0.27 g/cm^3 (Table 3.1). As shown in Figure 3.2, the temperature of a 17% w/v PCL solution in acetone, when placed in dry ice, decreases rapidly at the rate of 10°C per 30sec and tends to reach a constant value of around -78°C normally after 5min (Figure 3.2). Increasing the cooling time in dry ice from 2 min to 10 min results in higher percentage shrinkage of PCL matrices after air drying (Table 3.1). This behaviour may be explained by restricted growth of PCL crystals at low temperature which increases the number of polymer 'tie' chains excluded from the crystals. Chain recoiling on drying subsequently results in increased shrinkage.

Table 3.1 – Influence of cooling time in dry ice on shrinkage of unloaded-PCL matrices

2 min in dry ice	Tubes	Shrinkage (%)	Cylinders	Shrinkage (%)
Diameter on de-mould (mm)	11.1 ± 0.05		11.1 ± 0.05	
Diameter after methanol treatment	10.9 ± 0.12	2.4	10.9 ± 0.05	2.4
Diameter on drying	10.3 ± 0.05	7.2	10.3 ± 0.11	7.4

5 min in dry ice	Tubes	Shrinkage (%)	Cylinders	Shrinkage (%)
Diameter on de-mould (mm)	11.1 ± 0.56		11.1 ± 0.11	
Diameter after methanol treatment	10.9 ± 0.06	2.4	10.9 ± 0.05	1.8
Diameter on drying	10.1 ± 0.11	9.6	9.9 ± 0.22	11.3

10 min in dry ice	Tubes	Shrinkage (%)	Cylinders	Shrinkage (%)
Diameter on de-mould (mm)	11.1 ± 0.05		11.1 ± 0.12	
Diameter after methanol treatment.	10.8 ± 0.11	3.3	10.4 ± 0.11	6.7
Diameter on drying	10.0 ± 0.12	10.1	9.9 ± 0.06	10.5

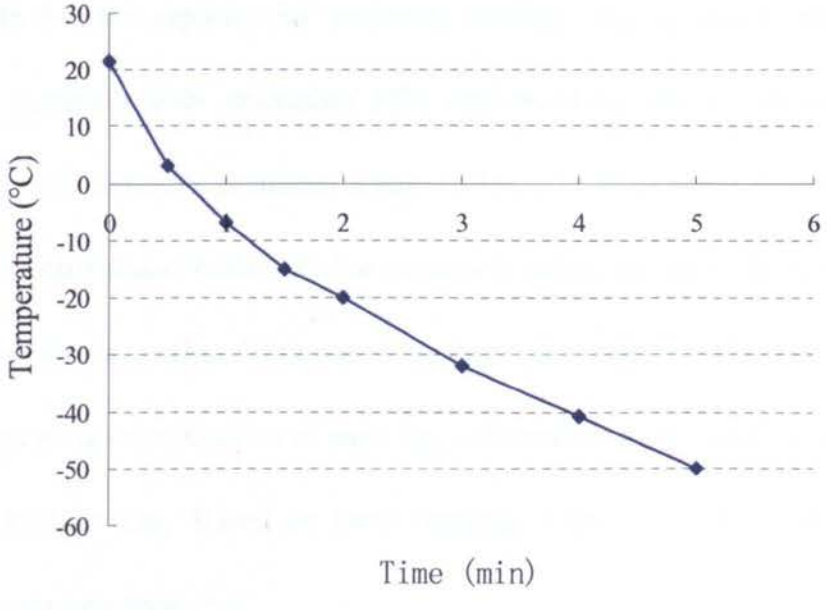

Figure 3.2 Temperature profile of PCL solution in acetone on immersing in dry ice

3.2 Effect of PCL solution concentration on particle loading

The effect of PCL solution concentration on particle loading was investigated using 12.5%, 15% and 20% (w/v) PCL solutions in acetone (Section 2.1.5). Low concentration PCL solutions (2.5% and 5% w/v) were also investigated at the beginning of this study, but hardened PCL samples were not formed after cooling in dry ice. Only a cloudy suspension was obtained. Gelatin particles were sieved to obtain a specific size range of 125-250 μm and suspended in 12.5%, 15% and 20% (w/v) PCL solutions respectively to produce three separate percentage loadings (28.6%, 37.5% and 44.4% w/w). Part of this study aimed to investigate the effect of PCL solution concentration on particle distribution throughout the matrix (to determine sample uniformity and to identify any effect on protein release. As shown in Table 3.2, the capacity for uniformly loading large gelatin particles in the PCL matrix increases with increasing PCL concentration which reduces sedimentation effects. PCL matrices produced using 12.5% w/v PCL solution resulted in a poor particle distribution (Table 3.2) due to particle sedimentation in the low viscosity PCL solution prior to casting. With use of medium concentration PCL solutions (15% w/v) and increasing concentration of particles, sedimentation was more apparent at the base of the PCL casting. Based on these findings, 17% w/v PCL solution was used in subsequent investigations.

Table 3.2 Weight distribution of gelatin particles (125-250μm) in PCL matrices produced using 12.5%, 15% 17% and 20% w/v PCL solution

Gelatin loading in PCL solution (% w/w)	Position in matrix	Gelatin loading in matrix (w/w) produced from various concentration PCL solutions (% w/v)			
		12.5	15	17	20
28.6	Top	11.4	20.2	17.5	26.6
	Middle	34.2	22.8	23.1	28.2
	Base	40.1	31.4	28.7	28.5
37.5	Top	22.5	27.5	27.5	33.7
	Middle	37.4	32.6	37.6	37.5
	Base	51.2	48.2	42.5	41.2
44.4	Top	4.5	22.5	35.6	44.1
	Middle	22.1	43.7	39.8	44.6
	Base	87.6	62.1	47.4	44.9

3.3 Morphology of unloaded PCL matrices

SEM examination of unloaded PCL matrices revealed a microporous surface morphology produced by an array of crystalline, lamellar structures giving rise to pores of irregular shape and size of the order of 5-10μm (Figure 3.3). PCL matrices formed using ethanol as non-solvent also showed a highly porous structure with irregular pores of size 5-20 μm (Figure 3.3 B), PCL matrices produced using water to extract solvent revealed a more compact, porous surface morphology with low numbers of smaller pores (< 10μm). PCL matrices produced using water as the non-solvent were distorted on drying due to higher shrinkage compared with materials

prepared using alcohols to extract solvent.

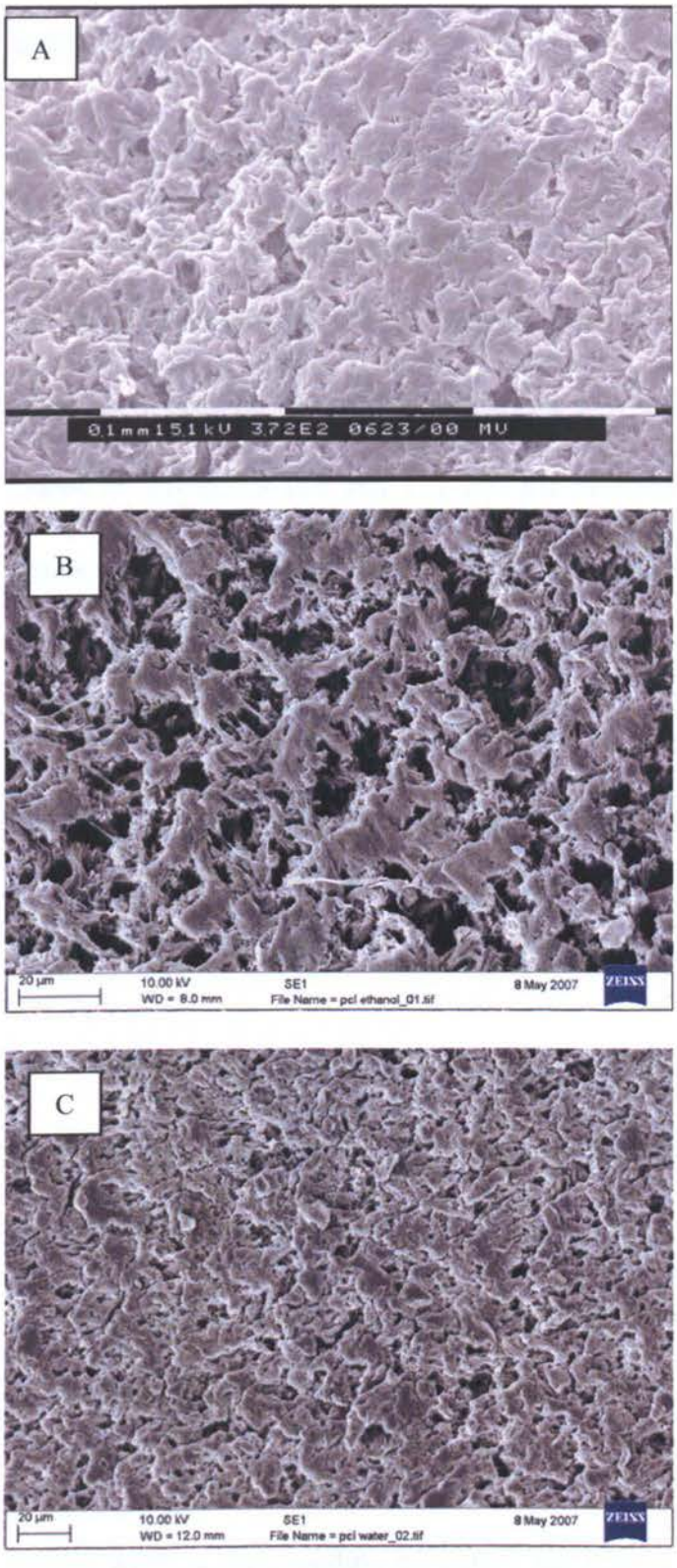

Figure 3.3 Surface morphology of PCL matrices formed using (A) methanol (B) ethanol (C) water as a non-solvent

3.4 Preparation and characterization of lactose-loaded PCL matrices

Lactose, the disaccharide commonly known as milk sugar, has been widely used in the manufacture of pharmaceuticals, such as the carrier material for dry powder inhalation preparations [214]. Lactose (Mw 360.3) is highly water-soluble but insoluble in acetone and methanol. Lactose powder was sieved to obtain particle size ranges of 45-90, 90-125 and 125-250 μm respectively, in order to produce a PCL matrix which would present a defined pore size after lactose solubilisation and extraction. Lactose particles were suspended in PCL solution and mixed well with a glass rod for 1 min, prior to casting in dry ice as described in Section 2. 6. The lactose content of the PCL matrix was measured in distilled water using HPLC as described in Section 2.6.1.

The weight distribution of lactose throughout PCL tubular matrices (OD=7.5mm, ID=6.5mm) produced using various particle size ranges is shown in Figure 3.4. The insolubility of lactose in methanol results in limited loss during formulation. A high proportion of the lactose particle content of the starting PCL solution was measured in the finished casting and a good particle distribution was obtained throughout the material from top to base indicating that sedimentation effects are limited. In the present work, a high loading of lactose particles was obtained by using a 17% w/v PCL solution containing a particle concentration of 29% w/w and various particle size ranges. No significant differences in distribution due to particle sedimentation were

apparent at the base of the PCL matrix with increasing particle size range. This can be attributed to rapid hardening of the suspension in dry ice over 2-3 min, the low density of lactose particles (1.525 g/cm^3 at 25 °C) and the relatively high viscosity of the PCL solution (approximately 300-350 cP) [215] which lowers the particle sedimentation rate.

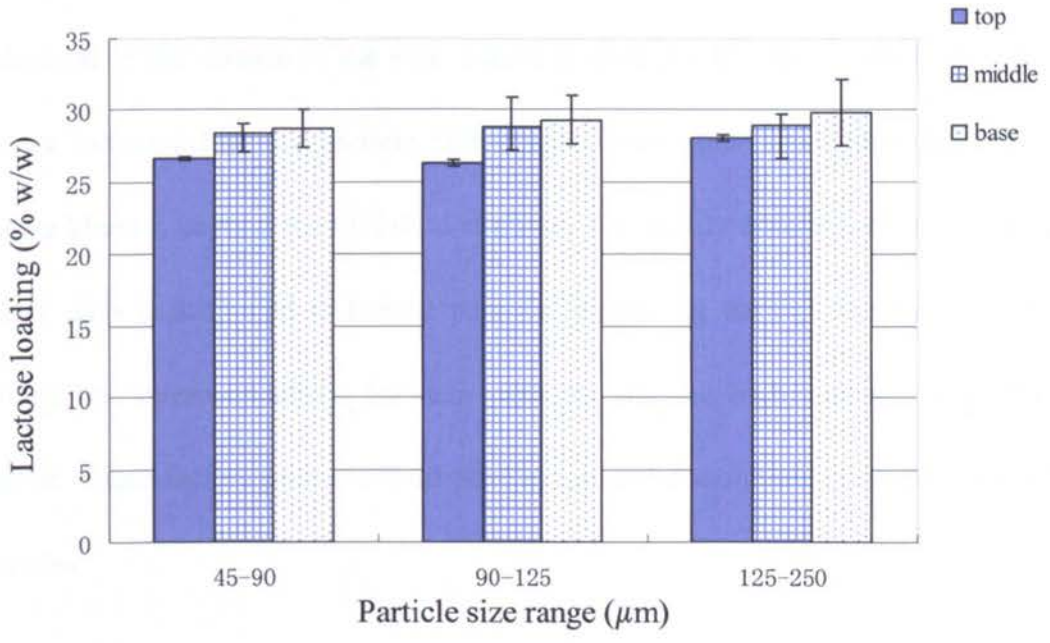

Figure 3.4 The weight distribution of lactose in microporous PCL matrices produced using various particle size ranges (starting suspension loading 29% w/w)

3.4.1 Lactose release from PCL matrices having various particle size ranges

In vitro release of lactose from PCL matrices is rapid as shown in Figure 3.5. Approximately 90% of the original lactose content of the PCL matrices was released over 9 days in PBS at 37°C. The release profiles obtained for each particle size range

were characterized by a major "initial burst" phase during the first 24h, followed by a plateau region after 3-4 days. The release of lactose was particularly rapid in the first day (approximately 75%) when particles in the size range 90-125 μm and 125-250 μm were used. The release amount of lactose in using particles in the size range of 45-90μm was lower (60%) in the first day. Burst release is normally associated with surface located species and could be caused by large amounts of lactose particles embedded in the surface of the PCL matrix (Figure 3.6 B). The similarity in release pattern indicates that the particle size ranges investigated have little influence on release kinetics beyond the initial burst phase. The highly efficient release behaviour over 9 days is attributed to lactose particles protruding through the matrix surface, contact and interconnections between particles and the high aqueous solubility of lactose. These factors promote fluid penetration and dissolution of deeply embedded particles.

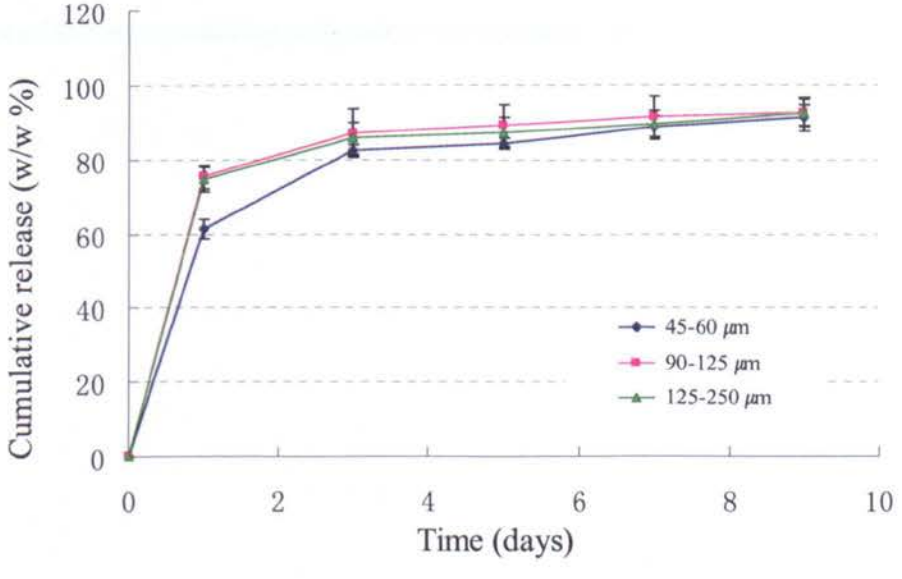

Figure 3.5 Cumulative lactose release from microporous PCL matrices (29% w/w particle loading) containing discrete particle size ranges

3.4.2 Morphology of lactose-loaded PCL matrices

PCL tubular castings exhibited a rough and porous surface morphology with pore sizes below 10 μm and an abundance of lactose particles embedded in and projecting from the surface (Figure.3.6 B). A distinct surface porosity developed after lactose release with irregular pore shape and size (Figure 3.6 C and D). Although the lactose particles used for matrix formulation were in the range of 90-125 μm, the pore size revealed by SEM was confined to the size range 10-20 μm (Figure 3.6 C and D). The surface porosity is likely to be formed by the proportion of fine lactose particles embedded in the surface or protrusion of only part of the larger particles through the matrix surface. These effects will limit surface porosity and exposure of the matrix interior. Lactose particles located within the matrix can be expected to produce similar effects on the surrounding polymer resulting in connections of small dimensions between pores, if the particle loading density, proximity and the wall thickness of the encapsulating polymer permit penetration.

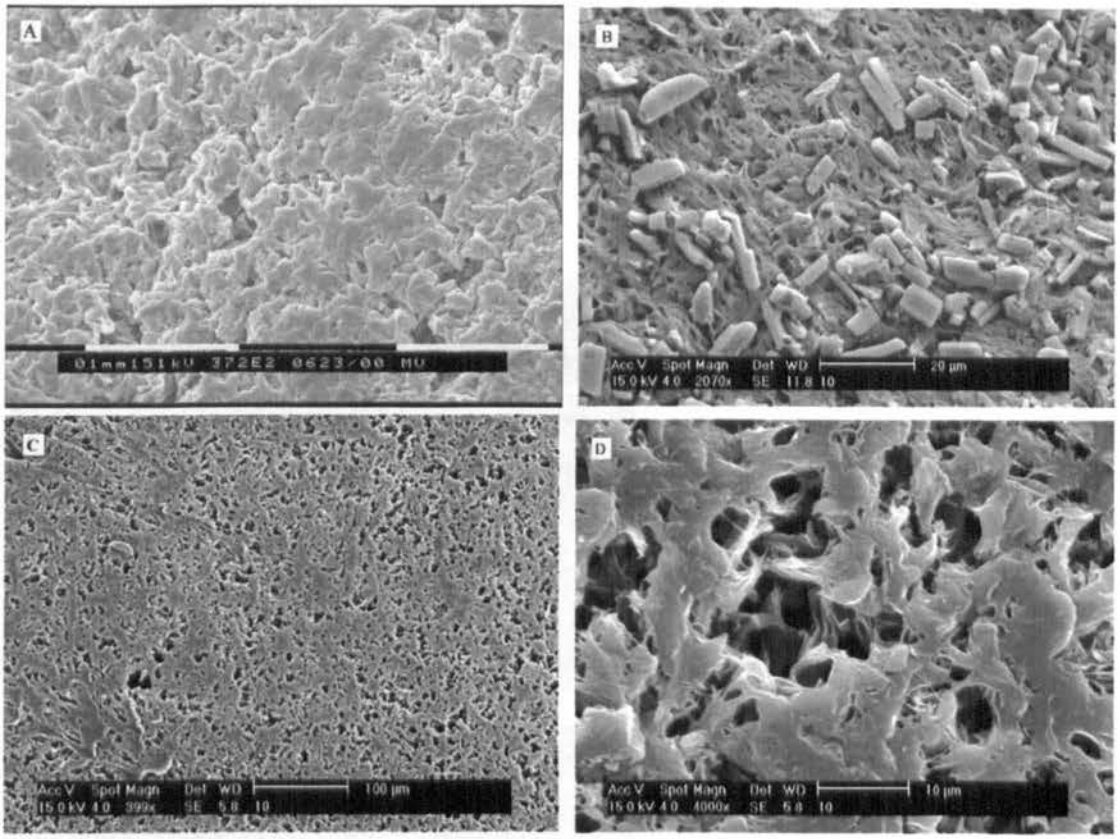

Figure 3.6 Scanning electron micrographs of (A) unloaded PCL matrix (B) Lactose (90-125μm): PCL matrix before release (C, D) Lactose (90-125μm): PCL matrix after release

3.4.3 Morphology of lactose particles before and after matrix formulation

Lactose particles prior to incorporation in PCL matrices exhibited a smooth, trapezoidal form and a fraction of powder fines, 10-20μm in size (Figure 3.7 A). SEM examination of lactose particles recovered from PCL matrices (using DCM to dissolve the polymer as described in Section 2.6.1) revealed particulates made up of aggregates of smaller particles of around 10μm with a more crystalline appearance (Figure 3.7 B

and C). A physical reduction in lactose particle size may occur during preparation of the lactose-PCL suspension and PCL matrix and could be another reason for the small pores in the external surface of PCL matrices following lactose release (Figure 3.6 C and D).

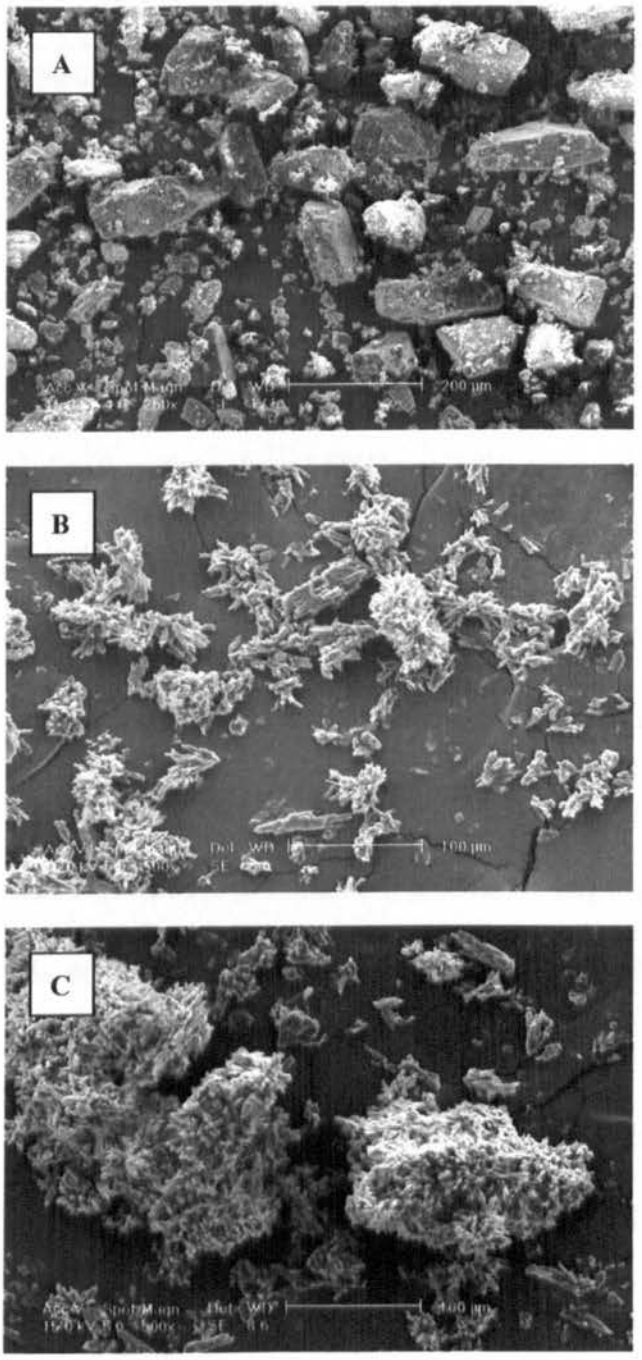

Figure 3.7 Scanning electron micrographs of lactose particles (A) before PCL matrix production (B, C) recovered from PCL matrix

3.4.4 Thermal properties and porosity analysis of PCL and lactose-loaded PCL matrices

Table 3.3 Thermal properties and porosity of PCL matrices and lactose-loaded PCL matrices

Matrix	PCL	Lactose-loaded PCL matrix		
Particle size range (μm)	—	45-90	90-125	125-250
Tm (°C)	68.2	64.9	64.0	66.1
Crystallinity (%)	71.5 ± 0. 7	74.5 ± 1.4	65.9 ± 5.7	74.9 ± 3.7
Porosity (%)	75.5 ± 2.1	74.5± 12.5	76.2±11.2	78.8 ± 8.8

The melting point of PCL matrices and lactose-loaded PCL matrices was, in general, higher than the value of 60°C normally quoted for PCL (Table 3.3). The incorporation of lactose particles in PCL matrices tended to result in a lower Tm compared with unloaded PCL matrices, suggesting the presence of smaller crystallites and/or crystal imperfections. The mean percentage crystallinity of PCL matrices containing intermediate size (90-125μm) lactose particles tended to be approximately 6% lower than PCL matrices containing smaller or larger particle size ranges. The reasons for this effect are unclear at present but may result from the morphology and surface characteristics of the 90-125μm powder fraction, impeding nucleation and growth of PCL crystals. The porosity of PCL matrices, measured using ethanol displacement after lactose release, was similar to unloaded PCL matrices.

3.5 Preparation and characterisation of gelatin-loaded PCL matrices

Gelatin has been used widely to achieve sustained drug delivery and for production of tissue engineering scaffolds (Section 1.7.1). In this study, gelatin was sieved to obtain three particle size ranges (45-90, 90-125 and 125-250μm) and suspended in a 17% w/v PCL solution in acetone prior to matrix formulation as described in Section 2.7. The aim was to investigate the ability of this novel low temperature casting method to produce a 3-D matrix with high particle loading and good particle distribution which would subsequently result in a highly porous material on extraction of the protein phase for cell ingrowth. At the same time, the kinetics of protein extraction would indicate the potential for growth factor release, A third advantage of using gelatin in these investigations concerned the possibility of residual gelatin in the matrix providing cell-adhesion sequences to improve cell attachment to the PCL matrix in tissue engineering.

As shown in Figure 3.8, a high proportion of the particle content of the starting PCL solution was measured in the finished casting and a good particle distribution was obtained throughout the material indicating that sedimentation effects are limited. The particle loading was more uniform throughout the final matrices when gelatin particles in the smaller size range of 45-90 and 90-125μm were incorporated in PCL matrices. This can be explained by the higher weight of the large particles which results in a higher sedimentation rate in the starting PCL solution.

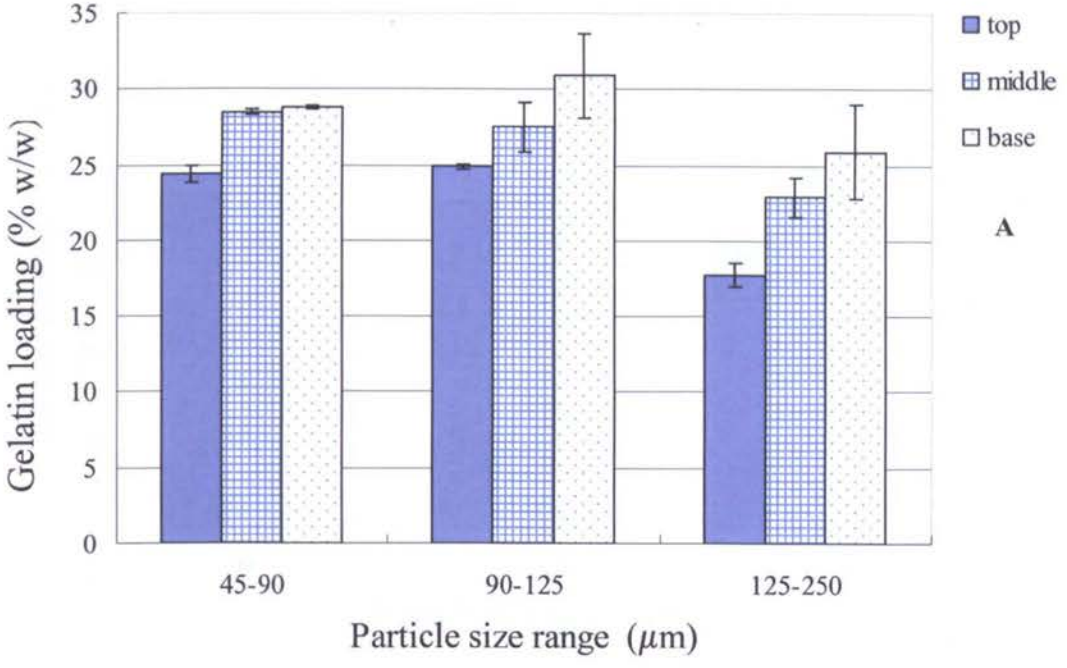
35
30
25
20
15
10
5
0
Gelatin loading (% w/w)
top
middle
base
A
45-90
90-125
125-250
Particle size range (μm)

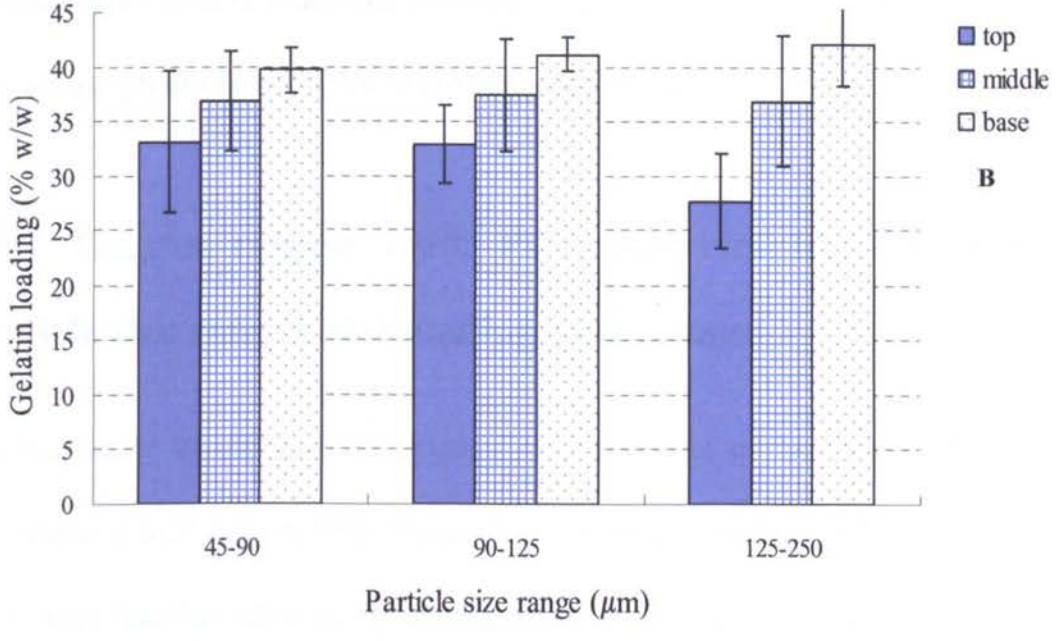
45
40
35
30
25
20
15
10
5
0
Gelatin loading (% w/w)
top
middle
base
B
45-90
90-125
125-250
Particle size range (μm)

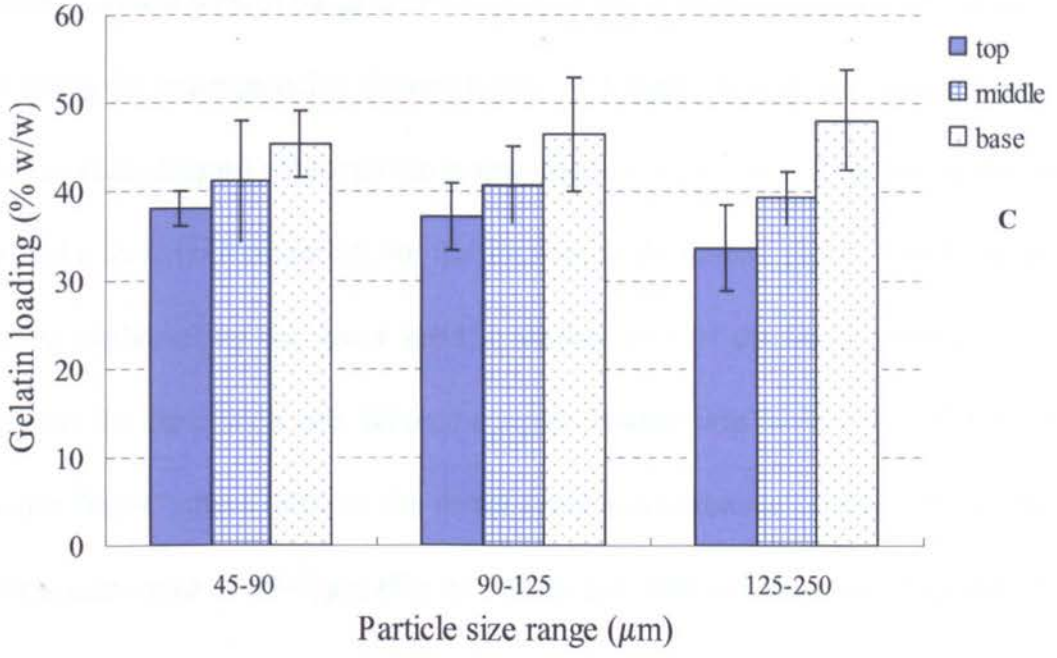

Figure 3.8 The weight distribution of gelatin particles in microporous PCL matrices produced using various particle size ranges (A) matrices prepared from 28.6% w/w particle suspensions (B) matrices prepared from 37.5% w/w particle suspensions (C) matrices prepared from 44.4% w/w particle suspensions

3.5.1 Gelatin release from PCL matrices having various particle size ranges and loading percentages

Approximately 80-100% of the original gelatin content of the PCL matrices was released over 3-21 days in PBS (Figure 3.9). The protein loading and the particle size range were found to influence the amount, duration and pattern of gelatin release. For PCL matrices with the lowest drug loading (28.6% w/w), around 40% of the gelatin content for 45-90 μm particles was released in 24 h, and the remaining protein was slowly and almost completely released over 11 days (Figure 3.9 A). Highly efficient

release of almost 90% of the gelatin load was obtained over 21 days for PCL matrices containing the larger particles. Gelatin-loaded PCL matrices prepared using the largest particles (125-250μm) exhibited the lowest amount of protein release during the first day, and a more uniform profile for the duration of the release period. This behaviour may be explained by the lower specific surface area of the larger particles which decreases the dissolution rate. When the gelatin loading was increased to 37.5% w/w, a major "burst" effect (80% of the initial load) was measured on the first day for a particle size range of 45-90μm (Figure 3.9 B) and 100% of the original gelatin load was released by day 7. Lower burst release (40-50%) and more gradual release of around 85% of the protein load were observed over 11 days for the matrices containing larger particles (90-125 and 125-250μm). With 44.4% w/w protein loading in the matrices, the release profiles obtained for each particle size range were very similar, characterized by a major (80%) "burst" phase during the first 24h and almost 100% protein release in 3 days. The trend of increased protein delivery over a shorter time scale correlates closely with increasing protein content of the matrix and may result from production of a highly interconnected network of pores and channels after protein solubilisation and extraction. These findings demonstrate the potential for controlling the kinetics of protein delivery by varying the matrix formulation conditions.

A

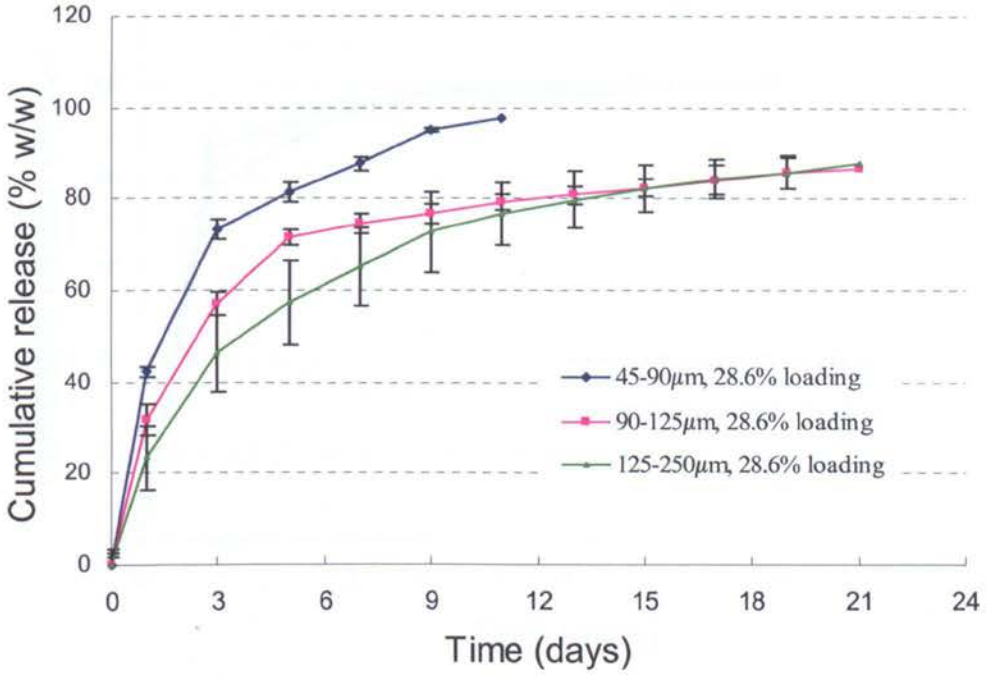
Cumulative release (% w/w)
120
100
80
60
40
20
0
0
3
6
9
12
15
18
21
24
Time (days)
45-90μm, 28.6% loading
90-125μm, 28.6% loading
125-250μm, 28.6% loading

B

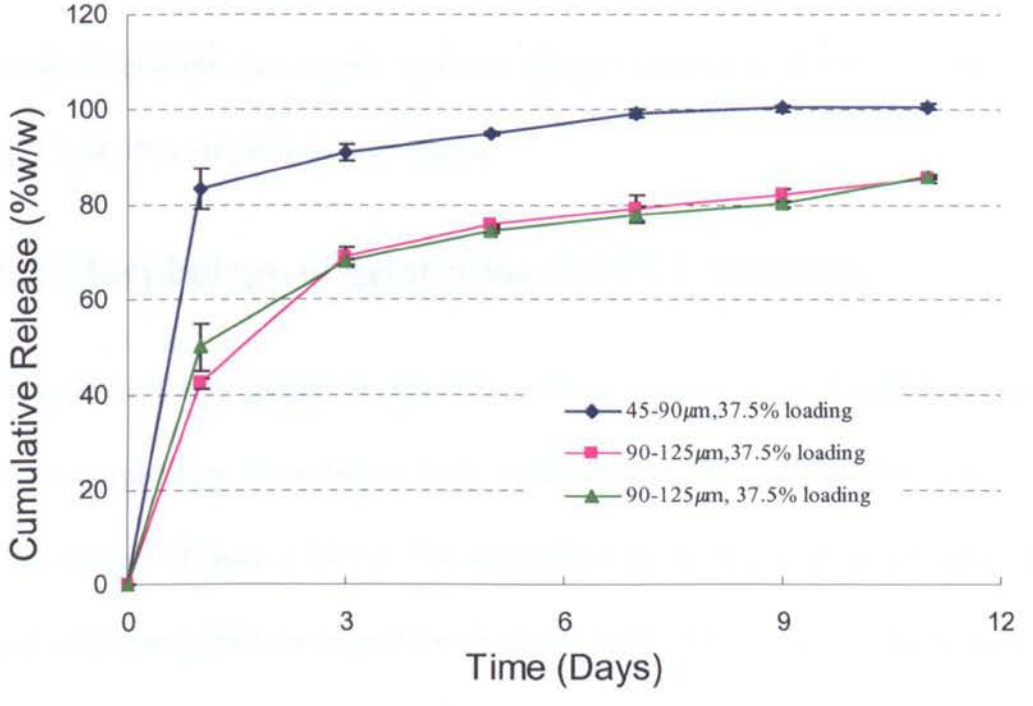
Cumulative Release (%w/w)
120
100
80
60
40
20
0
0
3
6
9
12
Time (Days)
45-90μm,37.5% loading
90-125μm,37.5% loading
90-125μm, 37.5% loading

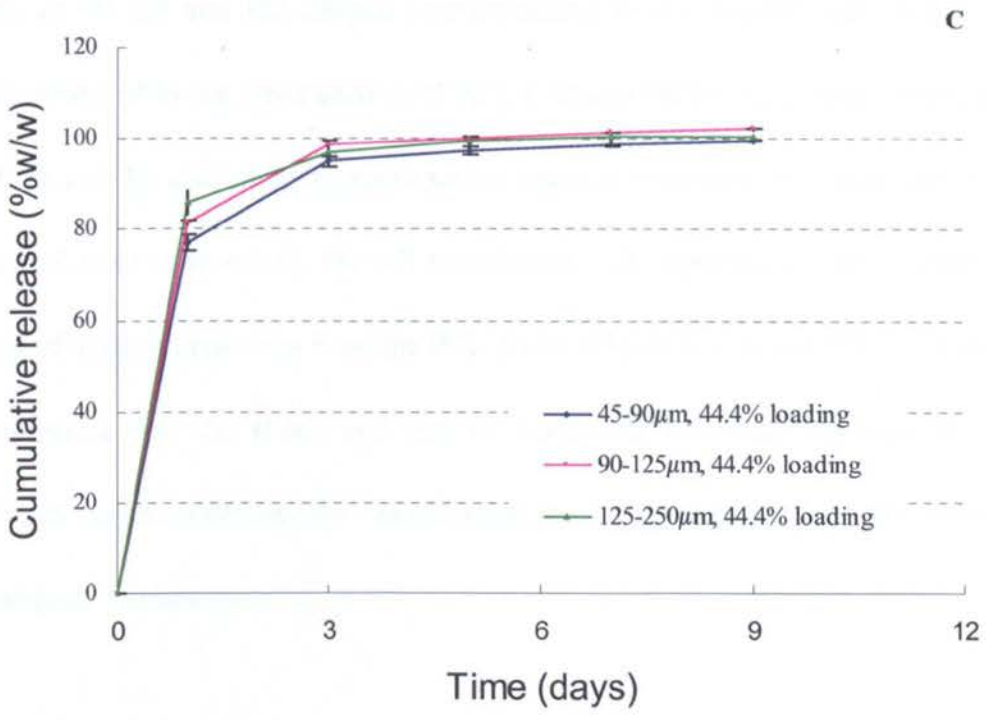

Figure 3.9 Cumulative gelatin release (%) from microporous PCL matrices containing particles of discrete size ranges. Matrices produced from (A) 28.6% w/w (B) 37.5% w/w (C) 44.4% w/w particle suspensions

3.5.2 Morphology of gelatin-loaded PCL matrices

SEM examination of gelatin-loaded PCL matrices revealed a rough and characteristic surface morphology formed by a fairly uniform dispersion of particles close to the matrix surface (Figure 3.10 A). The corresponding microporous and macroporous textures following protein release are shown in Figure 3.10 B and C. Deep pores and surface depressions formed by particle solubilisation are evident in the size range of 125-250μm, which corresponds to the original gelatin particle size. In addition, pores on the surface can be seen to connect with interior pores which is a key objective for controlling growth factor delivery and to promote cell ingrowth. Large pores in the

range of 90-125 and 125-250μm (corresponding to the original particle size range) were observed in the cross section of PCL matrices following gelatin release (Figure 3.10 D and E) indicating a macroporous internal structure with high porosity and potential inter connectivity for cell colonization. Microporosity is also visible in the range of 5-10 μm resulting from the PCL phase (Figure 3.10 C-E). These observations demonstrate that the shape and size of surface and internal macropores in PCL matrices may be controlled by incorporating soluble particles of defined geometry and subsequent extraction.

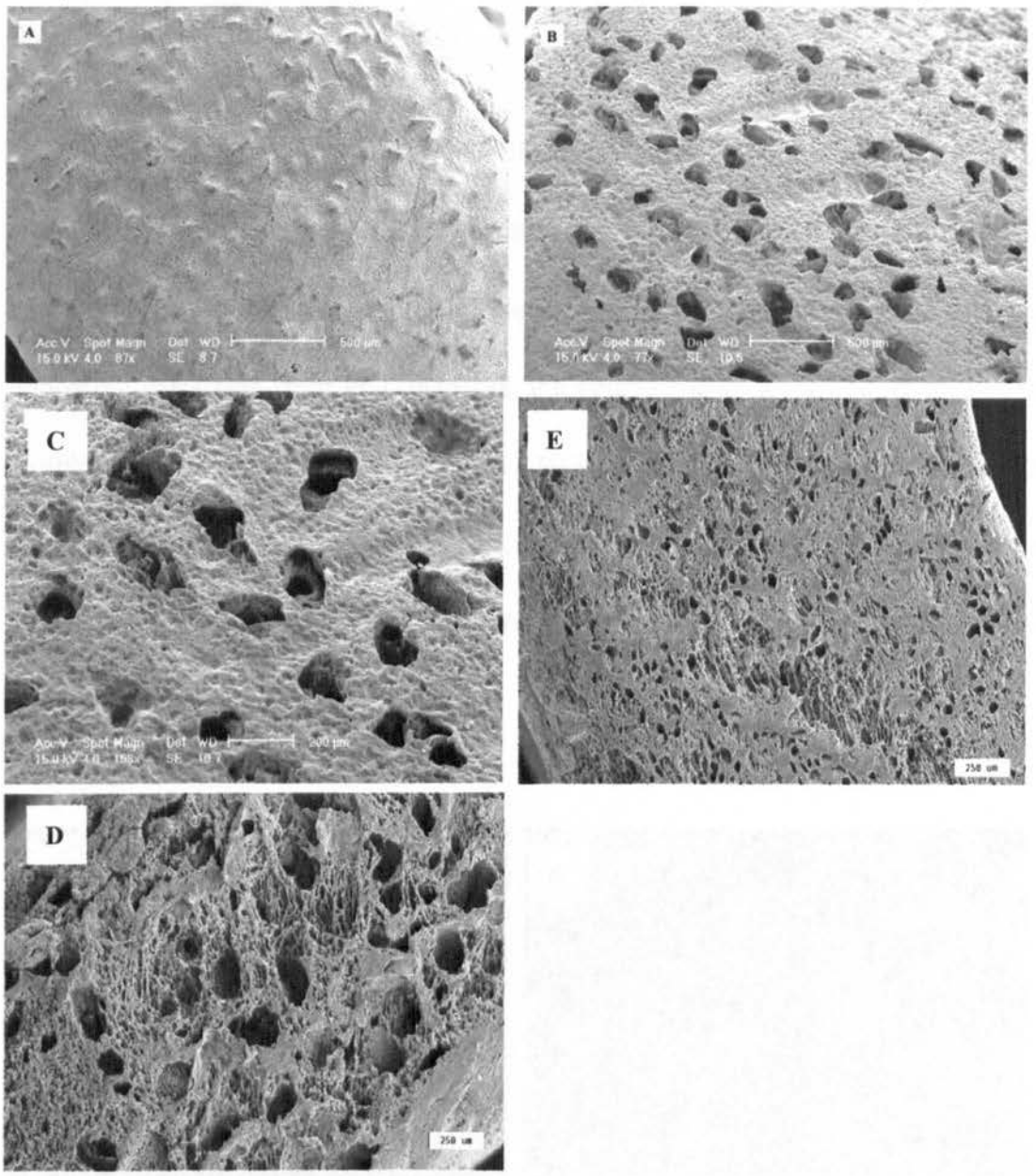

Figure 3.10 Scanning electron micrographs.(A) 28.6% w/w gelatin (125-250μm): PCL matrix before release (B, C) 28.6% w/w gelatin (125-250μm): PCL matrix after release (D) cross section of 44.4% w/w gelatin (90-125μm)-loaded PCL matrix after release (E) cross section of 44.4% w/w gelatin (125-250μm)-loaded PCL matrix after release

3.5.3 Morphology of gelatin particles before and after matrix formulation

Gelatin particles were extracted from PCL matrices using DCM to dissolve the PCL phase as described in Section 2.7.1. Gelatin particles exhibited a smooth and dense morphology and irregular, angular shapes before formulation (Figure 3.11 A). Following extraction from PCL matrices, the gelatin particles showed an unchanged morphology and particle size (Figure 3.11 B) in contrast to lactose particles (Section 3.4.2), This finding demonstrates that PCL matrices produced by rapid cooling in dry ice would result in macropores defined by the shape and size of the original gelatin particles following gelatin extraction.

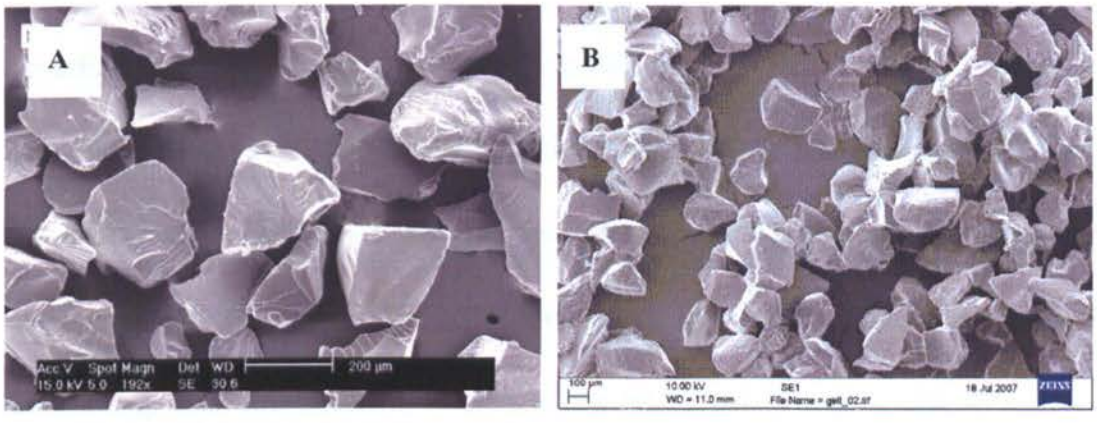

Figure 3.11 Scanning electron micrographs of 125-250μm gelatin particles (A) before PCL matrix formulation (B) following extraction from PCL matrices

3.5.4 Thermal properties and porosity analysis of PCL matricesand gelatin-loaded PCL matrices

Table 3.4 Thermal properties and porosity of PCL tubular castings

Matrix	PCL	Gelatin-loaded PCL matrix		
Particle size range (μm)	_	45-90	90-125	125-250
Tm (°C)	68.2	65.7	65.2	67.5
Crystallinity (%)	71.5 ± 0.7	71.8 ± 5.0	62.6 ± 2.1	72.0 ± 5.6
Porosity (%)	75.5 ± 2.1	73.9 ± 2.4	73.8 ± 10.5	80.8 ± 12.2

The melting point of PCL, and gelatin-loaded PCL matrices was, in general, higher than the value of 60°C normally quoted for PCL (Table 3.4). Incorporation of smaller gelatin particles in PCL matrices tended to result in a lower Tm compared with unloaded PCL matrices, suggesting the presence of smaller crystallites and/or crystal imperfections. The mean percentage crystallinity of PCL matrices containing intermediate size (90-125μm) gelatin particles tended to be approximately 6% lower than PCL matrices and 8% lower than matrices containing smaller or larger particle size ranges. The reasons for this effect are unclear at present but may result from the morphology and surface characteristics of the 90-125μm powder fraction, impeding nucleation and growth of PCL crystals. The porosity of PCL matrices, measured using ethanol displacement after gelatin release, was similar to unloaded PCL matrices.

3.6 Growth of 3T3 fibroblasts on PCL matrices

Swiss 3T3 fibroblasts (2×10^6) (European Collection of Cell Culture) were seeded successfully in 75 cm^2 tissue culture plastic (TCP). After 2 weeks growth, 90% of the

TCP surface was covered by a convergent layer of fibroblasts which displayed the characteristic long, spindle-shaped cell morphology (Figure 3.12). The proliferation rate of 3T3 fibroblasts on PCL matrices produced by extraction of lactose particles of various size ranges and 29% loading is shown in Fig.3.13. The number of attached fibroblasts on PCL matrices and lactose-extracted PCL matrices was similar to TCP on day 1 but lower than TCP by a factor of 2 and 3 at day 5 and 8 respectively. Enhanced cell attachment and proliferation on TCP has been recorded in many studies [216] and is due to the modified surface chemistry developed specifically for cell culture. Lactose-extracted matrices in general exhibit a surface pore size of 10-20μm (Figure 3.6). However, PCL matrices prepared by extraction of 90-125 μm lactose particles resulted in relatively higher fibroblast attachment on day 5 and 8 compared with matrices prepared by extraction of smaller or larger particles. Comparison of fibroblasts growth on microporous PCL scaffold and macroporous PCL scaffold (pore size 45-90, 90-125, 125-250μm) after lactose extraction, shows the cells number growing on PCL scaffold with pores in the range of 90-125μm at day 8 was statistically different from the PCL at the 95% confidence interval. In addition, cell numbers on PCL matrices were lower than on lactose-extracted matrices indicating that a pore size of 10-20μm enhances cell growth, at least over short times in culture.

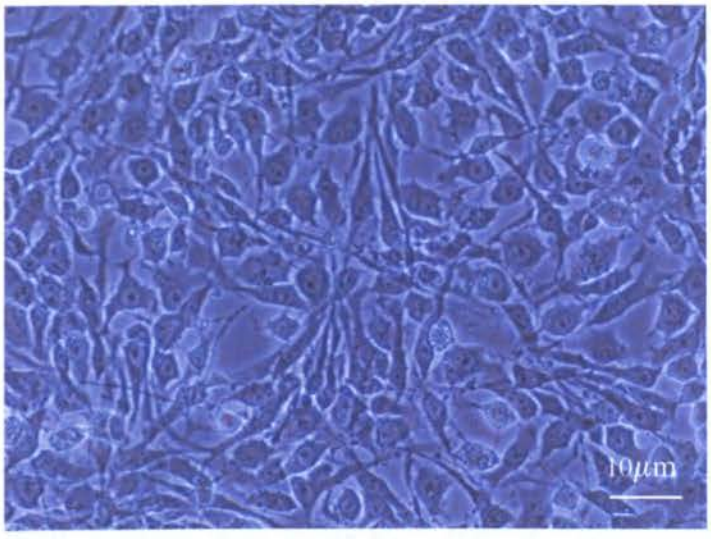

Figure 3.12 Light micrograph of 3T3 fibroblasts cultured on TCP at day 5

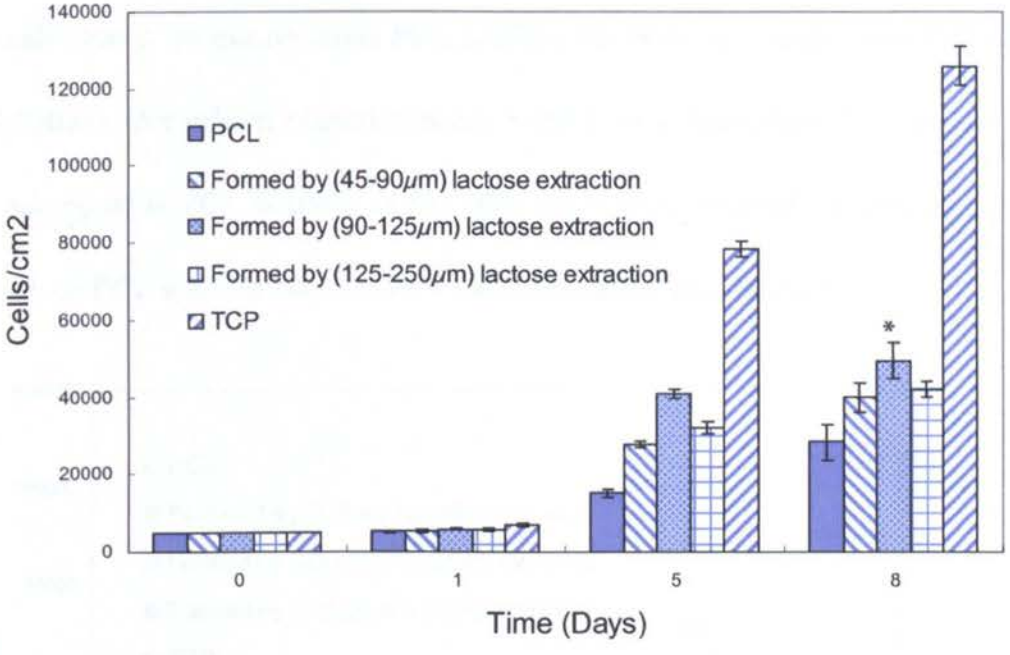

Figure 3.13 Proliferation rates of 3T3 mouse fibroblasts on TCP and porous PCL matrices produced by extraction of lactose particles (* $P<0.05$)

Swiss 3T3 fibroblasts (passage 5) supplied by Dr G. Astrid Limb, University College, London, were seeded in 75 cm^2 tissue culture plastic (TCP). The different cell source from the previous investigation resulted in cell with characteristic morphology but

lower growth rates (90% TCP surface coverage in 3-4 weeks). The proliferation rate of 3T3 fibroblasts on gelatine-extracted PCL matrices is shown in Figure 3.14. No significant difference in the number of attached cells on the various porous PCL matrices were observed at day. Higher cell numbers were recorded on PCL matrices having a pore size range of 90-125μm at day 5 and 8 compared with PCL matrices produced by extraction of smaller (45-90μm) and larger gelatin particles (125-250μm). (Cell numbers were lower by 1-5000 on gelatin-extracted matrices compared with lactose-extracted matrices at each culture time point). The paired t-test showed that the cell growth on macroporous PCL scaffold has pore size range from 45-90μm to 125-250μm after geltion extraction at day 5 and 8 were statistically different from that on microporous PCL scaffold at the 99% confidence interval, suggesting residual gelatin on PCL scaffold after delivery can enhance cell proliferation.

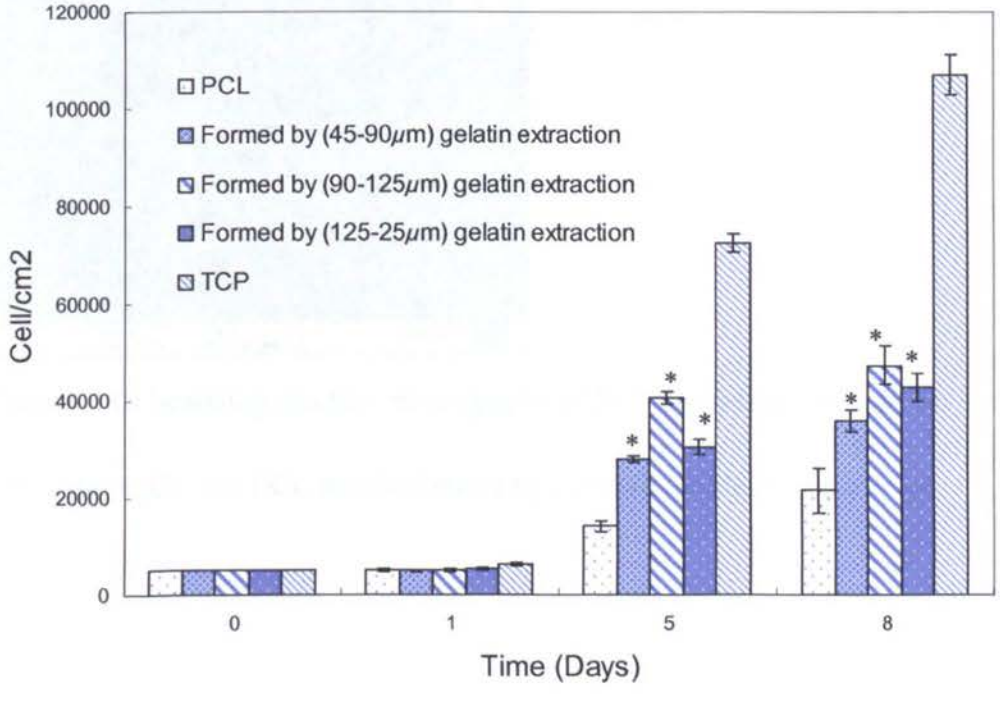

Figure 3.14 Proliferation rates of 3T3 fibroblasts on TCP and porous PCL matrices produced by extraction of gelatin particle (* P<0.01)

3.6.1 SEM analysis of 3T3 fibroblasts on PCL matrices

SEM analysis of seeded fibroblasts at day 1 on lactose-extracted PCL matrices (Figure 3.15) revealed large numbers of rounded cells in contact with the surface. Long process extensions linking the cells to the underlying matrix and to neighbouring cells are apparent, indicating favourable biocompatibility and cell adhesion. Some cells have started to spread on the PCL matrix (arrowed).

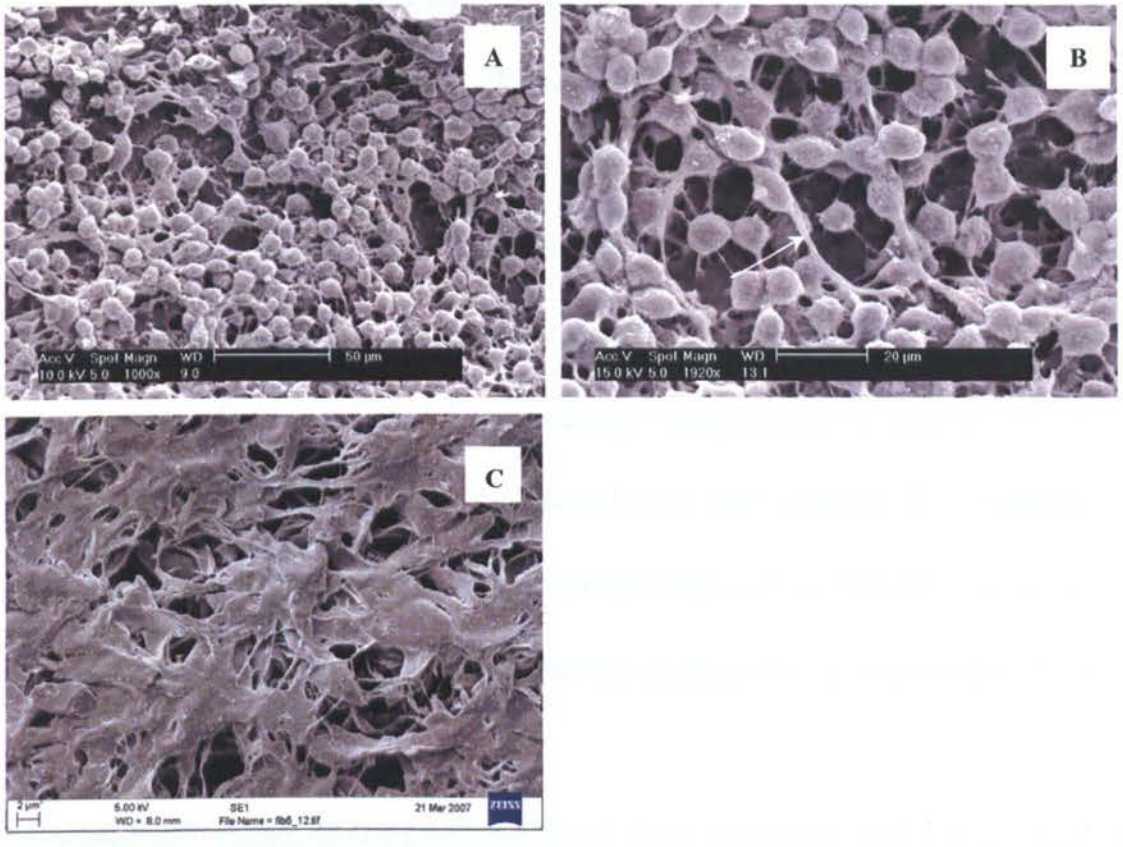

Figure 3.15 Scanning electron micrographs of 3T3 fibroblasts cultured for 1 day (A, B) and 3 days (C) on a PCL matrix formed by extraction of lactose particles.

3.10 Discussion and conclusions

Microporous polycaprolactone matrices have been formulated by precipitation casting for applications in drug delivery and tissue engineering in the past [217]. The method of manufacture relies on gradual extraction of solvent (acetone) from PCL solution by non-solvent (methanol) across a semi permeable membrane formed in situ at the PCL solution/non solvent interface. The materials have been used to achieve controlled delivery of a low molecular weight hydrophobic drug (progesterone [218]) and a hydrophilic antibiotic (gentamicin sulphate) with retained bioactivity in vitro [211]. However, incorporation of particulates of inulin polysaccharide (as a model of a hydropholic macromolecular entity) resulted in limited release of around 18% of the content in 12 months due to effective encapsulation by the PCL phase. In this chapter, a novel approach was described for producing microporous PCL matrices by rapid cooling of a PCL solution in dry ice followed by solvent extraction. The technique is applicable to manufacture of thick section components such as cylinders and tubes for pharmaceutical (e.g. depot devices) and medical application (e.g. vascular prostheses).

Compared with thermally-induced solid-liquid phase separation [48], precipitation of the PCL matrices is induced at low temperature in dry ice (-78°C) and the solvent (acetone, freezing point -94.7°C) remains liquid during the casting process. Solid-liquid phase separation involves solidification of the solvent (e.g. dioxane, DMSO) component of the polymer solution (e.g. PLA, PLGA) at low-temperature followed by sublimation of the solvent during freeze-drying. During phase separation,

the solvent solidifies in the direction of the temperature gradient resulting in formation of microtubule-like pores. A scaffold with oriented structure is obtained with pore size in the range of 10-120μm [26]. The direction of the temperature gradient and the speed of solvent crystallization need be carefully controlled in the above process which may be an obstacle for producing complex tissue engineering scaffolds. The limited pore size range formed by crystallization of the solvent would also be problematical for cell seeding and migration deep inside the scaffold. In liquid-liquid phase separation techniques, a polymer solution separates into two layers: a 'polymer-rich' and 'polymer-lean' phase when the concentration exceeds the sedimentation boundary caused by lowering the temperature. After phase separation, a porous scaffold is formed by solvent sublimation during freeze drying.

In the present study, a microporous scaffold is formed by rapid crystallization of the polymer (PCL) from solution when the temperature is decreased. This approach is simpler than TIPS since it avoids the need for solvent removal at low temperature. While PCL was used in these investigations, other synthetic polyesters such as poly-L-lactide [PLA] or high L-lactide-containing PLG copolymers which tend to crystallise from solution may also be suitable. PCL could also be blended with water soluble polymers such as polyethylene glycol (PEG) to prepare microporous polymer matrices having a water-soluble phase which may be useful for controlling drug release from the matrix.

The low temperature casting approach enabled high loadings of lactose (29% w/w) or gelatin (28.6-44.4% w/w) to be achieved in PCL matrices by suspension of particulates in the PCL solution prior to casting. The good particle distribution throughout the matrix and, importantly, efficient extraction of the water-soluble phase allow formation of a macroporous structure with defined pore architecture by incorporation of particles of a specific shape and size range. The increased crystallinity of PCL matrices resulting from inclusion of 45-90 and 125-250μm lactose particles suggests that PCL crystallized more rapidly due to an improved nucleating ability and decreased molecular mobility on contact with extraneous solid. Similar behaviour has been reported previously for gentamicin sulphate loaded PCL matrices [211]. However, the contrasting finding of reduced PCL crystallinity in both lactose and gelatin-loaded matrices containing intermediate size particles (90-125μm) is more noticeable and invites further studies of the particle shape and surface chemistry prevalent in this size fraction. In comparison, inhibition of PCL crystal nucleation and growth has been reported in PCL-based composites featuring a fibrous collagen phase [195].

A major burst release effect (60-75%) was observed for all lactose-loaded matrices in 24 h and 90% of the original content was extracted into PBS over 9 days. Burst release is normally associated with surface located species. The highly efficient release behaviour is attributed to lactose particles protruding through the matrix surface, contact and interconnections between particles and the high aqueous

solubility of lactose. These factors promote fluid penetration and dissolution of deeply embedded particles.

The amount and duration of protein delivery from 28.6% gelatin loaded PCL matrices was sensitive to the size range of incorporated particles. The amount released over time decreased substantially with increasing particle size range and may be explained simply by the reduction in dissolution rate with decreasing specific surface area of large particles. With increased protein loading from 28.6% to 37.5% and 44.4% w/w the initial 'burst' phase increased and the duration of release decreased. This behavior may be explained by production of a highly interconnected network of pores and channels which allows efficient protein solubilisation and extraction.

A number of studies of protein delivery from polymeric scaffolds or matrices have been carried out, but differences in scaffold material (e.g. natural polymer, non-biodegradable, biodegradable), dimensions and geometry (e.g. film, fiber) make comparisons difficult. Various proteins such as myoglobin [219], bovine serum albumin (BSA), histone [220], horseradish peroxidase (HRP) [221], lysozyme [222] and bone morphogenetic protein (BMP-2) [223] have been incorporated in scaffolds and their release profiles determined. Zilberman [221] found that 20%-80% w/w HRP was released in PBS from PLGA based composite fibers containing 5% HRP in the first day. Sohier et al [219] measured release of 10%-100% w/w of myoglobin and lysozyme from PEGT/PBT films over similarly short timescales (*24* hours) which

could be varied by PEG molecular weight and PEGT/PBT weigh ratio. Lee et al obtained only 25% BSA release from PCL scaffolds in PBS over 7 days [220]. Coombes et al [217] demonstrated limited release (18% of the content in 12 month) of a macromolecule (inulin polysaccharide) from PCL matrices due to effective encapsulation by the PCL phase.

In the present study, efficient release of almost 90% of a high protein load (29-44% w/w) was attained over time periods ranging from 3 days to three weeks in PBS at 37°C, by adjusting the initial loading and size of particles in the PCL matrix. This behavior demonstrates a potential for efficient delivery of co-incorporated growth factors such as b-FGF and active protein C to improve tissue regeneration.

SEM analysis, supported by extensive release of gelatin and lactose from PCL matrices, demonstrated that the low temperature casting technique combined with extraction of the water soluble phase produces highly porous surface and internal structures. The scaffold component of tissue engineering constructs provides a framework for cell attachment, migration, proliferation and tissue organization. The pore shape has been shown to influence the arrangement of seeded cells [224] and this parameter may be adjusted in PCL matrices by controlling the shape and size of incorporated particles. However, cell migration and colonization of the matrices requires an additional level of control over macropore and channel size, geometry and continuity.

Fibroblast growth in cell culture on PCL matrices was significantly lower than on lactose-extracted and gelatin-extracted matrices over 8 days, indicating that a wide range of pore sizes (10-20μm to 250μm) can enhance fibroblast growth over short time scales. The use of fibroblasts from different sources prevents strict comparisons but similar cell growth rates were obtained on lactose extracted PCL matrices (10-20 μm pores) and gelatin-extracted PCL matrices (45-250μm pores) despite the large variation in surface macropore size. Thus the higher cell numbers on the 90-125 μm particle-extracted matrices (Figure 3.13 and Figure 3.14) may be influenced more by the reduced crystallinity of the PCL phase in these materials (Table 3.3 and 3.4).

The present chapter also served to illustrate the potential for production of microporous PCL matrices in the form of tubes for vascular tissue engineering. The persistence of gelatin in the interior and surface of PCL tubular matrices may advantageously display cell adhesion sequences for binding with integrin cell surface receptors. The surface pore structure is anticipated to encourage integration with host tissue. In addition, the capacity for incorporating various growth factors (e.g. VEGF), anticoagulants (e.g. heparin) and anti-bacterial (eg gentamicin) recommends further investigation of PCL matrices to overcome the limitations of conventional blood vessel substitutes based on Dacron and ePTFE.

Chapter 4

Quantification of the internal pore structure of PCL matrices using micro-CT

Chapter 3 described a novel method for producing PCL-based scaffolds with defined internal pore structure using rapid cooling of PCL solutions. The composition and structure of tissue engineering scaffolds is known to play an important role in tissue regeneration by influencing cell distribution, morphology and organisation and, importantly, cell proliferation and differentiation [225, 226]. An effective scaffold should have high porosity, maximum surface area for cell attachment and sufficiently large pores and interconnectivity for cell ingrowth. The porosity of the scaffold also controls the key processes of nutrient supply to cells, metabolite dispersal, cell signaling and tissue ingrowth such as vascularisation. The objective of this chapter is to provide a detailed qualitative and quantitative assessment of the internal structure of PCL-based matrices using micro-computed tomography (Micro-CT) and related image analysis for correlation with cell ingrowth potential and protein release behaviour.

4.1 Qualitative assessment of the internal pore structure of PCL matrices

The internal structure of 1) PCL matrices 2) gelatin-loaded PCL matrices and 3) PCL matrices after solubilisation and extraction of gelatin particles was analysed using micro-computed tomography. Samples were cut from PCL tubular matrices and the length was controlled at 10mm with 2 mm^2 cross sections. In Micro-CT, the combination of X-ray transmission techniques with tomographical reconstruction allow one to visualize and measure the complete internal structure based on thousands of 2D x-ray shadow images. Micro-CT scans the sample vertically over 360 degrees to gain thousands of flat, cross section images from which the 3-D internal structure can be reconstructed. Two and three-dimensional morphological parameters such as porosity and pore size can also be analysed. As shown in Figure 4.1 A and Figure 4.2 A, the Skyscan micro-CT facility used in the early investigations did not clearly resolve the characteristic 5-10 μm pore dimension of unloaded PCL matrices due to a low voxel resolution of 15 μm, resulting in a low detail image of the polymeric phase. However, density differences between the PCL phase (0.38 g/cm^3) and gelatin particulates (1.0 g/cm^3) were sufficient to allow resolution of each component of the biocomposite (Figure 4.2 B).

Micro-CT analysis of the internal 3-D structure of PCL matrices, following extraction of gelatin, clearly defined the solid phase and pore component (Figure 4.1 B, C and 4.2 C-F). The pore shape and size corresponds closely with the particles used for

matrix production (Figure 4.1B, C and 4.2F) with extraction of high gelatin loaded materials providing more pores and internal connections. The high pore density revealed following extraction of 44.4% w/w gelatin-loaded matrices (particle size range 45-90μm) is particularly striking (Figure 4.4E) and tends to suggest that a network of interconnected pores would be produced due to particle contact and subsequent particle dissolution

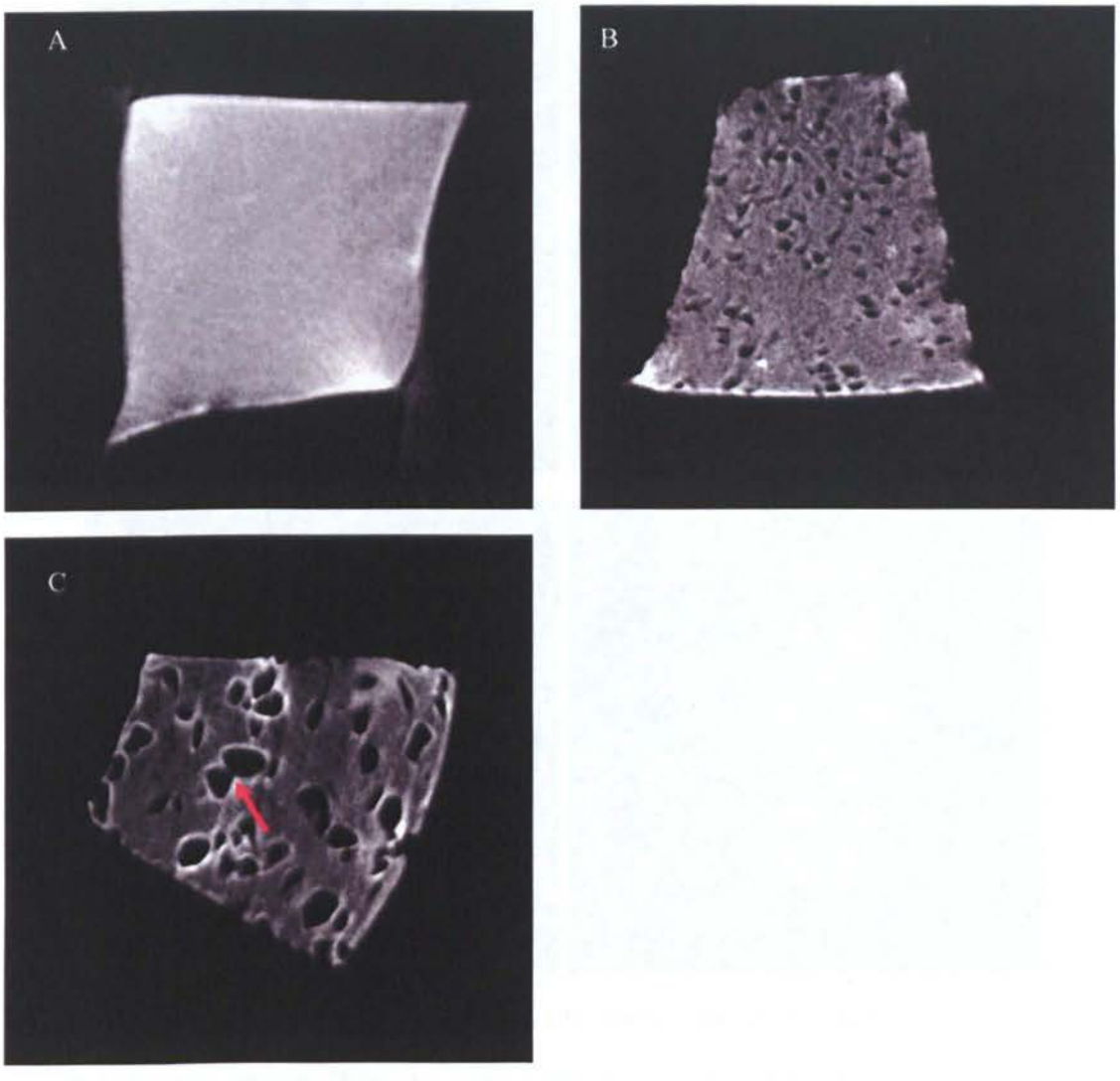

Figure 4.1 2D shadow images of (A) PCL matrix (B) 28.6% w/w gelatin (90-125μm): PCL matrix (polymer phase) after release (C) 28.6% w/w gelatin (125-250μm): PCL matrix (polymer phase) after release

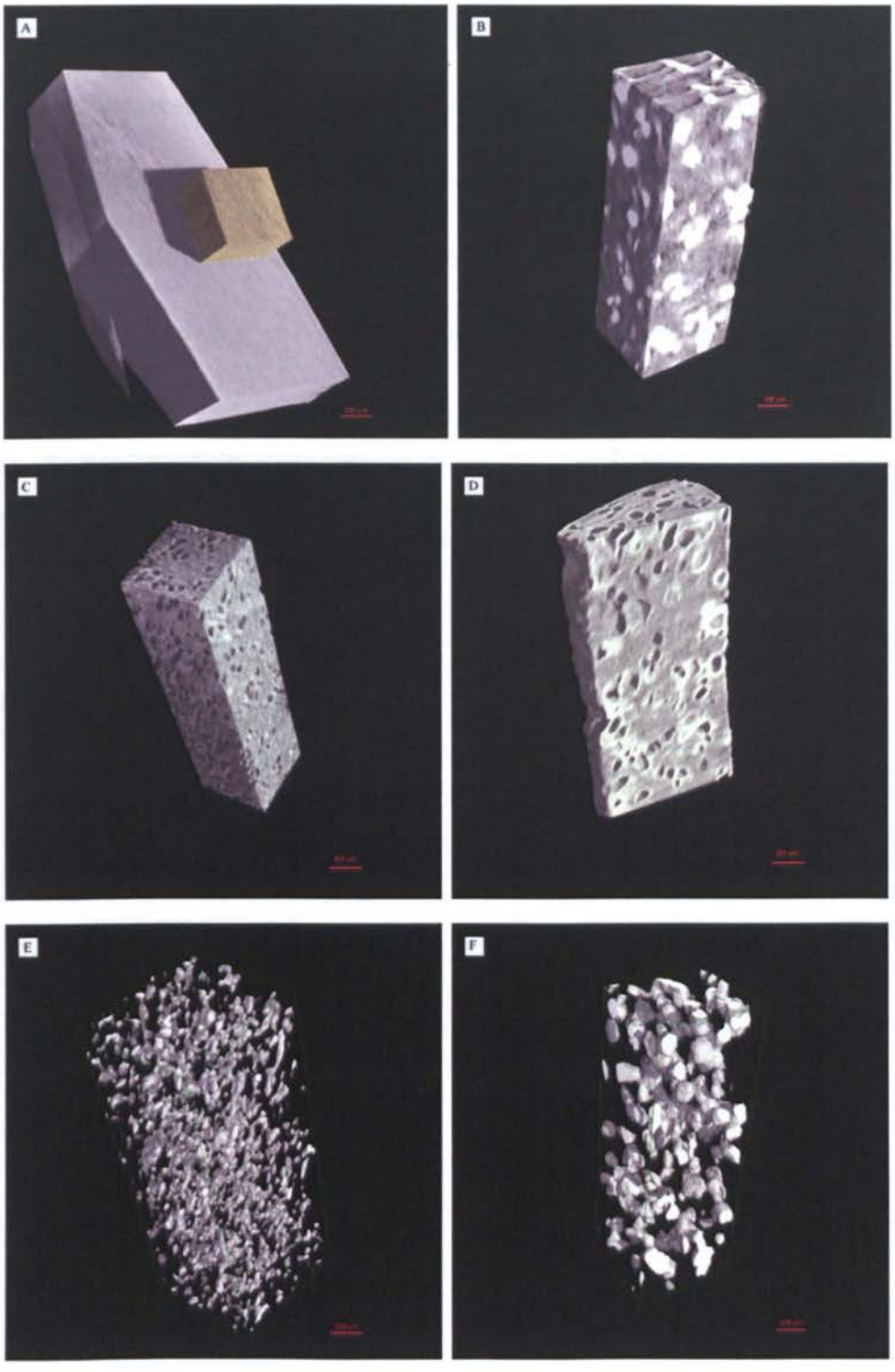

Figure 4.2 Internal microtomographs of (A) Polymeric phase of PCL matrix

(B) Polymeric phase of 28.6% w/w gelatin (90-125 μm): PCL matrix before release

(C) Polymeric phase of 28.6% w/w gelatin (45-90 μm): PCL matrix after release

(D) Polymeric phase of 28.6% w/w gelatin (125-250 μm): PCL matrix after release

(E) Pore phase of 28.6% w/w gelatin (45-90μm): PCL matrix after particle release

(F) Pore phase of 28.6% w/w gelatin (125-250μm): PCL matrix after particle release

A second generation Skyscan micro-CT facility was used later in the investigation, offering higher resolution which enabled visualization of the 10-20μm pore component of the PCL matrix as a rough surface morphology (Figure 4.3 A and B). Small pores are visible in the 2-D shadow images and the 3-D view of pore structure (Figure 4.4 E). However, the microporous structure in the size range of 5-10μm (corresponding to the PCL phase) was still not clearly shown in the final images.

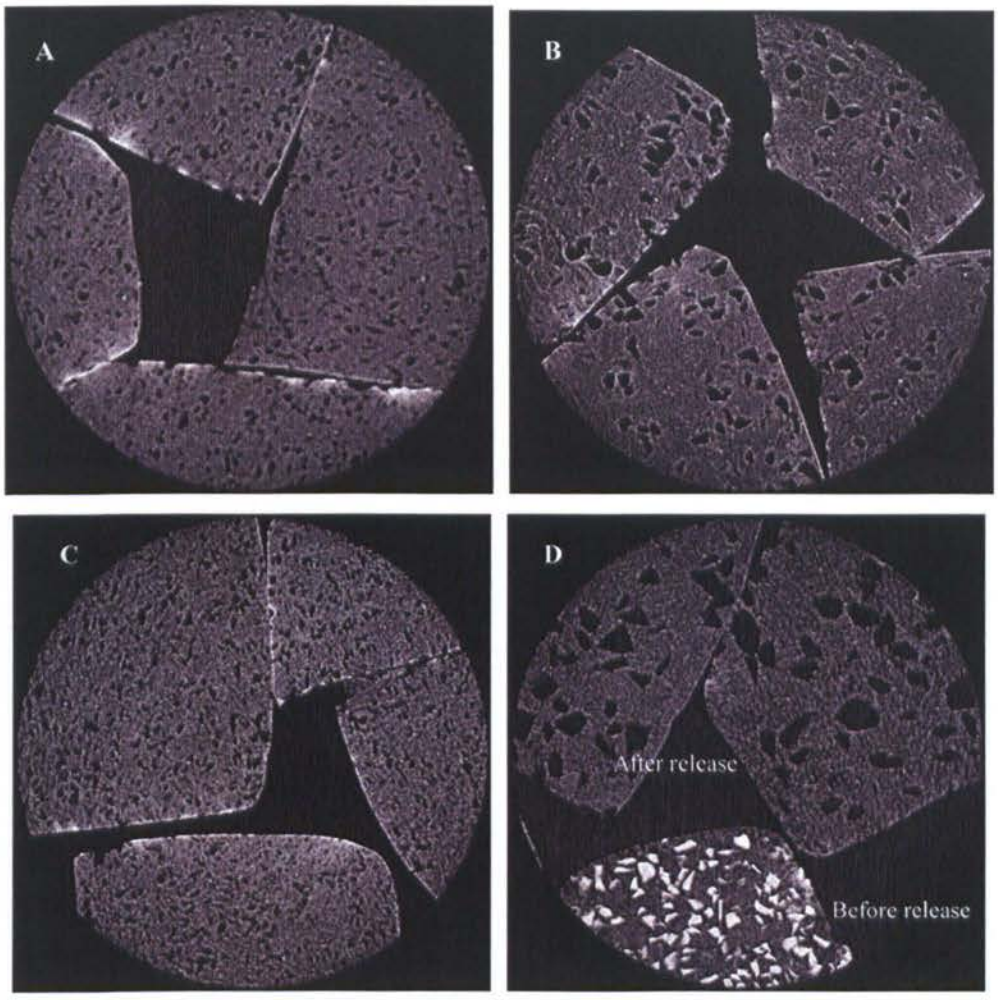

Figure 4.3 2D shadow images of (A) 37.5% w/w gelatin (90-125μm): PCL matrix (polymer phase) after release (B) 37.5% w/w gelatin (90-125μm): PCL matrix (polymer phase) after release (C) 44.4% w/w gelatin (45-90μm): PCL matrix (polymer phase) after release (D) 44.4% w/w gelatin (90-125,125-250μm): PCL matrix (polymer phase) before/after release

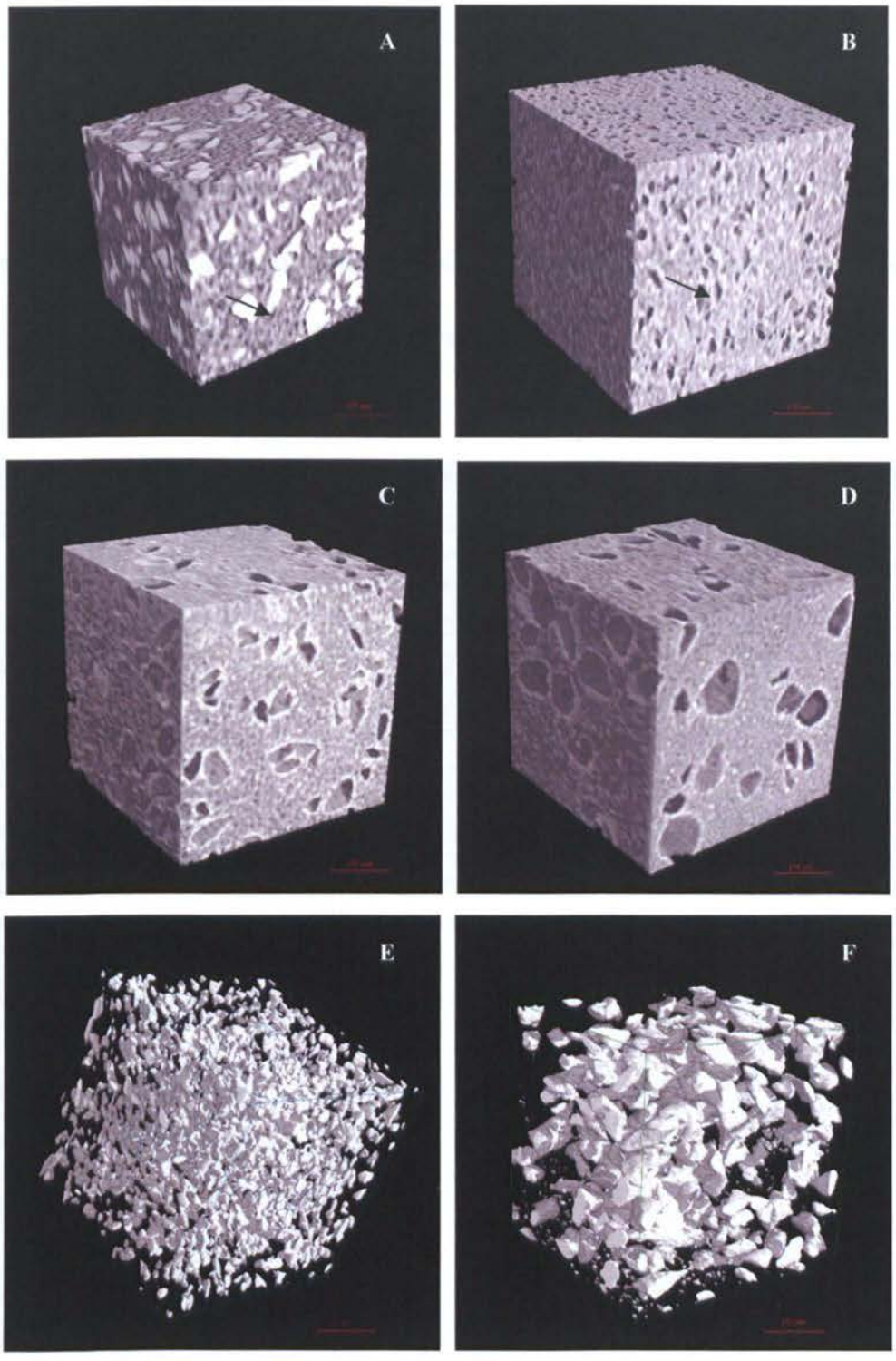

Figure 4.4 Internal microtomographs of (A) Polymeric phase of 44.4% w/w gelatin (90-125 μm): PCL matrix before release (B) Polymeric phase of 44.4% w/w gelatin (45-90 μm): PCL matrix after release (C) Polymeric phase of 37.5 % w/w gelatin (90-125 μm): PCL matrix after release (D) Polymeric phase of 37.5% w/w gelatin (125-250 μm): PCL matrix after release (E) pore structure of 37.5% w/w gelatin (45-90 μm): PCL matrix after release (F) pore structure of 37.5% w/w gelatin (90-125 μm): PCL matrix after release

As shown in the series of 3-D images of PCL matrices (Figure 4.5 A-D) inter-connections between pores become more widespread with increasing gelatin particle loading and isolated pores are also present (Figure 4.5 D). Regions of pore coalescence are visible in most regions, indicating initial particle contact in the matrix which produces a network of high volume channels on subsequent particle solubilisation and extraction.

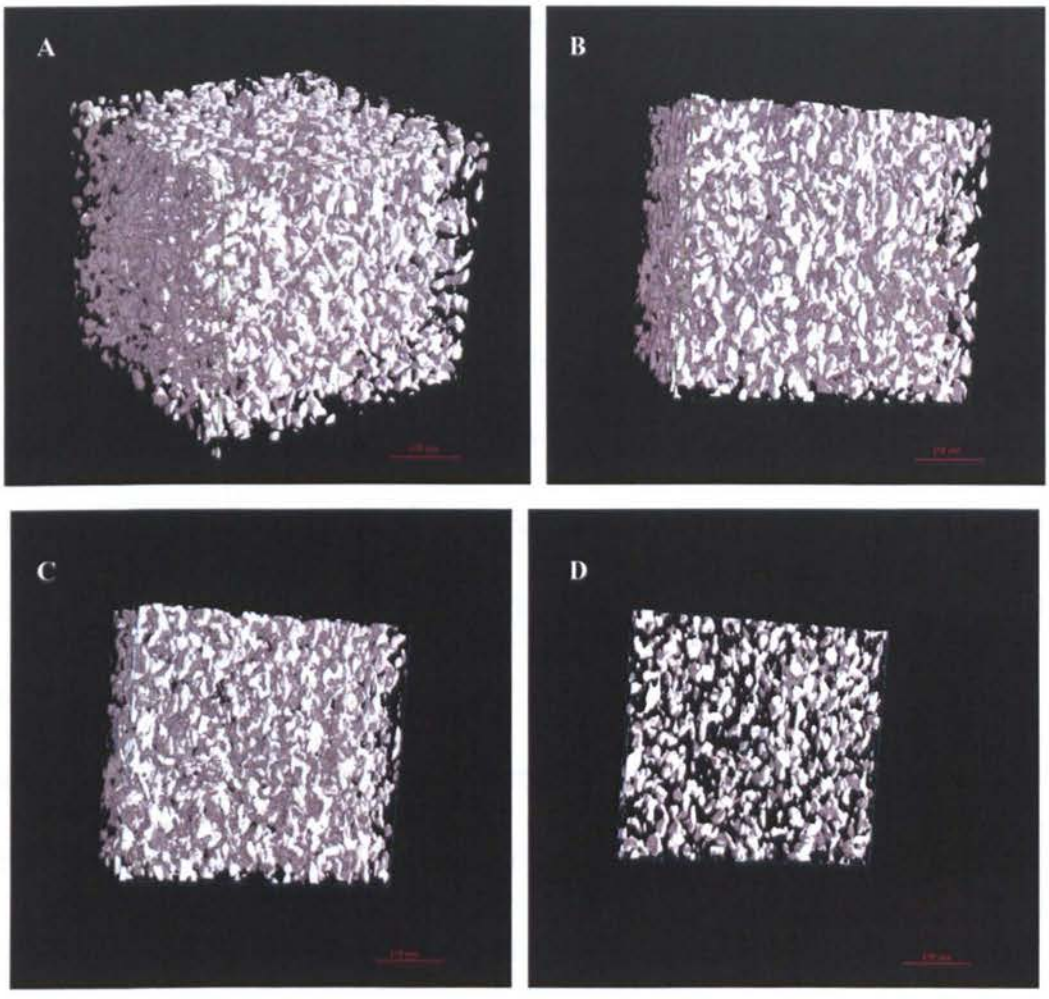

Figure 4.5 Internal microtomographs (A) pore structure of 44.4% w/w gelatin (45-90 μm): PCL matrix after release (complete section) (B) pore structure of 44.4% w/w gelatin (125-250 μm):PCL matrix after release (complete section) (C) pore structure of 44.4% w/w gelatin (45-90 μm): PCL matrix after release (half section) (D) pore structure of 44 % w/w gelatin (45-90 μm): PCL matrix after release (quarter section)

4.2 Quantitative assessment of the internal pore structure of PCL matrices

4.2.1 Image processing

Analysis of transverse 2D Micro-CT images obtained at 1000μm intervals along the sample long-axis (10mm total length) was performed to provide quantitative estimates of pore size and frequency distribution of pore size in the matrices. The image analysis protocol was developed by our group specifically for the micro-CT images of PCL matrices. All images were converted and processed to grey scale image using Paint Shop Pro (Jasc Software Inc., USA) prior to detecting pores by in-house developed software based on Vision Assistant.8.0 and MATLAB (The MathWorks, Inc, USA). During image processing, a 11×11 median filter was applied to the 2-D micro-CT image to remove noise (Figure 4.6 A step 1). A threshold (grey level intensity) was applied (Figure 4.6 B step 2) to classify each voxel as either scaffold or pore by representing the polymeric phase as dark and the pore phase as white. The median filter size and threshold are important parameters which influence resolution of the polymeric region and pores. After adjusting filter size, contrast and threshold, a square area was defined (Figure 4.6 D step 4) on the grey scale image to identify the original area of interest in the matrices. Finally, all selected squares with determined size were used to investigate 'equivalent pore diameter' and pore size frequency distribution using MINITAB (Mintab Inc,USA) and to reconstruct 3D images of pore structure for porosity analysis using Amira 4.0.

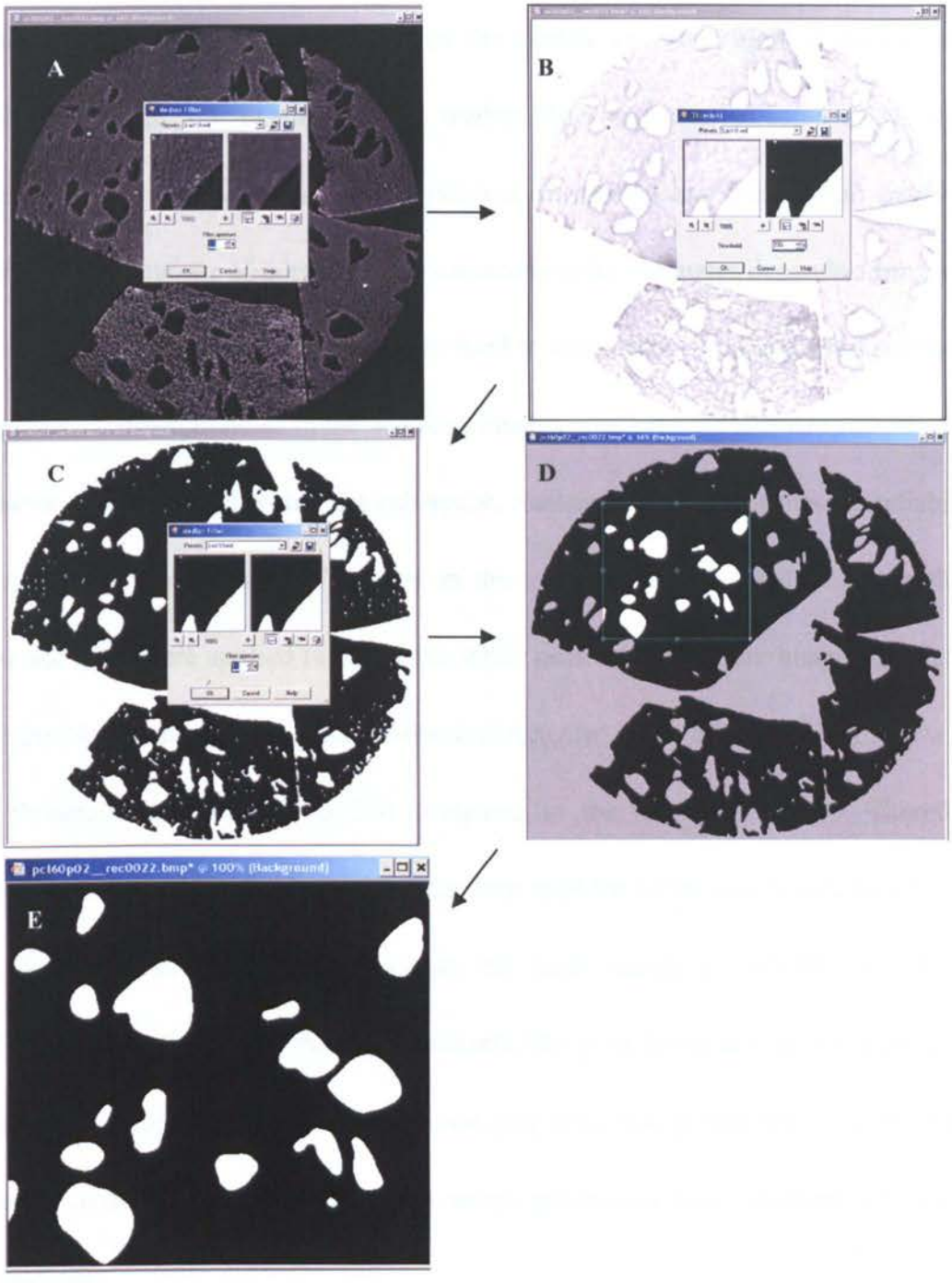

Figure 4.6 Step-by-step process of image processing of 2D shadow images from Micro-CT data of PCL matrices

(A) 2D image showing the difference after filtering

(B) 2D image showing the difference after contrast adjustment

(C) 2D image showing the image after threshold adjustment

(D) Modified 2D image and a defined square area of interest

(E) Final image used for quantitative analysis

Median filter size and threshold govern the quality and resolution of the resulting grey-scale image. For example, if the median filter size was adjusted to 11, small objects will be removed from the analysis and interpreted as a dark region (scaffold) instead. The accuracy of porosity and interconnectivity estimates depends strongly on the robustness of the threshold technique used to identify the pore and solid sub-space (Figure 4.7). Inherent noise in the acquired images coupled with ambient illumination, variation of grey levels within the sub-space, inadequate contrast limits the reliability of scaffold characterization. Therefore in the present study, two values of threshold (250 and 230) were applied to detect the white pore regions of the image. As Shown in Figure 4.7 B and C, more small pores were detected in the original 2-D image when the threshold was adjusted to 230 compared to the threshold of 250. Therefore, although the same threshold and filter size was used for all images in a particular data set, different thresholds were necessary for each sample (ie 45-90, 90-125 and 125-250μm gelatin-loaded PCL). Importantly, the pore boundary detected using the software was superimposed on the original grey-scale image and inspected by eye in order to confirm that pore detection by image processing was consistent with visual assessment.

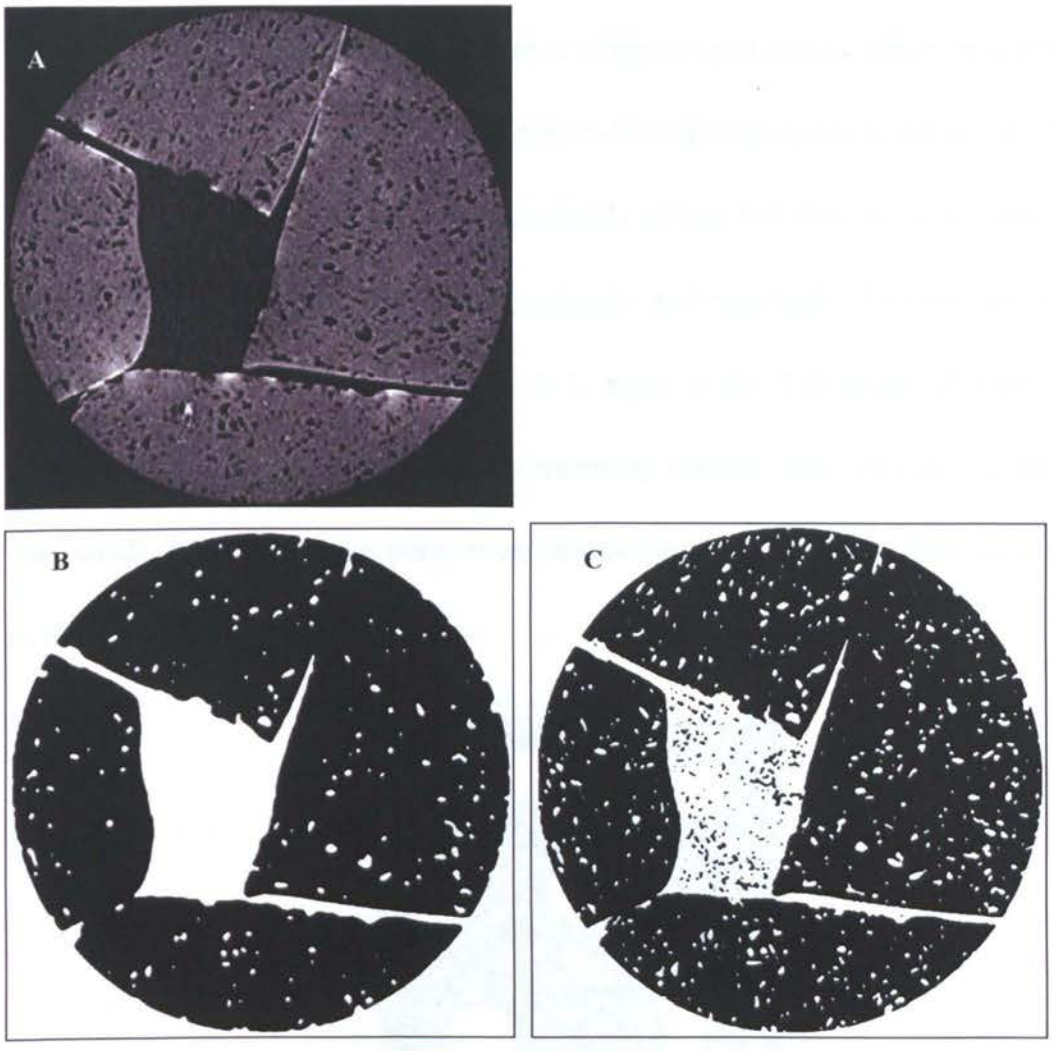

Figure 4.7 Image processing of MicroCT data. Original shadow image (A), and grey-scale image analysis using a threshold of 250 (B) and 230 (C)

For a particular matrix type, the variation of pore area in each image slice (10μm thick) was assessed using MINITAB and converted to an 'equivalent pore diameter'. In addition the pore area data for all sequential Micro-CT image slices at 1000μm intervals along the sample 'Z' axis (which equates to 10 images) in a particular sample were used to provide a measure of the frequency distribution of equivalent pore diameters throughout the PCL matrix. The principle of 'equivalent pore diameter' determination using MINITAB is explained below. The sample image

contains pores of varying shape (circular or irregular) and size as shown in white on a black background (Figure 4.8). The in-house developed program based on MATLAB analysed the image in x and y directions finally giving full detailed information (e.g. area, equivalent diameter, coordinates, perimeter and circularity) for each pore (Table 4.1). Since a circle exhibits circularity ≥ 1, pores in the 2-D image of a particular matrix with circularity <1 were deleted manually because they are more likely to be very small and noise. Those pores were assumed to be noise in the grey-scale image or too small to be analysed.

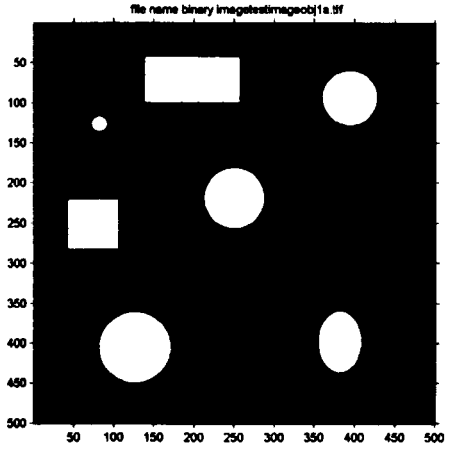

Figure 4.8 Illustration of the variation of pore shape in a 2-D image sample.

Table 4.1 Typical information generated on the pore structure within a sample

Number of labels	Label	Area filled	Equivalent Diameter (μm)	Stats (n). Centroid (1)	Stats (n). Centroid (2)	Perimeter (μm)	Circularity
7	1	4356	74.5	74.5	251.5	260	1.2
7	2	385	22.1	82.3	126.4	69.94	1.0
7	3	6668	92.1	126.4	405.5	303.07	1.1
7	4	7260	96.1	198	71.5	358	1.4
7	5	4790	78.1	250.5	219.5	256.45	1.1
7	6	3525	66.9	381.4	398.49	225.82	1.2
7	7	3973	71.1	393.9	94	233.13	1.1

The sample border region was neglected, any pores on the edge of the area of interest (Typically 6 per image slice depending on the total number of pores) were not included in the analysis (Figure 4.9) because these pores would not be completed and hence could give misleading measurement. With increasing numbers of pores in the image resulting from high-gelatin loaded PCL matrices, more pores on the edge of the area of interest were excluded by the MATLAB-based program. This limitation may cause errors in the analysis of pore size frequency distribution, 'equivalent pore diameter' and porosity as fewer pores would be involved in the analysis compared with the actual or theoretical values. The error will be more significant in the analysis of samples which contain large pores in the ranges of 125-250μm, due to the large potential 'negative pores' on the edge of the area of interest.

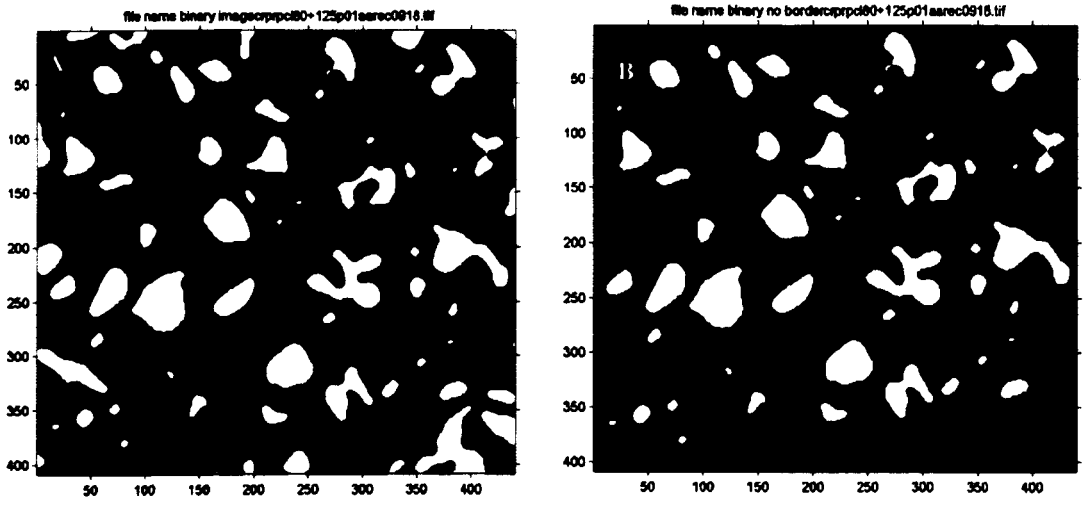

Figure 4.9 (A) Grey scale micro-CT image of a PCL matrix following extraction of 37.5 % w/w gelatin particles (90-125μm). (A) original defined area of interest (B) Image analysed after exclusion of pores on edge of area of interest

4.2.2 Determination of pore size and frequency distribution of equivalent pore diameter

Analysis of sequential Micro-CT images at 1000μm intervals along the sample long axis enabled detailed information to be gathered on the range of pore sizes and pore size distribution within the matrix which is useful for assessing cell ingrowth potential and correlating with drug delivery behaviour (Figures 4.10 and 4.11). The 28.6% w/w (45-90 μm) particle-loaded materials after lactose or gelatin extraction could not be reliably analysed using the selected approach, due to limitations in feature resolution and some intensity variation across the images. However, the Micro-CT shadow images from 37.5% and 44.4%w/w gelatin-loaded matrices containing small pores in the range of 45-90μm were analysed due to the improved resolution of the Skyscan (generation 2) facility used for these materials.

The presentation of 'equivalent pore diameters' for 28.6% w/w lactose (90-125 or 125-250μm)-loaded PCL matrices in Figure 4.10 highlights the reduced numbers of macropores in the latter sample, resulting in a very low fractional pore area of 2.9% compared with 7.3% for the 90-125μm sample. The mean 'equivalent pore diameter' of PCL matrices after release of 90-125μm lactose particles was around 75μm (Figure 4.10A), which is smaller than the original mean particle size (108μm). Similar observations were found for PCL matrices following extraction of large lactose particles. The micro-CT attribute of mean pore size was recorded at 75 and 100μm. Micro-CT and image analysis of lactose-loaded PCL matrices is complicated by the

presence of 10-20 μm powder 'fines' in the sieved powders as discussed in Section 3.4.3 (probably resulting from de-agglomeration and electrostatic binding) which reduces the weight of the large 'primary' particles in the matrix and subsequently the macroporosity. Such effects are apparently more pronounced in the case of lactose-loaded matrices produced using the 125-250μm particles.

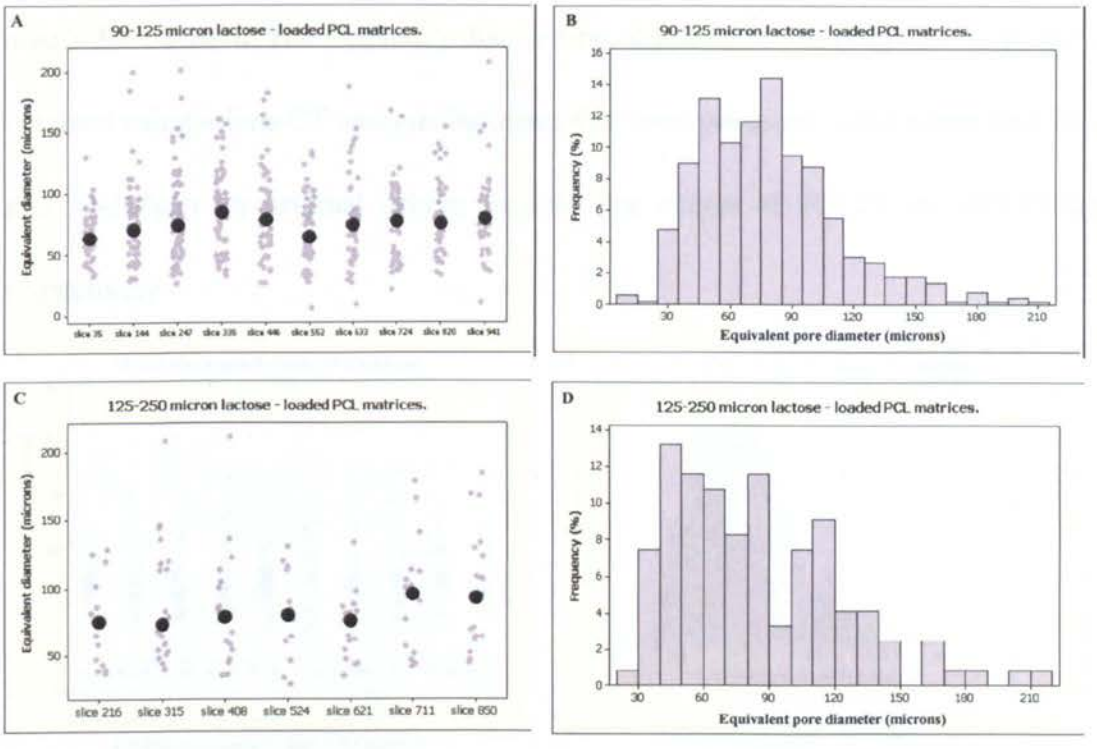

Figure 4.10 Analysis of macroporosity using micro-CT images of PCL matrices following extraction of 28.6% w/w lactose particles

(A) Variation in equivalent pore diameter (90-125μm lactose-loaded PCL)

(B) Frequency distribution of equivalent pore diameter (90-125μm lactose-loaded PCL)

(C) Variation in equivalent pore diameter (125-250μm lactose-loaded PCL)

(D) Frequency distribution of equivalent pore diameter (125-250μm lactose-loaded PCL)

The presentation of 'equivalent pore diameters' for 28.6% w/w gelatin (90-125 and 125-250μm)-loaded PCL matrices in Figure 4.11 confirms the visual impression of uniformity of pore distribution within the materials. Compared with lactose-loaded PCL matrices, more pores were detected in sequential Micro-CT images after gelatin extraction, suggesting that aggregation of gelatin particle is not significant during matrix formulation. The frequency distribution of pore size (%) (Figure 4.11 B and D) obtained using micro-CT analysis indicates that most pores are in the range 36-108μm and 50-200μm for original gelatin particle size ranges of 90-125 and 125-250μm, respectively.

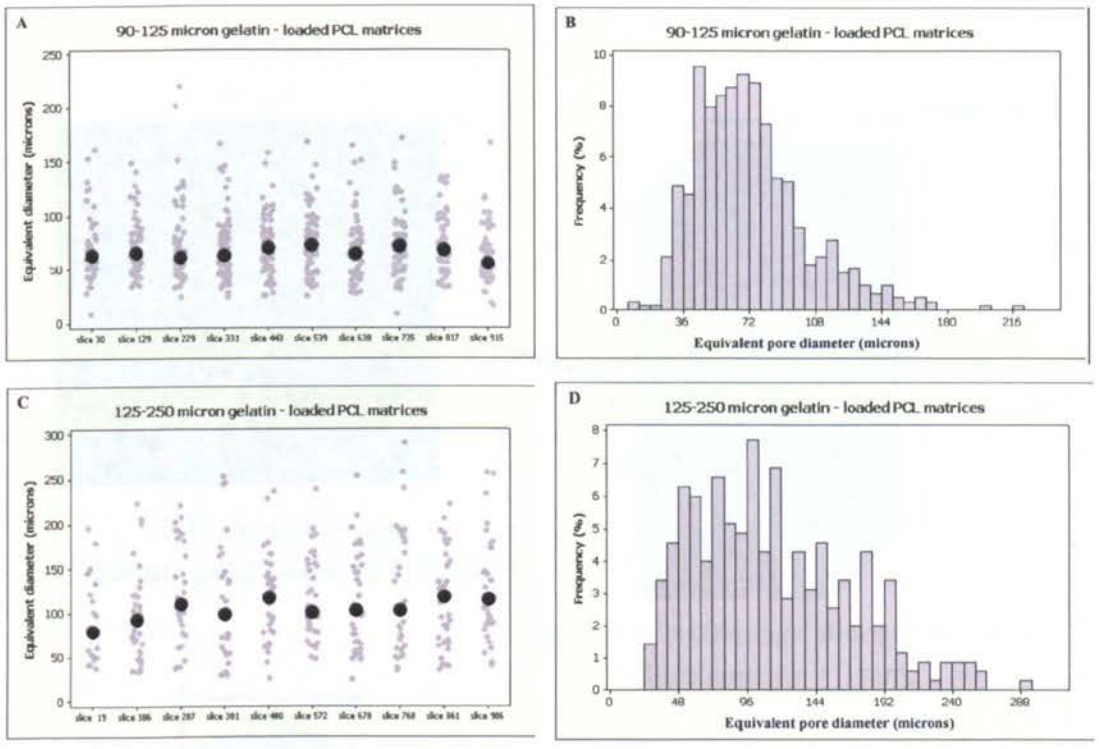

Figure 4.11 Analysis of macroporosity using micro-CT images of PCL matrices following extraction of 28.6%w/w gelatin particles (A) Variation in equivalent pore diameter (90-125μm gelatin-loaded PCL) (B) Frequency distribution of equivalent pore diameter (90-125μm gelatin-loaded PCL) (C) Variation in equivalent pore diameter (125-250μm gelatin-loaded PCL) (D) Frequency distribution of equivalent pore diameter (125-250μm gelatin-loaded PCL)

Micro-CT image analysis detected effectively the upper bound of the particle size range but recorded a significantly lower pore size than the sieved powder classification. This effect may be explained by the 'sectioning' Micro-CT technique used and subsequent image analysis of sample slices which would not be expected to coincide consistently with the largest dimension of asymmetric gelatin particles (Figure 3.5D and Figure 4.12). Sieving is designed, in principle, to separate particles based on the largest dimension. The low values of fractional pore area of 6.6% and 10.5% estimated for the 90-125 and 125-250μm gelatin-loaded matrices, respectively, is consistent with the range of cross-section of detected pores.

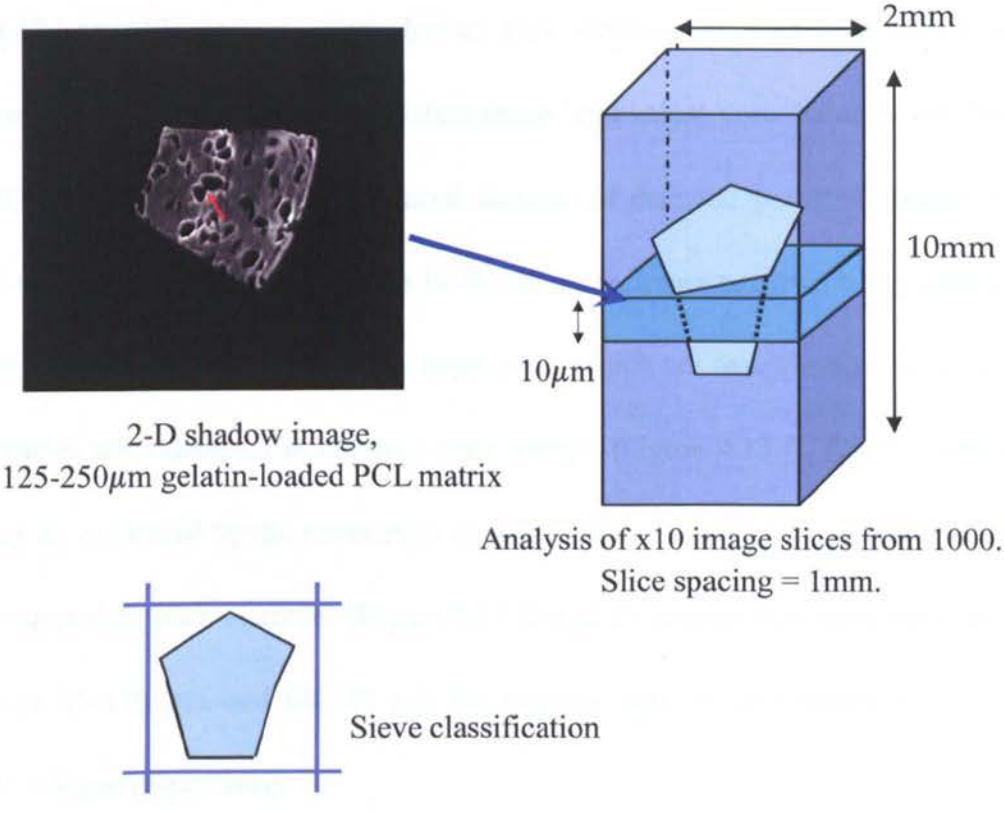

Figure 4.12 Schematic illustrating the difference between pore size measurement using Micro-CT and sieving.

The 2-D shadow image of 37.5% w/w gelatin-loaded PCL matrices after gelatin extraction showed a uniform pore structure for the various pore size ranges investigated (45-90, 90-125 and 125-250μm) and increased pore numbers compared with the 28.6% loaded sample (Figure 4.1 B and 4.3 A). Subsequent image analysis provided detailed information on the pore size range and frequency distribution of pore size. The 45-90μm particle-loaded matrices revealed a fairly limited spread of pore sizes and fairly uniform mean 'equivalent pore diameter' of around 40μm (Figure 4.13 A). The frequency distribution of equivalent pore diameter (Figure 4.13 B) indicates that most pores are small around 20-40μm which may be explained by the micro-CT 'sectioning' effect described above and illustrated in Figure 4.12. The 90-125 and 125-250μm gelatin-loaded PCL matrices after particle extraction were also characterised by a fairly constant mean 'equivalent pore diameter' of 75μm and 120 μm respectively. The decreased number of detected pores compared with the 45-90μm particle-loaded matrices is due to fewer, larger particles being loaded in the starting matrix. In addition, some large pores which are over the size range of sieved particles were detected in the grey scale images (Figure 4.13 C, E). This observation may be explained by the connection of two or more pores. The frequency distribution of equivalent pore diameter (Figure 4.13 D and F) reveals that most pores are in the range 30-120 μm and 60-180 μm for original particle size ranges of 90-125 and 125-250μm respectively.

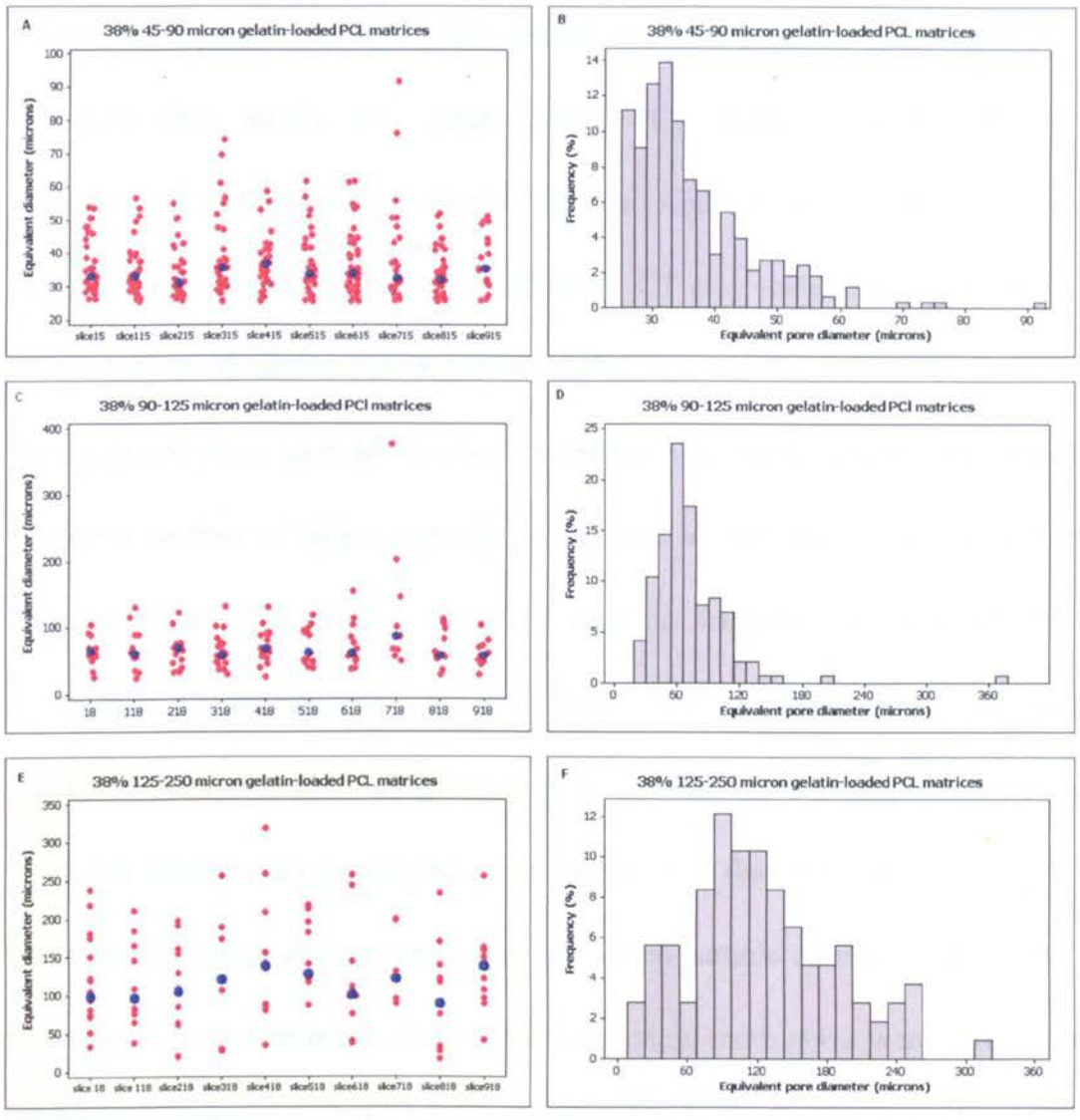

Figure 4.13 Analysis of macroporosity using micro-CT images of PCL matrices following extraction of 37.5% w/w gelatin particles

(A) Variation in equivalent pore diameter (45-90μm gelatin-loaded PCL)

(B) Frequency distribution of equivalent pore diameter (45-90μm gelatin-loaded PCL)

(C) Variation in equivalent pore diameter (90-125μm gelatin-loaded PCL

(D) Frequency distribution of equivalent pore diameter (90-125μm gelatin-loaded PCL)

(E) Variation in equivalent pore diameter (125-250μm gelatin-loaded PCL)

(F) Frequency distribution of equivalent pore diameter (125-250μm gelatin-loaded PCL)

The presentation of 'equivalent pore diameter' for three pore size ranges after particle extraction from 44.4% w/w gelatin-loaded PCL matrices confirms the visual impression of a highly porous internal structure (Figure 4.14). A fairly large number of pores were detected in the sequential Micro-CT grey scale images obtained from the original 45-90 and 90-125μm gelatin-loaded PCL matrices. However, fewer pores were detected when particles of size 125-250μm were used. This may be caused by the lower number of larger particles present and by the analysis method whereby pores on the edge of the area of interest were not included. Similar to 28.6% and 37.5% gelatin-loaded materials, the mean 'equivalent pore diameter' is fairly constant through sequential shadow images (40μm, 60 μm and 100 μm respectively) (Figure 4.14), but smaller than the original mean particle size due to the non-coincidence of the micro-CT image analysis technique and sieved particle classification. For 44.4% w/w gelatin-loaded matrices after protein extraction, more pores were detected with equivalent diameter over the original particle size ranges (Figure 4.14 A and C), indicating the possibility of pore connection and coalescence. In addition, the frequency distribution of equivalent pore diameter for 90-125 and 125-250μm particle-loaded PCL matrices showed a large proportion of small pores around 40μm (Figure 4.14 D and F) compared with the lower loaded matrices. This effect may be due to detection of interconnecting channels (connects) between the larger pores (Figure 4.3 C and D).

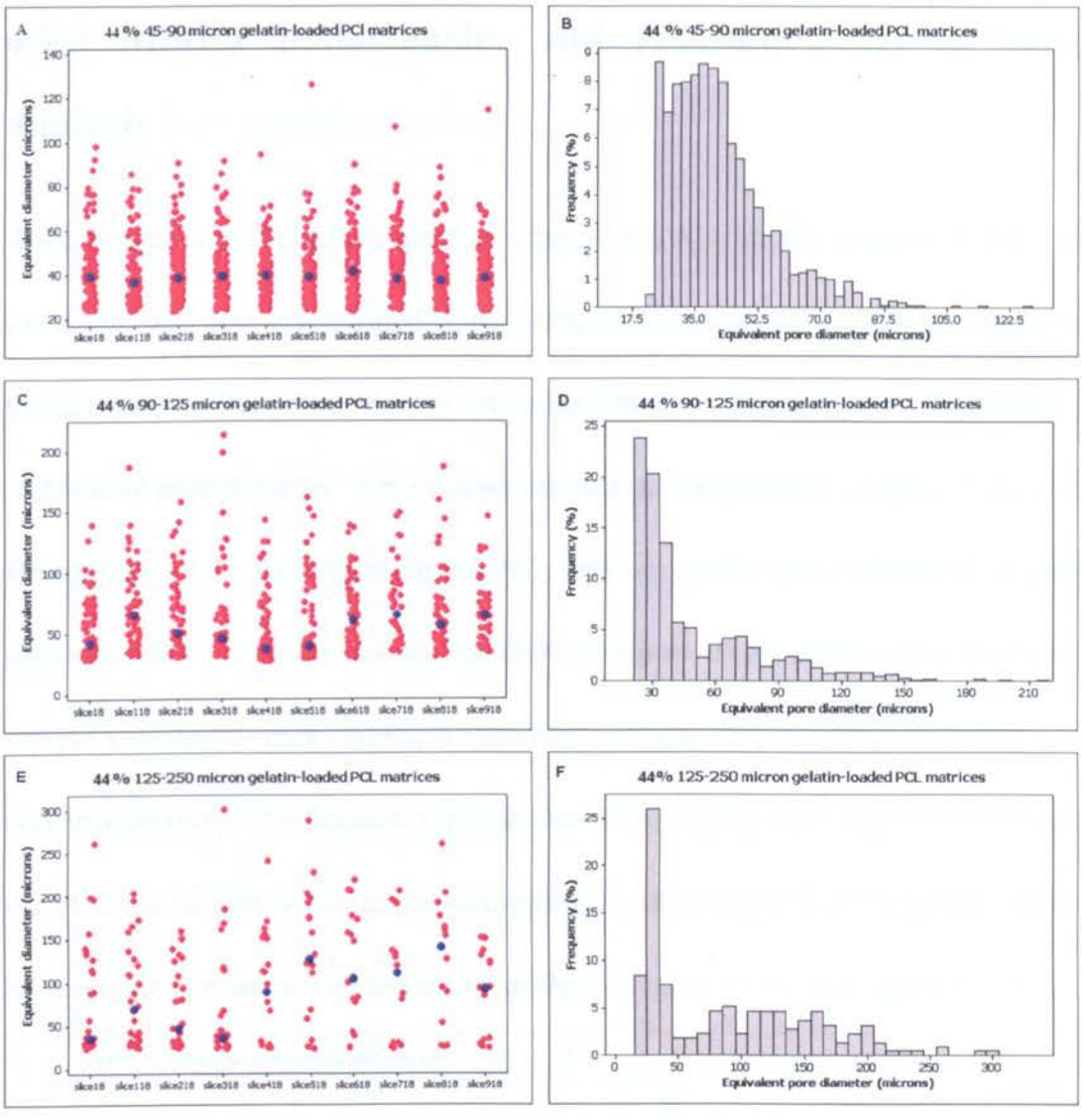

Figure 4.14 Analysis of macroporosity using micro-CT images of PCL matrices following extraction of 44.4% w/w gelatin particles

(A) Variation in equivalent pore diameter (45-90μm gelatin-loaded PCL).

(B) Frequency distribution of equivalent pore diameter (45-90μm gelatin-loaded PCL)

(C) Variation in equivalent pore diameter (90-125μm gelatin-loaded PCL)

(D) Frequency distribution of equivalent pore diameter (90-125μm gelatin-loaded PCL)

(E) Variation in equivalent pore diameter (125-250μm gelatin-loaded PCL)

(F) Frequency distribution of equivalent pore diameter (125-250μm gelatin-loaded PCL)

* Data is not comparable to those on Figure 4.11 due to advanced instrument was used for this study.

4.2.3 Matrix homogeneity and reproducibility of image analysis

The homogeneity of the PCL matrices after 44.4% w/w gelatin particle (125-250μm) extraction was also investigated using MINITAB after image processing. Sequential images starting from slice number 36 to number 936 were analysed. The results for 'equivalent pore diameter' were almost identical to the previous analysis (Figure 4.14 E and Figure 4.15 A), indicating the PCL matrices produced by extraction of gelatin particles have a uniform internal structure and pore distribution over a fairly large sample volume (40 mm^3) which is important for achieving consistent cell interaction and drug delivery. The frequency distribution of equivalent pore diameters throughout the PCL matrix also confirms the homogeneity and uniformity of the porous structure by revealing similarity with the earlier analysis (Figure 4.14 F and Figure 4.15 B).

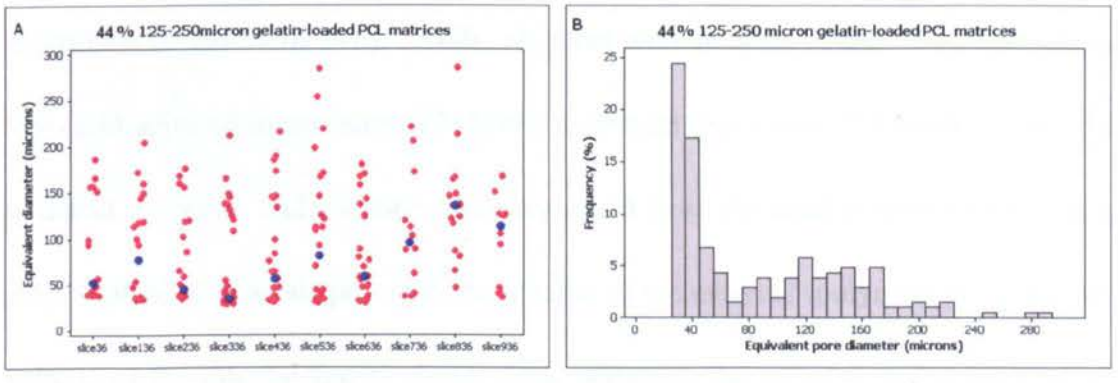

Figure 4.15 (A) Variation in equivalent pore diameter (125-250μm) (B) frequency distribution of equivalent pore diameter following gelatin particle (125-250μm) extraction from 44.4% w/w loaded PCL matrices. Sequential images starting from No. 36

4.3 Micro-CT evaluation of macroporosity of PCL matrices produced by gelatin particle extraction

The macroporosity (%) of PCL matrices produced by extraction of 28.6%, 37.5% or 44.4% w/w gelatin particles was analysed using available algorithms (Amira 4.0, VGStudioMAX) based on the total volume of the pore phase compared with the total volume of the matrix (polymer + pore phase). After converting the 2D Micro-CT shadow images to grey scale using Paint Shop Pro, sequential grey scale images (300 slices) were reconstructed to produce a 3D image using the Amira 4.0 software programme (Figure 4.16A). The individual pores and interconnected pores were shown in yellow, while the polymer phase was removed using a median filter (Section 4.2.2) within a volume of interest which defined the original dimensions of the porous PCL matrix. The total volume of pore phase was calculated by in-house computed algorithms (Figure 4.16 B-E). Briefly, all pores were selected (Figure 4.16 C) with the threshold adjusted to maximum (255) and minimum (5) (white=255 black=0) in order to detect all pores, and all pores were separated from the total volume of the matrix cube. Statistical analysis provided the volume of the external (polymer) phase and the volume of the internal (pore) phase. After summing the external and internal phase volume, the porosity was calculated by comparing the volume of the pore phase with the total volume of the matrix cube. Since each sample contains approximately 1000 sequential grey scale images, blocks of 300 images were reconstructed and analysed to assess the uniformity of macroporosity through the sample. Samples prepared by extraction of 45-90μm gelatin particles from 28.6% w/w loaded matrices were not

investigated due to insufficient resolution of original raw data.

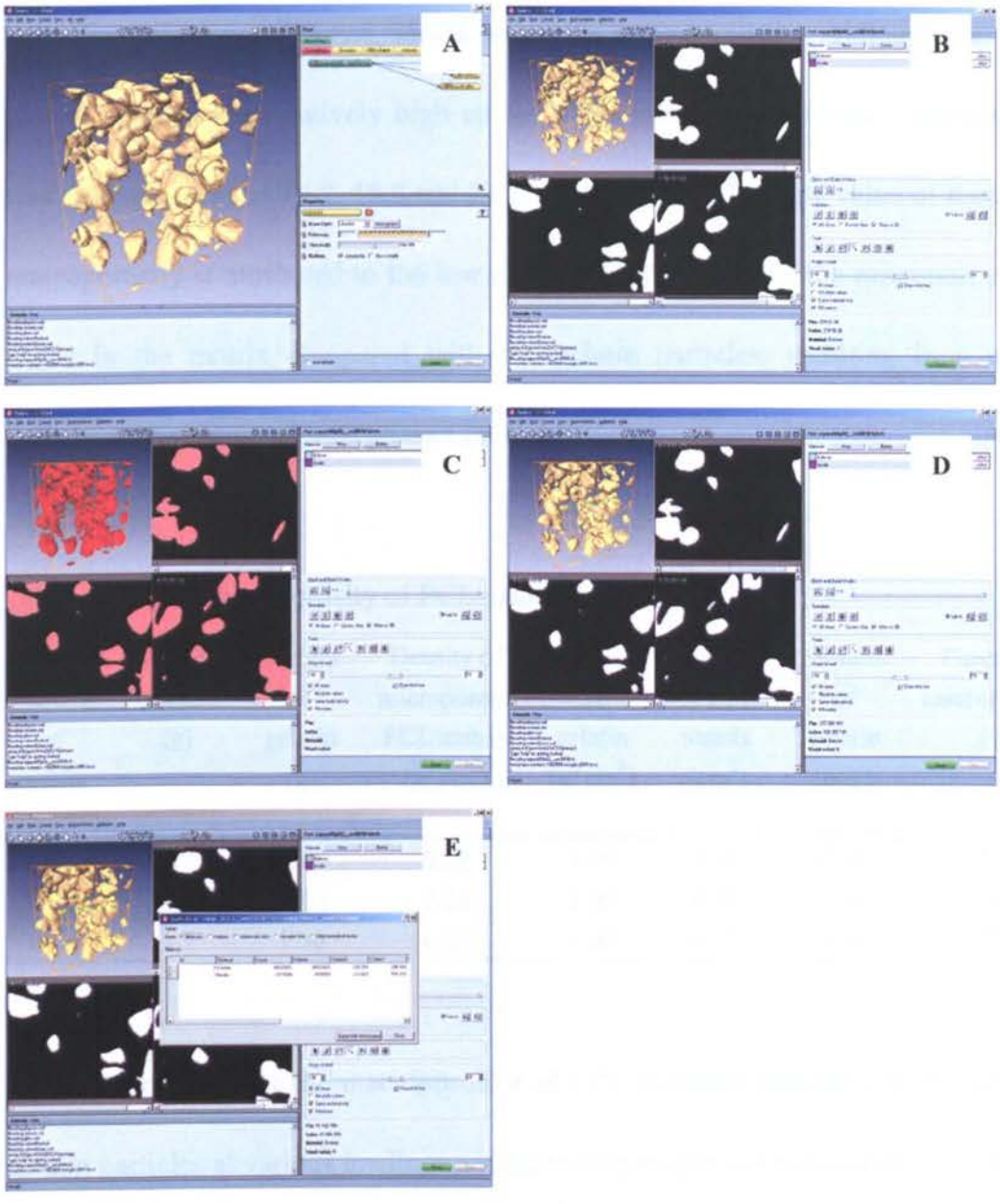

Figure 4.16 Step-by-step process of porosity analysis using micro-CT images

(A) 3D view of pore structure

(B) 3D view of sample with 2D view in x-y, x-z and y-z direction

(C) Pores were rendered in red before analysis

(D) All rendered pores were selected for analysis

(E) Presentation of results

Table 4.2 shows the theoretical macroporosity of PCL matrices produced by extraction of 28.6, 37.5 and 44.4% w/w gelatin respectively. Although the initial gelatin loading was relatively high up to 44.4% w/w, the theoretical macroporosity was determined to be 13.2, 18.6 and 23.3% respectively. The low value of theoretical macroporosity is attributed to the low density (0.38 g/ cm^3) of the microporous PCL phase in the matrix compared with the gelatin particles, resulting in a notable difference in volume of each phase (Table 4.2).

Table 4.2 Theoretical porosity of PCL matrices

Gelatin loading of matrix (% w/w)	Weight of PCL (g)	Weight of gelatin (g)	Density of microporous PCL matrix (g/ cm^3)	Density of gelatin (g/ cm^3)	Volume of PCL matrix (cm^3)	Volume of gelatin (cm^3)	Theoretical macroporosity (%)
28.6	1.7	0.68	0.38	1.00	4.47	0.68	13.2
37.5	1.7	1.02	0.38	1.00	4.47	1.02	18.6
44.4	1.7	1.36	0.38	1.00	4.47	1.36	23.3

Micro-CT analysis of the macroporosity of PCL matrices prepared by extraction of gelatin particles at various loadings and three size ranges are summarised in Table 4.3 and 4.4, The results are based on micro-CT grey scale images analysed using threshold (250) (Table 4.3) and threshold values (230) (Table 4.4). In general, micro-CT measurements of macroporosity increased when the higher threshold value was applied to grey-scale images. The micro-CT determined macroporosity produced by extraction of 45-90μm particles was found to be significantly lower (70-80%) than the theoretical macroporosity using a threshold value of 250 (Figure 4.17). Micro-CT

values were still 50-70% lower when the threshold was decreased to 230. This may be explained by a limitation of image processing, where small pores are removed as noise from grey scale images. When the pore size increased to 90-125 or 125-250μm, higher macroporosity values were generally recorded due to more visible and detectable pores in the grey-scale images. Micro-CT estimates were 15-40% and 0-30% lower than theoretical values of macroporosity using a threshold of 250 and 230 respectively. The reason for the relatively low values measured for 38% w/w gelatin loaded PCL matrices is unclear at present. The macroporosity of PCL matrices produced by extraction of 44.4% w/w gelatin particles (125-250μm) was higher than the theoretical value, which could be due to inclusion of pores which are smaller than 125μm in the porosity analysis. Visual evidence is shown in Figure 4.17, where considerable numbers of small pores are evident around the large pores (arrowed). Table 4.3 and 4.4 also reveal that there is no significant difference in macroporosity from top to base of the sample, indicating production of a uniform structure in PCL matrices produced by rapid cooling. The data in Tables 4.3 and 4.4 also suggest that micro-CT is capable of providing good estimates of macroporosity (within 85 and 100%) for materials containing pores larger than 90μm.

Table 4.3 Macroporosity of PCL matrices determined by analysis of micro-CT images using low threshold (250)

Gelatin loading of PCL matrix % w/w	Theoretical macroporosity %	Number of sample Slices	Macroporosity (%) of PCL matrices prepared from extraction of gelatin particles of three size ranges		
			45-90μm	90-125μm	125-250μm
28.6	13.2	001-330	--	10.5	10.3
		331-660	--	9.3	10.7
		661-1000	--	10.1	11.1
		001-1000	--	9.7	10.8
37.5	18.6	001-330	3.0	11.1	15.1
		331-660	2.9	11.7	15.3
		661-1000	2.8	12.0	15.4
		001-1000	2.9	11.9	15.2
44.4	23.3	001-300	7.6	17.5	21.8
		331-660	7.8	17.8	19.6
		661-1000	7.6	17.5	19.8
		001-1000	7.6	17.7	21.1

Table 4.4 Macroporosity of PCL matrices determined by analysis of micro-CT images using high threshold (230)

Gelatin loading of PCL matrix % w/w	Theoretical macroporosity %	Number of sample Slices	Macroporosity (%) of PCL matrices prepared from extraction of gelatin particles of three size ranges		
			45-90μm	90-125μm	125-250μm
28.6	13.2	001-330	--	11.4	11.8
		331-660	--	11.1	11.9
		661-1000	--	11.6	12.1
		001-1000	--	11.5	11.9
37.5	18.6	001-330	6.6	12.8	15.6
		331-660	6.4	13.1	15.6
		661-1000	5.9	12.8	15.9
		001-1000	6.3	12.9	15.8
44.4	23.3	001-300	12.3	24.1	26.2
		331-660	12.5	22.7	24.4
		661-1000	11.9	22.9	25.9
		001-1000	12.2	23.1	25.8

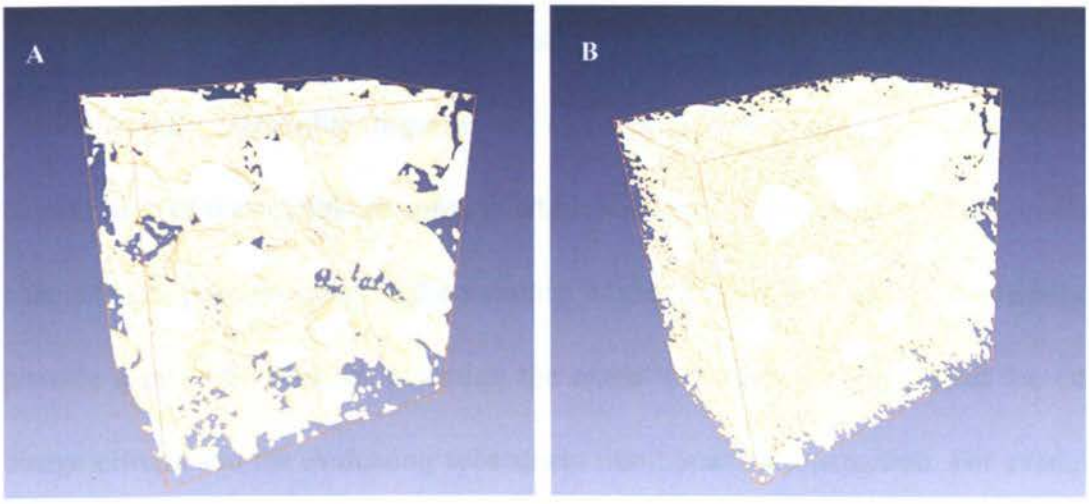

Figure 4.17 Internal macropores in PCL matrices detected using (A) low threshold (250) (B) high threshold (230) processing of micro-CT images. Matrices produced by extraction of 44.4% w/w gelatin particles (125 -250 μm)

4.4 Discussion and Conclusions

X-ray micro-computed tomography (Micro-CT or μCT) has been used previously in medical applications to characterise 3D bone microstructure, to evaluate microvascular architecture and to evaluate the porous architecture of biomaterials [227]. The advantages of Micro-CT include the fact that it is a non-destructive technique and 3D images of samples are acquired at microscopic resolution. In addition, it overcomes the inherent weakness of SEM which is limited to surface anaysis on relatively small fields of view. Micro-CT provides full information regarding isolated pores or deep pores connected by narrow throats in complex porous structures [228]. In the present chapter, Micro-CT was used to analyse the pore size distribution (and thus the original particle size distribution) in PCL matrices following solubilisation and release of particulates of non-uniform size and shape. Pore

interconnections in tissue engineering scaffolds are essential to allow, at one level, nutrient supply, metabolite dispersal and cell signaling. However, cell migration and colonization of the scaffold requires an additional level of control over macropore and channel size, pore geometry and continuity. Micro-CT has been shown previously to provide a powerful tool for assessing the extent to which scaffolds meet the latter design criteria and for evaluating subsequent tissue/scaffold interaction. For example, the regularity of pore size, shape and distribution in scaffolds produced by solid free-form fabrication techniques can result in 100% interconnectivity and facilitates image analysis and quantification of porosity by Micro-CT [229]. Micro-CT analysis of samples based on the structural indices applied in bone, confirmed the presence (though not the quantity) of interconnecting pores parallel and perpendicular to the foaming direction, high total porosity (>75%), high specific surface area ($44m^2$) and mean pore diameter of 400μm. In the work of Lin et al on oriented, porous polymer scaffolds [39], high average porosity values around 80% and pore interconnectivity greater than 99% were recorded in poly($_L$-lactide-$_{DL}$-lactide) scaffolds using micro-CT analysis. However, measurements of longitudinal connectivity, transverse pore size and pore connectivity were not differentiated.

In the present study, micro-CT provided detailed 3-D images of macroporosity which confirmed that pore shape could be controlled by using soluble particles of defined shape. Micro-CT also provided a detailed quantitative measure of the frequency distribution of equivalent pore diameters throughout a PCL matrix or scaffold

produced by extraction of gelatin or lactose particles, which is useful for optimizing scaffold design, production and performance. For example, only around 50% of the macropores in the highest porosity sample (23%, 125-250μm) are larger than 100μm (Figure 4.14 F) which will influence the extent of cell ingrowth. In addition, analysis of micro-CT images was shown to be capable of providing good estimates of macroporosity in materials containing irregular pores greater than 90μm.

The resolution of the Micro-CT facility used in this study prevented visualization and quantitative analysis of the fine-scale (<15μm) pore architecture and tortuosity present in the PCL matrices but revealed an extensive internal system of macropores. However, it is evident from 2-D shadow images that the network of high volume inter-pore channels required for cell infiltration of the material is absent in the low particle loading (28.6%) matrices (Figure 4.1B and C). Thus tissue integration would be confined initially to the matrix surface for these designs with the core potentially providing a depot system for controlled delivery of growth factors via the 5-10μm microporous system inherent in the PCL phase. The extent of macroporosity and interconnections between pores increases with particle loading of PCL matrix. A maximum of around 23% macroporosity was achieved in the present materials (Table 4.2). However, the extent of pore interconnections and their dimensions were not evaluated.

Several other researchers have previously used Micro-CT images to qualitatively and

quantitatively depict scaffolds. Moore et at [227] did quantify some aspects of the interconnectivity of a polymer scaffold produced by the salt-leaching process using micro-CT namely the volume fraction of porosity that was connected via a minimum interconnect size. Otsuki et al [228] mapped the path length from the surface to connected interior pores and the pore throat size of bioactive porous titanium implants using an algorithm developed for percolation studies in rock. Jones et al [19] recently identified and quantified the pore content, interconnects and pore size distributions in sol-gel derived bioactive glasses using micro-CT. Similar approaches are recommended in future work to characterize the interconnectivity of macropores in the higher porosity PCL matrices to further assess the potential for cell ingrowth.

Chapter 5

Characterisation of microporous PCL tubes for vascular tissue engineering under fluid flow conditions

Cardiovascular disease (CVD), including peripheral vascular and coronary artery disease, is the largest cause of mortality of women and men of all ages and all races world wide. Tissue engineering offers a potential alternative to existing treatment and devices such as substitution of occluded vessels by knitted Dacron or ePTFE prostheses. However, one of the major requirements of tissue engineered vascular grafts for wide clinical usage is sufficient mechanical performance and endurance under the high systemic blood pressure experienced by cardiovascular structures. Compliance mismatch between the implant and host artery resulting in disrupted blood flow conditions at the anastomosis or graft/artery junction, has long been implicated in prosthesis failure arising from anastomotic pseudointimal hyperplasia. Thus a long standing design criterion for replacement blood vessels is that they should display a dynamic mechanical response in vivo similar to the host artery. The pressure of the circulating blood decreases as blood moves through arteries, arterioles, capillaries, and veins; Typical values of arterial pressure in healthy adults are approximately 120mm Hg systolic and 80 mm Hg diastolic, while venous pressure in a vein or atria of the heart is much less than arterial pressure, with common values of

5 mm Hg in the right atrium and 8 mm Hg in the left atrium. The rupture strength of saphenous veins and tissue engineered grafts have been recorded as 1680±307 and 2150±709 mm Hg, respectively [230, 231]. In the present study, a potential polycaprolactone-based vascular graft was produced using the rapid cooling method described in Chapter 3. The aim of this chapter is to report the mechanical properties of the resulting microporous PCL tubes (nominal OD 7.5 mm ID 6.5 mm) under short-term hydrostatic and hydrodynamic loading conditions which simulate blood flow in vivo.

The hydrodynamic parameters that need to be considered when designing vascular prostheses are: the constant flow rates, blood pressure exerted within specific blood vessels e.g. artery and vein and pulse frequency. Fluid flow through a blood vessel generates a shear stress or tangential drag force at the wall of the vessel. The magnitude of this stress is directly proportional to the viscosity and blood flow rate and inversely proportional to the cube of the vessel radius. Fluid flow through a tube, if it is sufficiently compliant, will cause it to dilate by an amount related to the pressure of the fluid, i.e. it generates a hoop or circumferential strain. Thus, modulating fluid flow through a tube to mimic the pulsatile nature of the circulatory system will result in a corresponding cyclic change in the hoop strain in the wall of the tube by an amount that depends on the tube dimensions and its viscoelastic properties. The high compliance of microporous PCL tubes and degree of elasticity resulting from use of PCL (tensile modulus (E) 0.4 GPa, tensile strength 29 MPa, >

700% failure extension) [232] is expected to provide a better match with the mechanical properties of the natural artery than existing Dacron and ePTFE designs.

5.1 Measurement of the changes in diameter of PCL tubes under a constant flow rate of 300 ml/min at 37° C

The outer diameter of microporous PCL tubes increased by approximately 10μm from the starting diameter of 7.46 mm to around 7.47 mm over 1hr under a constant flow rate of 300ml/min at 37°C. A significant fluctuation in diameter was measured at 30min which may be caused by errors in response of the laser scanning micrometer or bubbles on the external tube surface. Although measurements of the tube diameter are affected by 'noise' associated with the operation of the laser micrometer, in general, fluid flow through the tube induced dilation and the amount of dilation increased with the duration of flow.

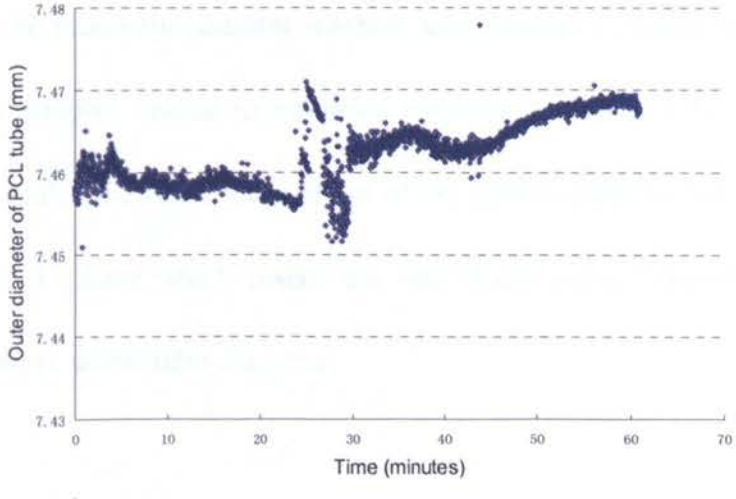

Figure 5.1 The changes in outer diameter of a microporous PCL tube over 1 hr at 37°C under a constant flow rate of 300ml/min

The changes in outer diameter of gelatin-loaded PCL tubes (28.6, 37.5 and 44.4% w/w loading) under a constant flow rate of 300 ml/min at 37 °C was also measured using a laser scanning micrometer. In contrast to microporous PCL tubes, a reduction of outer diameter was observed initially for all three gelatin-loaded PCL tubes followed by a relatively constant diameter during the 1 hour study (Figure 5.2). The initial gelatin loading affects the magnitude of the change and the time over which the changes in outer diameter occurred. For 28.6% gelatin-loaded PCL tubes, the outer diameter dropped quickly from approximately 7.6 mm to 7.5 mm (100μm) in 15 min (Figure 5.2 A) compared with approximately 150μm in 40 min for 37.5% gelatin-loaded tubes PCL tubes and 200 μm in 25 minutes for 44.4% loaded tubes (Figure 5.2 C). This behaviour may be attributed to the solubilisation of protruding gelatin particles at the external surface of PCL tubes resulting in a reduction of outer diameter. After a certain time, the outer diameter of 37.5 and 44.4% gelatin-loaded tubes tends to be relatively constant whereas tube dilation (10 μm) increased for the 28.6% loaded sample, similar to unloaded specimens (Figure 5.1). This behaviour may be attributed to the reinforcing affect of the gelatin particles incorporated in the microporous PCL phase which resists the wall shear stress induced by fluid flow, resulting in a more stable tube diameter.

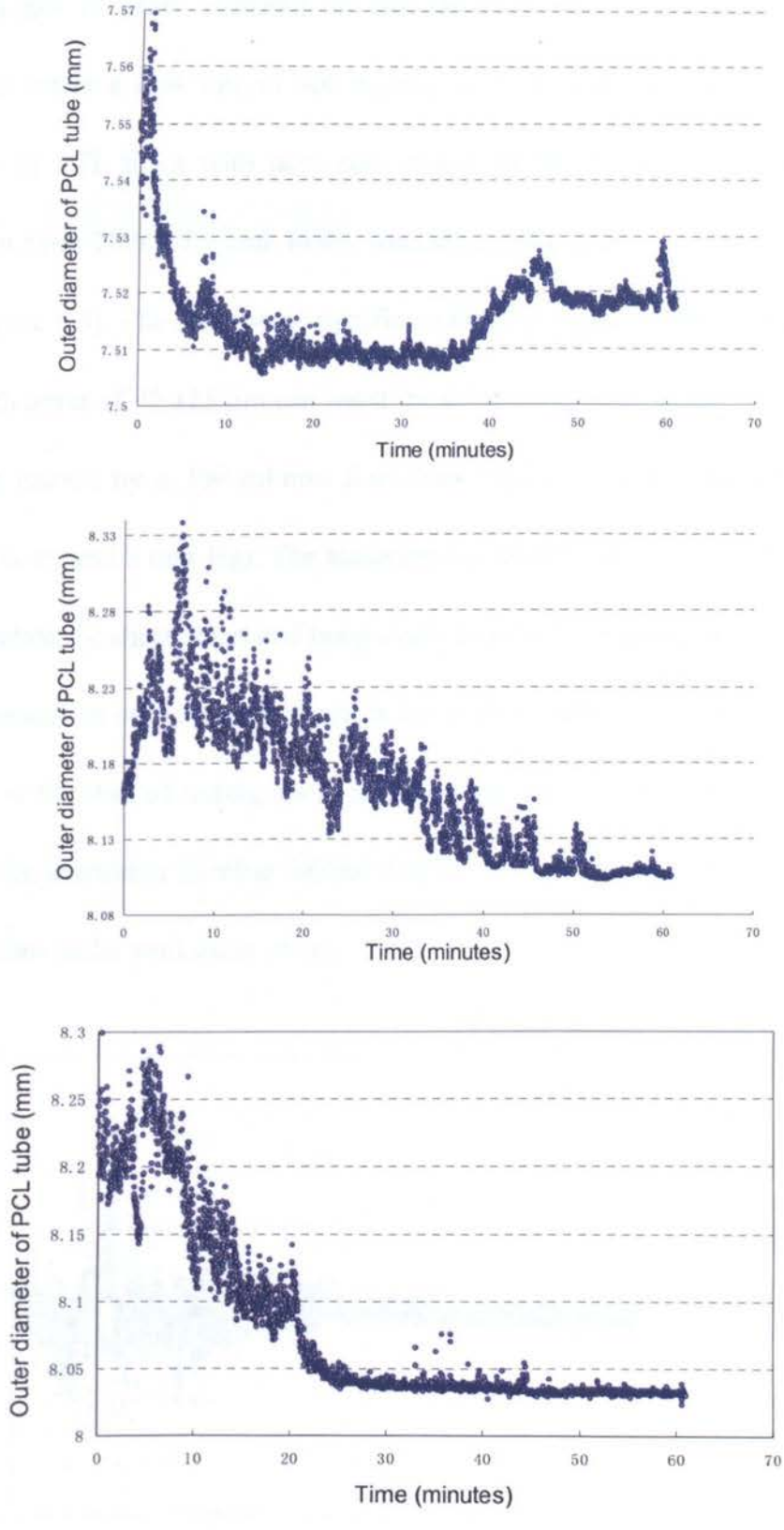

Figure 5.2 The changes in outer diameter of microporous PCL tubes containing (A) 28.6%, (B) 37.5% and (C) 44.4% w/w gelatin particles over 1 hour under a constant flow rate of 300ml/min at 37 ºC

The changes in outer diameter of macroporous PCL tubes formed by gelatin extraction under a flow rate of 300 ml/min at 37 °C were also recorded. The outer diameter of PCL tubes with pore size ranges of 90-125 μm produced by gelatin extraction from 28.6, 37.5 and 44.4% loaded samples remained fairly constant for 1 hour (Figure 5.3). The absence of significant dilation suggests that macroporous PCL tubes with pores of 90-125 μm can resist the shear stress and internal pressure of 20 + 5mm Hg caused by a 300 ml/min fluid flow rate over short time scales. (venous pressure is around 8 mm Hg). The macroporous internal structure of PCL tubes may accommodate the shear stress and hoop strain induced by hydrodynamic fluid flow by local deformation of the pore network at the luminal surface. The oscillation of outer diameter at the start of testing could be caused by the air remaining inside the pores after gelatin extraction forming bubbles which are released from the external surface of PCL tubes under wall shear stress.

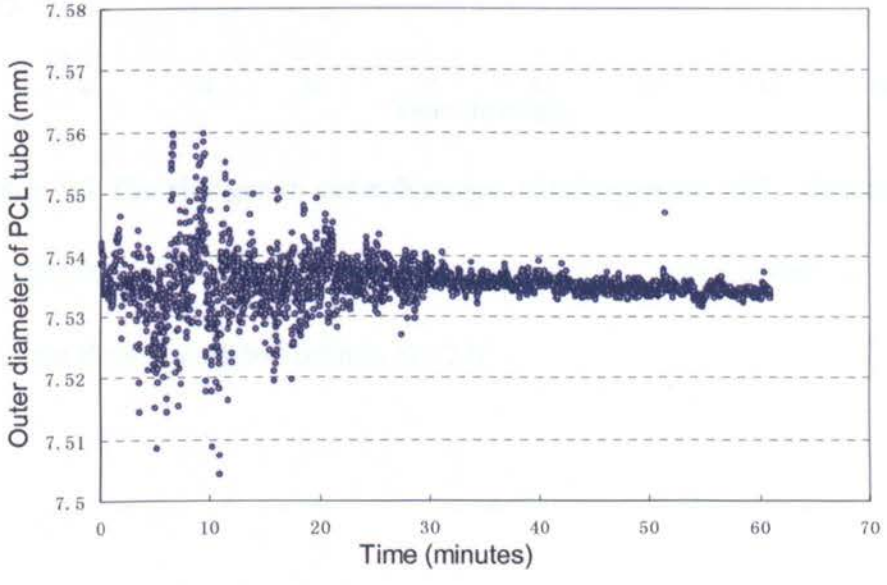

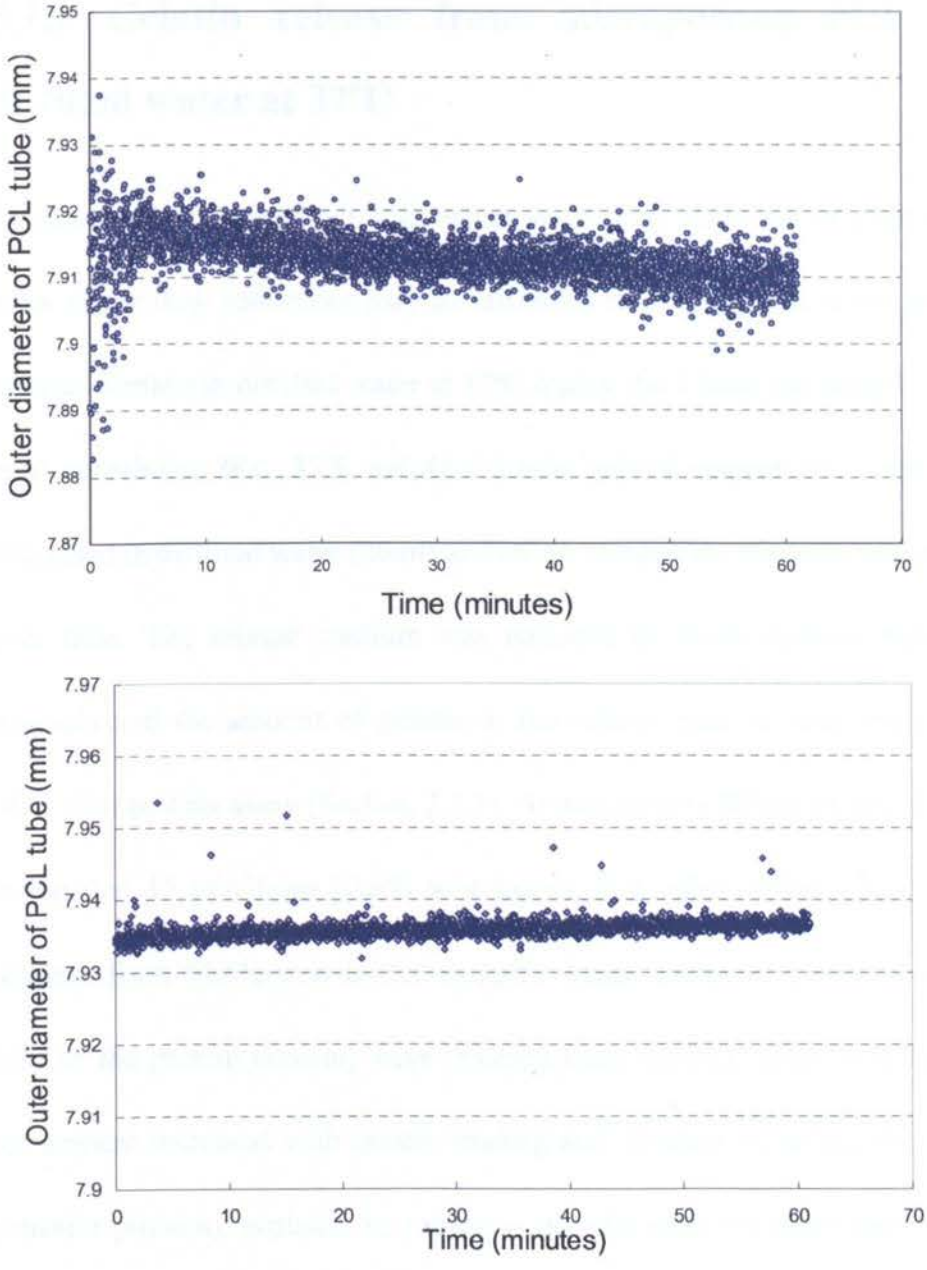

Figure 5.3 The changes in outer diameter of microporous PCL tubes after (A) 28.6%, (B) 37.5% and (C) 44.4% w/w gelatin extraction. Tubes tested for 1 hour under a constant flow rate of 300 ml/min at 37 °C

5.1.1 Gelatin release from microporous PCL tubes in distilled water at 37°C

As discussed in Section 5.1, the reduction of outer diameter of gelatin-loaded PCL tubes under flow conditions may be attributed to protein particle extraction from the external surface in distilled water at 37°C during the 1 hour test period, PCL tubes (50 mm) containing 28.6, 37.5 and 44.4% w/w gelatin respectively were consequently immersed in distilled water (20ml) at 37°C to monitor the diameter and protein release over time. The release medium was replaced by fresh distilled water at 15 min intervals and the amount of gelatin in the release medium was analysed using the BCA total protein assay (Section 2.7.1). Approximately 800μg of gelatin was released in the first 15 min from 28.6% w/w-loaded PCL tubes while around 2500 μg was released from 44.4% w/w-loaded samples. Large amounts of gelatin (approximately 15% of the protein content) were released from the PCL tubes over 15 minutes and the amount increased with gelatin loading and duration of testing (Figure 5.4). This behavior probably explains the reduction in outer diameter under hydrodynamic flow conditions (Figure 5.2).

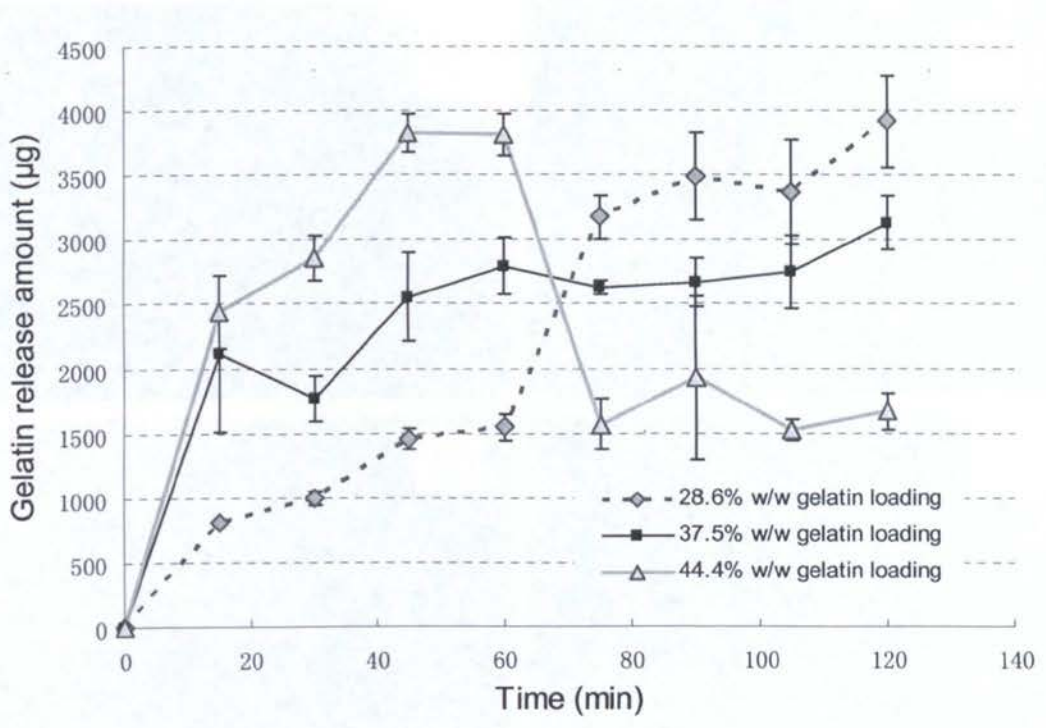

Figure 5.4 The amount of gelatin released from microporous PCL tubes in distilled water at 37°C

5.1.2 Morphology of the external surface of microporous PCL tubes before and after gelatin release

SEM examination of the external surface of gelatin-loaded PCL tubes revealed a characteristic rough and microporous surface formed by a fairly uniform dispersion of gelatin particles close to and protruding slightly from the tube surface (Figure 5.5 A and B). The 5-10µm micropores were also visible (Figure 5.5 B). After two hours release, macroporosity in the range of 90-125µm is apparent on the external surface of the PCL tubes (Figure 5.5 C and D). The significant changes of surface morphology before and after gelatin release are probably responsible for the reduction of outer diameter of PCL tubes under flow conditions (Figure 5.6).

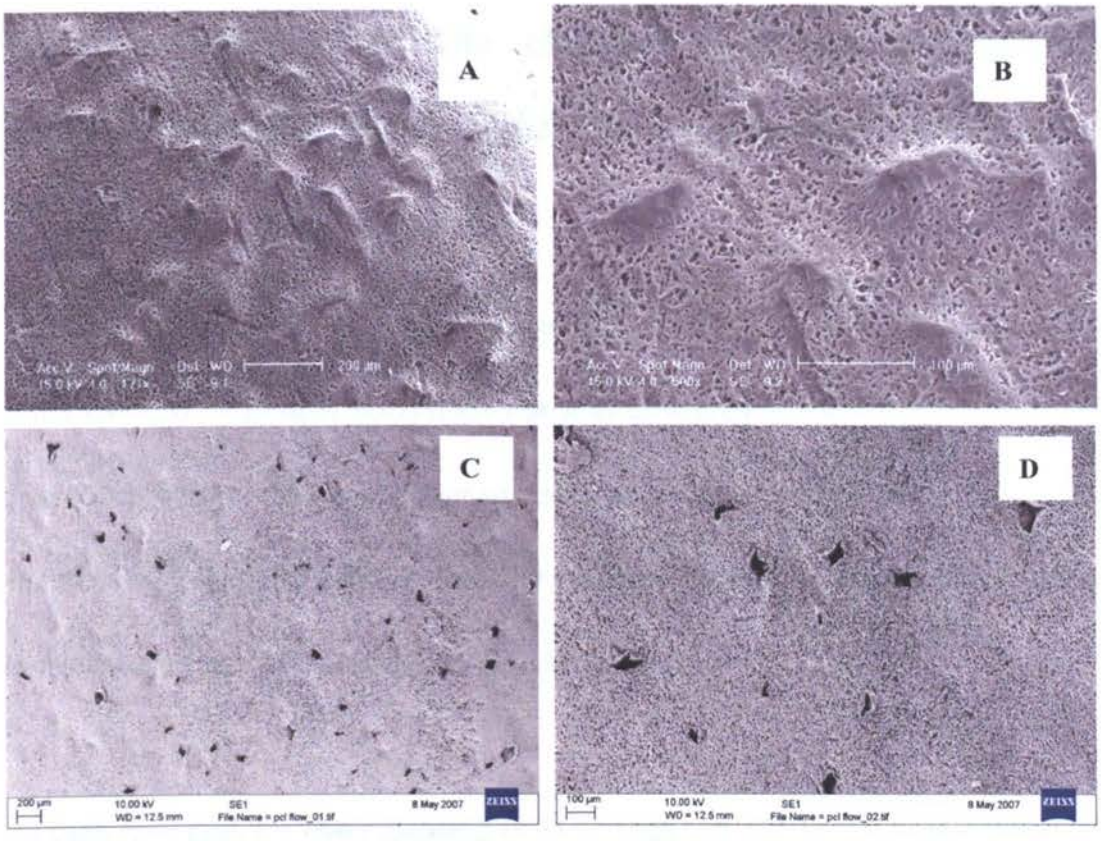

Figure 5.5 Scanning electron micrographs of 44% w/w gelatin-loaded PCL tube before gelatin release (A, B) after gelatin release (C, D)

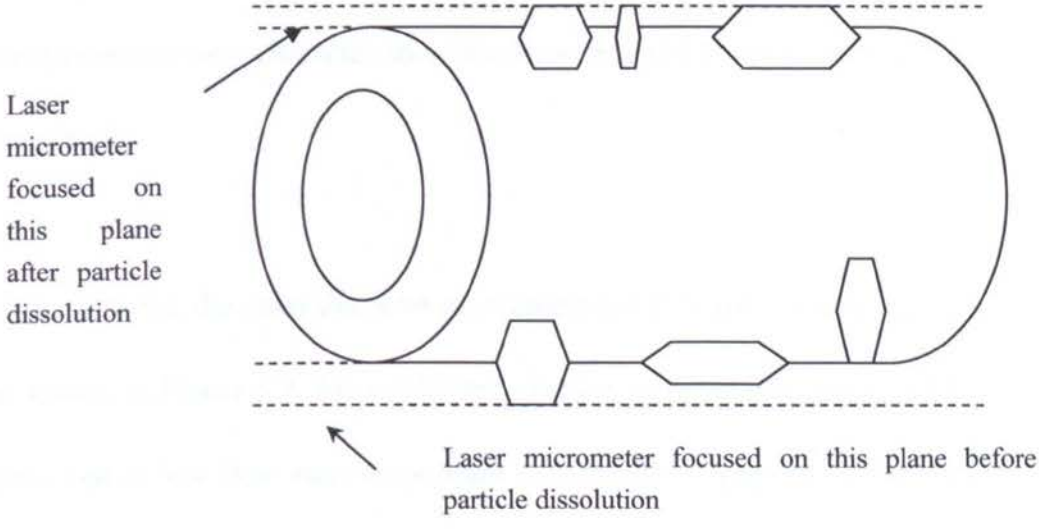

Figure 5.6 Explanation of the reduction in outer diameter determination of gelatin-loaded PCL tubes under flow conditions

5.2 Measurement of the changes in outer diameter of microporous PCL tubes under continuous flow conditions at 37°C

The outer diameter of PCL tubes, gelatin-loaded PCL tubes and macroporous PCL tubes (formed by protein extraction) was also measured under increasing flow rates from 50-1000 ml/min using a laser scanning micrometer. Similar to the above study (Section 5.1) nominal OD=7.5 mm, ID= 6.5mm, PCL tube length-55mm and the diameter changes were measured at the tube mid-point.

At each flow rate, the outer diameter of PCL tubes was measured at least 1000 times over a time interval of 2min at a rate of 10 measurements/sec in order to obtain the mean diameter. In addition, three repeat tests under increasing flow rates (50-1000 ml/min) were applied to each sample consecutively to generate information on the short-term recovery characteristics of microporous PCL tubes subjected to fluid flow conditions.

In the first run, the outer diameter of microporous PCL tubes increased with flow rate as shown in Figure 5.7. No significant changes in outer diameter of PCL tubes was measured at low flow rates from 50ml to 200ml/min, suggesting that PCL tube can resist the resulting shear stress and internal pressure without dilation. However, with increased rates of fluid flow, the PCL tube expanded from around 7.44 mm at 200ml/min to around 7.48 mm at 1000 ml/min (40μm) in a short time period (2

minutes). After 2 min at 1000ml/min, the flow rate was reduced to 50ml/min and the outer diameter of the PCL tube was recorded at around 7.45mm, which is at least 10μm larger than the starting diameter. Thus the PCL tube does not return immediately to its original diameter (recover) after being subjected to high flow rates. In the second run, the outer tube diameter first decreased and then gradually increased with increasing flow rate. This finding indicates that some recovery occurs over time following tube dilation. In the third run, the diameter of the PCL tube at each flow rate was similar to the second run, suggesting that permanent deformation ('set') of PCL tubes is produced initially by high flow rates but the recovery characteristics of the 'stress modified' material limits further deformation.

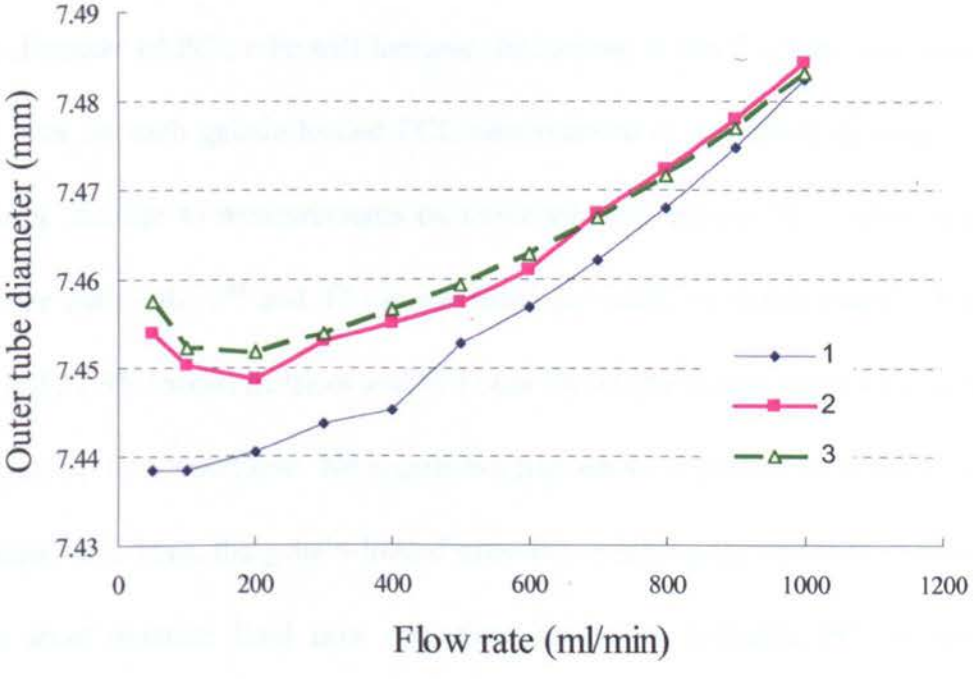

Figure 5.7 The changes in outer diameter of a microporous PCL tube under increasing continuous flow rates at 37°C

*1, 2 and 3 are repeated measurement of the same tube

5.2.1 Measurement of the changes in diameter of gelatin-loaded PCL tubes under continuous flow conditions at 37 °C

PCL tubes containing 28.6, 37.5 and 44.4% w/w gelatin loading respectively exhibited three patterns of behaviour in outer diameter under continuous flow conditions at 37°C (Figure 5.8). As discussed above in the constant flow rate study (300ml/min Section 5.1) gelatin particles start dissolving from the surface of PCL tubes from the beginning of the test at 37°C. Therefore, the peak in outer diameters under continuous flow in the first run may be attributed to the difference between the reduction of diameter caused by gelatin extraction and tube dilation. For example, if the tube dilation is larger than the diameter decrease induced by gelatin extraction, the outer diameter of PCL tube will increase. In contrast to the first run, the second and third tests on each gelatin-loaded PCL tube resulted in a gradual increase of outer diameter. Similar to measurements on unloaded microporous PCL tubes, the outer diameter during the 2^{nd} and 3^{rd} run increased gradually by approximately 30μm for 28.6 and 37.5% loaded matrices and by 60μm for 44.4%-loaded tubes with increasing flow rate up to 1000ml/min. No significant permanent deformation of the PCL tubes was observed. Thus, the gelatin-loaded materials exhibit good recovery characteristic under short duration fluid flow conditions similar to unloaded PCL matrices. In addition, tube dilation appears to increase with increasing gelatin content of the matrices indicating increased compliance of the material.

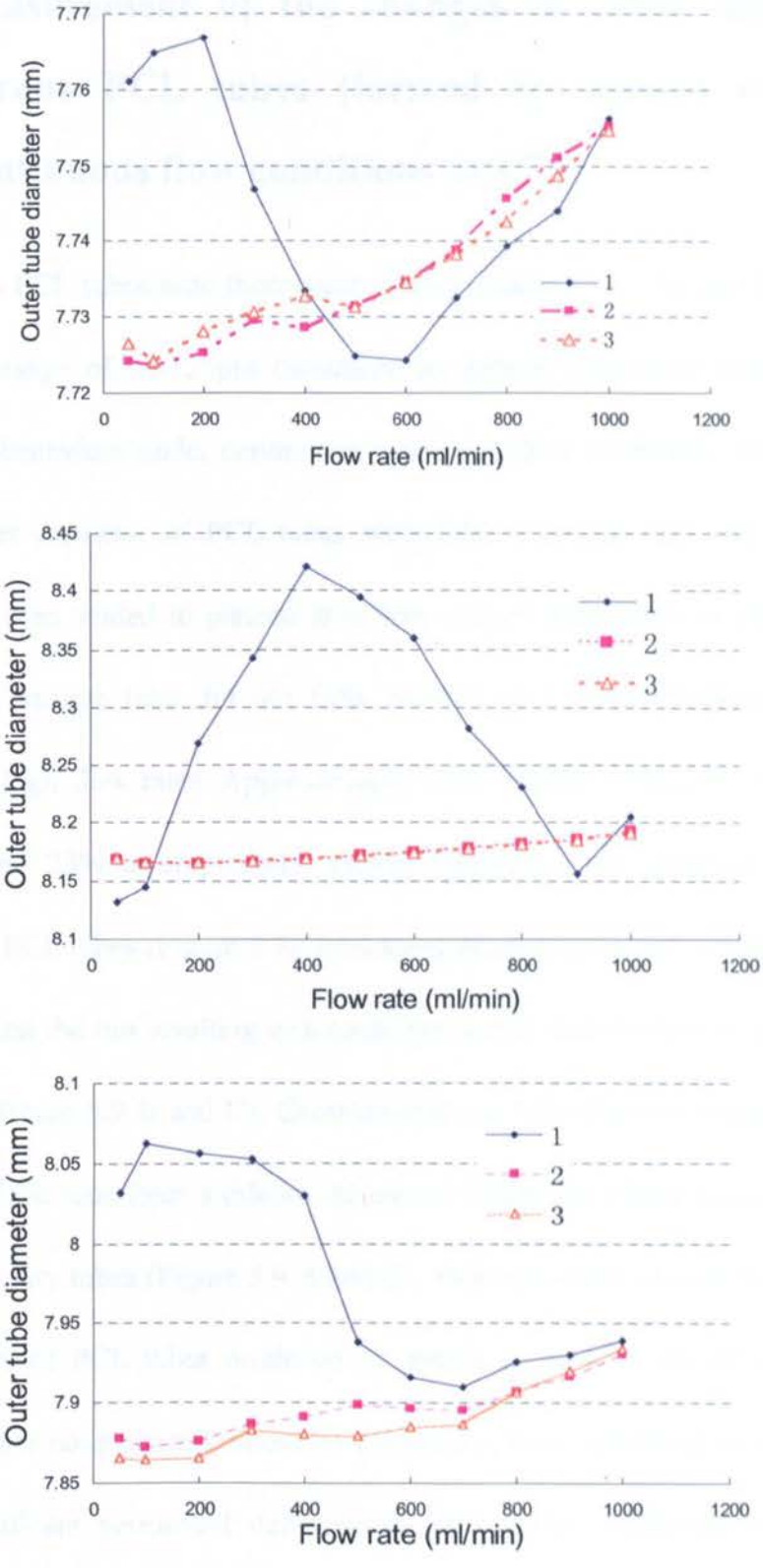

Figure 5.8 The changes in outer diameter of (A) 28.6% (B) 37.5% and (C) 44.4% gelatin-loaded PCL tubes under continuous increasing flow conditions at 37°C

*Run 1, 2 and 3 are repeated measurement on the same tube

5.2.2 Measurement of the changes in outer diameter of macroporous PCL tubes (formed by gelatin extraction) under continuous flow conditions at 37° C

Macroporous PCL tubes with theoretical macroporosity of 13, 19 and 23% and pore sizes in the range of 90-125μm (produced by gelatin extraction) exhibited similar deformation behaviour under continuous increasing flow conditions. During the first run, the outer diameter of PCL tubes with 13% macroporosity increased rapidly initially and then tended to plateau at a flow rate of 400ml/min to 1000ml/min. In addition, the sample tube did not fully recover its original diameter after being subjected to high flow rates. Approximately 5μm dilation remained. For PCL tubes with 19% and 23% macroporosity, similar behaviour was observed to unloaded microporous PCL tubes (Figure 5.7). Increasing dilation occurred with increased flow rate during first the run resulting in a small permanent deformation of approximately 5 to 10μm (Figure 5.9 B and C). Good recovery of tube diameter occurred after the second and third runs from a dilation of around 15μm and 40μm respectively for 19 and 23% porosity tubes (Figure 5.9 B and C). This behaviour reveals that the internal pore structure of PCL tubes produced by gelatin extraction can accommodate the shear stress and hoop strain induced by continuous flow conditions in the short term without significant permanent deformation. The extent of dilation increases with increasing porosity of the matrix due to the reduction in the polymer phase content and consequent increase in material compliance.

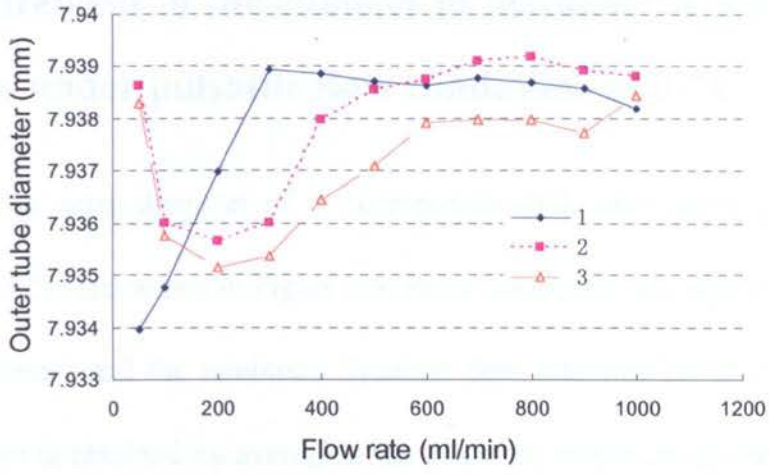

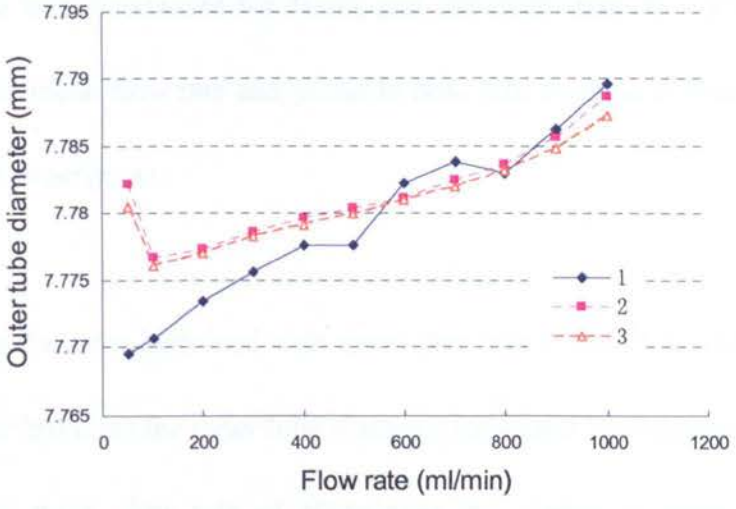

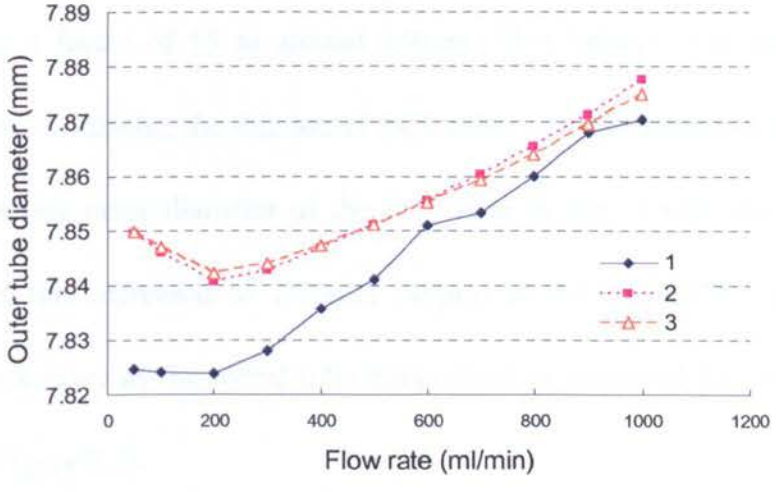

Figure 5.9 The changes in outer diameter of macroporous PCL tubes produced by gelatin extraction under continuous increasing flow conditions at 37°C. (A) 13% macroporosity (B) 19% macroporosity(C) 23% macroporosity

*Run 1 2 and 3 are repeated measurement on the same tube

5.3 Measurement of the changes in diameter of microporous PCL tubes under pulsatile flow conditions at 37°C

The changes in outer diameter of a microporous PCL tube under pulsatile flow conditions at 37°C are shown in Figure 5.9. Pulse frequency was adjusted to 1Hz (60 pulses per minute) and the minimum dynamic flow rate was set at 0 ml/min. The mean flow rate is obtained by averaging the peak and minimum dynamic flow rate. Each flow rate was maintained for 5mins and the outer diameter of PCL tubes was measured under mean flow rate and pulsatile flow rate conditions over 50 secs in the middle of each experiment.

The outer tube diameter increased with mean flow rate (Table 5.2). When mean flow rate was low (50ml/min) the outer tube diameter increased by approximately 5-10μm. With increased mean flow rate of 600ml/min the change in outer tube diameter increased by a factor of 15 to around 150μm. This behaviour reveals that under pulsatile flow conditions, the dilation of PCL tubes is proportional to the mean flow rate. The starting outer diameter of the PCL tube in Exp 1 tube was measured as 7.69mm and this increased to 7.73mm (40μm) at the end of the test indicating incomplete recovery of the initial tube dimensions as observed for continuous flow conditions (Figure 5.7).

Table 5.1 The effect of conditions of pulsatile flow on the deformation of microporous PCL tubes

Exp. No.	Max dynamic flow (ml/min)	Mean flow rate (ml/min)	Change in outer tube diameter (mm)
1	100	50	0.01
2	200	100	0.02
3	300	150	0.03
4	400	200	0.04
5	500	250	0.05
6	600	300	0.055
7	700	350	0.075
8	800	400	0.08
9	900	450	0.09
10	1000	500	0.10
11	1100	550	0.13
12	1200	600	0.15

Pulse frequency 1Hz. Minimum dynamic flow rate = 0ml/min

PCL tube length = 60mm PCL tube outer diameter =7.68mm

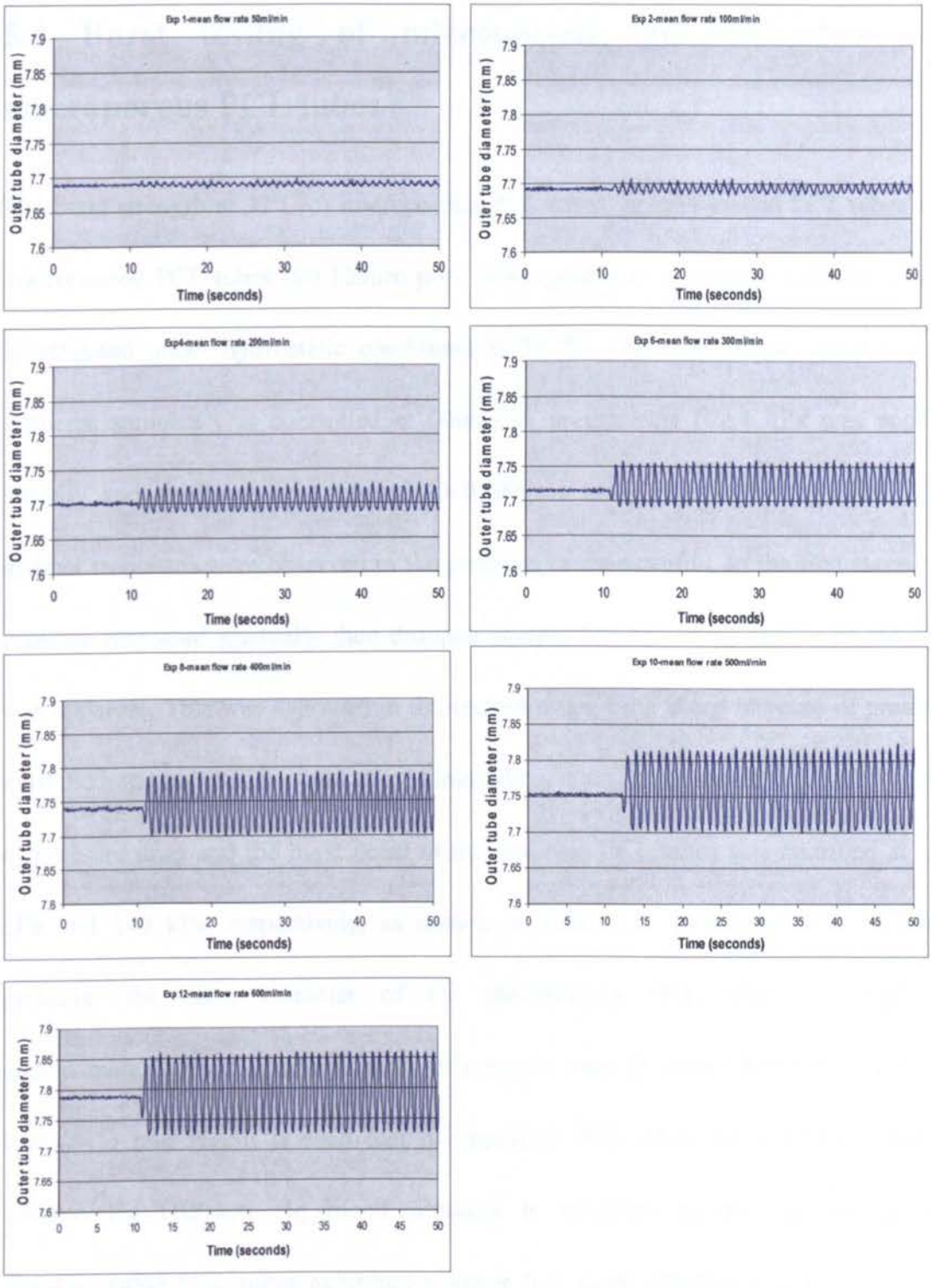

Figure 5.10 The changes in outer diameter of microporous PCL tube under pulsatile flow conditions at 37 °C

5.4 Burst testing of microporous, gelatin-loaded and macroporous PCL tubes

The burst strength at 37°C of microporous PCL tubes, gelatin-loaded PCL tubes and macroporous PCL tubes (90-125μm pore size) (produced by gelatin extraction) was investigated under hydrostatic conditions at 37 °C. The tube length under test of triplicate samples was controlled at 60mm. A pressure of 102.4 kPa was applied initially and increased at a rate of 50-200Pa/sec using a pressure regulator. Two distinct responses were observed in the pressure vs time profile. In the first stage, the pressure increased gradually then dropped sharply but no visible failure of the tube was apparent. This was followed in the second stage, by a sharp increase of pressure until the burst point of the tube when longitudinal cracking is apparent. The first point of pressure drop and the burst point of microporous PCL tubes was recorded at 132 kPa and 149 kPa, respectively, as shown in Table 5.3. With gradually increased pressure, the outer diameter of the microporous PCL tubes increased by approximately 20μm until first point of pressure drop (Figure 5.10). On converting Pascals to mm Hg, it is seen that microporous PCL tubes can withstand around 200mm Hg (120mm Hg blood pressure is recorded in healthy individuals). Gelatin-loaded PCL tubes exhibited a lower first point pressure and burst strength than PCL tubes resulting in around 130 mm Hg pressure resistance. No significant difference in burst strength was apparent for 28.6%, 37.5% and 44.4% w/w gelatin-loaded PCL tubes in the present study. However the gelatin particles embedded in the PCL phase reduced the overall strength of the tube relative to

microporous PCL samples by reducing the PCL content and/or acting as stress raisers to initiate crack formation. Similarly, macroporous PCL tubes formed by gelatin particle extraction also revealed decreased burst strength and a low first point pressure compared with microporous PCL tubes (Table 5.10). Increased porosity resulting from gelatin extraction reduces the PCL content of the tube wall and the continuity of the PCL phase. Therefore, lower burst strength is anticipated.

Table 5.2 Burst strength of microporous PCL tubes, gelatin-loaded PCL tubes and macroporous PCL tubes formed by gelatin extraction

Sample	1st point of pressure drop (kPa)	Burst point (kPa)
PCL tube	131.7 ± 4.8	148.7 ± 12.4
28.6 w/w gelatin-loaded	120.6 ± 2.1	123.7± 1.4
37.5 w/w gelatin-loaded	118.5 ± 3.3	128.9 ± 2.2
44.4 w/w gelatin-loaded	115.0 ± 7.1	131.7 ± 4.8
13% macroporous PCL tube	114.6 ± 3.9	126.6 ± 5.4
19% macroporous PCL tube	115.6 ± 1.1	125.3 ± 5.7
23% macroporous PCL tube	115.1 ± 2.5	120.6 ± 6.6

- Macroporous PCL tubes produced by extraction of 90-125μm gelatin particles at 37°C

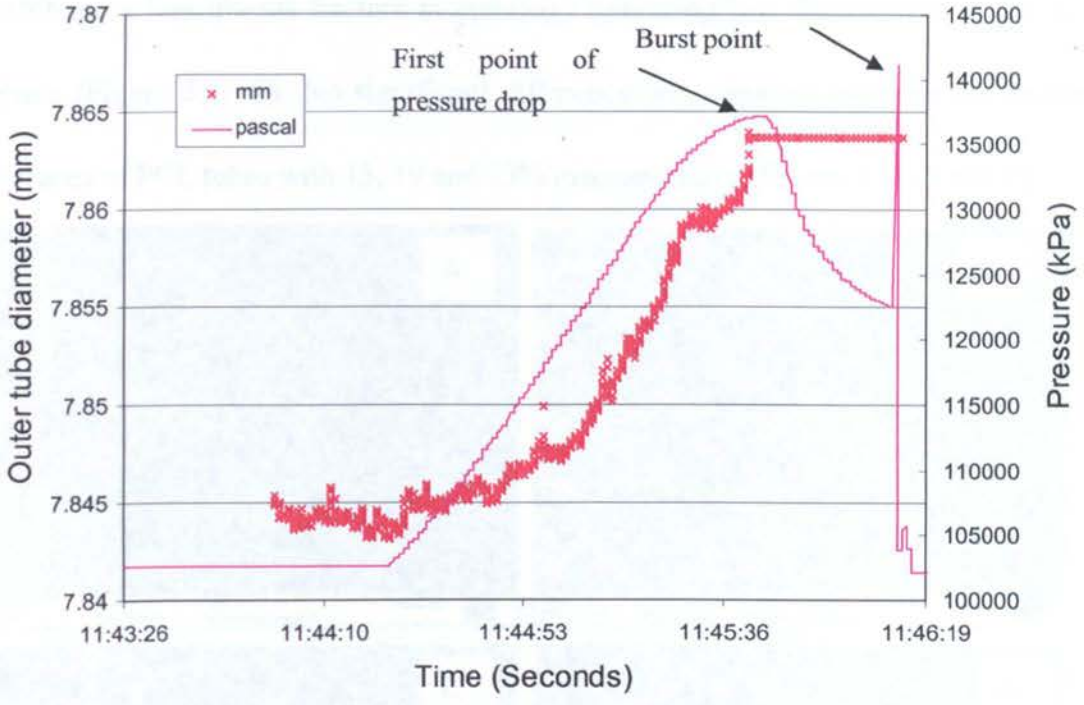

Figure 5.11 The changes of outer tube diameter and internal pressure during burst testing of PCL tubes

5.4.1 Morphology of fracture surface of PCL tubes following burst testing

The fracture surface of microporous PCL tubes following burst testing was characterized by a rough, microporous morphology with irregular pore shape and size of 5-20μm (Figure 5.11 A and B). The PCL fibrils visible in the fracture area might be formed by deformation of the PCL phase caused by increased internal pressure at the burst point. SEM analysis of macroporous PCL tubes formed by gelatin extraction also revealed a microporous fracture surface and the presence of irregular large pores of size of 90-125μm (Figure 5.11 C D and E) which can be attributed to the original gelatin particles. Compared with microporous PCL tubes, macroporous tubes

exhibited a less fibrous fracture morphology indicating less deformation of the PCL phase (Figure 5.11 C). No significant difference was apparent between the fracture surfaces of PCL tubes with 13, 19 and 23% macroporosity (Figure 5.11 D and E).

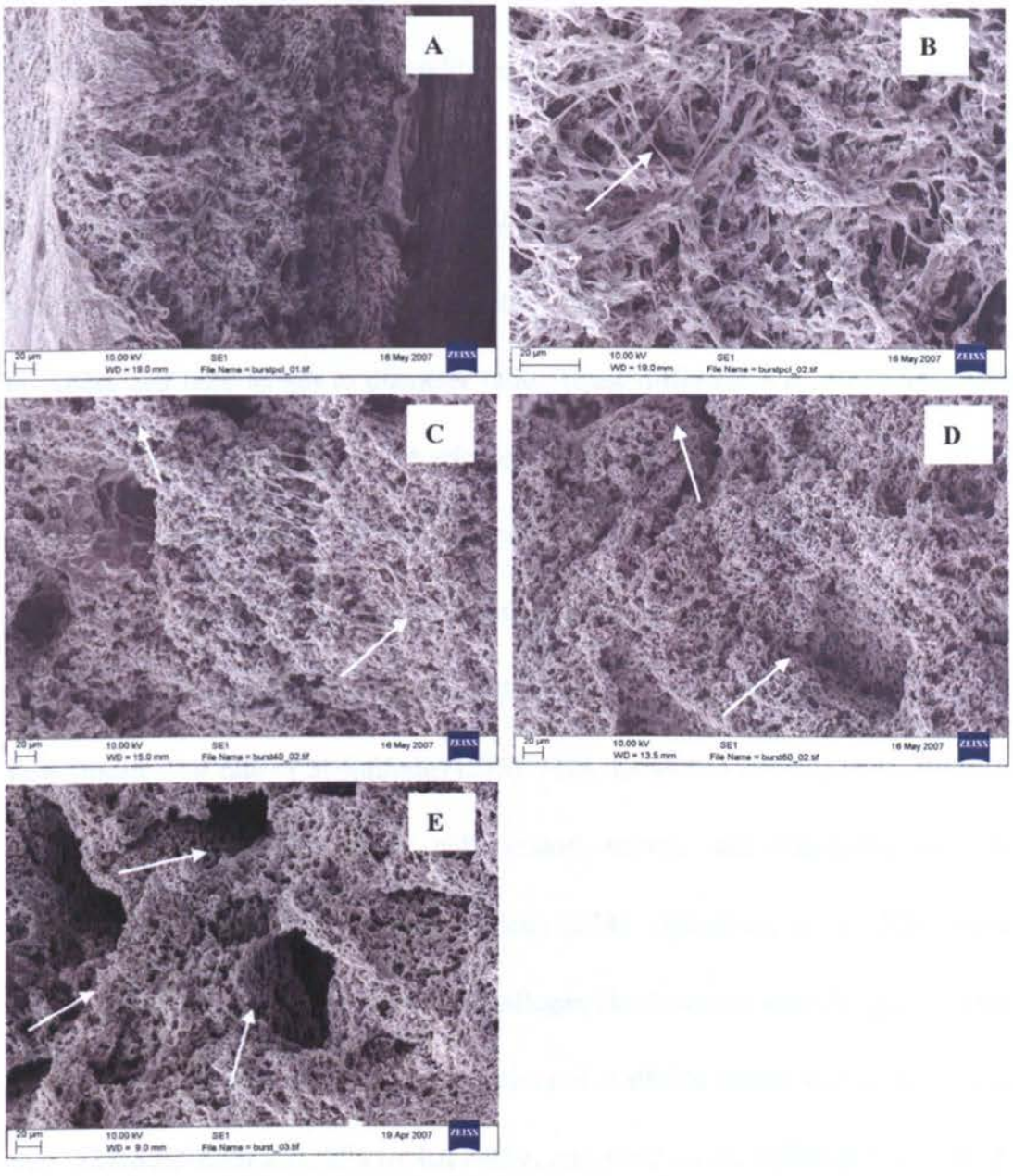

Figure 5.12 Scanning electron micrographs of fracture surface of PCL tubes following burst testing (A,B)microporous PCL (C)13% macroporous PCL (D)19% macroporous PCL (E) 23% macroporous PCL

5.5 Discussion and conclusions

The study described in this chapter was designed to evaluate the changes in diameter, recovery characteristics and burst strength of PCL--based tubes under hydrostatic/hydrodynamic flow conditions to assess their potential as vascular grafts. In previous studies, both synthetic and natural materials have been used in tissue engineering of blood vessels (mostly biodegradable) [233, 234]. Vascular grafts have been fabricated in a range of tube geometries that have significant differences in wall thickness and tube length to diameter ratio. These differences in geometry together with porosity and polymer physico-chemical properties would all influence mechanical performance. Polylactic acid-based tissue engineered blood vessels (20mm in diameter, 80mm length and with over 95% porosity) have shown favorable interaction with smooth muscle-like cells under dynamic fluid stress and pulsatile flow (mean flow rate of 500ml/min) [233]. PGA nonwoven tubes have been used for sequential seeding of constructs with smooth muscle and endothelial cells in a perfusion bioreactor under flow conditions [234]. Buttafoco, et al [235] recently characterised the physical properties of collagen/elastin-based vascular grafts cultured in a bioreactor. During 7 days, the yield stress of scaffolds seeded with smooth muscle cells increased from 20±1kPa to 40±10kPa, and yield strain increased from 90±20% to 160±30% under both dynamic and static flow conditions.

In the present study, the changes in outer diameter (dilation) of microporous and macroporous PCL tubes were investigated under hydrostatic and hydrodynamic

conditions. No significant dilation of microporous PCL tubes (10μm) was recorded at a constant flow rate of 300ml/min during limited testing (1 hour) at 37°C. Flow testing of gelatin-loaded tubes at a constant flow rate of 300ml/min resulted in a gradual decrease of tube diameter, probably due to solubilisation of protruding gelatin particles at the tube surface. (Figure 5.2) This behaviour may be advantageous for delivery of antibacterials or thrombolytic agents immediately flowing implantation of PCL tubes as vascular prosthesis. Enhanced macroporosity of the graft surface may improve interaction of host cells such as fibroblasts with the scaffold external surface or the interaction of seeded cells with the scaffold in a bioreactor prior to implantation. Under continuous increasing flow conditions, microporous PCL tubes exhibited minor dilation (30μm) under high flow rates (1000ml/min), but no craze or crack formation. Gelatin-loaded PCL tubes and macroporous PCL tubes, formed by gelatin extraction, exhibited good recovery of diameter following continuous increasing fluid flow rates (Figure 5.7) similar to unloaded, microporous PCL tubes. In this case, tube dilation increased with gelatin content and macroporosity, reflecting the importance of the PCL phase for resisting hydrodynamic stresses. These findings demonstrate the importance of adjusting the scaffold composition to meet the mechanical property requirement of potential vascular prostheses.

The dilation of microporous PCL tubes under pulsatile flow conditions (1Hz) at 37°C increased from 5μm to 150μm with increasing mean flow rate from 50-600 ml/min. This behaviour is attributed to the particular mechanical properties of

polycaprolactone, 750% elongation, low tensile modulus (0.4 GPa) tensile strength 29MPa. Importantly, the microporous PCL tubes tend to show very good recovery after deformation under high flow rate conditions (Figure 5.7) but not to the original tube diameters, indicating the limited elasticity of polycaprolactone. Cell seeding including fibroblasts, smooth muscle cells and/or incorporation of a natural polymer such as elastin may overcome this limitation of the present designs. Alternatively, pre-stressing of microporous PCL tubes could be applied to introduce permanent 'set' prior to implantation. Increasing tube dilation of 15 and 40μm respectively occurred for macroporous PCL tubes with theoretical porosity of 19 and 23% under a high continuous flow rate of 1000ml/min, this behaviour again indicates the importance of controlling the scaffold porosity to optimize cell interaction, drug delivery and mechanical properties.

Microporous PCL tubes revealed a relatively high burst strength of around 200-300 mm Hg of PCL tubes compared with gelatin-loaded PCL tube (around 130mm Hg) and macroporous PCL tubes formed by gelatin particle extraction (around 115 mm Hg). The burst strength may be varied if necessary in future work by controlling factors, such as the starting molecular weight and crystallinity of polycaprolactone, the thickness of the tube wall, porosity and uniformity of pores etc. If a cylindrical body is distended radially (due to internal pressure), then to conserve volume, the cylinder's length will decrease (Poisson's ratio), generating a reaction force parallel to the tube axis. Transverse cracking may be expected on tube failure. Longitudinal tube

cracking was observed during burst testing suggesting that radial tube extension is responsible for tube failure. However, because of the degree of elasticity of polycaprolactone both longitudinal and radial elongation could occur, with volume being conserved by thinning of the porous tube wall. This phenomenon is known as hyper elasticity and has been shown to occur in vascular tissue [236]. Non-uniformity of PCL tubes may influence the burst strength. The sharp drop in pressure recorded during burst testing of PCL tubes may be explained by localized dilation of the porous tube wall or failure of the luminal surface, prior to final crack propagation through the entire tube wall. This capacity for 'pressure relief' could be advantageous in avoiding catastrophic failure of implanted tubes.

More extensive testing is necessary to assess whether PCL tubes can be utilized in vivo as vascular graft over long time periods of at least 7-10 years. The mechanical properties may be reinforced by growth of smooth muscle cells, endothelial cells and fibroblasts in vitro or in vivo in longer term investigations. Further work in required to assess for example:

1. the long term mechanical behaviour under flow conditions
2. the interaction of the PCL tubes with blood components
3. endothelial cell/scaffold interaction with the aim of producing an endothelialised luminal surface
4. fibroblasts interaction with the external tube surface to promote integration with host tissue

Chapter 6

Controlled delivery of enzymes and a steroid, dexamethasone, from microporous PCL matrices

Chapter 3 described the incorporation of lactose and gelatin particles in microporous PCL matrices in order to achieve 1) controlled drug delivery and 2) macroporous PCL scaffolds with defined pore structure to enhance cell ingrowth. PCL matrices revealed sustained release of gelatin in PBS at 37°C. However, the formulation approach using organic solvent may denature proteins resulting in loss of biological activity. The aim of this chapter is to investigate the influence of PCL matrix formulation on enzyme loading and release characteristics and biological activity in vitro as a model for growth factor delivery in tissue engineering.

Various enzymes such as lysozyme, ribonuclease A and horseradish peroxidase (HRP) have been used as model proteins to investigate the stability and activity of proteins during processing and storage [219, 221, 222]. In this study, lysozyme, collagenase and catalase were incorporated within PCL matrices, respectively, by rapid precipitation of an enzyme suspension in PCL solution in dry ice followed by solvent extraction (Section 2. 4). The choice of these enzymes was based upon 1) the availability of a convenient and well validated biological assay in vitro 2) protein

molecular weight characteristics covering a wide range from 14.3 to 240kDa and 3) their supra-molecular structures (secondary, tertiary and quaternary structures) which play an important role in controlling enzyme activity.

6.1 Preparation and analysis of lysozyme-loaded PCL matrices

6.1.1 Lysozyme as a model protein in tissue engineering

Chicken egg white lysozyme is a low molecular-weight protein (14.3kDa) comprising 129 amino acids with secondary and tertiary structure Figure 6.1. Lysozyme consists of 40-45% α–helix, 19% β-sheet, 23-27% turn and 13-14% random structures. The enzyme is widely distributed in animals and plants and has been used in the pharmaceutical industry due to its bacteriolytic properties for treatment of sore throats. Lysozyme has been investigated frequently for a number of years as a model protein to determine the effects of scaffold or microsphere formulation on release behavior and activity [237-239].

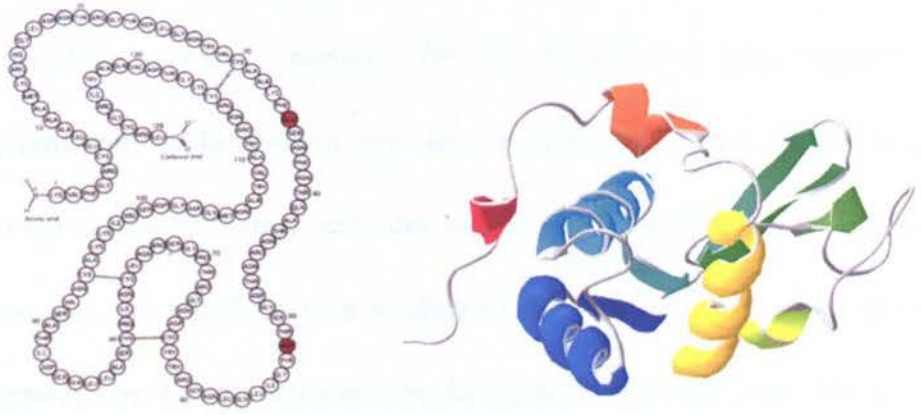

Figure 6.1 Native structure of chicken egg white lysozyme

6.1.2 Formulation of lysozyme-loaded PCL matrices

Lysozyme is insoluble in acetone but soluble in water (15mg/ml) and methanol. Lysozyme lyophilized powder containing 50,000 units/mg was ground using a glass pestle and mortar resulting in particles of size 100-200μm with irregular particle shape (Figure 6.7 D). Lysozyme particles were suspended in 17% w/v PCL solution to produce 10%, 20% and 40% w/w suspensions and lysozyme-loaded PCL matrices were subsequently produced by rapid cooling of the suspensions in dry ice as described in Section 2.1.2.

PCL microporous matrices containing lysozyme particles display soft and flexible characteristics and are free of large scale cracks and voids in the surface and interior. The lysozyme loading in the final matrix was around 3.1 % w/w and 10.5% w/w for matrices produced from 10% and 20% w/w particle suspensions, respectively (Figure 6.2). This reduction in loading compared with the starting suspension may be explained by the solubility of lysozyme in methanol which is used during matrix formulation to extract acetone. The lysozyme-loaded PCL matrices exhibited a uniform particle distribution from the top layer to the base (Figure 6.2) confirming that the casting technique using dry ice can significantly limit particle sedimentation. Increasing the initial enzyme loading of the PCL solution from 10% to 20% w/w improved the loading efficiency in the finished matrices from 30% to around 50%. PCL matrices were also produced from suspensions containing 40% w/w lysozyme powder. However, the poor mechanical strength of the finished matrix indicates that

interactions between lysozyme and the PCL phase lead to a reduction in physical and mechanical properties.

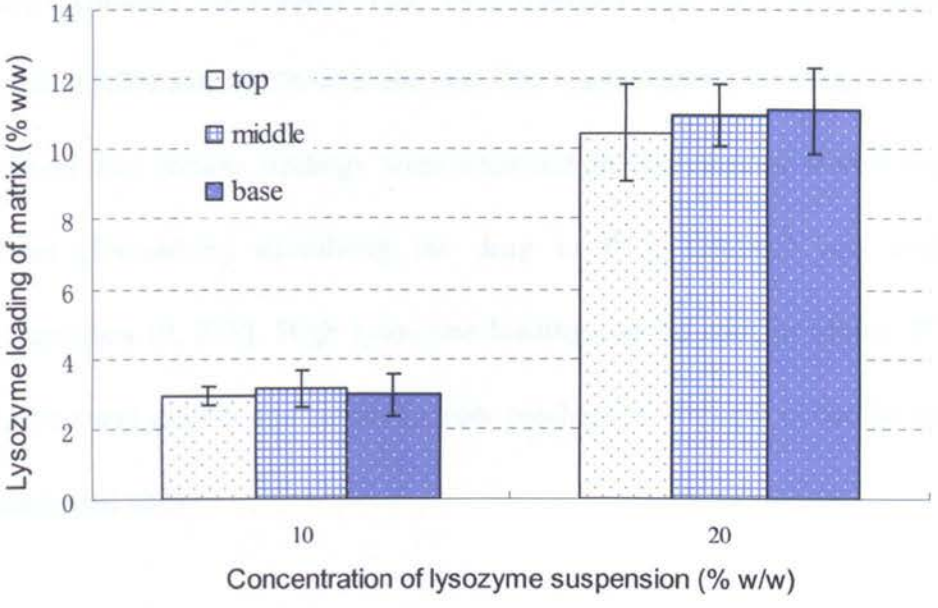

Figure 6.2 The weight distribution of lysozyme in microporous PCL matrices

6.1.3 Thermal properties of lysozyme-loaded PCL matrices

Polymer crystallinity affects the permeability to fluids, biodegradation rate and density of polymeric matrices because the close-packed polymer chains in the crystalline phase are less accessible to water and other solvents which may influence protein or drug release from the material [240]. The melting point of PCL and lysozyme-loaded PCL matrices produced by rapid cooling was, in general, higher than the value of 58-60°C normally quoted for PCL (Table 6.1). The melting temperature of lysozyme-loaded matrices was approximately 2 °C lower than enzyme-free matrices suggesting the presence of smaller crystallites and/or crystal imperfections. Low lysozyme loading results in increased PCL crystallinity suggesting enhanced

crystal nucleation and growth due to the presence of the particulate. However, the % crystallinity of PCL matrices having the highest enzyme loading (40%) was found to be approximately 10% lower than PCL matrices and 15% lower than matrices containing 3.2% and 10.5% w/w enzyme. The reason behind this behaviour is unclear at present but similar findings were recorded in the case of steroid-loaded PCL matrices (formed by dissolving the drug in PCL solution) and collagen:PCL biocomposites [9, 218]. High lysozyme loading can be seen to inhibit PCL crystal nucleation and growth and results in poor mechanical strength of the finished matrix as mentioned above.

Table 6.1 Thermal properties of PCL and lysozyme-loaded PCL matrices

Formulation of PCL matrix	PCL	lysozyme-loaded PCL matrix		
Lysozyme loading (% w/w)		3.2	10.5	40
Tm (°C)	68.2	66.1	66.1	66.8
ΔH_f	99.7	107.8	105.7	83.7
Crystallinity (%)	71.5 ± 0.71	77.3 ± 0.43	75.8 ± 1.16	60.2 ± 2.57

6.1.4 Lysozyme release from microporous PCL matrices

The amount of lysozyme released from PCL matrices in PBS solution at 37 °C was measured using the BCA total protein assay (Figure 6.3). A burst release phase of 30 and 45% was observed for enzyme-loading of 3.1% and 10.5% respectively during the first day followed by gradual release up to day 7 when the release profile plateaued. The initial enzyme loading affects the initial burst effect. There was no marked difference in the release pattern of the two formulations, around 80% of the

initial enzyme content was delivered from the 10.5% w/w lysozyme-loaded PCL matrix within 12 days compared with 60% from the 3.1% w/w lysozyme-loaded PCL matrix. This behaviour indicates a more highly developed network of interconnections between lysozyme particles in the more highly loaded matrices. The remaining enzyme content may be efficiently encapsulated by polymer therefore taking longer to release or not being released [217].

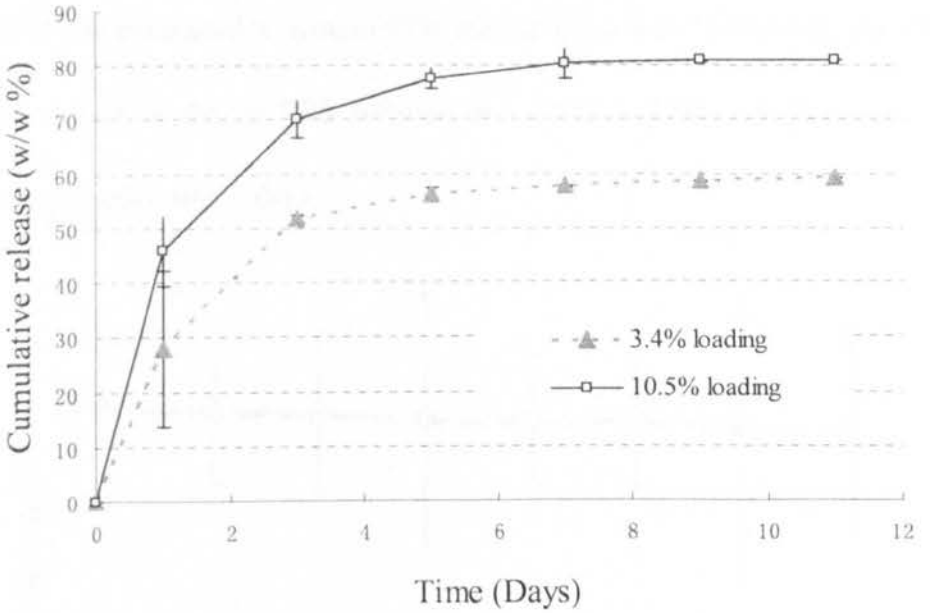

Figure 6.3 Cumulative lysozyme release from microporous PCL matrices in PBS at 37°C

6.1.5 Biological activity of lysozyme

Most of the biochemical assays for lysozyme are based on its lytic activity since lysozyme can hydrolyze the 1-4 glycosidic linkage between alternating N-acetylglucosamine (NAG) and N-acetylmuramic acid [50] residues on the cell wall of micro-organisms. In the present study, the activity of lysozyme was determined by

measuring the turbidity degree of lysis induced by the enzyme on *Micrococcus lysodeikticus* cells as described in Section 2.4.5 [241].

Fresh lysozyme solution in PBS of concentrations 1mg/ml and 2mg/ml was stored at -20°C for one week and the activity of thawed enzyme solution was determined every 24 hours to investigate the effect of storage condition on activity. As shown in Figure 6.4, enzyme activity appeared to be constant and close to 100% after 5 days storage at - 20°C and decreased to around 97% during day 6 and 7 indicating that the enzyme is fairly stable in frozen PBS solution at - 20°C and no significant loss of enzyme activity occurs over 7 days.

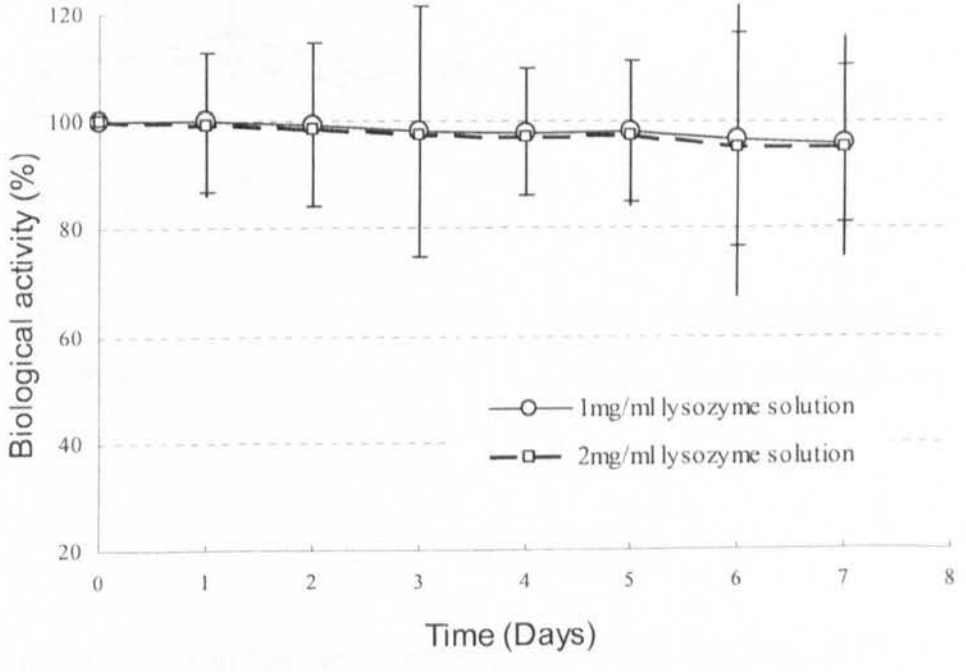

Figure 6.4 Activity of lysozyme solution in PBS following storage at - 20°C

Fresh lysozyme solution in PBS at concentrations of 1mg/ml and 2mg/ml was also

stored at 37°C for one week and activity was recorded every day over one week. The enzyme appeared to be stable for the first three days (95-100% retained activity) compared to native enzyme solution and slightly decreased (by approximately 5%) over the following 4 days. Protein stability mainly depends on the interactions of the amino acid side chains with secondary structure elements and/or the solvent to which it is exposed [242]. The loss of activity of lysozyme during 7 days storage in PBS (pH 7.4) at 37°C may be attributed to time dependent unfolding of its secondary structure elements at 37°C or to the pH of the medium which is outside the most stable range of 3.5-5.0 for lysozyme [243-245].

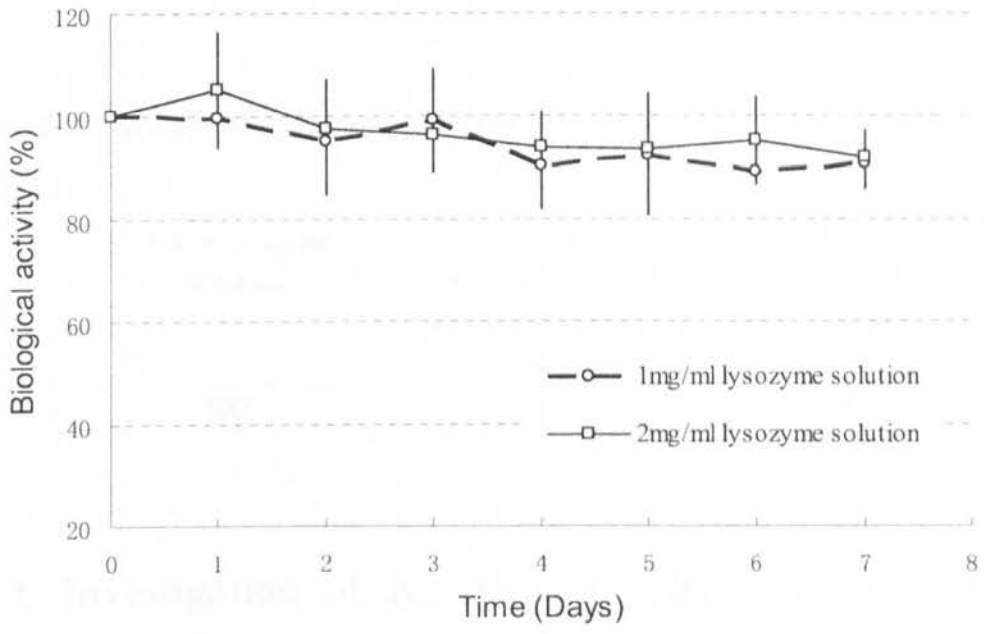

Figure 6.5 Activity of lysozyme solution in PBS following storage at 37°C

Lysozyme powder (approximately 2mg) was exposed to 2ml acetone or dissolved in methanol for 1 hour respectively to investigate the effect of matrix formulation

conditions on enzyme activity. After solvent evaporation in air, the dried lysozyme powder was accurately weighed and re-dissolved in PBS solution to make a 1mg/ml enzyme solution for activity measurement. Native lysozyme powder was also dissolved in PBS as a control. As shown in Table 6.2, no significant loss of bioactivity of lysozyme was measured after immersion of the powder in acetone or methanol for 1 hour indicating that the organic solvents used in matrix formulation do not cause unfolding of the enzyme secondary structure resulting in denaturation or degradation of the native enzyme. This result suggests that the technique of PCL matrix formulation by rapid cooling may be useful for incorporating growth factors or other active molecules with retained activity.

Table 6.2 Activity of lysozyme solution following powder exposure to organic solvents

	Native lysozyme solution	Lysozyme solution (50μg /ml) prepared from powder exposed to acetone	Lysozyme solution (50μg /ml) prepared from powder exposed to methanol
Activity	100%	99.62 ± 1.58%	99.17 ± 0.98%

6.1.6 Investigation of lysozyme activity following release from PCL matrices

An important aspect of protein or enzyme delivery is the stability of the protein in the delivery device during the release period. In the present study, the complete lysozyme release medium in PBS was collected every two days and stored at - 20°C prior to

analysis (Section 2.4.7). The activity of lysozyme released into PBS over the first 8 hours was recorded as 99.8 ± 0.6% compared to native lysozyme and was similar for 3.4% and 10.5% enzyme loaded PCL matrices (Figure 6.6 A). The activity of released lysozyme decreased gradually over 11 days to around 80% of the activity of fresh lysozyme solution. This behaviour, as discussed above, may result from denaturation of released enzyme over the 2 days period in PBS caused by unfolding of the secondary structure at 37°C. It can be inferred that neither degradation nor unfolding of lysozyme occurred during preparation of the matrices, since enzyme activity was conserved following exposure of the powder to acetone and methanol. The enzyme may be denatured in the matrix at 37°C and released in degraded form. The results indicate that the hydrophobic nature of PCL (which is normally responsible for poor compatibility with proteins, resulting in protein adsorption onto the polymer surface, denaturation and aggregation [246, 247]) may not be a major problem since 60-80% of the enzyme load was released in PBS (Figure 6.6). Increasing enzyme degradation may occur in the matrix and/or release medium over extended time periods. However this biological examination of lysozyme revealed the potential of the microporous PCL matrix to allow controlled release of active growth factors for use in tissue engineering.

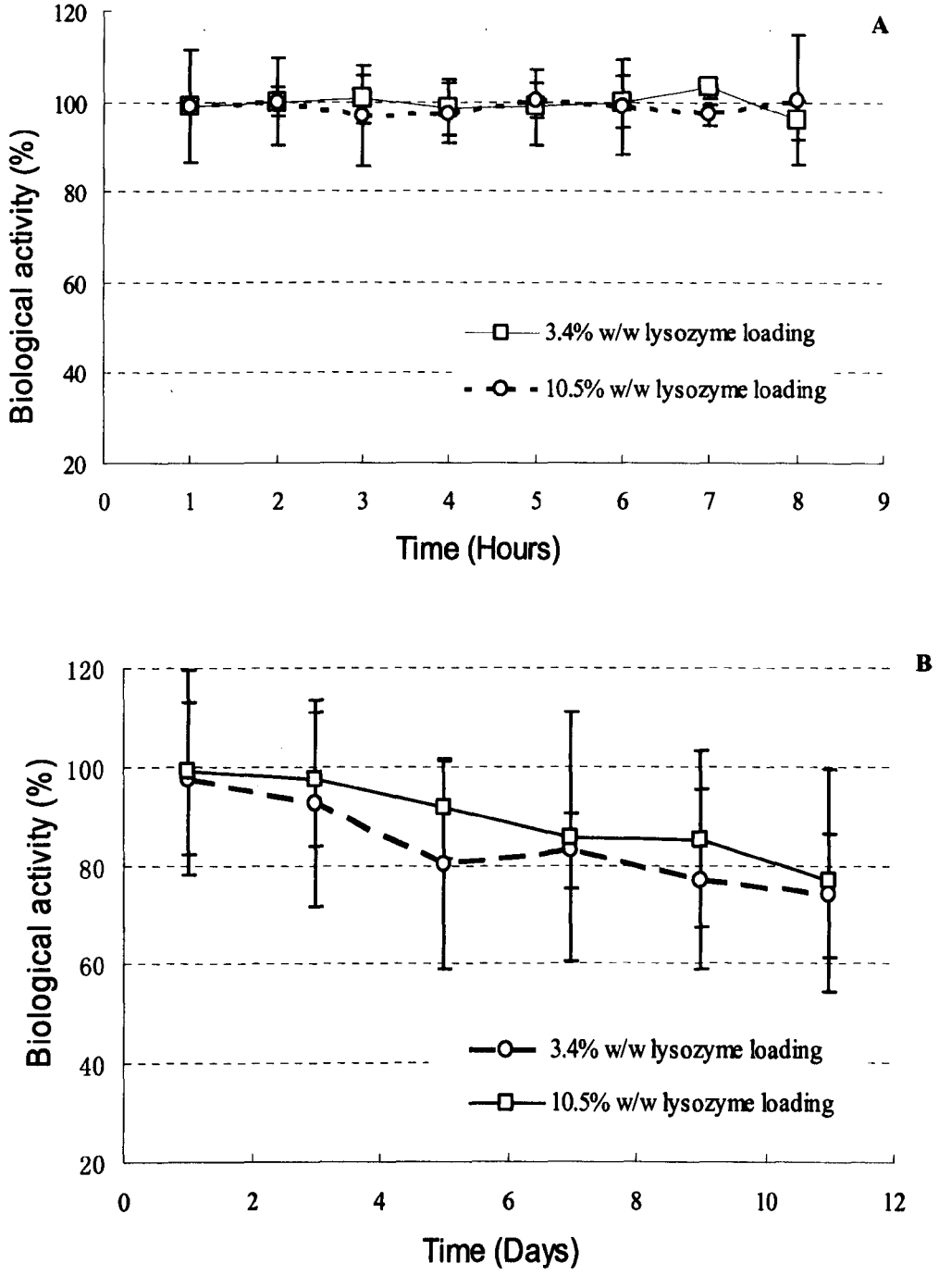

Figure 6.6 Activity of lysozyme released from PCL matrices into PBS at 37°C (A) during 8 hours (B) during 11 days

6.1.7 Morphology of lysozyme-loaded PCL matrices

Lysozyme particles produced by grinding exhibited a laminar morphology of irregular shape with size in the range of 100-200 μm (Figure 6.7). No significant morphological differences between enzyme-loaded PCL matrices and enzyme-free PCL matrices were apparent. Lysozyme loaded PCL matrices before and after release were characterized by a rough, microporous morphology with irregular pore shape and size of 5-10μm. Lysozyme particles are visible on the surface before release (Figure 6.7A).

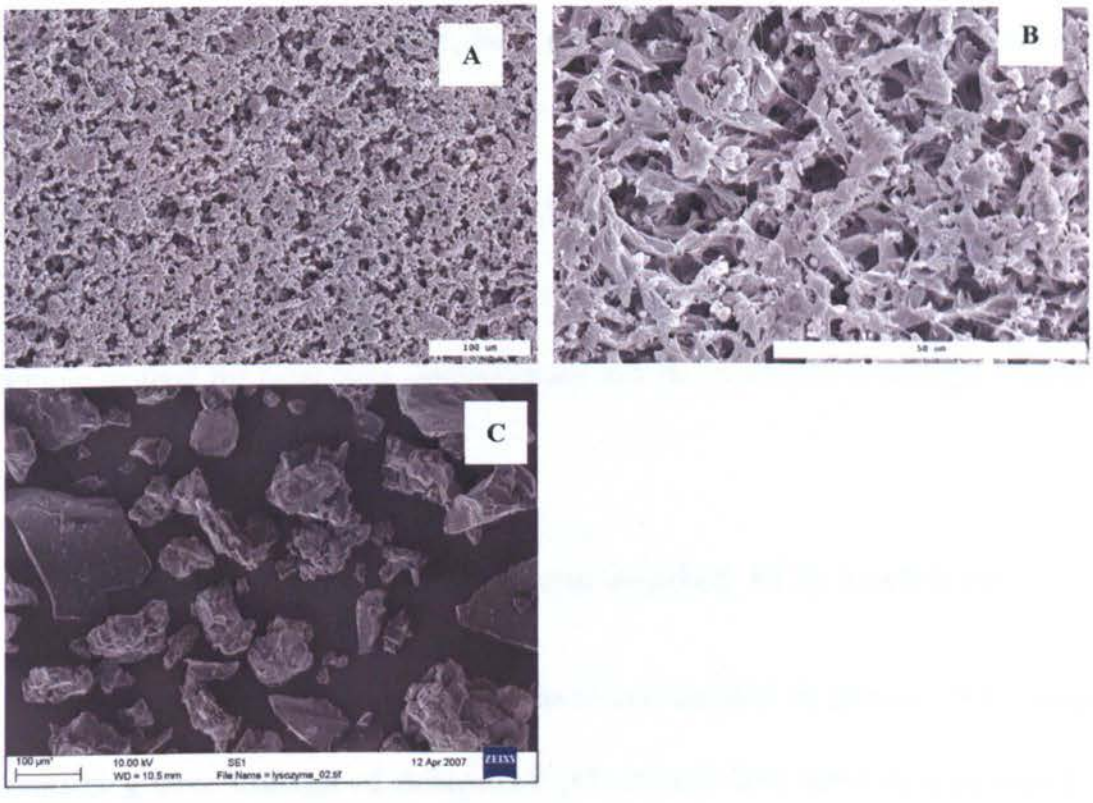

Figure 6.7 Scanning electron micrographs (A) 20% w/w lysozyme: PCL matrix before release (B) lysozyme: PCL matrix after release (C) lysozyme particles

6.2 Preparation and analysis of collagenase-loaded PCL matrices

Collagenase from *Clostridium histolyticum* is a medium molecular-weight protein with molecular weight ranging from 68,000 to 125,000Mw. Collagenase can break down the native collagen in connective tissue and is made by a variety of micro-organisms and many different animal cells [248]. Collagenase has been widely used for disaggregating human tumour, mouse kidney, human adult and fetal brain, lung and many other tissues, particularly endothelium [249-251]. It is also used in liver and kidney perfusion studies, for digestion of the pancreas and for isolation of nonparenchymal rat liver cells [252, 253]. However, no controlled drug delivery study was found using collagenase as a model protein. Collagenase was chosen as a model protein in the present study due to its medium molecular weight characteristic, a simple method for bioactivity determination and its sensitivity to storage conditions when in solution.

6.2.1 Formulation of collagenase-loaded PCL matrices

Collagenase is soluble in water and methanol but insoluble in acetone. PCL matrices containing three loadings of collagenase (10, 20 and 40% w/w) were produced by rapid cooling in dry ice, collagenase dispersions in PCL solution (Section 2.1.2). The dried microporous PCL matrices containing collagenase exhibited a light brown, soft and flexible characteristic without large scale cracks and voids in the surface or interior. The weight distribution of collagenase throughout the PCL matrices prepared

using 17% w/v PCL solutions is shown in Figure 6.8. The top, middle and base of the finished microporous PCL matrix exhibited similar enzyme loading and no significant sedimentation effect was apparent. Since collagenase is soluble in methanol, around 30% of the enzyme was lost from the final matrix due to partition into the non-solvent used in matrix production.

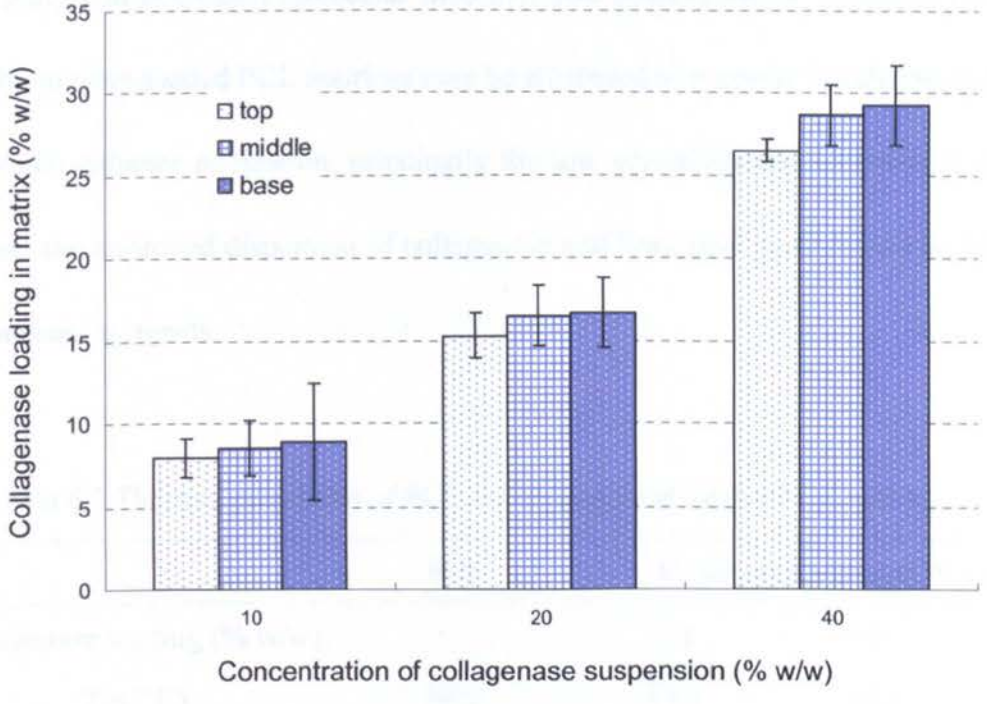

Figure 6.8 The weight distribution of collagenase in microporous PCL matrices

6.2.2 Thermal properties of collagenase-loaded PCL matrices

The thermal characteristics of collagenase-loaded PCL matrices are shown in Table 6.3. The melting point of PCL matrices containing collagenase particles was similar to the value of 58-61°C normally quoted for PCL. The incorporation of collagenase resulted in an increase in crystallinity from 71.5% for unloaded PCL matrices to

approximately 74% for all three collagenase incorporated PCL matrices. A similar effect was found for lysozyme-loaded PCL matrices (except for 40% w/w lysozyme loading Table 6.1), indicating a crystal nucleating effect due to the presence of the collagenase particles. In previous studies, Skoglund et al reported that PCL melts crystallized more rapidly with heterogeneity addition due to an improved nucleating ability and decreased molecular mobility. The observation of increased crystallinity for enzyme-loaded PCL matrices may be attributed to a similar combination of factors which enhance nucleation, principally the low crystallization temperature in dry ice and the improved dispersion of collagenase and lysozyme particles which function as nucleating agents.

Table 6.3 Thermal properties of PCL and collagenase-loaded PCL matrices

	PCL	Collagenase-loaded PCL matrix		
collagenase loading (% w/w)	-	7.4	16.3	28.6
Tm (°C)	68.2	60.2	62.1	61.3
ΔH_f	99.7	103.6	103.1	104.1
Crystallinity (%)	71.5 ± 0. 7	74.3 ± 3.02	73.9 ± 1.07	74.6 ± 1.98

6.2.3 Collagenase release from microprous PCL matrices in vitro

Cumulative release of collagenase from PCL matrices in PBS at 37°C was measured using the BCA total protein assay from day 1 to day 3 and the QuantiPro™ BCA assay for the remainder of the release study due to the low collagenase concentration

in PBS. Approximately 85% of the original collagenase content of the PCL matrices was released over 17 days in PBS (Figure 6.9). A burst phase of 30-60% was observed in the first 24h. The initial enzyme loading of the PCL matrices was found to influence the magnitude of release. For example 30% of the collagenase content was released in day 1 from 7.4% w/w enzyme-loaded matrices compared with approximately 60% from PCL matrices containing 28.6% w/w initial enzyme loading. This behaviour may be explained by the high solubility of collagenase in water and good connectivity between collagenase particles in the matrix resulting in large amounts of enzyme released in the first 3 days. The release profiles tended to plateau at 8 days. However, there are no marked differences in collagenase release duration and pattern among the PCL matrices containing three different enzyme loadings.

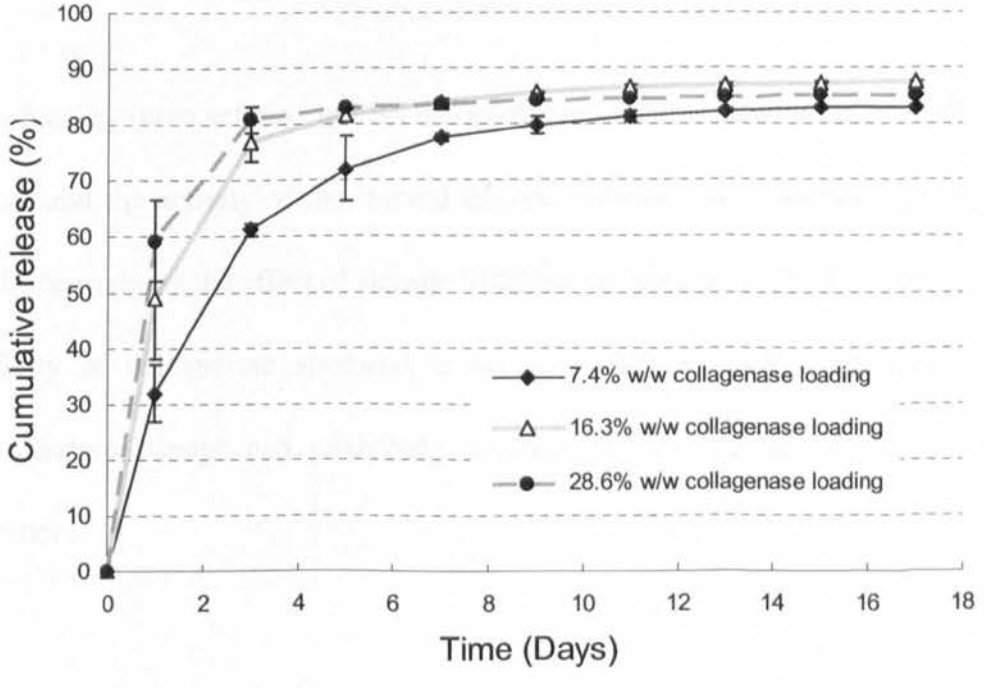

Figure 6.9 Cumulative collagenase release from miroporous PCL matrices

6.2.4 Investigation of collagenase activity in solution and after exposure to the solvents used for matrix formulation.

The collagenase from *Clostridium histolyticum* used in PCL matrix preparation contains 0.25-1.0 FALGPA units/mg solid, >125 CDU/mg solid (CDU = collagen digestion units). The activity of collagenase can be determined using a collagenase digestion unit (CDU) assay based on cleaving two of the three helical chains in the long, undenatured collagen protein [254]or by measuring the enzyme's ability to cut a short synthetic peptide, N-[3-2-Furyl]acryloyl)]-Leu-Gly-pro-Ala (FALGPA). In the present study, the activity of collagenase was determined by measuring the changes of absorbance of the fragment at 565nm caused by enzyme-specific hydrolyse of a synthetic substrate, carbobenzoxy-Gly-Pro-Gly-Gly-Pro-Ala-OH to carbobenzoxy-Gly-Pro-Gly and Gly-Pro-Ala.

Fresh collagenase solution in PBS (concentration 1mg/ml) was stored at -20°C for one week and the activity of the thawed enzyme solution was determined every day in order to examine the effect of storage condition on enzyme activity (Figure 6.10). The activity of collagenase appeared to be very close to 100% indicating that low temperature storage can effectively preserve the activity of the enzyme in PBS solution.

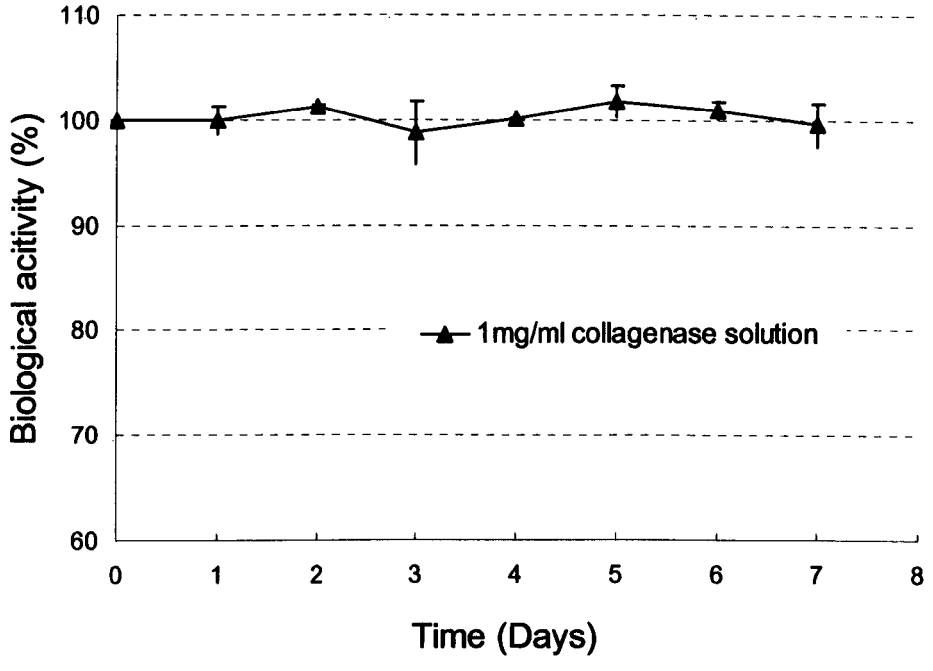

Figure 6.10 Activity of collagenase solution in PBS stored at -20°C

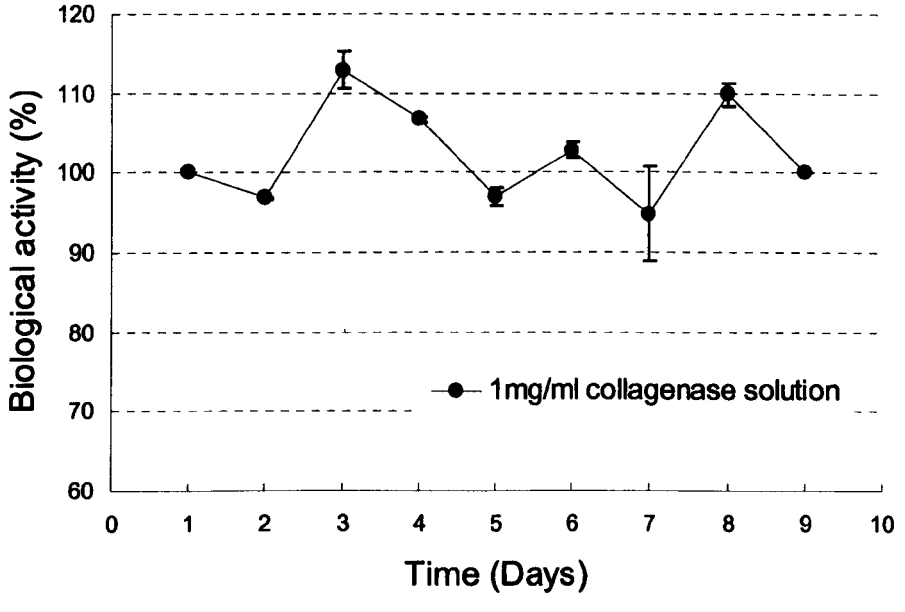

Figure 6.11 Activity of collagenase solution in PBS stored at 37°C

Native collagenase in PBS solution (concentration 1mg/ml) was also stored at 37°C

for one week to investigate if activity was affected by the release conditions used for testing enzyme-loaded PCL matrices. As shown in Figure 6.11, the activity of collagenase in PBS assessed every 24 hours over 7 days seems to be constant and fairly stable compared to native fresh collagenase solution. A biological activity in excess of 100% was recorded at day 3, 4 and 8. The reason behind this effect is unclear at present, but it may be caused by localized aggregation or association of enzyme molecules in specific regions of the solution.

Collagenase powder (approximately 2mg) was also suspended in 2ml acetone or methanol for 24h to simulate exposure of enzyme to the solvents used in PCL matrix formulation. The collagenase powder was collected, and dried and subsequently redissolved in PBS to produce a 1mg/ml solution. Native collagenase powder was also dissolved in PBS as a control (1mg/ml). The retained activity of collagenase after exposure to the solvents used in PCL matrix formulation was found to be approximately 100% (Table 6.4) suggesting that enzyme activity would not be lost during matrix formulation.

Table 6.4 Activity of collagenase following exposure of powder in organic solvent

	Native collagenase solution	Collagenase solution (1mg /ml) prepared from powder exposed to acetone	Collagenase solution (1mg /ml) prepared from powder exposed to methanol
Activity	100%	101.37 ± 0.91%	98.97 ± 1.46%

6.2.5 Bioactivity of collagenase released from PCL matrices

The activity of collagenase released from 7.4% w/w enzyme-loaded matrices was examined. However, the low concentration of collagenase in the release medium results in unreliable data. The activity of collagenase released from 16.3% and 28.6% enzyme-loaded PCL matrices appeared to be stable (around 95-120%-retained activity) compared with native collagenase over the first 8 hours and no significant difference in activity was found between the two enzyme loadings. Similar to the study of collagenase solutions at 37°C, over 100% activity was measured in the release medium over 2-5 h for the 20% enzyme-loaded matrices and at 5h for the 40% enzyme-loaded PCL matrices. The reason for this behaviour is unclear at present, but it may be result from self-association of collagenase in the release medium. The activity of released collagenase was determined for 11 days only due to insufficient release from 11-17 days (Figure 6.9). The activity of released collagenase was fairly constant over 11 days (99-110%) compared to native collagenase and no marked difference was found between the two loadings. In conclusion, no degradation or denaturation of collagenase occurred during matrix formulation, and enzyme release, suggesting that the rapid cooling technique could be suitable for growth factor incorporation and delivery from PCL matrices for tissue engineering.

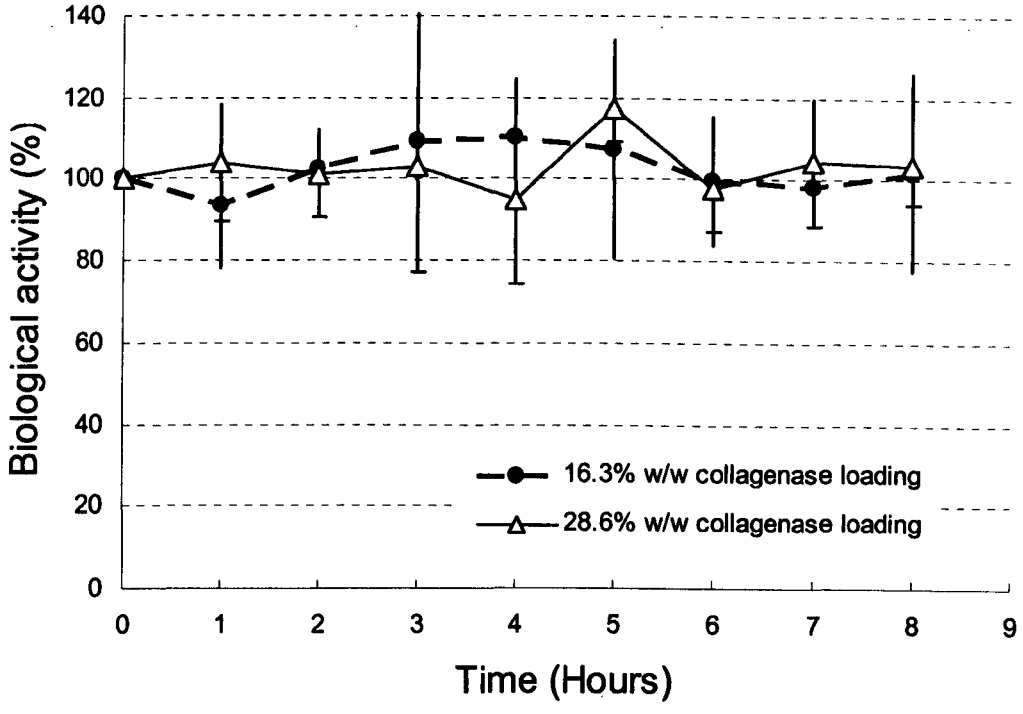

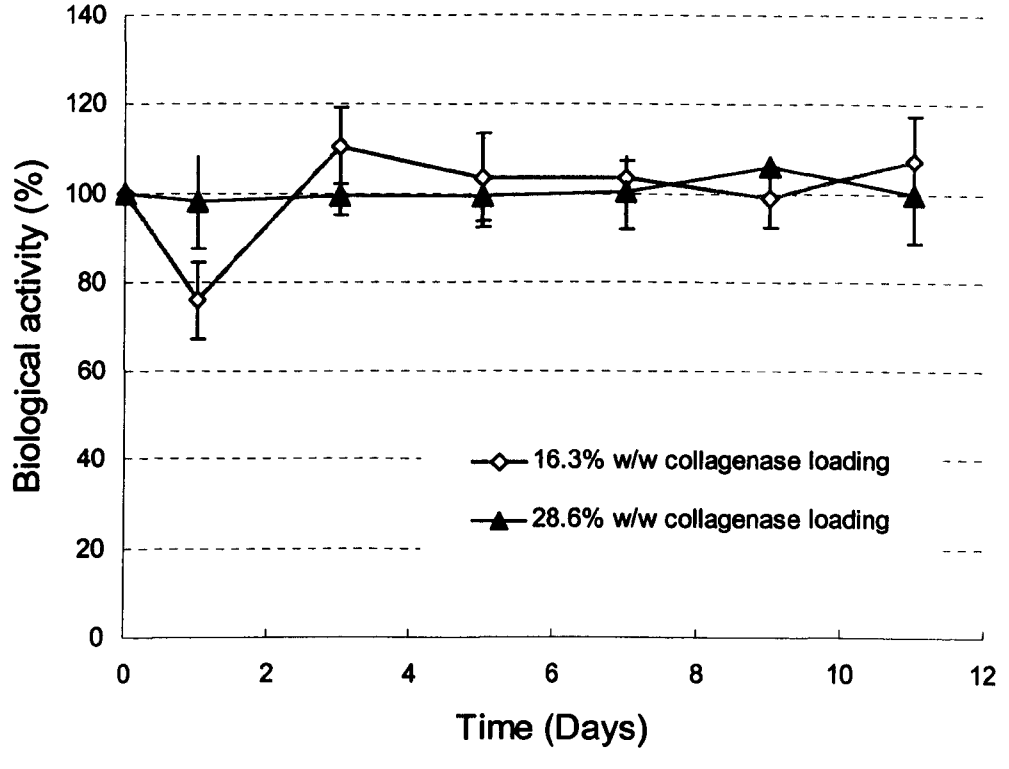

Figure 6.12 Activity of collagenase released from PCL matrices in PBS at 37°C

(A) during 8 hours (B) during 11days

6.2.6 Surface morphology of collagenase-loaded PCL matrices

SEM examination of 16.3% and 28.6% collagenase-loaded PCL matrices revealed a porous surface morphology with irregular pore shape and size in the 5 to 20μm size range (Figure 6.13 A). No significant differences were observed for matrices before or after collagenase release. Collagenase particles showed an irregular laminar or flattened shape with sizes in the range of 50 to 500 μm (Figure 6.13 C), but no particles were detected on the external surface or through the cross section of PCL matrices (Figure 6.13 A, B). This indicates formation of afine-scale particle dispersion, efficient particle coverage by the PCL phase or particles may be masked by PCL (Figure 6.13 A, arrowed).

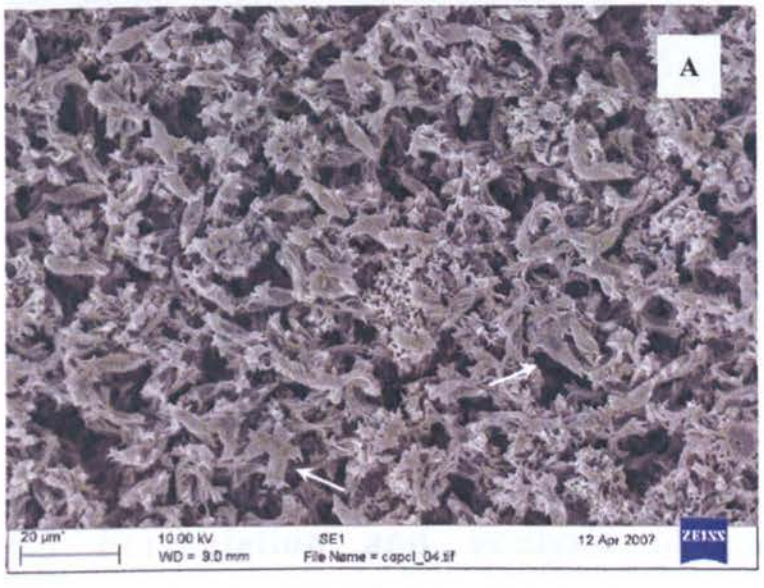

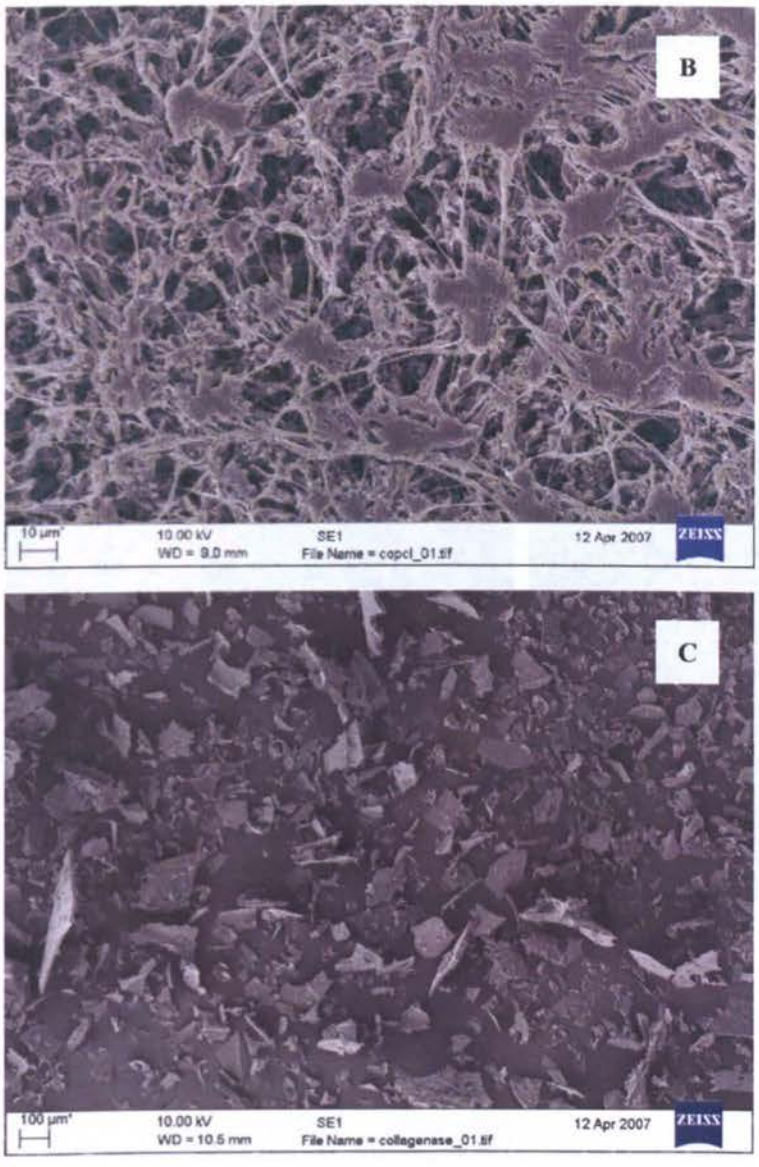

Figure 6.13 Scanning electron micrographs of (A) external surface of 16.3% w/w collagenase-loaded PCL matrices (B) cross section of 16.3% w/w collagenase-loaded PCL matrices (C) collagenase particles

6.3 Formulation and analysis of catalase-loaded PCL matrices

Bovine liver catalase has been investigated previously as a model protein to study the effects of formulation and preparation on activity [255]. The enzyme has a large

molecular weight (243 kDa) and exists as a tetramer of four identical subunits, each of which consists of 506 amino acids plus one heme group and one NADH molecule. Catalase is found in nearly all aerobic cells of animals and bacteria, fungi and plants and its function is to protect the cells from the toxic effects of hydrogen peroxide by catalyzing its decomposition to H_2O and O_2.

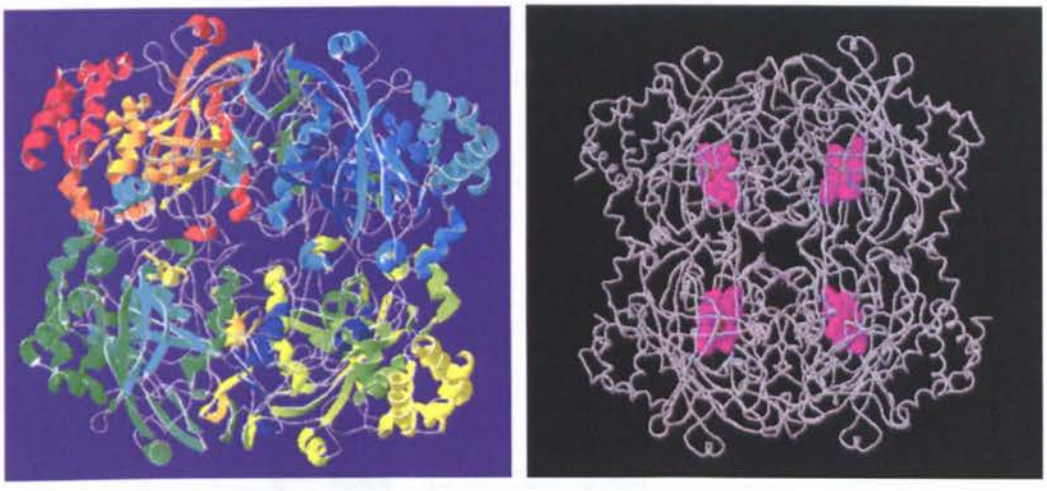

Figure 6.14 Native structure of catalase

6.3.1 Formulation of catalase-loaded PCL matrices

Catalase was loaded into PCL microporous matrices using the rapid cooling technique described in Section 2.1.2. Briefly, catalase powder was suspended in PCL solution prior to cooling in dry ice followed by solvent extraction using methanol as non-solvent. The weight distribution of catalase throughout the dried PCL matrices is shown in Figure 6.15. Only 50% of the starting catalase content of the PCL solution was incorporated in the final PCL matrices probably because of catalase's solubility in methanol which was used for solvent extraction. A uniform distribution of catalase was obtained throughout the material from top to base showing that sedimentation

effects are limited. However, the catalase particles, after loading in PCL matrices, exhibited a characteristic colour change from the original light celadon to yellow brown indicating possible denaturation of the enzyme during matrix formulation.

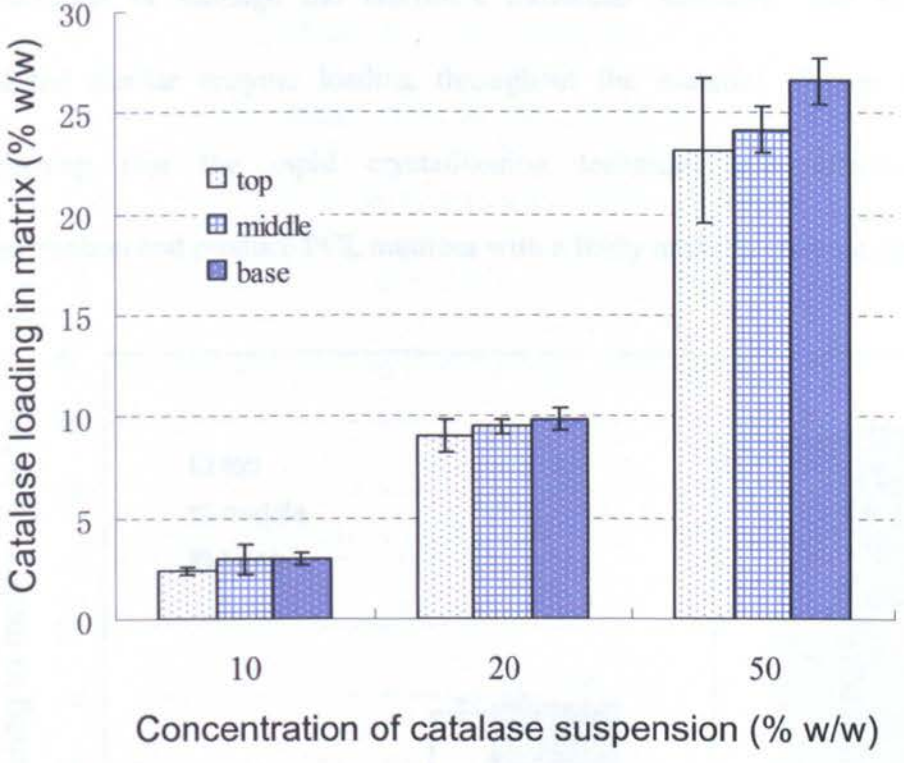

Figure 6.15 The weight distribution of catalase in microporous PCL matrices produced using methanol as a non-solvent and 10, 20% and 50% w/w particle suspensions

In an alternative approach, methanol was replaced by ethanol to extract the solvent (acetone) remaining inside the hardened PCL matrices. The incorporation efficiency of catalase in the final material was increased from around 50% to 97% compared with PCL matrices produced using methanol to extract the solvent. The reason for this behaviour is not clear at present, but it may be explained by reduced solubility of

catalase in ethanol. In addition, catalase particles incorporated in the dried PCL matrices did not display any colour or morphology changes suggesting that rapid PCL crystallization in dry ice, followed by the use of ethanol as non-solvent may not cause denaturation or damage the enzyme's molecular structure. The PCL matrices exhibited similar enzyme loading throughout the material (Figure 6.11) again, confirming that the rapid crystallization technique can effectively reduce sedimentation and produce PCL matrices with a fairly uniform enzyme distribution.

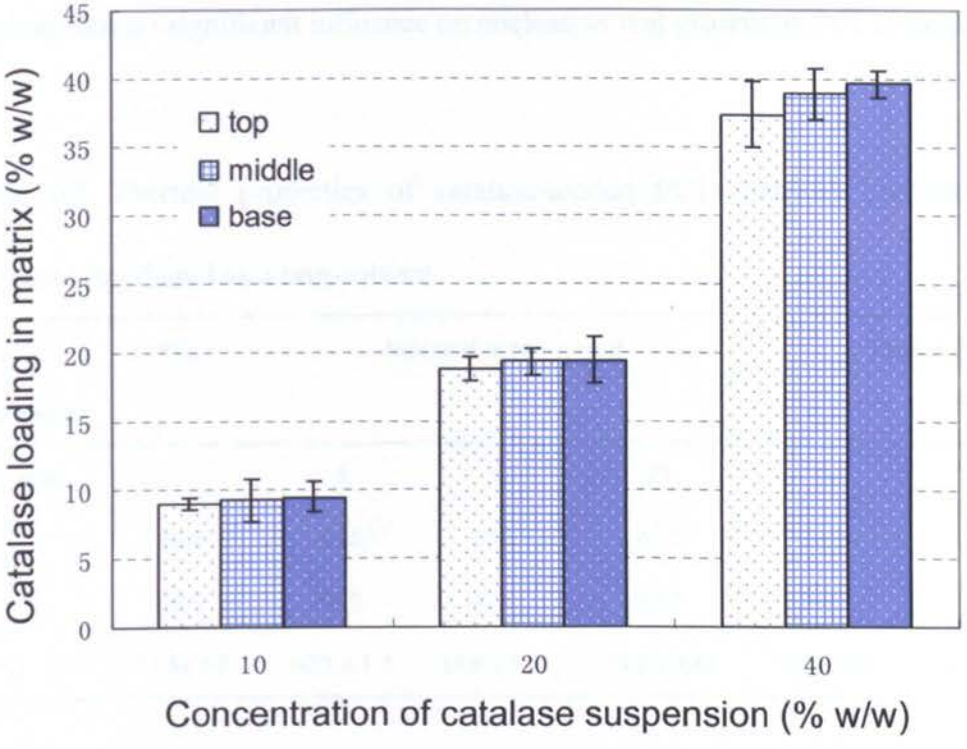

Figure 6.16 The weight distribution of catalase in microporous PCL matrices produced using ethanol as a non-solvent and 10, 20% and 40% w/w particle suspensions

6.3.2 Thermal properties of catalase-loaded PCL matrices produced using methanol or ethanol as the non-solvent

As shown in Table 6.6, the melting point of catalase-loaded PCL matrices produced using either methanol or ethanol as a non solvent was similar (around 65°C) which is higher than the usually quoted values for PCL (58-61 °C). The mean crystallinity of catalase-loaded PCL matrices produced using methanol or ethanol as a non-solvent was similar to enzyme-free PCL matrices, indicating that the presence of catalase particles has no significant influence on nucleation and growth of PCL crystals.

Table 6.5 Thermal properties of catalase-loaded PCL matrices produced using methanol or ethanol as a non-solvent

Formulation of catalase-loaded PCL matrix	PCL	Methanol as non-solvent			Ethanol as non-solvent		
catalase loading (% w/w)		5	10	25	10	20	40
Tm (°C)	68.2	65.5	65.2	65.2	64.2	63.9	63.8
ΔH_f	99.7	96.2	97.4	98.7	100.4	100.3	99.7
Crystallinity (%)	71.5± 0.7	69.3 ± 1.2	69.8 ± 1.62	70.8 ± 0.84	72.2 ± 3.02	71.9 ± 1.07	71.5 ± 8.88

6.3.3 Bioactivity of catalase

Assays for determination of catalase activity are based on the measurement of H_2O_2 decomposition, the liberation of O_2 and the production of heat [256]. The spectrophotometeric method used for catalase determination is based upon the enzymatic decomposition of H_2O_2, which is a first order reaction when the H_2O_2

concentration is between 10μg and 50μg. The reaction constant (k) as function of time follows:

$$2H_2O_2 \xrightarrow{\text{Catalase}} 2H_2O + O_2$$

$$k = \frac{1}{\Delta t} \times \ln \frac{S_1}{S_2}$$

Where $\Delta t = t_2 - t_1$ represents the measured time interval, and S_1 and S_2 are the concentrations of H_2O_2 at times t_1 and t_2 respectively.

Catalase powder (approximately 2mg) was exposed to 2ml acetone, methanol or ethanol respectively for 1 hour. After solvent evaporation in air, the powder was collected, accurately weighed and re-dissolved in PBS to produce a 50μg/ml enzyme solution for activity testing. Native catalase powder was also dissolved in PBS as a control. As shown in Table 6.5, 98-99% bioactivity was retained after exposure to acetone or ethanol but all enzyme activity was lost following exposure to methanol. This result suggests that the rapid crystallization method using ethanol as the non-solvent will not damage catalase.

Table 6.6 Activity of catalase following exposure of the powder to organic solvents

	Native catalase solution	Catalase solution (50μg/ml) prepared from powder exposed to acetone	Catalase solution (50μg/ml) prepared from powder exposed to methanol	Catalase solution (50μg/ml) prepared from powder exposed to ethanol
Activity retention (%)	100	98.3 ± 5.8	0	99.1± 4.8

Fresh catalase solution in PBS was prepared in a series of concentrations from 10μg/ml to 50μg/ml and stored at 37°C for 8 hours or 7 days respectively. The bioactivity of catalase was assessed by measuring the conversion of hydrogen peroxide to water and molecular oxygen as described in Section 6.3.2. The activity of catalase solution (concentration 50μg/ml) recorded every hour over 8 hours was constant at 99-100% compared to native enzyme solution (Figure 6.17). Catalase solutions of lower concentration (10-40 μg/ml) were found to be less stable, exhibiting approximately 30-40% activity loss in 8 hours. Similar results for the stability of native catalase (approximately 30% activity loss in PBS after 5 hours incubation at 37°C) have been reported by Cetinus.S.A et al [257] and suggest that catalase is thermally sensitive. However, the activity loss may be attributed to a number of factors such as dilution, ionic strength, pH of the solution and temperature. Over a 7 days storage period in PBS, the activity of catalase fell to between 50 and 65% at day 1 and 20-30% at day 3 compared to native catalase solution. The activity decreased gradually after day 3 until no biological activity was detected at day 5. The stability of catalase solution in PBS following storage at -20°C was not assessed in this study since Sigma's product information states that freezing stock solution will cause a 50-70% loss in enzyme activity.

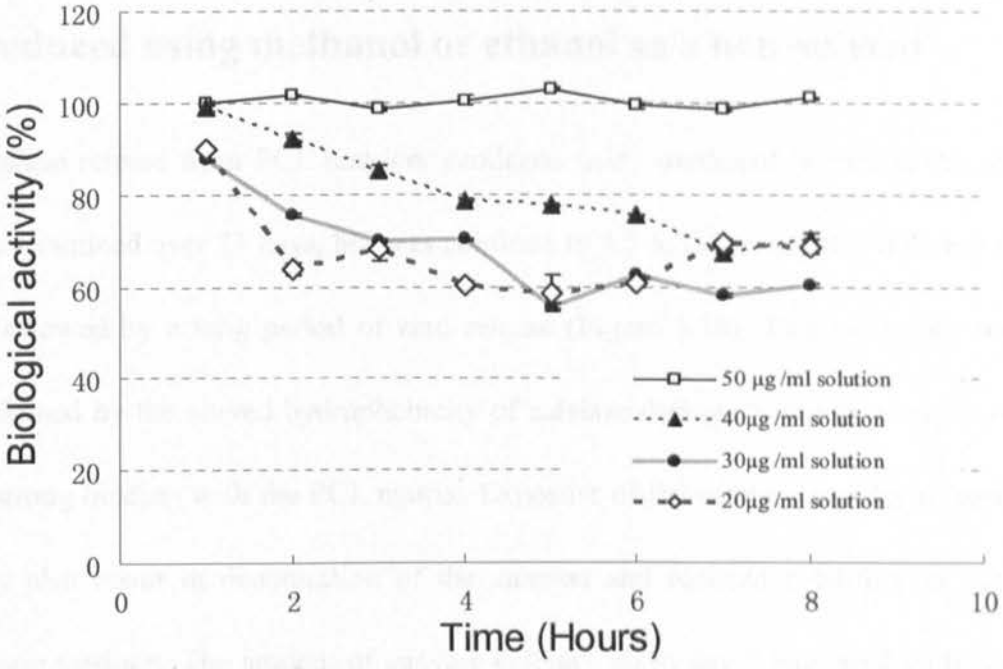

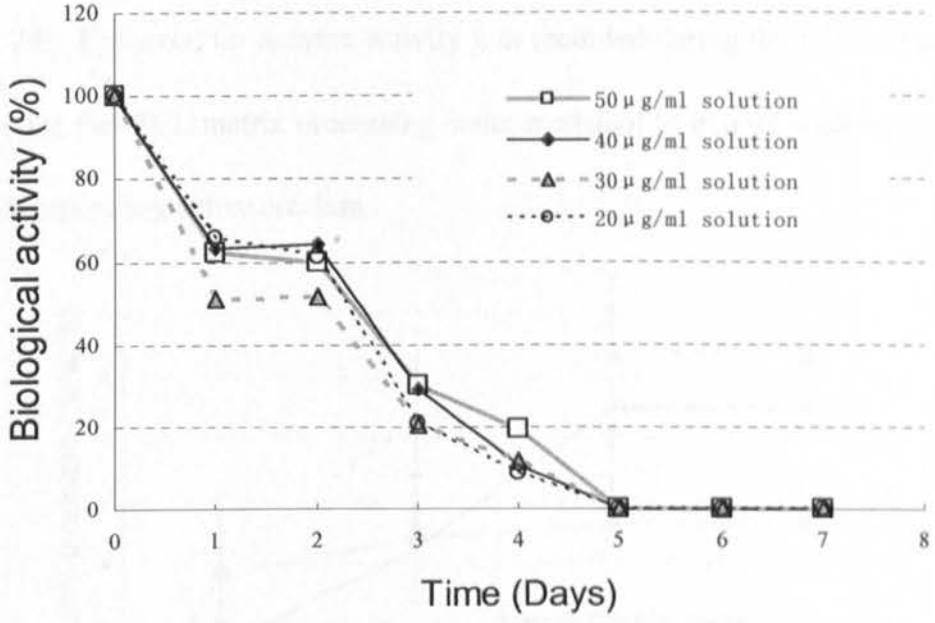

Figure 6.17 Activity of catalase solution in PBS following storage at 37 ºC (A) during 8 hours (B) during 7 days

6.3.4 Catalase release from microporous PCL matrices produced using methanol or ethanol as a non-solvent

Catalase release from PCL matrices produced using methanol to extract the solvent was examined over 21 days, but was confined to 3.5-6.5% cumulative delivery at day 7, followed by a long period of zero release (Figure 6.18). This behaviour may be explained by the altered hydrophobicity of catalase during formulation which results in strong binding with the PCL matrix. Exposure of the catalase powder to methanol may also result in denaturation of the enzyme and reduced solubility in the PBS release medium. The amount of enzyme delivery up to day 7 increased with catalase loading of the PCL matrix and no major "initial burst" phase was found during the first 24h. However, no enzyme activity was recorded during the release study, which indicates that PCL matrix processing using methanol to extract acetone is unsuitable for incorporating active catalase.

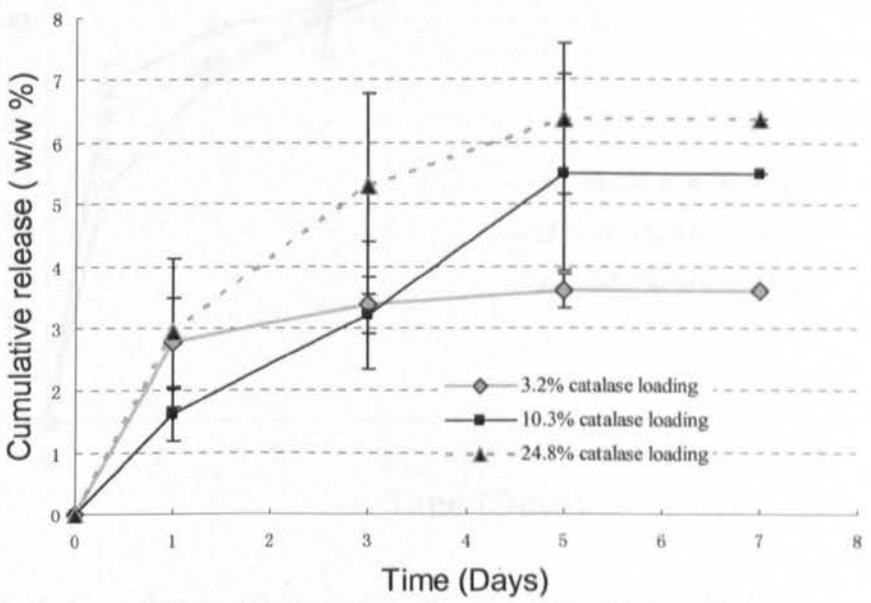

Figure 6.18 Cumulative catalase release from microporous PCL matrices produced using methanol as a non-solvent

Compared to the approach using methanol, cumulative catalase release from the matrices was significantly increased from approximately 6% in 7 days to around 50% over 15 days when ethanol was used to extract solvent (Figure 6.18 and 6.19). This behaviour indicates that catalase does not bind strongly with the PCL phase of the matrices when ethanol is used as the non-solvent. The release profile obtained for all three enzyme loadings was similar apart from the magnitude of the initial burst release phase (Figure 6.19) which increased with enzyme loading. Similar behaviour was observed for lysozyme-loaded matrices (Figure 6.3). Around 23-33% of the catalase content of the matrices was released in 24 hours followed by slow gradual release over 15 days.

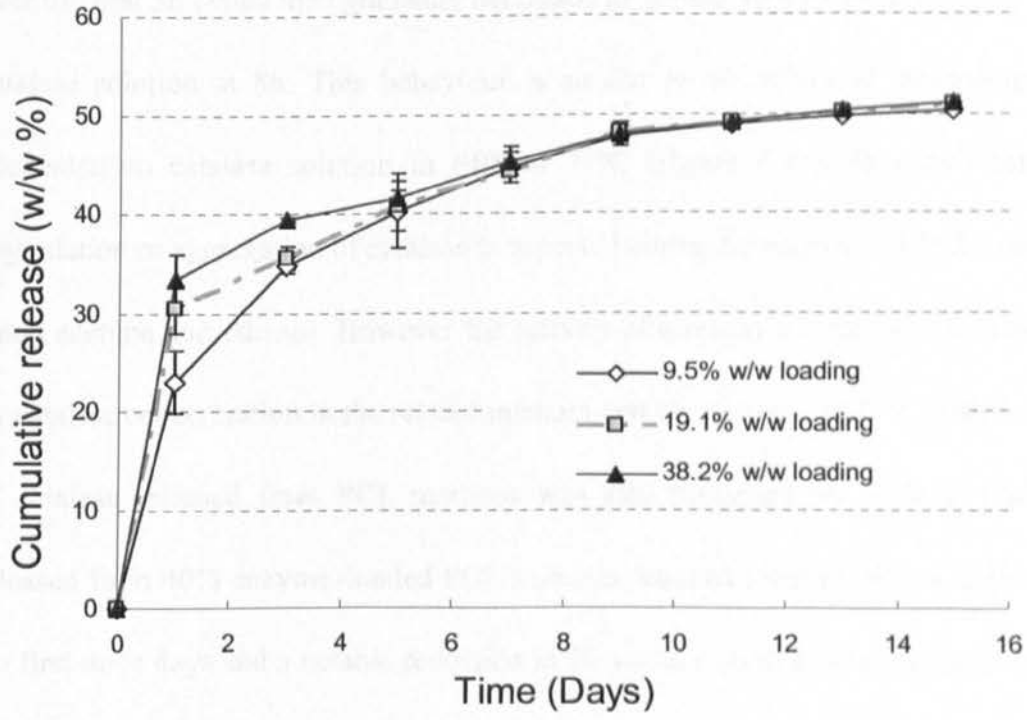

Figure 6.19 Cumulative catalase release from microporous PCL matrices produced using ethanol as the non-solvent (PBS 37°C)

6.3.6 Biological activity of catalase released from microporous PCL matrices

During this study, the biological activity of catalase was determined immediately after collection of samples of the release medium (PBS 37°C) by measuring the conversion of hydrogen peroxide to water and molecular oxygen. Catalase released from PCL matrices over the first 8 hours retained approximately 40% to 99% activity compared to native catalase in PBS. Catalase released from 38.2% w/w loaded PCL matrices appeared to be fairly stable during the first 8 hours (Fig 6.20) which may result from its high concentration in the release medium (over 500μg/ml). In contrast, enzyme released from 8.5% loaded-PCL matrices was found to retain around 80% activity over the first 3h which then gradually decreased to around 40% of the activity of fresh catalase solution at 8h. This behaviour is similar to the effect of incubating low concentration catalase solution in PBS at 37°C (Figure 6.17). In conclusion, no degradation or aggregation of catalase is expected during formulation of PCL matrices using acetone and ethanol. However the activity of released enzyme will be affected by catalase concentration in the release medium and storage time at 37°C. The activity of catalase released from PCL matrices was also measured for 9 days. Catalase released from 40% enzyme–loaded PCL matrices retained close to 95% activity over the first three days and a notable reduction to 20% was recorded between day 3 and 5. With decreasing enzyme loading of the matrix from 38.2% to 8.5%, only 40% activity of released catalase remained after 1 day, approximately 20% at day 3 and no activity was left at day 5. Catalase is expected to be stable during matrix formulation using

ethanol as a non-solvent. However, analysis of catalase activity is complicated by the possibility of denaturation of non-released enzyme during incubation of the PCL matrices in PBS at 37°C and by denaturation of released enzyme. Catalase in solution in PBS (20-50 μg/ml in PBS retained approximately 60%, 30% and 0% activity at day 1, 3 and 5. Catalase released from 19.1% enzyme loaded-PCL matrices retained 80%, 60% and 10% activity at the same time intervals suggesting that the PCL matrix may provide a protective effect for encapsulated enzyme.

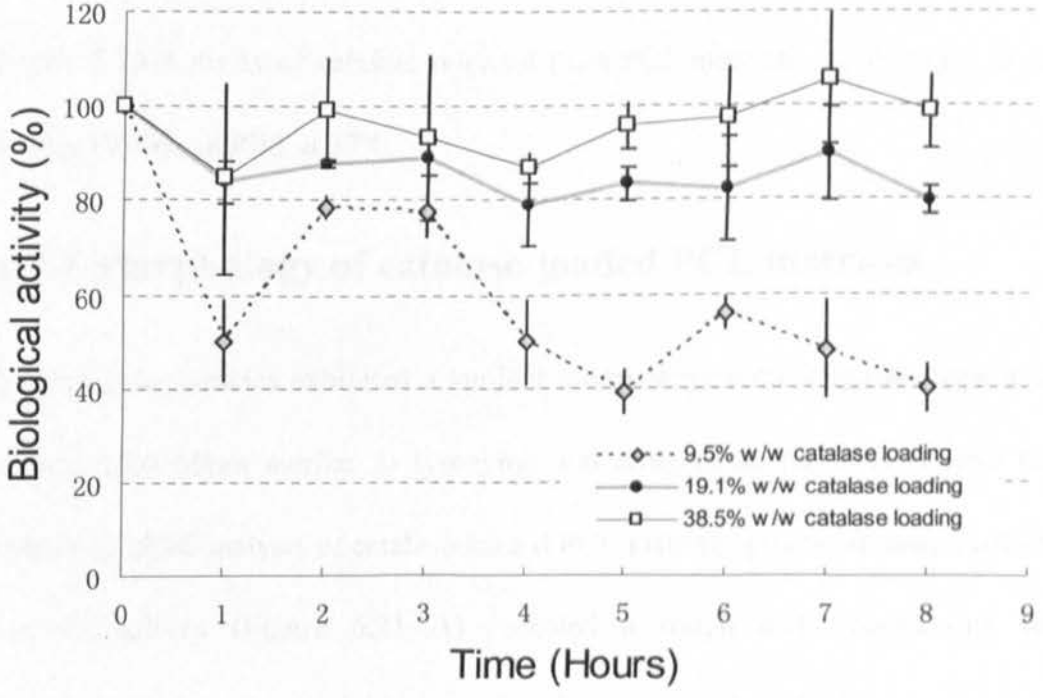

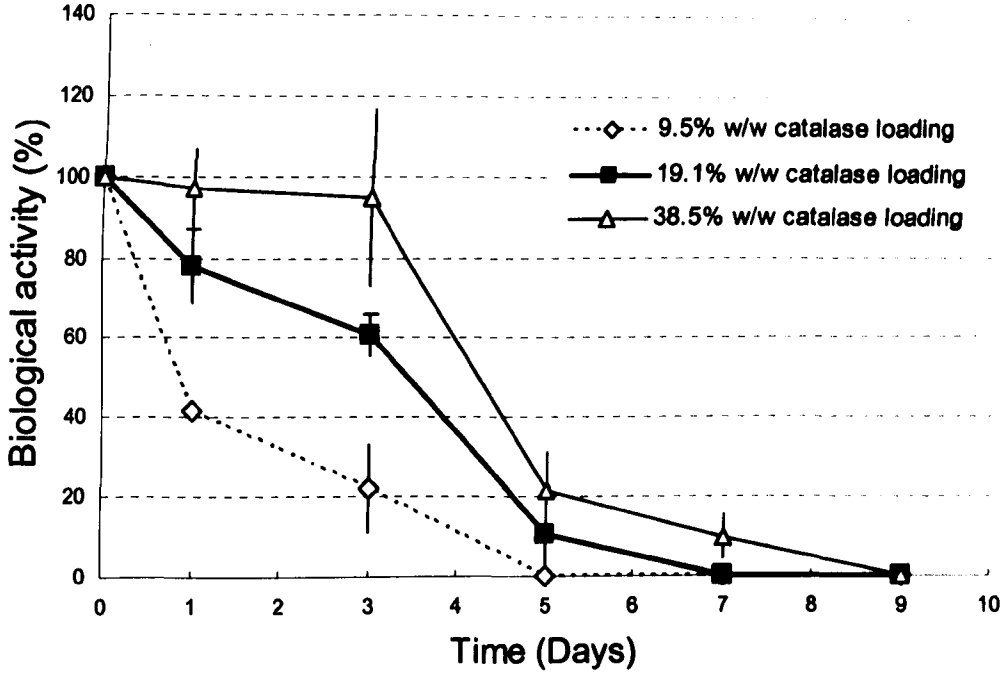

Figure 6.20 Activity of catalase released from PCL matrices (A) during 8 hours (B) during 10 days in PBS at 37°C

6.3.7 Morphology of catalase-loaded PCL matrices

The catalase particles exhibited a laminar morphology with irregular shape and size around 100-200μm similar to lysozyme and collagenase particles (Figure 6.21 E arrowed). SEM analysis of catalase-loaded PCL matrices produced using methanol as the non-solvent (Figure 6.21 A) revealed a rough and microporous surface morphology. Catalase particles were found to be evenly embedded inside the PCL matrix on sectioning of samples (Figure 6.21 B arrowed). The surface morphology of catalase-loaded PCL matrices formed fusing ethanol to extract solvent exhibited a rough and more porous surface morphology (Figure 6.21 C). Similarly, catalase particles were not clearly observed on the surface but a uniform distribution of

catalase particles was found inside the PCL matrix after sectioning (Figure 6.21 D, arrowed).

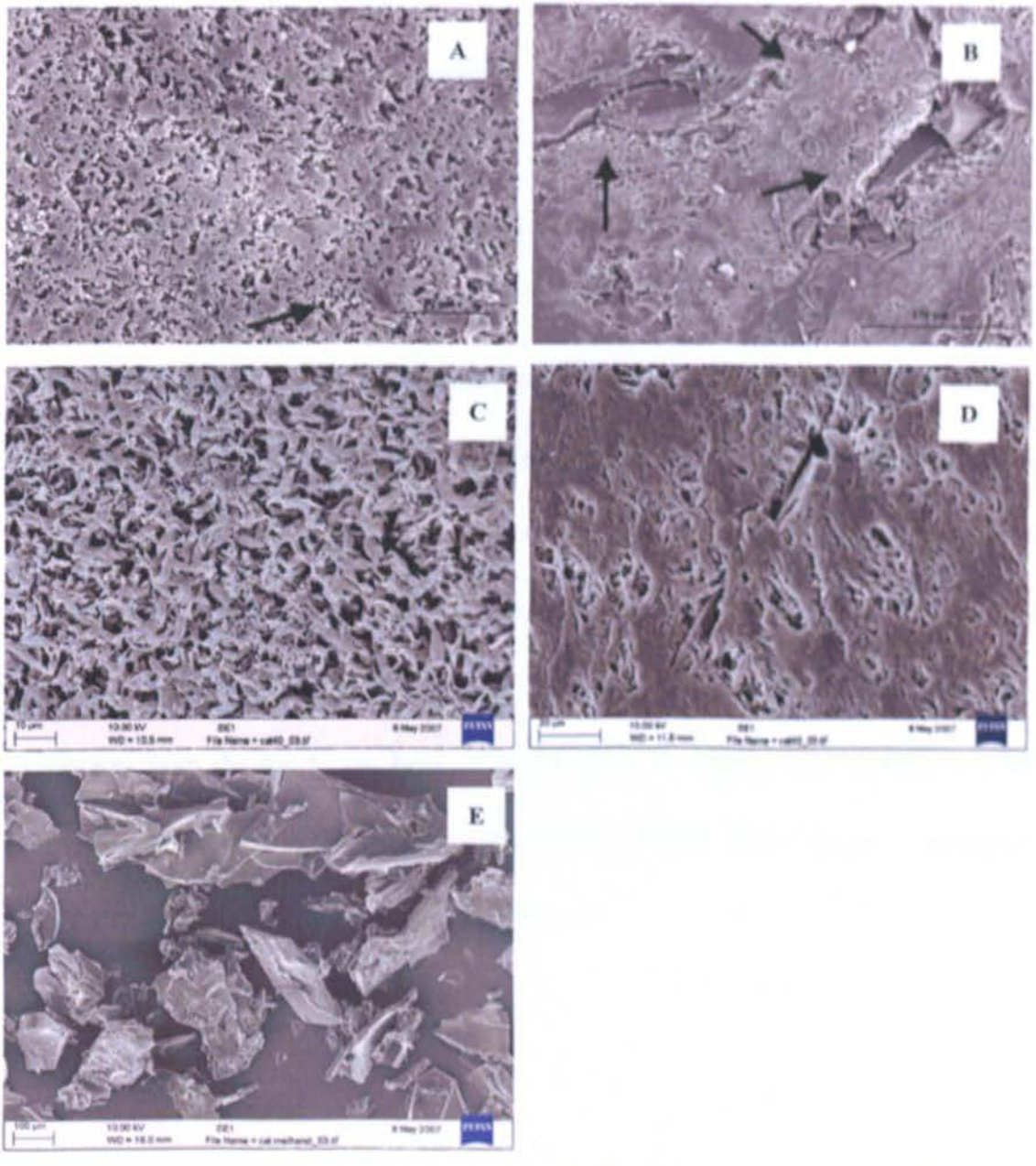

Figure 6.21 Scanning electron micrographs of 20% w/w catalase-loaded: PCL matrix produced using methanol as the non-solvent (A) surface region (B) section through matrix and using ethanol as the non-solvent (C) surface region (D) section through matrix (E) catalase powder

6.4. Formulation and characterization of dexamethasone-loaded PCL matrices

Dexamethasone was readily incorporated into PCL matrices using the co-solution approach, since the steroid is completely soluble in acetone. However, the efficiency of drug loading was confined to around 70-75% of the original drug content of the PCL solution (Figure 6.22). The extent of dexamethasone loss during formulation is considered to arise from its high solubility in methanol leading to partition into the non-solvent layer during matrix formation. The solubility of dexamethasone in methanol is 25mg/ml (Sigma). A fairly uniform drug distribution is apparent throughout the PCL matrices apart from the base region (Figure 6.22). Since the PCL matrices were left in the mould to dry, the acetone/methanol mixture gradually evaporates from the top to the base of the matrices. A higher drug loading may be anticipated in the base of the moulding due to the tendency of the steroid to associate with the residual solvent during the drying process.

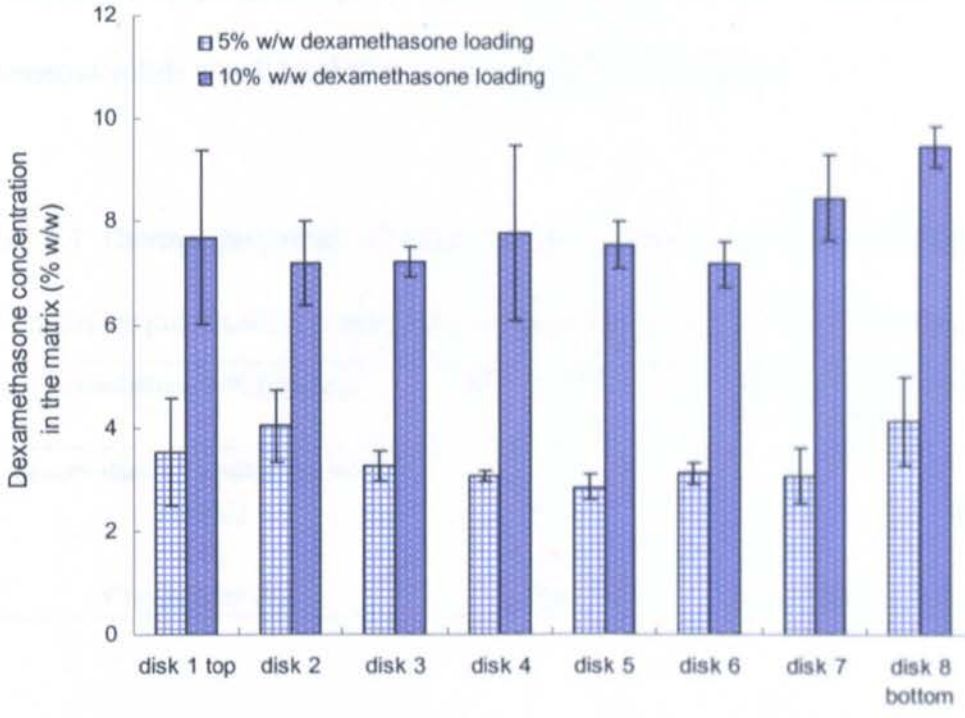

Figure 6.22 The weight distribution of dexamethasone in PCL matrices produced using 5% and 10%w/w concentration drug solution

6.4.1 Thermal properties of dexamethasone-loaded PCL matrices

The melting temperature of dexamethasone-loaded matrices was similar to drug free matrices (Table 6.7). In addition, the crystallinity decreased from approximately 71.5% to 62.4% for PCL matrices prepared using 17% w/v and 12.5% w/v PCL solution, respectively. This behaviour suggests that a more favourable environment for crystallization exists under the conditions of reduced chain mobility existing in more concentrated PCL solutions. Dexamethasone incorporation resulted in a reduction in crystallinity of the PCL matrix of around 20%. Similar findings were recorded in the case of progesterone-loaded PCL matrices [218] and collagen:PCL

biocomposites [9] indicating a 'contact sensitivity' of PCL solutions to certain extraneous solids which inhibits crystal nucleation and growth.

Table 6.7 Thermal properties of drug free-PCL matrices and dexamethasone-loaded PCL matrices produced by precipitation casting using 12.5% w/v PCL solutions

Formulation of PCL matrix	PCL (12.5% w/v)	dexamethasone-loaded PCL matrix	
dexamethasone loading (% w/w)	-	3.9	7.9
Tm (°C)	67.5	65.8	66.1
ΔH_f	87.2	69.8	71.2
Crystallinity (%)	62.4± 2.7	50.1 ± 0.4	50.8 ± 1.1

6.4.2 Dexamethasone release from microporous PCL matrices in vitro

The characteristics of dexamethasone release from 3.9% and 7.9% w/w drug loaded matrices prepared by the co-solution approach using a PCL solution concentration of 12.5% w/v are shown in Figure 6.24 and Figure 6.25. The steroid loading was founded to influence the amount and the duration of drug release. The 3.9% w/w dexamethasone-loaded matrices tended to sustain delivery longer than the higher loaded matrices. The amount of dexamethasone released decreased rapidly over the first 1-2 days and then more gradually over the remaining 6-7 days of the study. The initial burst effect recorded in the first few hours was probably caused by drug located near the surface of the matrix. The variability in the amount of drug released at a particular time period (Figure 6.23) may be explained by localised non-uniform drug distribution in the matrix. The amount of dexamethasone delivered from the matrices

over time increased with drug loading, correlating with the response of diffusing species to a higher concentration gradient. However, less than 50% of the steroid was from the matrices in 8 days (Figure 6.24) indicating a low efficiency of 'pore-type' and 'partition-type' diffusion mechanisms.

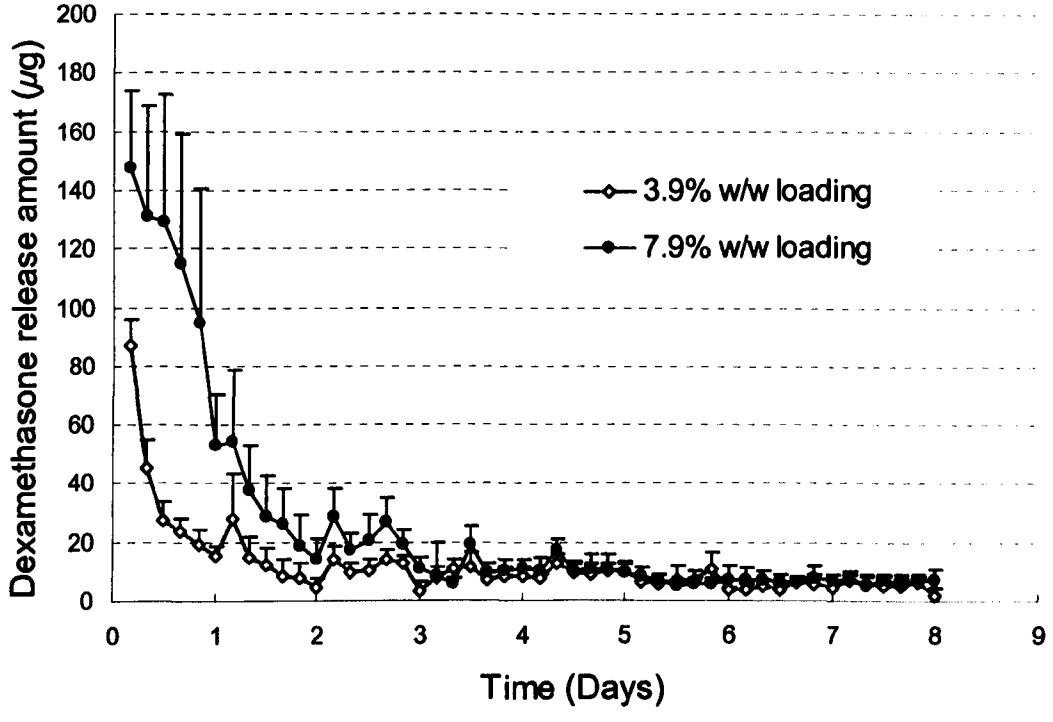

Figure 6.23 Release of dexamethasone (μg) from microporous PCL matrices containing 3.9% and 7.9% w/w initial drug loading

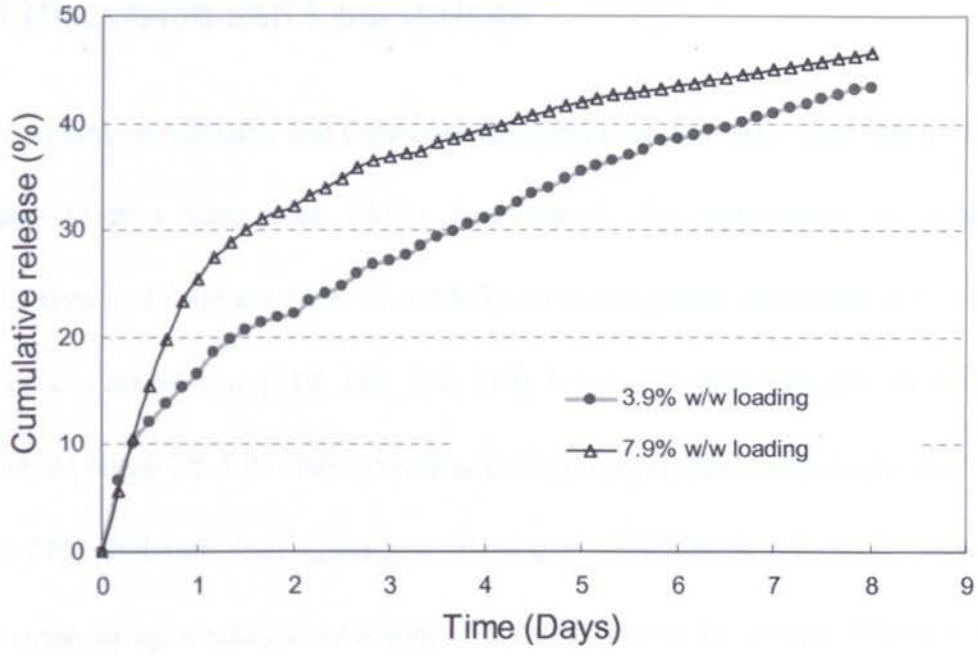

Figure 6.24 Cumulative release of dexamethasone (%) from PCL matrices containing 3.9% and 7.9% w/w initial drug loading

6.4.3 Morphology of dexamethasone-loaded PCL matrices

Dexamethasone particles were not observed on SEM examination of steroid-loaded PCL matrices (Figure 6.25 A and B), suggesting that dexamethasone is produced as fine dispersion of particles during matrix production by the co-solution technique.

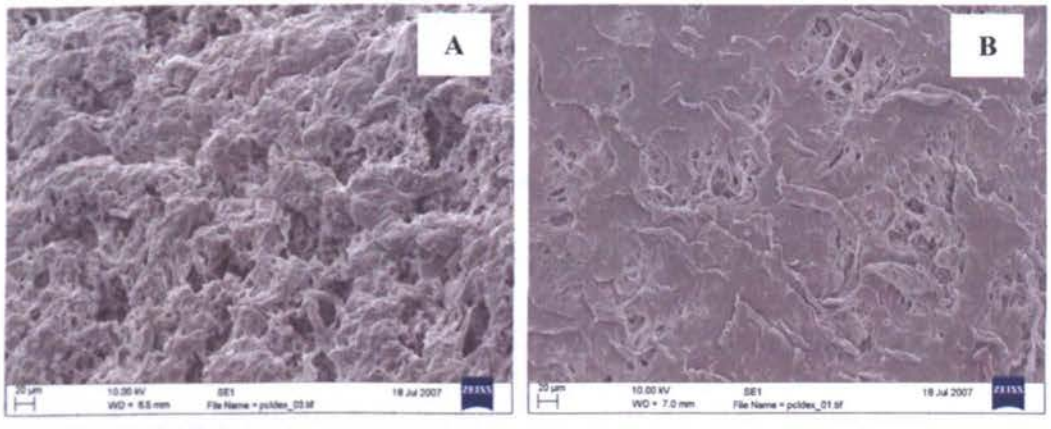

Figure 6.25 Scanning electron micrographs of 7.9% w/w dexamethasone-loaded PCL matrix produced using the co-solution technique (A) Surface region (B) section through matrix

6.5 Discussion and Conclusions

In regenerative medicine and controlled drug delivery research, lysozyme loading and release kinetics have been widely investigated for optimizing the design and performance of different types of scaffolds or microspheres for potential biomolecule delivery in active form [219, 222, 258, 259]. It is known that lysozyme is most stable in the pH range 3.5-5.0, where the denaturation temperature is reported to be 75-80°C [243-245]. Poly(ethylene glycol)/poly(butylene terephthalate) matrices loaded with lysozyme using emulsion techniques revealed zero-order release kinetics and no reduction of lysozyme activity over a 50 days release period [260]. Lysozyme (positive charged) encapsulated in dextran based hydrogel microspheres exhibited 80% w/w release in active form over 60 days and mathematical modelling revealed that the release kinetics were governed by Fickian diffusion [259]. PLGA microparticles containing lysozyme which were produced by supercritical fluid processing also indicated undamaged protein function after formulation but no release kinetics was documented [222]. Sohier et al [219] investigated dual release of lysozyme together with myoglobin from poly(ether-ester) multiblock copolymer matrices as microspheres and found that protein release can be influenced by matrix and coating characteristics. The achievement of controlled delivery of up to 80% of the lysozyme (Mw 14.3 kDa) load over 11 days from PCL matrices, with retained activity around 80% is consistent with the above studies although over shorter time period. Similarly, approximately 80% of the collagenase (Mw 68-125kDa) load was gradually released in 8-10 days from microporous PCL matrices with complete

retention of activity. In contrast, catalase (Mw 243 kDa) release was limited to around 6% in 7 days with complete loss in activity occurring during PCL matrix formulation using methanol as the non-solvent. The use of ethanol rather than methanol resulted in 50% catalase release from PCL matrices in PBS at 37°C over 14 days but a maximum of 20% activity was retained over a 5 day release period. However, a protective effect of the PCL matrix towards encapsulated enzyme is suggested since the activity of catalase solutions in PBS is completely lost in 5 days.

Although catalase has not been used as a model protein in previous studies of scaffold formulation, its stability has been widely investigated under various storage conditions such as high temperature, pressure, pH, ionic strength [261] and additives. In general, catalase is most efficient in the temperature range of 20-50°C and pH 6-8, but Costa. et al [262] showed that the half-life of native catalase at 30 °C is 11 days which may due to a time-related unfolding of the protein structure under thermal stress. In addition, Cetinus' group reports that native catalase in PBS lost around 30% activity in 5 hours at 37°C [257]. Similarly, the loss of enzymatic activity of catalase in the present release study may be caused by temperature induced changes in protein conformation and structure.

Taken together, the findings of this chapter show the potential for incorporation of growth factors or other active molecules with a wide range of molecular weights in PCL matrices and releasing them with retained activity for applications in tissue

engineering and drug delivery.

The investigations of formulation, drug loading and release kinetics for dexamethasone-loaded PCL matrices are important for optimizing the design and performance of microporous PCL devices for delivery of steroids. For example, controlled co-administration of a corticosteroid (dexamethasone) and antibiotic (gentamicin sulphate) from ocular inserts has been investigated to limit the precorneal damage caused by external ophthalmic infections [263]. In regenerative medicine research, the marked influence of dexamethasone on proliferation and differentiation of a range of cell types has been widely documented [264-270]. Human mesenchymal stem cells (MSC), following SOX-9 transfection, differentiated into chondrocyte-like cells in media containing dexamethasone and retained their phenotype when attached to 3-D, poly(L-lactic acid) scaffolds [266]. Human adipose-derived adult stem cells, seeded on gelatin scaffolds, form cartilage-like tissue when cultured in chondrogenic medium containing dexamethasone [268]. Similarly, bone marrow stromal cells (BMSC) cultured on 3-D scaffolds of poly(lactic co-glycolic acid) selectively differentiated into cartilaginous or bone-like tissues by supplementing the external growth medium with dexamethasone [265]. Enhanced proliferation and mineralization of cultured fetal and adult bone cells has also been reported in the presence of dexamethasone [264]. In this latter case, the steroid is considered to exert its osteogenic effect through targeting of specific sub-populations of osteoprogenitor cells which respond to glucocorticoids [269, 270]. Yoon et al [271] envisaged that

dexamethasone release from porous, poly(DL lactic co-glycolic acid) scaffolds would stimulate differentiation of migrating bone marrow stem cells into osteoblasts within bone defects. Microporous PCL matrices produced by precipitation casting have been shown previously to provide a favourable substrate for attachment and growth of primary human osteoblasts [217]. The control over dexamethasone delivery from PCL matrices demonstrated in this chapter may, therefore, provide a further advantage for production of tissue engineering scaffolds which are capable of inducing the correct phenotype of proliferating cells and functional tissue.

Chapter 7

Overall conclusions and future work

Microporous PCL matrices in the form of tubes and cylinders were produced by rapid cooling solutions of PCL in acetone followed by solvent extraction from the hardened matrices using methanol. The novel casting approach enabled high loadings (29-44% w/w) of water soluble particles (gelatin) to be achieved in PCL matrices by suspension of particulates in the PCL solution prior to casting. The good particle distribution throughout the matrix and, importantly, efficient extraction of the water-soluble phase allowed formation of a macroporous structure with defined pore architecture by incorporation of particles of a specific shape and size range (45-90, 90-125, 125-250μm).

Gradual and sustained release of almost 90% of a high protein load (29-44% w/w) was achieved over time periods of 3 days to 3 weeks depending on particle loading. The extent and duration of gelatin release from low -loaded- PCL matrices (29% w/w) was sensitive to the size range of incorporated particles reflecting the lower dissolution rate of larger particles. The duration of protein release decreased with increasing gelatin loading up to 44% w/w and may be explained by facilitated dissolution with increasing interconnectivity of particles.

Investigation of fibroblasts growth in cell culture on macroporous PCL matrices produced by extraction of lactose or gelatin particles demonstrated good cell attachment but no significant effect of particle size was found. The porous surface structure is anticipated to encourage integration of the implanted material with host tissue.

Visualisation and quantitative assessment of the internal macroporous structure of PCL matrices was investigated using Micro-CT and image analysis. The mean pore diameter detected by micro-CT is less than the original particle size since the 2-D sample sections do not coincide with the largest particle diameter. The frequency distribution of equivalent pore diameter was obtained for macroporous PCL matrices prepared by extraction of gelatin particles in three size ranges (45-90, 90-125 and 125-250 μm). This type of detailed evaluation is useful for correlating with protein release kinetics and for assessing the potential for cell ingrowth. The analysis is probably the first to be applied to matrix-type drug delivery systems containing irregular size and shape particles. The Micro-CT determined macroporosity of PCL matrices was close to the theoretical porosity for materials containing macropores of 90μm and above.

Micro-CT analysis showed that the extensive network of high volume channels required for cell infiltration is absent in the PCL matrices produced by extraction of

low particle loads (29%). Thus tissue integration with the matrix surface is more likely for this design with the core potentially providing a depot system for controlled delivery of growth factors via the 5-10 μm pore system inherent in the PCL phase.

The study of the mechanical behaviour of PCL tubes under hydrostatic conditions at 37°C revealed burst strength of approximately 150kPa, 123kPa, and 128kPa for microporous PCL, gelatin-loaded PCL and macroporous PCL tubes respectively. Short-term testing under fluid flow conditions (constant flow, continuous flow and pulsatile flow) at 37°C revealed small changes in outer tube diameter (20 μm dilation) at a maximum flow rate of 1000 ml/min. Good dimensional recovery was found following the first application of hydrodynamic load. Micro-macropoprous PCL tubes may be useful for blood vessel substitution.

The study of enzyme-loaded microporous PCL matrices produced by rapid crystallization of the polymer phase in dry ice showed sustained release of the entrapped enzyme with retained activity dependent on the particular enzyme used (75-80% for lysozyme, at 11 days, 100% for collagenase, at 11 days, 10-20% at 5 days for catalase). These findings reveal a potential for controlled delivery of growth factors in active form for tissue engineering.

Further Micro-CT analysis of the internal structure of PCL matrices is required to clarify the pore connectivity, tortuosity and the shape and size of pore

interconnections which is key for guiding cells migration and proliferation. Images of cells seeded on porous PCL matrices would reveal the relationship between the internal architecture of matrices and cell ingrowth.

Fibroblast cell culture on PCL matrices produced by gelatin particle extraction may reveal more clearly the influence of pore size on cell interaction since the surface macroporosity reflected the original gelatin particle size and shape. The surface pores in PCL matrices following lactose extraction reflected the size of the (10-20μm) powder fines.

The potential for retaining bioactivity of incorporated growth factors (e.g. VEGF), anticoagulants (e.g. heparin) and anti-bacterial (e.g. gentamicin) recommends further investigation of PCL matrices to overcome the limitations of conventional blood vessel substitutes based on Dacron and ePTFE.

Endothelialisation of micro/macroporous PCL tubes is desirable to overcome thrombosis and infection of cardiovascular prostheses. Further experiments could focus on cell seeding and EC monolayer formation. It is important to elucidate the behavior of the endothelial cell lining under simulated blood flow conditions, because EC cultures are extremely sensitive to shear stress, leading to cell elongation in the flow direction, increases in DNA synthesis and production of prostacyclin and growth factors.

The incorporation of cell adhesion molecules and specific growth factors in micro/macroporous PCL matrices may be advantageous for improving the performance of tissue engineering scaffolds. Growth factor release kinetics would need to be controlled to match the specific requirements of tissue repair. Controlled delivery of a wide range of bioactives including microbicides, steroids, antibiotics and vaccines could be investigated to widen the utilization of PCL matrices in different pharmaceutical fields.

References

1. Tabata, Y. (2000) Significance of release technology in tissue engineering, *Drug Discovery Today. 10*, 1639-1646.
2. Kusama, K., Donegan, W. L. & Samter, T. G. (1989) An investigation of colon cancer associated with urinary diversion, *Diseases of the Colon and Rectum. 32*, 694-697.
3. Regan, J. J., McAfee, P. C., Blumenthal, S. L., Guyer, R. D., Geisler, F. H., Garcia, R. & Maxwell, J. H. (2006) Evaluation of surgical volume and the early experience with lumbar total disc replacement as part of the investigational device exemption study of the charite artificial disc, *Spine. 31*, 2270-2276.
4. Ohlstein, B., Kai, T., Decotto, E. & Spradling, A. (2004) The stem cell niche: theme and variations, *Current Opinion in Cell Biology. 16*, 693-699.
5. Ferretti, P. & Geraudie, J. (1997) Cellular and molecular basis of regeneration: From invertebrates to humans, *John Wiley & Sons Ltd, Chichester, UK.*
6. Thomas, A. C., Campbell, G. R. & Campbell, J. H. (2003) Advances in vascular tissue engineering, *Cardiovascular Pathology. 12*, 271-676.
7. Levenberg.S. & Langer, R. (2004) Advances in tissue engineering, *Current Topics in Developmental Biology. 61*, 113-134.
8. Aubert, J. H. & Clough, R. L. (1985) Low-density, microcellular polystyrene foams, *Polymer. 26*, 2047-2055.
9. Dai, N. T., Williamson, M. R., Khammo, N., Adams, E. F. & Coombes, A. G. (2004) Composite cell support membranes based on collagen and polycaprolactone for tissue engineering of skin, *Biomaterials. 25*, 4263-4271.
10. Saltzman, W. M. (2002) Delivery of Molecular Agents in Tissue Engineering in *Tissue Engineering.8*, 355-356.
11. Ranucci, C. S., Kumar, A., Batra, S. P. & Moghe, P. V. (2000) Vascular grafts *Biomaterials. 21*, 783-793.
12. Hou, Q., Grijpma, D. W. & Feijen, J. (2000) Porous polymeric structures for tissue engineering prepared by a coagulation, compression moulding and salt leaching technique, *Biomaterials. 24*, 1937-1947.
13. Yang.J, Shi, G., Bei, J., Wang, S., Cao, Y., Shang, Q., Yang, G. & Wang, W. (2002) Fabrication and surface modification of macroporous poly(L-lactic acid) and poly(L-lactic co-glycolic acid) (70/30) cell scaffolds for human skin fibroblasts cell culture, *Journal of Biomedical Materials Research. 62*, 438-446.
14. Ashman, A. & Moss, M. L. (1977) Implantation of porous polymethlmethacrylate resin for tooth and bone replacement, *The Journal of Prosthetic Dentistry 37*, 657-665.
15. deGroot, J. H., de Vrijer, R., Pennings, A. J., Klompmaker, J., Veth, R. P. H. & Jansen, H. W. B. (1996) Use of porous polyurethanes for meniscal reconstruction and meniscal prostheses, *Biomaterials. 17*, 163-173.
16. Lu, Q., Ganesan, K., Simionescu, D. T. & Vyavahare, N. R. (2004) Novel porous

aortic elastin and collagen scaffolds for tissue engineering, *Biomaterials. 25*, 5227-5237.

17. Yannas, I. V. (2000) In vivo synthesis of tissues and organs In: *Principles of tissue engineering* (Lanza, R. p., Langer, R. & Vacanti, J. P.) pp. 167-178.

18. Freed, L. E. & Vunjak-Novakovic, G. (1998) Culture of organized cell communities, *Advanced Drug Delivery Reviews. 33*, 15-30.

19. Jones, J. R., Poologasundarampillai, G., Atwood, R. C., Bernard, D. & Lee, P. D. (2007) Non-destructive quantitative 3D analysis for the optimisation of tissue scaffolds, *Biomaterials. 28*, 1404-1413.

20. Yannas, I. V., Lee, E., Orgill, D. P., SKrabut, E. M. & Murphy, G. F. (1989) Synthesis and characterization of a model extracellular matrix that induces partial regeneration of adult mammalian skin, *Proceedings of the National Academy of Sciences of the United States of America. 86*, 933-937.

21. O'Brien, F. J., Harley, B. A., Yannas, I. V. & Gibson, L. J. (2005) The effect of pore size on cell-adhesion in collagen-GAG scaffolds, *Biomaterials. 26*, 433-441.

22. Zeltinger, J., Sherwood, J. K., Graham, D. A., Mueller, R. & Griffith, L. G. (2001) Effect of pore size and void fraction on cellular adhesion, proliferation, and matrix depostion, *Tissue Engineering. 7*, 557-572.

23. Salem, A. K., Stevens, R., Pearson, R. G, Davies, M. C., Tendler, S. J. & Roberts, C. J. (2002) Interactions of 3T3 fibroblasts and endothelial cells with defined pore features, *Journal of Biomedical Materials Research. 61*, 212-217.

24. Zein, I., Hutmacher, D. W., Tan, K. C. & Teoh, S. H. (2002) Fused deposition modeling of novel scaffold architectures for tissue engineering applications, *Biomaterials*, 1169-1185.

25. Woodfield, T. B. F., Malda, J., Wijin, J. D., Peters, F., Riesle, J. & Blitterswijk, C. A. V. (2002) Design of porous scaffolds for cartilage tissue engineering using a tree-dimensional fiber-deposition technique, *Biomaterials. 25*, 4149-4161.

26. Ma, P. X. & Zhang, R. (2001) Microtubular architecture of biodegradable polymer scaffolds, *Journal of Biomedical Materials Research. 48*, 469-477.

27. Chu, T. M. G, Orton, D. G, Hollister, S. J., Feinberg, S. E. & Halloran, J. W. (2002) Mechanical and in vivo performance of hydroxyapatite implants with controlled architectures, *Biomaterials. 23*, 1283-93.

28. Ramay, H. R. & Zhang, M. (2003) Preparation of porous hydroxyapatite scaffolds by combination of the gel-casting and polymer sponge methods, *Biomaterials. 24*. 2017-2032.

29. Zhang, R. & Ma, P. X. (1999) Poly(alpha-hydroxyl acids)/hydroxyapatite porous composites for bone-tissue engineering. I. Preparation and morphology, *Journal of Biomedical Materials Research. 44*, 446-455.

30. Kellomake, M., Niiranen, H., Puumanen, K., Ashammakhi, N., Waris, T. & tormala, P. (2000) Bioabsorbable scaffolds for guided bone regeneration and generation, *Biomaterials. 21*, 2495-2505.

31. Walsh, D., Furuzono, T. & Tanaka, J. (2001) Preparation of porous composite implant materials by in situ polymerization of prous apatite containing caprolactone or methyl methacrylate, *Biomaterials. 22*, 1205-1212.

32. Ma, P. X. (2004) Scaffolds for tissue fabrication, *Material today. 7*, 30-40.
33. Feldkamp, L. A., Goldstein, S. A., Parfitt, A. M., Jesion, G & Kleerekope, M. (1989) The direct examination of three-dimensional bone architecture in vitro by computed tomography, *Journal of Bone and Mineral Research. 4*, 3-11.
34. Williams, J. M., Adewunmi, A., Schek, R., Flanagan, C. L., Krebsbach, P. H., Feiberg, S. E., Hollister, S. J. & Das, S. (2005) Bone tissue engineering using polycaprolactone scaffolds fabricated via selective laser sintering, *Biomaterials. 26*, 4817-4827.
35. Washburn, N. R., Weir, M., Anderson, P. & Potter, K. (2004) Bone formation in polymeric scaffolds evaluated by proton magnetic resonance microscopy and X-ray microtomography, *Journal of Biomedical Materials Research. Part A. 69*, 738-747.
36. Darling, A. L. & Sun, W. (2004) 3D microtomographic characterization of precision extruded poly-epsilon-caprolactone scaffolds, *Journal of Biomedical Materials Research. Part B. Applied Biomaterials. 70B. 2*, 311-317.
37. Thurner, P., Muller, R., Raeber, G., Sennhauser, U. & Hubbell, J. A. (2005) 3D morphology of cell cultures: a quantitative approach using micrometer synchrotron light tomography, *Microscopy Research and Technique. 66*, 289-298.
38. Thurner, P., Muller, R., Sennhauser, U., Hubbell, J. A. & Muller, B. (2004) Tomography studies of biological cells on polymer scaffolds, *Journal of Physical condensed matter. 16*. S3499-3510.
39. Lin, A. S., Barrows, T. H., Cartmell, S. H. & Guldberg, R. E. (2003) Microarchitectural and mechanical characterization of oriented porous polymer scaffolds, *Biomaterials. 24*, 481-489.
40. Foster, T. P. & Parrott, E. L. (1990) Release of highly water-soluble medicinal compounds from inert, heterogeneous matrixes, *Journal of Pharmaceutical Sciences. 79*, 806-810.
41. Desai, S. J., Singh, P., Simonelli, A. P. & Higuchi, W. I. (1966) Investigation of factors influencing release of solid drug dispersed in inert matrices II, *Journal of Pharmaceutical Sciences. 55*, 1224-1229.
42. Papadokostaki, K. G., Amarantos, S. G. & Petropoulos, J. H. (1998) Kinetics of release of particulate solutes incorporated in cellulosic polymer matrices as a function of solute solubility and polymer swellability, *Journal of Applied Polymer Science. 67*, 227-287.
43. Wu, Y. S., Lucas, J., Frijlink, H. W. & Maarscalk, K. (2006) The determination of relative path length as a measure for tortuosity in compacts using image analysis, *European Journal of Pharmaceutical Sciences. 28*, 433-440.
44. Bullitt, E., Gerig, G., Aylward, S., Joshi, S., Smith, K., Ewendl, M. & Lin, W. (2003) Tortuosity in *Attributes and Malignant Brain Tumors In MICCAI 2003 proceedings LNCS 2878* pp. 671-679.
45. Coombes, A. & Heckman, J. D. (1992) Gel casting of resorbable polymers in vitro degradation of bone graft substitutes, *Biomaterials. 13*, 297-307.
46. Mooney, D. J., Baldwin, D. F., Suh, N. P., Vacanti, J. P. & Langer, R. (1996) Novel approach to fabricate porous sponges of poly(D,L-lactic-co-glycolic acid) without the use of organic solvents, *Biomaterials. 17*, 1417-1422.

47. Whitaker, M. J., Quirk, R. A., Howdle, S. M. & Shakesheff, K. M. (2001) Growth factor release from tissue engineering scaffolds, *Journal of Pharmacy and Pharmacology. 53*, 1427-1437.
48. Yang, F., Xue, Q., Cui, W., Bei, J., Yu, F., Lu, S. & Wang, S. (2006) Manufacturing and morphology structure of polylactide-type microtubules orientation-structured scaffolds, *Biomaterials. 27*, 4923-4933.
49. Schugens, C., Maquet, V., Grandfils, C., Jerome, R. & Teyssie, P. (1996) Biodegradable and macroporous polylactide implants for cell transplantation: 1. Preparation of macroporous polylactide supports by solid-liquid phase separation, *Polymer. 37*, 1027-1038.
50. Nam, Y. S., Yoon, J. J. & Park, G. (2000) A novel fabrication method of macroporous biodegradable polymer scaffolds using gas foaming salt as a progen additive, *Journal of Biomedical Materials Research. 53*, 1-7.
51. Pego, A. P., Poot, A. A., Grijpma, D. W. & Feijen, J. (2001) Copolymers of trimethylene carbonate and epsilon-caprolactone for porous nerve guides: synthesis and properties, *Journal of Biomaterial Science. 12*, 35-53.
52. Thomson, R. C., Yaszemski, M. J., Powers, J. M. & Mikos, A. G. (1995) Fabrication of biodegradable polymer scaffolds to engineer trabecular bone, *Journal of Biomaterial Science. 7*, 23-38.
53. Cao, Y., Vacanti, J. P., Ma, P., Paige, K. T., Upton, J., Chowanski, Z., Schloo, B., Langer, R. & Vacanti, C. A. (1994) Generation of neotendon using synthetic polymers seeded with tenocytes, *Transplantation proceedings. 26*, 3390-3392.
54. Freed, L. E., Vunjack-Novakovic, G., Biron, R. J., Eagles, D. B., Lesnoy, D. C., Barlow, S. K. & Langer, R. (1994) Biodegradable polymer scaffolds for tissue engineering, *Biotechnology. 12*, 689-693.
55. Kim, D. H. (1997) Human osteoblast response in vitro to platelet-derived growth factor and transforming growth factor-beta delivered from controlled-release polymer rods, *Biomaterials. 18*, 1175-1184.
56. Vacanti, C. A., Langer, R., Schloo, B. & Vacanti, J. P. (1991) Synthetic polymers seeded with chondrocytes provide a template for new cartilage formation, *Plastic and Reconstructure Surgery. 88*, 753-759.
57. de Dunnen, W. F. A., Stokroos, I., Blaauw, E. H., Holwerda, A., Pennings, A. J., Robinson, P. H. & Schakenraad, J. M. (1996) Light microscopic and eletron-microscopic evaluation of short-term nerve regeneration using a biodegradable poly(DL-lactide-caprolactone) nerve guide, *Journal of Biomedical Materials Research. 31*, 105-115.
58. Kaufmann, P. M., Heimrath, S., Kim, B. S. & Mooney, D. J. (1997) Highly porous polymer matrices as a three-dimensional culture system for hepatocytes, *Cell Transplant. 6*, 463-468.
59. Murphy, W. F., Kohn, D. H. & Mooney, D. J. (2000) Growth of continuous bonelike mineral within porous poly(lactide-co-glycolide) scaffolds in vitro, *Journal of Biomedical Materials Research. 50*, 50-58.
60. Evans, G. R. D., Brandt, K., Widmer, M. S., Lu, L., Meszlenyi, R. K., Gupta, P. K., Mikos, A. G., Hodges, J., Williams, J., Gurlek, A. & Patrick, C. W. (1999) In vivo

evaluation of poly(L-lactic acid) porous conduits for peripheral nerve regeneration, *Biomaterials. 20*, 1109-1115.

61. Kim, B. S., Nikolovski, J., Bonadio, J., Smiley, E. & Mooney, D. J. (1999) Engineered smooth muscle tissues: regulating cell phenotype with the scaffold, *Experimental Cell Research. 251*, 318-328.

62. Falk, R., Randolph, T. W., Meyer, J. D., Kelly, R. M. & Manning, M. C. (1997) Controlled release of ionic compounds from poly(L-lactide) microspheres produced by precipitation with a compressed antisolvent, *Journal of Controlled Release. 44*, 77-85.

63. Hile, D. D., Amirpour, M. L., Akgerman, A. & Pishko, M. V. (2000) Active growth factor delivery from poly(D.L-lactide-co-glycolide) foams prepared in supercritical CO_2, *Journal of Controlled Release. 66*, 177-185.

64. Howdle, S. M., Watson, M. S., Whitaker, M. J., Popov, V. K., Davies, M. C., Mandel, F. S., Wang, J. D. & Shakesheff, K. M. (2001) Supercritical fluid mixing: preparation of thermally sensitive polymer composites containing bioactive materials, *Chemical Communication, 11*,109-110.

65. Kim, S. S., Utsunomiya, H., Koski, J. A., Wu, B. M., Cima, M. J., Sohn, J., Mukai, K., Griffith, L. G. & Vacanti, J. P. (1998) Survival and function of hepatocytes on a novel three-dimensional synthetic biodegradable polymer scaffold with an intrinsic network of channels, *Annals of Surgery. 228*, 8-13.

66. Park, A., Wu, B. & Griffith, L. G. (1998) Integration of surface modification and 3D fabrication techniques to prepare patterned poly(L-lactide) substrates allowing regionally selective cell adhesion, *Journal of Biomaterials Science Polymer Edition. 9*, 89-110.

67. An, Y. J. & Hubbell, J. A. (2000) Intraarterial protein delivery via intimally-adherent bilayer hydrogels, *Journal of Controlled Release. 64*, 205-215.

68. Cruise, G. M., Scharp, D. S. & Hubbell, J. A. (1998) Characterization of permeability and network structure of interfacially photopolymerized poly(ethylene glycol) diacrylate hydrogels, *Biomaterials. 19*, 1287-1294.

69. Drumheller, P. D., Elbert, D. L. & Hubbell, J. A. (1994) Multifunctional poly(ethylene glycol) semi-interpenetrating polymer networks as highly selective adhesive substrates for bioadhesive peptide grafting, *Biotechnology and Bioengineering. 43*, 772-780.

70. Hern, D. L. & Hubbell, J. A. (1998) Incorporation of adhesion peptides into nonadhesive hydrogels useful for tissue resurfacting, *Journal of Biomedical Materials Research. 39*, 266-276.

71. Han, D. K. & Hubbell, J. A. (1997) Synthesis of polymer network scaffolds from L-lactide and poly(ethylene glycol) and their interactions with cells, *Macromolecules. 30*, 6077-6083.

72. Metters, A. T., Anseth, K. S. & Bowman, C. N. (2000) Fundamental studies of a novel, biodegradable PEG-b-PLA hydrogel, *Polymer. 41*, 3993-4004.

73. Elisseeff, J., Anseth, K., Langer, R. & Hrkach, J. S. (1997) Synthesis and characterization of photo-gross-linked polymers based on poly(l-lactic acid-co-l-aspartic acid), *Macromolecules. 30*, 2182-2184.

74. Sakiyama-Elbert, S. E. & Hubbell, J. A. (2000) Development of fibrin derivatives for controlled release of heparin-binding growth factors, *Journal of Controlled Release. 65*, 389-402.
75. Peter, S. J., Nolley, J. A., Widmer, M. S., Merwin, J. E., Yaszemski, M. J., Yasko, A. W., Engel, P. S. & Mikos, A. G (1997) In vitro degradation of a poly(propylene fumarate)/beta-tricalcium phosphate composite orthopaedic scaffold, *Tissue Engineering. 3*, 207-215.
76. Suggs, L. J., West, J. L. & Mikos, A. G (1999) Platelet adhesion on a bioresorbable poly(propylene fumarate-co-ethylene glycol) copolymer, *Biomaterials. 20*, 683-690.
77. Davis, M. & Vacanti, J. P. (1996) Toward development of an implantable tissue engineered liver, *Biomaterials. 17*, 365-372.
78. Li, R. H., Whtie, M., Williams, S. & Hazlett, T. (1998) Poly(vinyl alcohol) synthetic polyer foams as scaffolds for cell encapsulation, *Journal of Biomaterials Science Polymer Edition. 9*, 239-258.
79. Tokiwa, T. & Kodama, M. (1997) Multilayer aggregate culture of rat hepatocytes on a porous material: three dimensional cellular organization and maintenance of hepatic functions, *Tissue Engineering. 2*, 97-103.
80. Ma, T., Li, Y., Yang, S. T. & Kniss, D. A. (2000) Effects of pore size in 3-D fibrous matrix on human trophoblast tissue development, *Biotechnology and Bioengineering. 21*, 606-618.
81. Mayer, J., Karamuk, E., Akaike, T. & Wintermantel, E. (2000) Fundamental studies of a novel, biodegradable PEG-b-PLA hydrogel, *Polymer. 41*, 3993-4004.
82. Chenite, A., Chaput, C., Wang, D., Combes, C., Buschmann, M. D., Hoemann, C. D., Lerous, J. C., Atkinson, B. L., Binette, F. & Selmani, A. (2000) Novel injectable neutral solutions of chitosan form biodegradable gels in situ, *Biomaterials. 21*, 2155-2161.
83. Rowley, J. A., Madlambayan, G & Mooney, D. J. (1999) Alginate hydrogels as synthetic extracellular matrix materials, *Biomaterials. 20*, 45-53.
84. Xiong, Z., Yan, Y. N., Zhang, R. J. & Sun, L. (2001) Fabrication of porous poly(l-lactic acid) scaffolds for bone tissue engineering via precise extrusion, *Scripta Materialia. 45*, 773-779.
85. Giordano, R. A., Wu, B. M., Borland, S. W., Cima, L. G & Sachs, E. M. (1996) Mechanical properties of dense polylactic acid structures fabricated by three dimensional printing, *Journal of Biomaterials Science. 8*, 63-75.
86. Draghi, L., Resta, S., Pirozzolo, M. G & Tanzi, M. C. (2005) Microspheres leaching for scaffold porosity control, *Journal of Materials Science: Materials in Medicine. 16*, 1093-1097.
87. Hutmacher, D. W. (2001) Scaffold design and fabrication technologies for engineering tissues--state of the art and future perspectives, *Journal of Biomaterials Science. 12*, 107-124.
88. Hollister, S. J. (2005) Porous scaffold design for tissue engineering, *Nature Materials. 4*, 518-524.
89. Ingber, D. E. (2003) How structural networks influence cellular information

processing networks, *Journal of Cell Science. 116*, 1397-1408.
90. Goulet, R. W., Goldstein, S. A., Ciarelli, M. J., Kuhn, J. L., Brown, M. B. & Feldkamp, L. A. (1994) The relationship between the structural and orthogonal compressive properties of trabecular bone, *Journal of Biomaterial Science. 17*, 375.
91. Cavalcanti-Adam, E. A., Shapiro, I. M., Composto, R. J., Macarak, E. J. & Adams, C. S. (2002) RGD peptides immobilized on a mechanically deformable surface promote osteoblast differentiation, *Journal of Bone and Mineral Research. 17*, 2130-2140.
92. Benoit, J. P., Faisant, X. & Menei, P. (2000) Development of microspheres for neurological disorders: from basics to clinical applications, *Journal of Controlled Release. 65*, 285-296.
93. Fujisato, T., Sajiki, T. & Ikada, Q. (1996) Effect of basic fibroblasts growth factor on cartilage regeneration in chondrocyteseeded collagen sponge scaffold, *Biomaterials. 17*, 155-162.
94. Lohmann, C. H., Schwartz, Z., Niederauer, G. G., Carnes, D. L., Dean, D. D. & Boyan, B. B. (2000) Pretreatment with platelet derived growth factor-BB modulates the ability of costochondral resting zone chondrocytes incorporated into PLA/PGA scaffolds to from new cartilage in vivo, *Biomaterials. 21*, 49-61.
95. Park, Y. J., Lee, Y. M., Lee, J. Y., Seol, Y. J., Chung, C. P. & Lee, S. J. (2000) Controlled release of platelet-derived growth factor-BB from chondroitin sulfate-chitosan sponge for guided bone regeneration, *Journal of Controlled Release. 67*, 385-394.
96. Park, Y. J., Lee, Y. M., Park, S. N., Sheen, S. Y., Chung, C. P. & Lee, S. J. (2000) Platelet derived growth factor releasing chitosan sponge for periodontal bone regeneration, *Biomaterials. 21*, 153-159.
97. Kang, S. S., Grosselin, C., Ren, D. W. & Greisler, H. P. (1995) Selective stimulation of endothelial-cell proliferation with inhibition of smooth-muscle cell-proliferation by fibroblast growth -factor-1 plus heparin delivered from fibrin glue suspensions, *Surgery. 118*, 280-287.
98. Martin, I., Vunjak-Novakovic, G., Yang, J., Langer, R. & Freed, L. E. (1999) Mammalian chondrocytes expanded in the presence of fibroblast growth factor 2 maintain the ability to differentiate and regenerate three-dimensional cartilaginous tissue, *Experimental Cell Research. 253*, 681-688.
99. Shireman, P. K., Hampton, B., Burgess, W. H. & Greisler, H. P. (1999) Modulation of vascular cell growth kinetics by local cytokine delivery from fibrin glue suspensions, *Journal of Vascular Surgery. 29*, 852-861.
100. Krewson, C. E. & Saltzman, W. M. (1996) Transport and elimination of recombinant human NGF during long-term delivery to the brain, *Brain Research. 727*, 169-181.
101. Cao, X. D. & Shoichet, M. S. (1999) Delivering neuroactive molecules from biodegradable microspheres for application in central nervous system disorders, *Biomaterials. 20*, 329-339.
102. Saltzman, W. M., Mak, M. W., Mahoney, M. J., Duenas, E. T. & Cleland, J. L. (1999) Intracranial delivery of recombinant nerve growth factor: release kinetics and

protein distribution for three delivery systems, *Pharmaceutical Research. 16*, 232-240.

103. Mooney, D. J., Kaufmann, P. M., Sano, K., Schwendeman, S. P., Majahod, K., Schloo, B., Vacanti, J. P. & Langer, R. (1996) Localised delivery of epidermal growth factor improves the survival of transplanted hepatocytes, *Biotechnology and Bioengineering. 50*, 422-429.

104. Chen, G. F., Ito, Y. & Imanishi, Y. (1997) Photo-immobilization of epidermal growth factor enhances its mitogenic effect by artificial juxtacrine signaling, *Biochimica et Biophysica Acta. 1358*, 200-208.

105. King, T. W. & Patrick, C. W. (2000) Development and in vitro characterization of vascular endothelial growth factor (VEGF)-loaded poly(DL-lactic-co-glycolic acid)/poly(ethylene glycol) microspheres using a solid encapsulation/single emulsion/solvent extraction technique, *Journal of Biomedical Materials Research. 51*, 383-390.

106. Lee, Y. K., Peters, M. C., Anderson, K. W. & Mooney, D. J. (2000) Controlled growth factor release from synthetic extracellular matrices, *Nature. 208*, 998-1000.

107. Murphy, W. L., Peters, M. C., Kohn, D. H. & Mooney, D. J. (2000) Sustained release of vascular endothelial growth factor from mineralized poly(lactide-co-glycolide) scaffolds for tissue engineering, *Biomaterials. 21*, 2521-2527.

108. Sheridan, M. H., Shea, L. D., Peters, M. C. & Mooney, D. J. (2000) Bioadsorbable polymer scaffolds for tissue engineering capable of sustained growth factor delivery, *Journal of Controlled Release. 64*, 91-102.

109. Hollinger, J. O. & Leong, K. (1997) Poly(alpha-hydroxy acids): carriers for bone morphogenetic proteins, *Biomaterials. 17*, 187-194.

110. Lind, M., Overgaard, S., Glerup, H., Soballe, K. & Bunger, C. (2001) Transforming growth factor-beta 1 adsorbed to tricalciumphosphate coated implants increases pre-implant bone remodeling, *Biomaterials. 22*, 189-193.

111. Mann, B. K., Schmedlen, R. H. & West, J. L. (2001) Tethered-TGF-beta increases extracellular matrix production of vascular smooth muscle cells, *Biomaterials. 22*, 439-444.

112. Kwangwoo, N., Watanabe, J. & Ishihara, K. (2004) The characteristics of spontaneously forming physically cross-linked hydrogels composed of two water-soluble phospholipid polymers for oral drug delivery carrier, *European Journal of Caner and Clinical. 23*, 261-270.

113. Nho, Y., Park, S., Kim, H. & Hwang, T. (2005) Oral delivery of insulin using PH-sensitive hydrogels based on polyvinyl alcohol grafted with acrylic acid/methacrylic acid by radiation, *Nuclear Instruments and Methods in Physic Research. 236*, 283-288.

114. Croxatto, H. B. (2000) Progestin implants, *Steroids. 65*, 681-685.

115. Vogelhubera, W., Sprusb, T., Bernhardtb, G., Buschauerb, A. & Gopferich, A. (2002) Efficacy of BCNU and paclitaxel loaded subcutaneous implants in the interstitial chemotherapy of U-87 MG human gioblastoma xenografts, *International Journal of Pharmaceutics. 238*, 111-121.

116. Krewson, C. E., Dause, R., Mak, M. & Saltzman, W. M. (1996) Stabilization of nerve growth factor in controlled release polymers and in tissue, *Journal of Biomaterial Science. 8*, 103-117.
117. Gombotz, W. R., Pankey, S. C., Bouchard, L. S., Ranchalis, J. & Puolakkainen, P. (1993) Controlled release of TGF-beta 1 from a biodegradable matrix for bone regeneration, *Journal of Biomaterials Science. 5*, 49-63.
118. Johnson, O. L., Cleland, J. L., Lee, H., J., Charnis, M., Duenas, E., Jaworowicz, W., Shepard, D. & Shahzamani, A. (1996) A month-long effect from a single injection of microencapsulated human growth hormone, *Nature Medicine. 2*, 795-799.
119. Sherwood, J. K., Dause, R. B. & Saltzman, W. M. (1992) Controlled antibody delivery systems, *Biotechnology. 10*, 1446-1449.
120. Cleland, J. L. (1995) Design and production of single-immunization vaccines using polylactide polyglycolide microsphere systems, *Pharmaceutical Biotechnology. 6*, 439-462.
121. Marx, P. A., Compans, R. W., Gettie, A., Staas, J. K., Gilley, R. M., Mulligan, M. J., Yamshchikov, G. V., Chen, D. & Eldridge, J. H. (1993) Protection against vaginal SIV transmission with microencapsulated vaccine, *Science. 260*, 1323-1327.
122. Whittum-Hudson, J. A., An, L. L., Saltzman, W. M., Prendergast, R. A. & MacDonald, A. B. (1996) Oral immunization with an anti-idiotypic antibody to the exoglycolipid antigen protects against experimental Chlamydia trachomatis infection, *Nature Medicine. 2*, 1116-1121.
123. Luo, D., Woodrow-Mumford, K., Belcheva, N. & Saltzman, W. M. (1999) Controlled DNA delivery systems, *Pharmaceutical Research. 16*, 1300-1308.
124. Shea, L. D., Smiley, E., Bonadio, J. & Mooney, D. J. (1999) DNA delivery from polymer matrices for tissue engineering, *Naure Biotechnology. 17*, 551-554.
125. Freed, L. E., Martin, I. & Vunjak-Novakovic, G. (1999) Frontiers in tissue engineering. In vitro modulation of chondrogenesis, *Clinical Orthopaedics and Related Research. 367, 1002-1004.*
126. Lee, J. S. & Feldman, A. M. (1998) Gene therapy for therapeutic myocardial angiogenesis: a promising synthesis of two emerging technologies, *Nature Medicine. 4*, 739-742.
127. Bonadio, J. (1999) Localized, direct plsmid gene delivery in vivo: prolonged therapy results in reproducible tissue regeneration, *Nature Medicine. 5*, 753-759.
128. Hora, M. S., Rana, R. K., Nunberg, J. H., Tice, T. R., Gilley, R. M. & Hudson, M. E. (1999) Release of human serum albumin from poly(lactide-co-glycolide) microspheres, *Pharmaceutical Research. 7*, 1190-1114.
129. Cohen, S., Yoshioka, T., Lucarelli, M., Hwang, L. H. & Langer, R. (1991) Controlled delivery systems for proteins based on poly(lactic/glycolic acid) microspheres, *Pharmaceutical Research. 8*, 713-720.
130. Tamada, Y. & Ikada, Y. (1994) Fibroblasts growth on polymer surfaces and biosynthesis of collagen, *Journal of Biomedical Materials Research. 28*, 783-789.
131. van Wachem, P. B. (1987) Adhesion of cultured human endothelial cells onto methacrylate polymers with varying surface wettability and charge, *Biomaterials. 8*, 323-328.

132. Horbett, T. & Schway, M. (1988) Correlations between mouse 3T3 cell spreading and serum fibronectin adsorption on glass and hydroxyethylmethacrylate-ethylmethacrylate copolymers, *Journal of Biomedical Materials Research. 22*, 763-793.
133. Weiss, P. (1945) experiments on cell and axon orientation in vitro: The role of colloidal exudates in tissue organization, *Journal of Experimental Zool. 100*, 353-386.
134. Meyle, J., Gultig, K. & al, e. (1995) Variation in contact guidance by human cells on a microstructured surface, *Journal of Biomedical Materials Research. 29*, 81-88.
135. Langer, R. (1997) Tissue engineering: a new field and its challenges, *Pharmaceutical Research. 14*, 840-841.
136. Ye, Q., Zund, G, Benedikt, P., Jockenhoevel, S., Hoerstrup, S. P., Sakyama, S., Hubbell, J. A. & Turina, M. (2000) Fibrin gel as a three dimensional matrix in cardiovascular tissue engineering, *European Journal of Cardio Thoracic Surgery. 17*, 587-591.
137. Shin, H., Jo, S. & Mikos, A. G (2002) Modulation of marrow stromal osteoblast adhesion on biomimetic oligo(poly(ethylene glycol) fumarate) hydrogels modified with Arg-Gly-Asp peptides and a poly(ethylene glycol) spacer, *Journal of Biomedical Materials Research. 61*, 169-179.
138. Massia, S. P. & Hubbell, J. A. (1991) An RGD spacing of 440nm is sufficient for integrin -medicated fibroblast spreading and 140nm for focal contact and stress fiber formation, *Journal of Cell Biology. 114*, 1089-1100.
139. Massai, R. & Hubbell, J. A. (1991) Human endothelial cell interactions with surface-coupled adhesion peptides on a nonadhesive glass substrate and two polymeric biomaterials, *Journal of Biomedical Materials Research. 25*, 223-242.
140. Curtis, A. (1983) Adhesion of cells to polystyrene surfaces, *Journal of Cell Biology*, 1500-1507.
141. Lydon, M. T., Minett, T. & Tighe, B. (1985) Cellular interactions with synthetic polymer surfaces in culture, *Biomaterials. 6*, 396-402.
142. Chinn, J. (1989) Enhancement of serum fibronectin adsorption and the clonal plating efficiencies of Swiss mouse 3T3 fibroblast and MM14 mouse myoblast cells on polymer substrates modified by radiofrequency plasma deposition, *Journal of Collid and Interface Science. 127*, 67-87.
143. Stile, R. A. (2001) Thermo-responsive peptide-modified hydrogels for tissue regeneration, *Biomacromolecules. 2*, 185-194.
144. Elbert, D. L. & Hubbell, J. A. (2001) Conjugate addition reactions combined with free-radical cross-linking for the design of materials for tissue engineering, *Biomacromolecules. 2*, 430-441.
145. Borkenhagen, M., Clemence, J. F., Sigrist, H. & Aebischer, P. (1999) Three dimensional extracellular matrix engineering in the nervous system, *Journal of Biomedical Materials Research. 39*, 266-276.
146. Marler, J. J., Guha, A., Rawley, J., Koka, R., Mooney, D. J., Upton, J. & Vacanti, J. P. (2000) Soft-tissue augmentation with injectable alginate and syngeneic fibroblasts, *Plastic and Reconstructive Surgery. 105*, 2049-2058.

147. Wu, K., Liu, Y. L., Cui, B. & Han, z. (2006) Application of stem cells for cardiovascular grafts tissue engineering, *Transplant Immunology. 16*, 1-7.
148. Butcher, J. T. & Nerem, R. M. (2004) Porcine aortic valve interstitial cells in three dimensional culture: comparison of phenotype with aortic smooth muscle cells, *Journal of Heart Valve Discovery. 13*, 478-485.
149. Johnson, B. D., Page, R. C., Narayanan, A. S. & H.P., P. (1986) Effects of donor age on protein and collagen synthesis in vitro by human diploid fibroblasts, *Laboratory Investigation. 55*, 490-496.
150. Ruiz-Torres, A., Lozano, R., Melon, J. & Carraro, R. (2003) Age-dependent decline of in vitro migration (basale and stimulated by IGF-1 or insulin) of human vascular smooth muscle cells, *Journal of Gerontol A. 58*, 1074-1077.
151. Nerem, R. M. (2004) Critical issues in vascular tissue engineering, *International Congress Series. 1262*, 122-125.
152. Bolton, E. M. & Bradley, J. A. (2006) Co-stimulatory blockade-a pathway to tolerance, *American Journal of Transplantation. 6*, 857-858.
153. Clavijo-Avarez, J. A., Rubin, J. P., Bannett, J., Nguyen, K., Dudas, J. & Marra, K. G. (2006) A novel perfluoroelastomer seeded with adipose-derived stem cells for soft-tissue repair, *Plastic and Reconstructive Surgery. 5*, 1132-1142.
154. Nerem, R. M. (2004) Tissue engineering of the vascular system, *Vox Sanguinis. 2*, 158-160.
155. Kawai, K., Suzuki, S., Tabata, Y., Ikada, Y. & Nishi, S. (2000) Accelerated tissue regeneration through incorporation of basic fibroblasts growth factor-impregnated gelatin microspheres into artificial dermis, *Biomaterials. 21*, 489-499.
156. Yamamoto, M., Ikada, Y. & Tabata, Y. (2001) Controlled release of growth factors based on biodegradation of gelatin hydrogel, *Journal of Biomaterials Science. 12*, 77-88.
157. Fujita, M., Kinoshita, Y., Tabata, Y. & Kameyama, Y. (2005) Proliferation and differentiation of rat bone marrow stromal cells on poly(glycolic acid)-collagen sponge., *Tissue Engineering. 11*, 1346-1355.
158. Seal, B. L., Otero, T. C. & Panitch, A. (2001) Polymeric biomaterials for tissue and organ regeneration, *Material Science and Engineering. 7*, 147-230.
159. Cremers, H. F. M., feijen, G., Bae, Y. H., Kwon, G., Kim, S. W. & Noteborn, H. P. J. M. (1990) Albumin-heparin microspheres as carriers for cytostatic agents, *Journal of Controlled Release. 11*, 167-179.
160. Nastruzzi, C., Pastesini, C., Cortesi, R., Esposito, R., Menegatti, E. & Gambari, R. (1994) Production and in vitro evaluation of gelatin microspheres containing an antitumour tetra-amidine, *Journal of Microencapsulation. 11*, 249-260.
161. Weltz, M. M. & Ofner, C. M. (1992) Examination of self-crosslined gelatin as a hydrogel for controlled release, *Journal of Pharmaceutical Sciences. 81*, 85-90.
162. Santin, M., Huang, S. J., Iannace, I., Ambrosio, L., Nicolais, L. & Peluso, G. (1996) Synthesis and characterization of a new interpenetrated poly(-hydroxyethlmethacrylate)-gelatin composite polymer, *Biomaterials. 17*, 1459-1467.

163. Koide, M., Osaki, K., Konishi, J., Oyamada, K., Katakura, T. & Takahashi, A. (1993) A new type of biomaterial for artificial skin: dehydrothermally cross-linked composites of fibrillar and denatured collages, *Journal of Biomedical Materials Research. 27*, 79-87.
164. Drury, J. L. & Mooney, D. J. (2003) Hydrogels for tissue engineering: scaffolds design variables and application, *Biomaterials. 24*, 4337-4351.
165. Minenna, L., Herrero, F., Sanz, M. & Trombelli, L. (2005) Adjunctive effect of a polylactide/polyglycolide copolymer in the treatment of deep periodntal intraosseous defects: a randomized clinical trial, *Journal of Clinical Periodontology. 32*, 456-461.
166. Agnihotri, S. A., Mallikarjuna, N. N. & Aminabhavi, T. M. (2004) Recent advances on chitosan-based micro- and nanoparticles in drug delivery, *Journal of Controlled Release. 100*, 5-28.
167. Olsen, D., Ynag, C., Bodo, M., Chang, R., Leigh, S., Baez, J., Carmichael, D., Perala, M., Hamakainen, E., Jarvinen, M. & Polarek, J. (2003) Recombinant collagen and gelain for drug delivery, *Advanced Drug Delivery Reviews. 55*, 1547-1567.
168. Putnam, D. & Kopecek, J. (1995) Polymer conjugates with anticancer activity, *Advanced Polymer Science. 122*, 55-123.
169. Saettone, M. & Salminen, L. (1995) Ocular inserts for topical delivery, *Advanced Drug Delivery Reviews. 16*, 95-106.
170. Peppas, N. A., Bures, P., Leobandung, W. & Ichikawa, H. (2000) Hydrogels in pharmaceutical formulation, *European Journal of Pharmaceutics and Biopharmaceutics. 50*, 27-40.
171. Baldwin, S. P. & Saltzman, W. M. (1998) Materials for protein delivery in tissue engineering, *Advanced Drug Delivery Reviews. 33*, 71-86.
172. Eschbach, L. (2000) Non-resorbable polymers in bone surgery, *Injury. 4*, 22-27.
173. Xue, L. & Greisler, H. P. (2003) Biomaterials in the development and future of vascular grafts, *Journal of Vascular Surgery. 37*, 472-480.
174. Woofson, A. D., Malcolm, R. K., Morrow, R. J., Toner, C. F. & McCullagh, S. D. (2006) Intravaginal ring delivery of the reverse transcriptase inhibitor TMC 120 as an HIV microbicide, *International Journal of Pharmaceutics. 325*, 82-89.
175. Sparnacci, K., Laus, M., Endoli, B., Castaldello, A. & Caputo, A. (2005) Core-shell microspheres by dispersion polymerization as promising delivery systems for proteins, *Journal of Biomaterials Science. 16*, 1557-74.
176. Banakar, U. V. (1994) Materials used in controlled release technology-a primer in *Technomic publishing company: Lancaster* pp. pp132-154.
177. Malcolm, K., Woofson, A. D., Russell, J. & Andrews, C. (2003) In vitro release of nonoxynol-9 from silicone matrix intravaginal rings., *Journal of Controlled Release. 91*, 355-364.
178. Kurtz, S. M., Muratoglu, O. K., Evans, M. & Edidin, A. A. (1999) Advances in processing, sterilization, and crosslinking of ultra-high molecular weight polyethylene for total joint arthroplasty, *Biomaterials. 20*, 1659-1688.
179. Kulkarni, R. K. e. a. (1971) Biodegradble poly(lactic acid) polymers, *Journal*

of Biomedical Materials Research. 5, 169-181.
180. Woodland, J. H. e. a. (1973) Long-acting delivery systems for narcotic antagonists, *Journal of Medicinal Chemistry. 16*, 897-901.
181. Jacknicz, T. M. e. a. (1973) Polylactic acid as a biodegradable carrier for contraceptive steroids, *Contraception. 8*, 227-234.
182. Beck, L. R. e. a. (1979) New long-acting injectable microcapsule contraceptive system, *American Journal of Obstetrics and Gynecology. 135*, 419-426.
183. Agrawal, C. M. & Ray, R. B. (2001) Biodegradable polymeric scaffolds for musculoskeletal tissue engineering, *Journal of Biomedical Materials Research. 55*, 141-150.
184. Ranade, V. V. & Holliner, M. A. (2003) *Roles of polymers in drug delivery, In: Drug delivery systems* pp. 64-114, CRC press, Boca Raton..
185. Dijkman, G. A., Moral, P. E. D. & Plasman, J. W. (1990) A new extra long acting depot preparation of the LHRH analogue ZoladexT.First endocrinological and pharmacokinetic data in patients with advanced prostate cancer, *The Journal of Steroid Biochemistry and Molecular Biology. 37*, 933-936.
186. Pitt, C. G., Chasalow, F. I., Hibionada, Y. M., Klimas, D. M. & Schindler, A. (1981) Aliphatic polyesters.I.The degradation of polycaprolactone in vivo, *Journal of Applied Polymer Science. 26*, 3779-3787.
187. Pitt, C. G. (1990) Poly(e-caprolactone) and its copolymers *In: Biodegradable polymers as drug delivery systems* (Chasin, L. R. & Langer, R., eds) pp. 71-120, Marcel Dekker, New York.
188. Bao, Y. T., Samuel, N. K. P. & Pitt, C. G. (1988) The prediction of drug solubilites in ploymers, *Journal of Ploymer Science. 26*, 41-46.
189. Pitt, C. G. & Schindler, A. (1983) Biodegradation of polymer, *In*: *Controlled Drug delivery* pp. 53-80, CRC press, Boca Raton.
190. Holland, S. J. & Tighe, B. J. (1986) Polymers for biodegradable medical devices.1. The potential of polyesters as controlled macromolecular release systems, *Journal of Controlled Release. 4*, 155-180.
191. Pitt, C. G. & Schindler, A. (1984) Capronor *In: A biodegradable delivery system for levonorgestrel, in long-acting contraceptive delivery systems* (Zatuchni, G. I., Goldsmith, A., Shelton, J. D. & Sciarra, J. J., eds) pp. 48-63, Harper and Row, Philadelphia.
192. (1977) Report to NICHD, NIH, August in, Research Triangle Institute,
193. Wade, C. W. R., hegyeli, A. F. & Kulkarni, R. K. (1977) Standards for in-vitro and in-vivo comparison and qualification of bioabsorbable polymers, *Journal of Testing and Evaluation. 5*, 397-400.
194. Darney, P. D., Monroe, S. E., Klaisle, C. M. & Alvarado, A. (1989) Clinical evaluation of the Capronor contraceptive implant: preliminary report, *American Journal of Obstetrics and Gynecology. 160*, 1292-1295.
195. Coombes, A., Verderio, E., Shaw, B., LI, X. M., Griffin, M. & Downes, S. (2002) Biocomposites of non-crosslinked natural and synthetic polymers, *Biomaterials. 23*, 2113-2118.
196. Ziyuan, C. & Teoh, S. H. (2004) Surface modification of ultra thin

polycaprolactone films using acrylic acid and collagen, *Biomaterials. 25*, 1991-2001.
197. Schmidt, C., wens, R., Nies, B. & Moll, F. (1995) Antibiotic in vivo/in vitro release, histocompatibility and biodegradable of gentamicin implants based on lactic acid polymers and copolymers, *Journal of Controlled Release. 37*, 83-94.
198. Stewart, P. S. (2002) Mechanisms of antibiotic resistance in bacterial biofilms, *International Journal of Medical Microbiology. 292*, 107-113.
199. Hendricks, K. J., Lane, D., Burd, T. A., Lowry, K. J., Day, D., Phaup, J. G & Anglen, J. O. (2001) Elution characteristics of tobramycin from polycaprolactone in a rabbit model., *Clinical Orthopaedics and Related Research. 392*, 418-426.
200. Rutledge, B., Huyette, D., Day, D. & Anglen, J. O. (2003) Treatment of osteomyelitis with local antibiotics delivered via bioabsorbable polymer, *Clinical Orthopaedics and Related Research. 411*, 280-287.
201. Ciapetti, G., Ambrosio, L., Savarion, L., Granchi, D., Cenni, E., Baldini, N., Pagani, S., Guizzardi, S., Causa, F. & Giunti, A. (2003) Osteoblast growth and function in porous polycaprolactone matrices for bone repair: preliminary study, *Biomaterials. 24*, 3815-3824.
202. Marra, K. G., Szem, J. W., Kumta, P. N., DiMilla, P. A. & L.E., W. (1999) In vitro analysis of biodegradable polymer blend/hydroxyapatite composites for bone tissue engineering, *Journal of Biomedical Materials Research. 47*, 324-325.
203. Dai, N. T., Yeh, M. K., Liu, D. D., Adams, E. F., Chiang, C. H., Yen, C. Y., Shih, C. M., Sytwu, H. K., Chen, T. M., Wang, H. J., Williamson, M. R. & Coombes, A. G (2005) A co-cultured skin model based on cell support membranes, *Biochemical and Biophysical Research Communications. 329*, 905-908.
204. Zhou, S., Deng, X. & Yang, H. (2003) Biodegradable polycaprolactone-polyethyleneglycol block copolymers: characterization and their use as drug carriers for a controlled delivery system, *Biomaterials. 24*, 3563-3570.
205. Ray, A.-M. L., Chiffoleau, S., Iooss, P., Grimandi, G., Gouyette, A., Daculsi, G & Merle, C. (2003) Vancomycin encapsulation in biodegradable polycaprolactone microparticles for bone implantation. Influence of the formulation process on size, drug loading, in vitro release and cytocompatibility, *Biomaterials. 24*, 443-449.
206. Jeong, J. C., Lee, J. & Cho, K. (1992) Effects of crystalline microstructure on drug release behavior of polycaprolactone microspheres, *Journal of Controlled Release. 92*, 249-258.
207. Perez, M. H., Zinutti, C., Lamprecht, A., Ubrich, N., Astier, A., Hoffman, M., Bodmeier, R. & Maincent, P. (2000) The preparation and evaluation of polycaprolactone microparticles containing both a lipophilic and a hydrophilic drug, *Journal of Controlled Release. 65*, 429-438.
208. Polacco, G., Cascone, M. G., Lazzeri, L., Ferrara, S. & Giusti, P. (2002) Biodegradable hollow fibers containing drug-loaded nanoparticles as controlled release systems, *Polymer International. 51*, 1464-1472.
209. Williamson, M. R. & Coombes, A. G (2004) Gravity spinning of polycaprolactone fibres for applications in tissue engineering, *Biomaterials. 25*, 459-465.
210. Williamson, M. R., Chang, H. I. & Coombes, A. G (2004) Gravity spun

polycaprolactone fibres: controlling release of a hydrophilic macromolecule (ovalbumin) and a lipophilic drug (progesterone), *Biomaterials. 25*, 5053-5060.
211. Chang, H. I., Perrie, Y. & Coombes, A. G. (2006) Delivery of the antibiotic gentamicin sulphate from precipitation cast matrices of polycaprolactone, *Journal of Controlled Release. 110*, 414-421.
212. Aspden, R. M. & Li, B. (1998) Reproducibility of techniques using Archimedes' principle in measuring cancellous bone volume, *Medical Engineering and Physics. 20*, 393-395.
213. Keenan, M. J., Hegsted, M., Jones, K. L., Delany, J. P., Kime, J. C., Melancon, L. E., Tulley, R. T. & Hong, K. D. (1903) Comparison of bone density measurement techniques: DXA and Archimedes' principle, *Journal of Bone and Mineral Research. 12*, 1903-1907.
214. Young, P. M., Chan, H. K., Chiou, H., Edge, S., Tee, T. H. & Traini, D. (2007) The influence of mechanical processing of dry powder inhaler carriers on drug aerosolization performance, *Journal of Pharmaceutical Sciences. 96*, 1331-1341.
215. Kaheebu, L. & Coombes, A. G. A. (2006) *Production and characterisation of polycaprolactone fibres for tissue engineering*, Kingston University, London.
216. Williamson, M. R., Adams, E. F. & Coombes, A. G. (2005) Gravity spun polycaprolactone fibres for soft tissue engineering: interaction with fibroblasts and myoblasts in cell culture, *Biomaterials. 27*, 1019-1026.
217. Coombes, A. G., Rizzi, S. C., Williamson, M., Barralet, J. E., Downes, S. & Wallace, W. A. (2004) Precipitation casting of polycaprolactone for applications in tissue engineering and drug delivery, *Biomaterials. 25*, 315-325.
218. Chang, H. I., Williamson, M. R., Perrie, Y. & Coombes, A. G. (2005) Precipitation casting of drug-loaded microporous PCL matrices: incorporation of progesterone by co-dissolution, *Journal of Controlled Release. 106*, 263-272.
219. Sohier, J., Vlugt, T. J. H., Cabrol, N., Blitterswijk, C. A. V., Groot, K. & Bezemer, J. M. (2006) Dual release of proteins from porous polymeric scaffolds, *Journal of Controlled Release. 111*, 95-106.
220. Lee, T., Chen, T. T., Iruela-Arispe, M. L., Wu, B. M. & Dunn, J. C. Y. (2007) Modulation of protein delivery from modular polymer scaffolds, *Biomaterials. 28*, 1862-1870.
221. Zilberman, M. (2007) Novel composite fiber structures to provide drug/protein delivery for medical implants and tissue regeneration, *Acta Biomaterialia. 3*, 51-57.
222. Whitaker, M. J., Hao, J., Davies, O. R., Serhatkulu, G., Stolnik-Trenkic, S., Howdle, S. M. & Shakesheff, K. M. (2005) The production of protein-loaded microparticles by supercritical fluid enhanced mixing and spraying, *Journal of Controlled Release. 101*, 85-92.
223. Hosseinkhani, H., Hosseinkhani, M., Khademosseini, A. & Kobayashi, H. (2007) Bone regeneration through controlled release of bone morphogenetic protein-2 from 3-D tissue engineering nano-scaffold, *Journal of Controlled Release. 117*, 380-386.
224. Zmora, S., Glicklis, R. & Cohen, S. (2002) Tailoring the pore architecture in 3-D alginate scaffolds by controlling the freezing regime during fabrication,

Biomaterials. 23, 25-78.
225. Hubbell, J. A. (1995) Biomaterials in tissue engineering, *Biotechnology. 13*, 565-576.
226. Saltzman, W. M. (1999) Cell interactions with polymers in *Principles of tissue engineering* (Lanza, R. P., Langer, R. & Vacanti, J. P.) pp. 221, New York.
227. Moore, M. J., Jabbari, E., Ritaman, E. L., Lu, L., Currier, B. L., Windebank, A. J. & Yaszemski, M. J. (2004) Quantitative analysis of interconnectivity of porous biodegradable scaffolds with micro-computed tomography, *Journal of Biomedical Materials Research Part A. 71*, 258-267.
228. Otsuki, B., Takemoto, M., Fujibayashi, S., Neo, M., Kokubo, T. & Nakamura, T. (2006) Pore throat size and connectivity determine bone and tissue ingrowth into porous implants: Three-dimensional micro-CT based structural analyses of porous bioactive titanium implants, *Biomaterials. 27*, 5892-5900.
229. Mondrinos, M. J., Dembzynski, r., Lu, L., Byrapogu, V. K. C., Wooton, D. M. & Lelkes, P. (2006) Porogen-based solid freeform fabrication of polycaprolactone-calcium phosphate scaffolds for tissue engineering, *Biomaterials. 27*, 4399-4408.
230. Niklason, L. E., Gao, J., Abbott, W. M., Hirschi, K. K., Houser, S., Marini, R. & Langer, R. (1999) Functional arteries grown in vitro, *Science. 284*, 489-493.
231. L'Heureux, N., Paquet, S., Labbe, R., Germain, L. & Auger, F. A. (1998) A completely biological tissue-engineered human blood vessel, *The FASEB Journal: official publication of the Federation of American Societies for Experimental Biology. 12*, 47-56.
232. Moore, G. F. & S.M., S. (1997) Advances in biodegradable polymers, *Journal of Pharmaceutical Scienc. 9*, 19-21.
233. Narita, Y. U., Hata, K., Kagami, H., Usui, A., Ueda, M. & Ueda, Y. (2004) Novel pulse duplicating bioreactor system for tissue-engineered vascular construct, *Tissue Engineering. 10*, 1224-1233.
234. Williams, C. & Wick, T. M. (2004) Perfusion bioreactor for small diameter tissue-engineered arteries, *Tissue Engineering. 10*, 930-941.
235. Buttafoco, L., Engbers-Buijtenhuijs, P., Poot, A. A., Dijkstra, P. J., Vermes, I. & Feijen, J. (2006) Physical characterization of vascular grafts cultured in a bioreactor, *Biomaterials. 27*, 2380-2389.
236. Sandwick, R. E. (1999) Mechanical design in arteries, *Journal of Experimental Biology. 202*, 3305-3312.
237. Remmele, J. R. L., Stushnoff, C. & Carpenter, J. F. (1997) Real-time in situ monitoring of lysozyme during lyophilisation using infrared spectroscopy: dehydration stress in presence of sucrose, *Pharmaceutical Research. 86*, 1315-1318.
238. Sah, H. (1997) A new strategy to determine the actual protein content of poly(lactide-co-glycolide) microspheres, *Journal of Pharmaceutical Sciences. 86*, 1315-1318.
239. Ghaderi, R. & Carlfors, J. (1997) Biological activity of lysozyme after entrapment in poly(D,L-lactide-co-glycolide) microspheres, *Pharmaceutical Research. 14*, 1556-1562.

240. Pitt, C. G., Jeffcoat, A. R., Zweidinger, R. A. & Schindler, A. (1979) Sustained drug delivery systems. I. The permeability of poly(epsilon-caprolactone), poly(DL-lactic acid), and their copolymers, *Journal of Biomedical Materials Research. 13*, 497-507.
241. Grossowicz, N. & Ariel, M. (1983) Methods for determination of lysozyme activity, *Methods of Biochemistry. 29*, 435-446.
242. Petersen, S. B., Jonson, V., Fojan, P., Wimmer, R. & Pedersen, S. (2004) Sorbitol prevents the self-aggregation of unfolded lysozyme leading to an up to stabilisation of the folded form, *Journal of Biotechnology. 114,* 269-278.
243. Fujita, Y., Yasuhiko, I. & Yukinao, N. (1982) The effect of polyhydric alcohols on the thermal denaturation of lysozyme as measured by differential scanning calorimetry, *Bulletin of the Chemical Society of Japan. 55,* 1896-1900.
244. Fujita, Y. & Noda, Y. (1992) Effect of alkylation with different sized substituents on thermal stability of lysozyme, *International Journal of Peptide and Protein Research. 40,* 103-109.
245. Wimmer, H., Olsson, M., Petersen, M. T., Hatti-Kaul, R., Peterson, S. B. & Muller, N. (1997) Towards a molecular level understanding of protein stabilisation: the interaction between lysozyme and sorbitol, *Journal of Biotechnology. 55,* 85-100.
246. Crotts, G. & Park, T. G. (1997) Stability and release of bovine serum albumin encapsulated with poly(D,L-lactic acid-co-glycolic acide) microspheres, *Journal of Controlled Release. 44,* 123-134.
247. Crotts, G., Sah, H. & Park, T. G. (1997) Adsorption determines in-vitro protein release rate from biodegradable microspheres: quantitative analysis of surface area during degradation, *Journal of Controlled Release. 47,* 101-111.
248. Harper, E. (1980) Collagenases, *Annual Review of Biochemistry. 49,* 1063.
249. Peck, W., Birge, S. & Fedak, S. (1964) Bone cells: biochemical and biological studies after enzymatic isolation, *Science. 146,* 1476.
250. Kono, T. (1968) Purification and partial characterization of collagenolytic enzyme from Clostridium histolyticum, *Biochemistry. 7,* 1106.
251. Barker, C. (1975) Transplantation of the islets of langerhans and the histocompatibility of endocrine tissue, *Diabetes. 24,* 766.
252. Ewart, R., Kornfield, S. & Kipnis, D. (1975) Effect of lectins on hormone release from isolated islets of langerhans, *Diabetes. 24,* 705.
253. Seglen, P. (1973) Preparation of rat liver cells II. Effect of ions and chelators on tissue dispersion, *Experimental Cell Research. 76,* 25.
254. Moore, S. & Stein, W. H. (1948) Photometric Nihydrin Method, *Journal of Biological Chemistry. 176,* 367.
255. Sichak, S. P. & Dounce, A. L. (1987) A study of the catalase monomer produced by lyophilization, *Biochimica et Biophysica Acta. 925,* 282-289.
256. Aebi, H., Wyss, S. R., Scherz, B. & Skvaril, F. (1974) Heterogeneity of erythrocyte catalase II. Isolation and characterization of normal and variant erythrocyte catalase and their subunits, *European Journal of Biochemistry. 48,* 137-145.
257. Cetinus, S. A., Oztop, H. N. & Saraydin.D. (2007) Immobilization of catalase

onto chitosan and cibacron, *Enzyme and Microbial Technology. 12,* 78-93.
258. Bezemer, J. M., Radersma, R., Grijpma, D. W., Dijkstra, P. J., Feijen, J. & van Blitterswijk, C. A. (2000) Zero-order release of lysozyme from poly(ethylene glycol)/poly(butylene terephthalate) matrices, *Journal of Controlled Release. 64,* 179-192.
259. Van Tomme, S. R. V., De Geest, B. G., Braeckmans, K., De Smedt, S. C., Siepmann, F., Siepmann, J., Van Nostrum, C. F. & Hennink, W. E. (2005) Mobility of model proteins in hydrogels composed of oppositely charged dextran microspheres studied by protein release and fluorescence recovery after photobleaching, *Journal of Controlled Release. 110,* 67-78.
260. Bazemer, J. M., Radersma, R., Grijpma, D. W., Dijkstra, P. J., Feijen, J. & van Blitterswijk, C. A. (2000) Zero-order release of lysozyme from poly(ethylene glycol)/poly(butylene terephthalate) matrices, *Journal of Controlled Release. 64,* 179-192.
261. Michiaki, M., Koji, K. & Kazuo, K. (1997) Effects of polyols and organic solvents on thermostability of lipase, *Journal of Chemical Technology and Biotechnology. 70,* 188-192.
262. Costa, S. A., Tzanov, T., Carneiro, A. F., Paar, A., Gubitz, M. & Cavaco-Paulo, A. (2002) Studies of stabilization of native catalase using additives, *Enzyme and Microbial Technology. 30,* 387-391.
263. Baeyens, V., Kaltsatos, V., Boisrame, B., Varesio, E., Veuthey, J. L., Fathi, M., Balant, L. P., Gex-Fabry, M. & Gurny, R. (1998) Optimized release of dexamethasone and gentamicin from a soluble ocular insert for the treatment of external ophthalmic infections, *Journal of Controlled Release. 52,* 215-220.
264. Montjovent, M.-O., Burri, N., Silke, M., Federici, E., Scaletta, C., Zambelli, P.-Y., Hohlfield, P., Leyvraz, P.-F., Applegate, L. L. & Pioletti, D. P. (2004) Fetal bone cells for tissue engineering, *Bone. 35,* 1323-1333.
265. Martin, I., Shastri, V. P., Padera, R. F., Yang, J., Mackay, A. J., Langer, R., Vunjak-Novakovic, G. & Freed, L. E. (2001) Selective differentiation of mammalian bone marrow stromal cells cultured on three-dimensional polymer foams, *Journal of Biomedical Materials Research. 55,* 229-235.
266. Richardson, S. M., Curran, J. M., Chen, R., Vaughan-Thomas, A., Hunt, J. A., Freemont, A. J. & Hoyland, J. A. (2006) The differentiation of bone marrow mesenchymal stem cells into chondrocyte-like cells on poly-L-lactic acid (PLLA) scaffolds, *Biomaterials. 27,* 4069-4078.
267. Datta, N., Pham, Q. P., Sharma, U., Sikavitsas, V. I., Jansen, J. A. & Mikos, A. G. (2006) In vitro generated extracellular matrix and fluid shear stress synergistically enhance 3-D osteoblastic differentiation, *Proceeding of the National Academy of Sciences of the United States of America. 103,* 27-30.
268. Erickson, G. R., Gimble, J. M., Franklin, D. M., Rice, H. E., Awad, H. & Guilak, F. (2002) Chondrogenic potential of adipose tissue-derived stromal cells in vitro and in vivo, *Biochemical and Biophysical Research Communications. 290,* 763-769.
269. Fromigue, O., Marie, P. J. & Lomri, A. (1997) Differential effects of

transforming growth factor beta2,dexamethasone and 1,25-dihydroxyvitamin D on human bone marrow stromal cells, *Cytokine. 9,* 613-623.
270. Hodge, B. O. & Kream, B. E. (1988) Variable effects of dexamethasone on protein synthesis in clonal rat osteosarcoma cells, *Endocrinology. 122,* 2127-2133.
271. Yoon, J. J., Kim, J. H. & Park, T. G. (2003) Dexamethasone-releasing biodegradable polymer scaffolds fabricated by a gas-foaming/salt-leaching method, *Biomaterials. 24,* 2323-2329.